Dissertation
submitted to the
Combined Faculty of Natural Sciences and Mathematics
of the Ruperto Carola University Heidelberg, Germany
for the degree of
Doctor of Natural Sciences

Presented by
M.Sc. Elena von Molitor
born in: Sinsheim
Oral examination: 10.05.2021

Human tongue-cell derived spheroids suggest that multiple pathways and molecules are involved in the sweet gustatory sense

Referees: Prof. Dr. Stephan Frings

Prof. Dr. Rüdiger Rudolf

I dedicate this thesis to my parents and my family
who always encouraged me to go on adventures.
Thank you for your endless love and support.

Table of contents

Acknowledgements

First and foremost, I owe my deepest gratitude Prof. Dr. Rüdiger Rudolf. Thank you for all your expert advises, your dedicated support and patience. I appreciated that you always had time to listen to my struggles and I am especially grateful for your courage and trust in my work. I absolutely enjoyed working in your lab and your enthusiasm about science always motivated me to stay tuned. This allowed me not only to gain scientific experience but also to grow personally.

Many thanks go to Prof. Dr. Mathias Hafner for his guidance and overall insights in the cell biology field which have made this an inspiring experience for me. Further, I thank Dr. Katja Riedel, Dr. Torsten Ertongur-Fauth, Dr. Paul Scholz and Dr. Janina Trothe from BRAIN AG for their enthusiasm in this future orientated project. Thank you for your time and scientific expertise. Your profound knowledge, insightful discussions and assistance decisively contributed to the success of my thesis.

I am happy to acknowledge Dr. Tiziana Cesetti who jointly worked with me on this topic and emotionally shared all up and downs with me. Thank you for your mentorship and encouragement during my practical work and reviewing my thesis. I am grateful for your support and I am proud of our common achievements. We have been a good team.

I am thankful to Prof. Dr. Stephan Frings for the supervision and personal contribution to all my TAC meetings. Thank you for your time, your advice and ideas. It was always very valuable to have an independent opinion on my data. I also thank Prof. Dr. Hilmar Bading and Prof. Dr. Andreas Draguhn for the time invested in reviewing my thesis.

Exceptionally I would like to say thank you to all my MZB colleagues: Roman Bruch, Dr. Andreas Holloschi, Sarah Hörner, Florian Keller, Prof. Dr. Petra Kioschis, Dr. Hella-Monika Kuhn, Jessica Martin, Elina Nürnberg, Matteo Rigon, Valeh Rustamov, Max Schäfer, Ariane Tomsche, Mario Vitacolonna and Patrick Williams for their energy, understanding and help throughout my project. It was a pleasure to have Tatjana Straka, Julia Klicks, Anett Pomowski, and Franziska Ebeling as motivating, supportive and dedicating lab members but also as friends. Thank you so much for the good and frustrating moments we shared inside and outside the lab and the time we spent together on this journey.

Further, I would like to thank Dr. Heiko Flammann and Dr. Andreas Lux from QBios GmbH but also Dr. Manfred Frey, Cordula Stahl and Regina Martens from the Steinbeis-Transferzentrum for scientific discussions. It has been a pleasure to have you as colleagues.

To my parents I would like to express thanks from all my heart not only for their dedication, encouragement and the many years of support during my studies that provided the foundation for this work - but also for their love and implicitly standing behind me no matter which way I choose to go. Without you I would never have enjoyed so many great opportunities in my life, I would not have gone so far and I would have never made so many great and enriching experiences.

I am extremely thankful to Dario Frey who shared the great PhD adventure with me. Your understanding and patience in troubleshooting my experiments over and over again severely contributed to the success of this work. Thank you for your deep trust, your enthusiasm and motivation through all my doubts but also for the enriching timeouts during our backing adventures which gave me new inspiration and courage.

My family and my friends also receive my deepest gratitude for encouraging me to take the step to dare this PhD project. Thank you for sustaining me, for always having an open ear, your love and friendship.

Zusammenfassung

Kanonisch wird der Süßgeschmack durch spezifische T1R2/T1R3 G-Protein gekoppelte Süßrezeptoren vermittelt, die von Geschmacksknospenzellen der Zunge exprimiert werden. Mäuse, denen diese Rezeptoren oder ihre nachgeschalteten Signalkomponenten fehlen, können jedoch immer noch natürlichen Zucker erkennen. Künstlichen Süßstoffe hingegen können sie nicht mehr wahrnehmen, da diese hauptsächlich an die kanonischen Süßrezeptoren binden. Dies deutet auf die Existenz eines parallelen “alternativen Signalwegs“ für die Wahrnehmung von Zuckern hin. Um die zugrundeliegenden molekularen Wege, deren Komplexität und physiologische Relevanz zu beleuchten, wurden in der vorliegenden Arbeit umfassende Literaturrecherchen sowie experimentelle Arbeiten auf Basis von 3D-Zellkulturen immortalisierter humaner Zungenzellen (HTC-8) durchgeführt.

Die Literaturrecherche ergab, dass süßempfindliche Geschmackszellen Monosaccharide über Glukosetransporter (GLUT/SGLT1) aufnehmen können. Durch den anschließenden oxidativen Stoffwechsel wird vermehrt ATP gebildet, welches K_{ATP}-Kanäle blockiert. Dadurch depolarisieren die Zellen und Ca^{2+} strömt ein. Disaccharide können nach Spaltung, durch von Geschmackszellen exprimierten Bürstenrandenzymen, diesen Signalweg aktivieren. Alternativ könnten Disaccharide über noch unbekannte Transporter in das Zellinnere aufgenommen werden, wodurch eine osmotische Schwellung induziert und volumenregulierte Anionenkanäle aktiviert werden. Über noch nicht identifizierte neuronale und/oder endokrine Mechanismen könnten diese Signalwege zur Geschmackswahrnehmung beitragen, aber auch zur Insulinfreisetzung nach GLP-1-Sekretion von Geschmackszellen in der kephalischen Phase. Dies würde bedeuten, dass der alternative Signalweg den Körper auf die Verdauung vorbereitet, während der kanonische Weg eher für den hedonischen Wert verantwortlich ist. Da Geschmack artenspezifisch ist und der Zugang zu humanen Zungengewebeproben limitieret ist, bleiben die meisten Hypothesen des alternativen Weges eher vage und basieren häufig auf analogen Experimenten mit Zellen anderer Organe, die ebenfalls extraorale Süßrezeptoren und kanonische Signalmoleküle exprimieren, wie beispielsweise Magen-Darm- oder Pankreaszellen.

Da im Rahmen dieser Arbeit durchgeführte perfundierte Echtzeitexperimente lebender HTC-8 Sphäroide zeigten, dass einzelne HTC-8-Zellen auf Süß, Bitter und KCl reagieren, könnten diese zu den neu beschriebenen breitempfindlichen Geschmackszellen gehören. Dies steht im Gegensatz zu der Annahme, dass verschiedene Geschmacksmodalitäten unterschiedliche Signalwege in unterschiedlichen Zelltypen verwenden. Eine vorläufige Transkriptomanalyse von HTC-8 Sphäroiden bestärkte ferner die Hypothese, dass Geschmack nicht ausschließlich über den kanonischen Signalweg übertragen wird. Hieraus folgernd könnte der Bittergeschmack von HTC-8-Sphäroiden über Familienmitgliedern des kanonischen

Signalwegs vermittelt worden sein. Die Wahrnehmung von Zucker könnte hingegen den metabolisch alternativen Weg verwendet haben, da Sphäroide gegenüber dem künstlichen Süßstoff Acesulfam K nicht empfindlich waren und im 3D Verbund begannen verwandte Signalmoleküle des alternativen Signalwegs zu exprimieren. Obwohl das hier etablierte Modell Einschränkungen aufweist und weiterentwickelt werden muss, könnte es als vorläufige Testplattform dienen, um humane Daten zur Geschmacksphysiologie mit einem höheren Durchsatz als bei menschlichen Probanden zu generieren. Zusätzlich kann es für die Suche nach neuen Zuckerersatzstoffen genutzt werden, um dem ansteigendem Zuckerkonsum und den damit verbundenen Erkrankungen entgegen zu wirken.

Abstract

Canonically, sweet perception is mediated by specific T1R2/T1R3 sweet taste G-protein coupled receptors expressed in taste cells of the tongue. However, mice lacking these receptors or their downstream signaling components are still able to recognize natural sugars. Conversely, they do not perceive artificial sweeteners, which are mostly canonical sweet taste receptor agonists, suggesting the existence of a parallel “alternative pathway” for sweet perception. To address the molecular pathways, complexity and physiological relevance of sweet taste sensation, this study combines a deep literature survey on sweet taste biology with experimental work using 3D cell cultures of immortalized human tongue cells (HTC-8).

The literature research revealed that sweet-sensitive taste cells may take up monosaccharides via Glucose transporters (GLUT/SGLT1) to induce depolarization-dependent Ca^{2+} signals upon oxidative metabolism and K_{ATP} channel inactivation. Disaccharides can activate this signal path upon digestion from taste cell-expressed Brush Boarder enzymes. Alternatively, disaccharides may be taken up with elusive transporters, induce osmotic swelling and activate volume regulated anion channels. Via unidentified neuronal and/or endocrine mechanisms, sweet taste receptor-independent pathways may contribute to behavioral attraction but may also induce cephalic phase Insulin release upon GLP-1 secretion from taste cells. This would suggest that the alternative pathway may prepare the body for digestion, while the canonical pathway might be rather responsible for the hedonic value of sugars. Since taste differs among species and human samples are limited, most hypotheses of the alternative pathway remain rather vague and are often based on cells of other organs that express extraoral sweet taste receptors and canonical downstream molecules like gastro-intestinal or pancreatic cells.

Since perfused live imaging experiments conducted in this study revealed that individual HTC-8 cells responded to KCl, sweet and bitter stimulation, they might belong to the newly described broadly-sensitive taste cells, which is in contrast with the assumption that diverse taste modalities use different signaling pathways in distinct cell types. A preliminary transcriptome analysis of HTC-8 spheroids corroborated the finding that taste is not exclusively transduced by the canonical pathway. Accordingly, bitter responses of HTC-8 spheroids might have been mediated by family members of the canonical signaling pathway, while sugars may have used the alternative pathway, since spheroids were not sensitive to the artificial sweetener Acesulfame K and related signal molecules of the alternative signal pathway were expressed upon 3D culture of HTC-8 cells. Although the here established model contains several limitations and needs further adjustment it might serve as a first testing platform to obtain human-derived data on taste physiology in a higher throughput than in human subjects. Thereby, it may support the search for new sugar alternatives and to combat the current sugar overconsumption which goes along with a sickening society.

1 Introduction

Throughout evolution, animal behavior has been strongly influenced by taste and flavors and the awareness of the five basic taste modalities sweet, bitter, umami, sour and salty offers essential information to induce instinctive reactions for survival (Clark 1998; Kikut-Ligaj and Trzcielińska-Lorych 2015). Specific roles in body homeostasis are assigned to the individual modalities. Depending on their concentration, salty and sour taste can be repulsive or pleasant. Salty taste governs the intake of ions essential for body fluid maintenance and sour taste helps to maintain the acid-base ratio. Bitter taste unpleasantness serves as a warning signal for toxicity, while umami refers to the protein content in the food (Chaudhari and Roper 2010; Kikut-Ligaj and Trzcielińska-Lorych 2015; Beauchamp 2016). A biological predisposition makes sweet taste the most favored modality since sweet compounds are present in the amniotic fluid and sweetness of mother milk is associated with weight gain essential for development. Thus, sweetness can already be identified by premature babies (Tatzer et al. 1985; Beauchamp and Mennella 2011). Such predispositions guide our food choice through life, making energy-rich nutrients highly attractive. For our ancestors, this was essential to survive. However, thanks to growing food industries, high calorie palatable junk food is now provided in excess. In the US, 75% of beverages and meals contain added sugar, which increased sugar consumption by 30 times within the last 200 years (Li et al. 2011; Bray and Popkin 2014). With this over nutrition, severe health problems as type II diabetes, obesity and cardiovascular diseases dramatically increased in the 20th century (Bray and Popkin 2014; Borges et al. 2017). Thus, there is a high interest in replacing sugars by substitutes, such as artificial sweeteners, which are believed to be more healthy due to their lack in calories (Pepino 2015; Borges et al. 2017). In the US, daily intake dosages for the artificial sweeteners - Advantame, Cyclamate, Saccharin, Aspartame, Sucralose, Neotame and Acesulfame K - have been approved by the FDA (Li et al. 2011). However, their consumption is still hampered by a bitter, unpleasant off-taste (Moskowitz and Klarman 1975; Kuhn et al. 2004; Galindo-Cuspinera et al. 2006). Furthermore, as sweet taste receptors are not exclusively expressed in the oral cavity but also in multiple extraoral tissues, artificial sweeteners may have unknown actions in these tissues and may induce cancer, obesity and diabetes (Belpoggi et al. 2006; Pepino 2015). This prompted the search for alternatives, such as positive allosteric modulators of the sweet taste receptor. Such modulators are not sweet *per se,* but they increase sugar sweetness and, thus, reduce caloric intake (Servant et al. 2010).

1.1 Taste papillae and their projections to the central nervous system

Onion-shaped taste buds, embedded in papillae of the stratified epithelium of the tongue, plate and epiglottis of mammals, represent the taste organs (Lindemann 1999; Breslin and Huang 2006; Kikut-Ligaj and Trzcielińska-Lorych 2015; Roper and Chaudhari 2017). In mammals, there are three different types of taste papillae (Figure 1). First, about 300 fungiform papillae reside in the anterior two thirds of the human tongue. They contain ~3.5 taste buds each and convey information via the chorda tympani nerve (VII) (Breslin and Huang 2006; Behrens et al. 2011; Kikut-Ligaj and Trzcielińska-Lorych 2015). Second, circumvallate papillae are the largest with ~250 taste buds each. They are located on the dorsal tongue (Behrens et al. 2011). In humans, there are ~9 circumvallate papillae which are innervated by the cranial nerve (IX), a part of the glossopharyngeal nerve (Behrens et al. 2011; Kikut-Ligaj and Trzcielińska-Lorych 2015). Third, foliate papillae are buried on the lateral sides of the tongue and comprise multiple clefts with ~1300 taste buds in humans (Behrens et al. 2011). They convey information via both, the glossopharyngeal and the chorda tympani nerve (Breslin and Huang 2006; Kikut-Ligaj and Trzcielińska-Lorych 2015). In addition to taste buds organized in papillae, there are also single taste buds in the palate and the epiglottis, which project to the vagus nerve (X) (Barlow 2015).

Projection from the peripheral nerves to the brain occurs via the geniculate ganglia from the chorda tympani nerve, via petrosal ganglia from the glossopharyngeal nerve and via nodose ganglia from the vagus nerve (Ootani et al. 1995; Gutierrez et al. 2020). From there, information is transmitted to the rostral part of the nucleus of the solitary tract (NTS), where nerves make synapses with second order neurons. In humans, these directly connect to the thalamus (Ohla et al. 2019). In rodents, they first project to the parabrachial nucleus (PbN), from there to the amygdala (amy) and then to the hypothalamus and the medullary reticular (Figure 4, Karimnamazi et al. 2002). To finally decode gustation, the information travels from the thalamus to the gustatory cortex, also termed insula (Ohla et al. 2019). How taste information is represented in neurons, is still controversial. Two major theories are called “labelled line model” and “cross-fiber theory” (Lemon and Katz 2007). The labelled line model suggests that each taste modality is recognized by a specific peripheral taste cell that conveys its information to a specific neuron. For example, in chimpanzee it was shown that sweet taste stimulated a special set of chorda tympani fibers (“S-clusters”), whereas other fibers (“Q-clusters” and “N-clusters”) were activated by bitter tastants and salts. If a particular taste modality was not present, the other clusters were quiescent (Hellekant et al. 1998). In contrast, the cross-fiber theory proposes that taste is carried by an activity pattern across a population of neurons (Lemon and Katz 2007). In regard to this, it was reported that neurons responding to bitter molecules also received input from receptors that mediated other taste modalities (Lemon and Smith 2005).

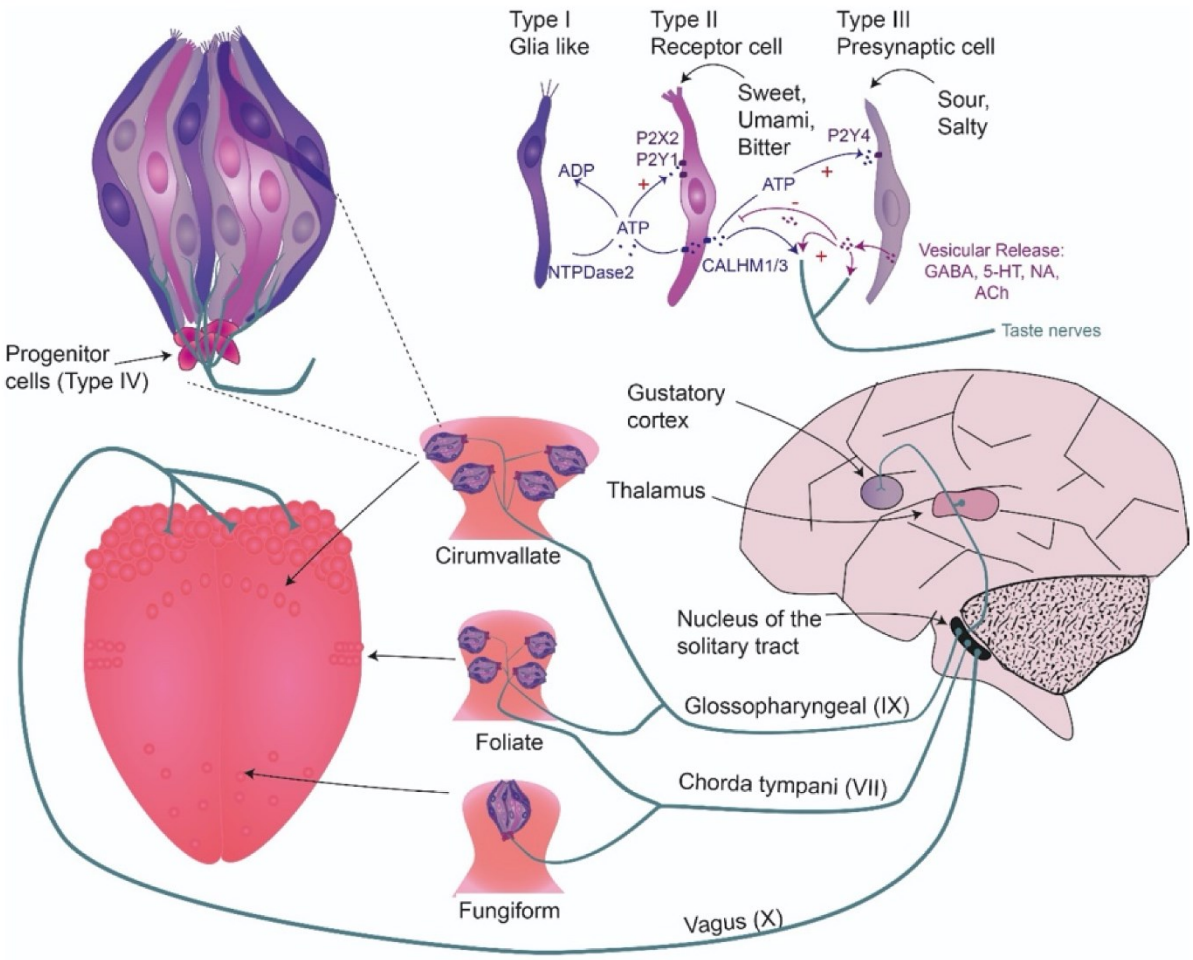

Figure 1: Anatomy of organs, tissues and cells involved in taste perception. As indicated, primary taste transduction uses different receptors and intra- and intercellular pathways that are mediated in three distinct taste cell types (upper right). Taste cells assemble to taste buds (upper left), which are embedded in circumvallate, foliate or fungiform papillae (center) of the tongue (lower left). Sensory information is conveyed via glossopharyngeal, chorda tympani and vagus nerves (lower right) to the nucleus of the solitary tract in the brain stem (right), from where they get relayed to the thalamus and then to the gustatory cortex (insula) for final processing. Abbreviations: 5-HT: Serotonin, NA: Noradrenaline, Ach: Acetylcholine. Figure adapted from von Molitor et al. 2020b.

1.2 Taste buds and their composition

Each taste bud is a cluster of about 60-100 polarized neuroepithelial taste cells. Four distinct types of taste cells (Figure 1) can be distinguished according to their morphology and expression profile (Breslin and Huang 2006; Chaudhari and Roper 2010; Roper and Chaudhari 2017). Most abundant are type I cells. They are described as “dark cells”, since they comprise an electron-dense cytoplasm, apical dark granules and long microvilli (Yee et al. 2001; Miura et al. 2006). Type I cells enwrap other cells and are believed to have glia-like function (Vandenbeuch et al. 2008). They release NTPDase to terminate synaptic transmission by degrading neurotransmitters secreted from other taste cells (Chaudhari and Roper 2010; Roper 2013). Recent findings postulate that type I cells may release GABA to provide negative feedback onto type II cells to terminate their taste-evoked ATP secretion (Huang and Wu 2018).

Type II cells are lighter with shorter and thicker microvilli and a more electron-lucent cytoplasm (Yee et al. 2001; Miura et al. 2006). They express G-protein coupled receptors of two different families, T1R for sweet and umami taste, and T2R to transduce bitter taste. Accordingly, type II cells are termed “receptor cells” (Chaudhari and Roper 2010; Roper 2013). To generate action potentials, they express voltage-gated Na^+ and K^+ channels (Cummings et al. 1996; Medler et al. 2003; Clapp et al. 2006) and a subpopulation may also express voltage-dependent Ca^{2+} channels (Medler et al. 2003; Hacker et al. 2008). Depolarization of type II cells mediates unconventional release of ATP, which has many functions within the taste bud: it activates nerve terminals, exerts positive autocrine feedback and stimulates type III cells (Huang et al. 2009; Dando and Roper 2012).

Type III cells are responsible for sour taste sensation (Gilbertson et al. 2000) and their electron density is intermediate (Miura et al. 2006). They are called “presynaptic cells” since they synapse with afferent nerve fibers and release neurotransmitters, such as Serotonin (Huang et al. 2009), Noradrenaline (Huang et al. 2008) and GABA (Huang et al. 2011). Serotonin and GABA exert an inhibitory feedback onto type II cells, while the function of Noradrenaline is not fully understood (Gilbertson et al. 2000).

Finally, type IV cells, termed “progenitor cells”, reside at the bottom of the taste bud and give constantly rise to new mature taste cells since their lifespan is limited to ~10 days (Chaudhari and Roper 2010; Roper and Chaudhari 2017).

1.3 The canonical sweet taste receptor is formed by T1R2/T1R3 GPCR heterodimers

Canonically, sweet taste perception in the oral cavity is mediated by T1R2/T1R3 heterodimers (Bachmanov et al. 2001; Kitagawa et al. 2001; Max et al. 2001; Montmayeur et al. 2001; Nelson et al. 2001; Sainz et al. 2001; Li et al. 2002), which belong to the class C of G-protein coupled receptors (GPCR). These are characterized by a seven-transmembrane domain, an extracellular venus flytrap-like domain on the N-terminus, comprising a cysteine-rich domain and an active site for ligands (Figure 2, DuBois 2016). Sweet taste receptors have at least six distinct binding sites and are, thus, target of ligands with different chemistries reaching from saccharides, artificial sweeteners, sweet proteins to new modulators (DuBois 2016). The Saccharin preference (*sac*) locus (Fuller 1974; Lush 1989) and D-Phenylalanine aversion (*dpa*) locus (Ninomiya et al. 1984) were both described to influence sweet sensitivity. This discovery was prompted by the observation that two mice strains, called tasters (C57BL/6 and DBA/2), were strongly attracted by Saccharin and D-Phenylalanine, compared to non-taster mice (129/sv) (Bachmanov et al. 1997). Indeed, the genes of T1R map to the *sac* locus, while the role of the *dpa* locus is not fully understood (Shigemura et al. 2005). In mice, the T1R family is encoded by three genes located on the distal chromosome 4 in the order: *TAS1R2* –

TAS1R1 – TAS1R3. Humans have the same order of the orthologue genes in a conserved synteny region of the short arm of chromosome 1 (1p36) (Bachmanov et al. 2011). T1R1 is not crucial for sweet taste but forms functional umami receptors with the T1R3 subunit (Chaudhari et al. 2000; Sainz et al. 2001; Nelson et al. 2002).

Besides *TAS1R,* also *TAS2R* is part of the *TAS* gene family and encodes ~25 different bitter receptors in humans (Adler et al. 2000; Chandrashekar et al. 2000; Matsunami et al. 2000), which can be co-expressed in different combinations in bitter-sensitive type II cells (Adler et al. 2000). Several structurally unrelated compounds can activate T2Rs. While some bitter compounds are specific for one receptor, others can activate more than one receptor (Kuhn et al. 2004; Meyerhof et al. 2010). The molecular taxonomy of T2Rs is still elusive: initially termed a class A-GPCR, they share only 20% sequence homology with this group of receptors (Di Pizio and Niv 2014). Thus, T2Rs might rather belong to the F-frizzled receptors (Fredriksson et al. 2003) or to a completely distinct new group (Horn et al. 2003).

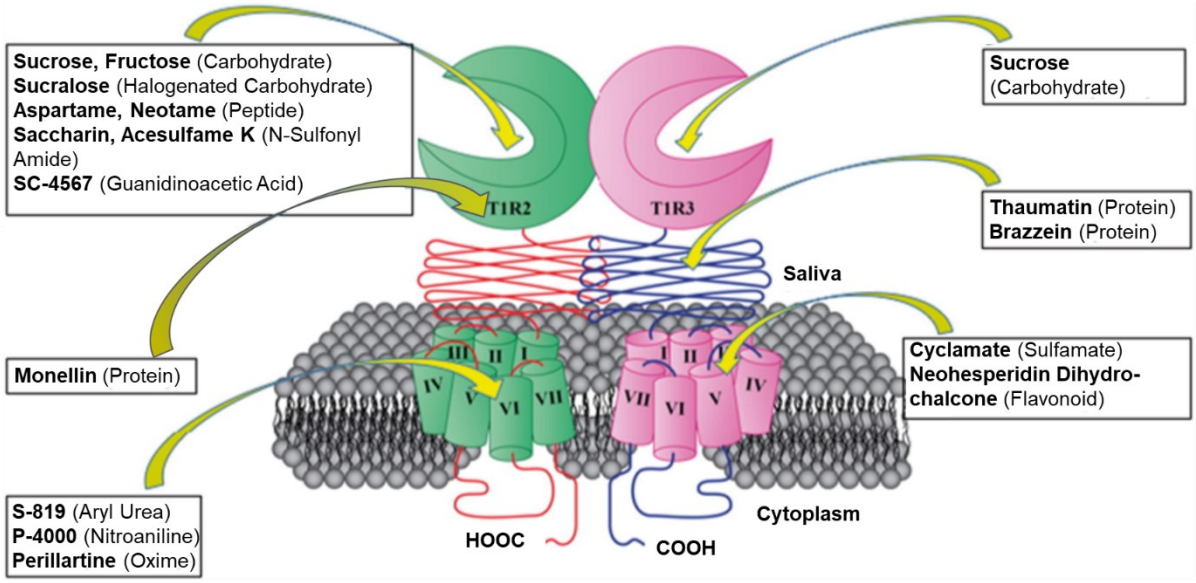

Figure 2: Structure of the human sweet taste receptor. The T1R2/T1R3 heterodimer is a C-GPCR. They comprise an N-terminal extracellular venus flytrap-like domain followed by a cysteine-rich domain attached to the typical seven-transmembrane domain. There are six distinct loci for allosteric binding of sweet molecules. Figure adapted from DuBois 2016.

1.4 Multiple G-protein subunits may transduce sweet taste

Upon ligand binding, taste receptors undergo a conformational change affecting their apposite heterotrimeric G-protein, i.e. GDP is exchanged for GTP on the Gα subunit. Consequently, this subunit dissociates from the receptor and the βγ subunit (Hoon et al. 1995). The first molecule found to transduce taste upon activation of the transmembrane taste receptor was gustducin, a G-protein related to the G_i family, which consists of $G\alpha_{gustducin}$ (McLaughlin et al. 1992; McLaughlin et al. 1993) and a $G\beta_3\gamma_{13}$ subunit (Huang et al. 1999). However, gustducin may not be the only player in sweet sensation as only a fraction of type II cells expressing sweet

taste receptors are also positive for gustducin (Hoon et al. 1999; Montmayeur et al. 2001; Max et al. 2001). In addition, gustducin-knockout mice exhibit a reduced but not abolished response to sweet (Wong et al. 1999; He et al. 2002; Danilova et al. 2006) and bitter compounds (Caicedo et al. 2003). Accordingly, $G\alpha_{transducin}$, $G\alpha_{q}$, $G\alpha_{i\text{-}2}$, $G\alpha_{i\text{-}3}$, $G\alpha_{s}$ and $G\alpha_{14,15}$ have been identified in taste tissue and might transduce the signal from the sweet taste receptor (McLaughlin et al. 1992; Kusakabe et al. 1998; Tizzano et al. 2008; Shindo et al. 2008). However, no functional experiments have been conducted with these additional subunits nor it is known, if they are used selectively or collectively to transduce sweet, bitter or umami taste.

1.5 Canonical sweet taste transduction downstream the sweet taste receptor

Sweet and bitter taste transduction have been largely studied in parallel (Table 1). The latter uses a variety of T2Rs. Upon receptor activation by a taste molecule, the $G\beta_3\gamma_{13}$ subunit (Huang et al. 1999; Rössler et al. 2000) mediates the generation of the second messenger Inositol-3-phosphate (IP3) (Hwang et al. 1990; Spielman et al. 1994) via Phospholipase Cβ2 (PLCβ2) activation (Figure 3, Rössler et al. 1998). Subsequently, IP3 binds to its receptor (IP3-R) on the endoplasmic reticulum (Clapp et al. 2001; Miyoshi et al. 2001) to release Ca^{2+} from stores (Akabas et al. 1988; Liu and Liman 2003). This stimulates cell depolarization by Na^{+} influx through the transient receptor potential M5 channel (TRPM5) (Pérez et al. 2002; Liu and Liman 2003; Zhao et al. 2003), followed by ATP release via pannexin 1 and/or calcium homeostasis modulator channel 1/3 (CALHM1/3) (Romanov et al. 2007; Ma et al. 2018). Finally, the secreted ATP activates the nerves either directly or indirectly by stimulating presynaptic type III cells (Huang et al. 2009). This signaling cascade has been described as “canonical bitter signaling” (Huang et al. 1999; Clapp et al. 2004). Canonical sweet and umami transduction pathways are considered to be similar, but mediated by T1R2/T1R3 and T1R1/T1R3, respectively (Roper 2013; Roper and Chaudhari 2017). Accordingly, knockout of PLCβ2 or TRPM5 reduced responses to sweet, bitter and amino acids (Zhang et al. 2003). However, an increasing wealth of evidence suggests that any single taste modality is not necessarily mediated by only one specific pathway, but may involve several different mechanisms (von Molitor et al. 2020c).

Indeed, before the discovery of the cascade using PLCβ2-IP3-TRPM5, research focused on a different downstream signaling pathway that involved cyclic adenosine monophosphate (cAMP) and Protein Kinase A (PKA)-induced cell depolarization (Figure 3). Already in 1972, Kurihara and Koyama suggested that cAMP plays a role in taste transduction since its synthesizing enzyme, Adenylyl Cyclase (AC), was enriched in bovine taste buds (Kurihara and Koyama 1972) and sugars as well as Saccharin were shown to stimulate AC in the presence of guanine nucleotides in frog, rat and pig tongue epithelium (Avenet and Lindemann 1987; Striem et al. 1989; Striem et al. 1991; Naim et al. 1991). Electrophysiological studies showed

that addition of cAMP analogues induced cell depolarization due to a decreased K^+ outward current via PKA-mediated phosphorylation (Avenet and Lindemann 1987; Striem et al. 1991). In addition, the sweet compounds Saccharin and NC01 were found to trigger Phosphodiesterase (PDE)-mediated hydrolysis of cAMP in frog cells, which in turn activated cyclic-nucleotide-suppressible channels (CNG), Ca^{2+} influx and cell depolarization (Kolesnikov and Margolskee 1995). Low cAMP levels further kept PKA activity low to create permissive conditions for PLCβ2 signaling (Margolskee 1993; Gilbertson et al. 2000).

Table 1: Canonical taste signaling molecules downstream bitter T2R or T1R2/T1R3 sweet taste receptors.

Signaling molecule	Bitter	Sweet
$G\beta_3$	Rössler et al. 2000	Max et al. 2001
$G\gamma_{13}$	Huang et al. 1999	Max et al. 2001
PLCβ2	Rössler et al. 1998; Miyoshi et al. 2001; Yan et al. 2001; Zhang et al. 2003	Asano-Miyoshi et al. 2000; Max et al. 2001; Miyoshi et al. 2001; Zhang et al. 2003
IP3	Hwang et al. 1990; Spielman et al. 1994; Ogura et al. 1997; Huang et al. 1999	Bernhardt et al. 1996; Uchida and Sato 1997; Usui-Aoki et al. 2005
IP3R	Clapp et al. 2001; Miyoshi et al. 2001	Miyoshi et al. 2001
Ca^{2+} release from stores	Akabas et al. 1988	Bernhardt et al. 1996; Uchida and Sato 1997
TRPM5	Pérez et al. 2002; Zhang et al. 2003	Pérez et al. 2002; Zhang et al. 2003; Talavera et al. 2005

Since sugars mediated a cAMP increase, while artificial sweeteners (Saccharin and SC45647) led to increased IP3 concentrations in rat taste buds, it was postulated that sugars and artificial sweeteners use distinct pathways downstream the sweet taste receptor (Striem et al. 1991; Bernhardt et al. 1996). Along these lines, extracellular Ca^{2+} was described to be only required for sugar-mediated responses, but not for artificial sweeteners (Bernhardt et al. 1996). However, further studies contested such a concept of differential signaling since i) in some studies Saccharin stimulated both pathways (Nakashima and Ninomiya 1999), ii) PLCβ2 deficient mice were insensitive to Sucrose and Glucose (Zhang et al. 2003), and iii) deletion of TRPM5 diminished the response to sugars (Zhang et al. 2003; Damak et al. 2006). More recently, most publications focused on the PCβ2/IP3 pathway, while only a few older studies support the cAMP/PKA pathway in frog, hamster, mouse and bovine cells (Avenet et al. 1988; Tonosaki and Funakoshi 1988; Béhé et al. 1990; Cummings et al. 1996). In summary, the issue of specific pathways for natural sugars and artificial sweeteners is still open, in particular, since following up studies and human data are still missing.

1.6 Caloric sugars may signal in a manner independent of the sweet taste receptor

Besides the canonical T1R2/T1R3-mediated pathway, there is evidence for the existence of an alternative sweet pathway independent of the sweet taste receptor. Although no nerve or behavioral responses to sweet compounds were observed in T1R2/T1R3-double-knockout mice, both, T1R3- and T1R2-single-knockout mice showed diminished responses to concentrated sugars, but not to artificial sweeteners, suggesting the involvement of low affinity T1R3-homomeric receptors (Zhao et al. 2003). Another T1R3-knockout mice strain showed preserved to only moderately diminished chorda tympani nerve responses to Sucrose and Maltose but abolished responses to artificial sweeteners and amino acids (Damak et al. 2003). Further, using threshold and discrimination tests, T1R3-knockout mice could still differentiate between Sucrose and the prototypical umami substance Monosodium Glutamate (Delay et al. 2006). Moreover, PLCβ2- (Zhang et al. 2003; Dotson et al. 2005), gustducin- (Danilova et al. 2006) or TRMP5-knockout mice (Damak et al. 2006) were still able to respond to monosaccharides, opening the question of the existence of an alternative sweet taste pathway that is independent of the canonical T1R2/T1R3 sweet taste receptor.

1.6.1 Type II cells may utilize Glucose transporter as sugar sensors alternative to T1R2/T1R3

Interestingly, some Glucose-sensing cells outside the oral cavity, such as pancreatic β-cells or enteroendocrine L-cells, also express sweet taste receptors and its downstream signaling molecules (Chapter 1.11, Cummings and Overduin 2007). In addition, intestinal cells are equipped with Glucose transporters (GLUTs) and sodium-driven Glucose symporters (SGLTs). The GLUT family contains 13 members with tissue specific expression and functional diversity (Table 2). They allow the transport not only of Glucose, but also of other monosaccharides, such as Galactose, Mannose, Fructose, Xylose and Glucosamine (Table 2, Scheepers et al. 2004). Glucose absorption has been long reported on the human tongue (Kurihara and Koyama 1972; Oyama et al. 1999) and indeed, GLUT8-10 and GLUT13 expression were described in primate fungiform papillae and circumvallate papillae (Hevezi et al. 2009). GLUT2, 4, 5 and SGLT1 were specifically expressed in T1R3-positive cells of mouse circumvallate and foliate papillae (Merigo et al. 2011; Yee et al. 2011), whereas GLUT1 co-localized with gustducin and IP3-R in mouse circumvallate papillae (Toyono et al. 2011). Thus, gastro-intestinal cells, β-cells and taste cells share principal components necessary for sweet sensation independent of the canonical sweet taste receptor (Figure 3).

Table 2: Overview of GLUT characteristics and their expression in taste tissue.

Channel	Properties	Expression	Source
GLUT2 *(SLC2A2)*	• Tissue expression: liver, intestine, kidney, β-cells, neurons, astrocytes, tanycytes • Substrates: Glucose, Mannose, Galactose, Fructose, Glucosamine • Source: Thorens 2015	mouse taste cells of circumvallate, foliate and fungiform papillae rat circumvallate papillae	Yee et al. 2011 Merigo et al. 2011
GLUT4 *(SLC2A4)*	• Tissue expression: adipose tissue, skeletal muscle, cardiac muscle • Substrates: Glucose, Dehydroacetic Acid • Source:Vargas et al. 2020; Huang and Czech 2007	mouse taste cells of circumvallate, foliate and fungiform papillae	Yee et al. 2011
GLUT5 *(SLC2A5)*	• Tissue expression: intestine and testis, kidney, skeletal muscle, fat tissue, brain • Substrates: Fructose • Source:Douard and Ferraris 2008	rat circumvallate papillae	Merigo et al. 2011
GLUT8 *(SLC2A8)*	• Tissue expression: testis, brain, spleen, liver, skeletal muscle, heart, adipose tissue • Substrates: Glucose, Fructose, Galactose • Source: Schmidt et al. 2009	mouse taste cells of circumvallate, foliate and fungiform papillae macaque taste bud gene expression	Yee et al. 2011 Hevezi et al. 2009
GLUT9 *(SLC2A9)*	• Tissue expression: kidney, liver, placenta, lung, brain, leukocytes, skeletal muscle, heart, testis, articular cartilage • Substrates: Glucose, Fructose, Urate • Source: Doblado and Moley 2009	mouse taste cells of circumvallate, foliate and fungiform papillae	Yee et al. 2011
GLUT10 *(SLC2A10)*	• Tissue expression: heart, lung, brain, liver, skeletal muscle, pancreas, placenta, kidney • Substrates: Glucose, Galactose • Source: Dawson et al. 2001	macaque taste bud gene expression macaque taste bud gene expression	Hevezi et al. 2009 Hevezi et al. 2009
GLUT13 *(SLC2A13)*	• Tissue expression: small intestine, skeletal muscle • Substrates: Glucose activated Na^+ channel, IP3 • Source: Zhao and Keating 2007	macaque taste bud gene expression	Hevezi et al. 2009
SGLT1 *(SLC5A1)*	• Tissue expression: intestine, kidney, parotid, submandibular salivary glands, heart • Substrates: Glucose, Galactose • Source: Sabino-Silva et al. 2010; Wright et al. 2011	mouse taste cells of circumvallate, foliate and fungiform papillae rat circumvallate papillae	Yee et al. 2011 Merigo et al. 2011

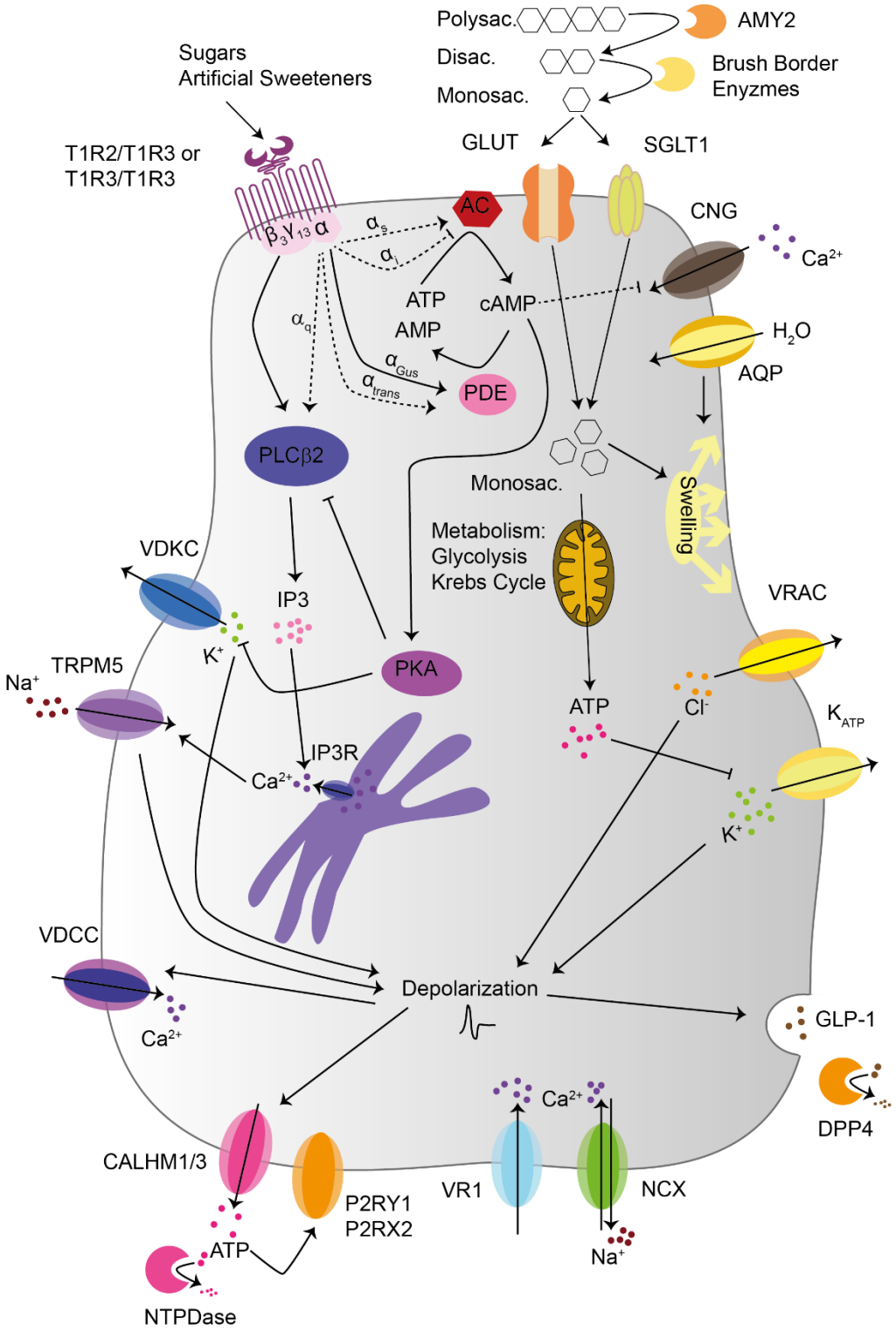

Figure 3: Pathways of sweet taste. Sweet taste can be transduced via the canonical sweet pathway employing the sweet taste receptor (left side), but also via an additional alternative pathway that utilizes GLUTs and/or SGLT1 (right side). The canonical pathway is mediated through heteromeric or homomeric sweet taste receptors that signal to a diversity of G-proteins. Activating diverse subunits, different pathways can be stimulated to release ATP: cAMP/PKA or PLCβ2/IP3. The alternative pathway allows monosaccharide entry via GLUTs and/or SGLT1, which leads to a metabolic rise in ATP levels and cell swelling. Taste cells are depolarized either by the inhibition of K^+ outward currents (K_{ATP}) and/or activation of Cl^- outward currents (VRAC). This results in Ca^{2+} entry via VDCC, vanilloid receptor 1 (VR1) or Na^+/Ca^{2+} exchanger (NCX) to finally release GLP-1 as neuromodulator. Abbreviations: CNG: cyclic-nucleotide-suppressible channel; VDKC: voltage-dependent K^+ channel; DDP4: Dipeptidyl-peptidase 4. Dashed arrows indicate presumed functions.

1.6.2 Possible pathways downstream GLUTs that may mediate cell depolarization

To mediate Glucose-induced depolarization of β- and gastro-intestinal cells, three potential pathways have been described. First, SGLT1 can promote cellular depolarization by the exchange of two Na^+ with Glucose and, hence, activate voltage-dependent calcium channels (VDCCs) to trigger hormone release (Gribble et al. 2003; Kuhre et al. 2015). Second, the entry of Glucose into β-cells via GLUT2 can increase ATP levels through enhanced oxidative metabolism (Ashcroft et al. 1984). This inhibits K_{ATP} channels, leading to cellular depolarization and release of Insulin (Best et al. 2010). Third, an indirect activation of outward Cl^- currents can be mediated by the uptake and intracellular accumulation of Glucose and its metabolites, which results in osmotic water entry and cell swelling via the aquaporins AQP7 and AQP8 (Matsumura et al. 2007; Best et al. 2010; Louchami et al. 2012). In the scope of regulatory volume decrease, Cl^- is then released via volume regulated anion channels (VRACs), which depolarizes cells and activates VDCCs, to finally mediate Insulin exocytosis (Best et al. 2010).

In contrast to GLUTs, SGLT1 was functionally investigated in taste cells and can be activated by non-metabolizable Glucose analogues (Yasumatsu et al. 2020). Accordingly, in wild type and T1R3-knockout mice NaCl selectively increased sweet responses to Glucose and Sucrose, but not to artificial sweeteners (Yasumatsu et al. 2020). This response was blocked with the SGLT1 antagonist Phlorizin. Investigation of afferent sweet responsive fibers revealed three different response patterns: i) fibers with a maximum response to caloric sugars were sensitive to NaCl and Phlorizin, ii) fibers with a maximum response to artificial sweeteners were unaffected by NaCl and Phlorizin, and iii) fibers stimulated with sugars and artificial sweeteners responded to NaCl and Phlorizin suggesting that there are i) SGLT-expressing cells, ii) sweet taste receptor-expressing cells, and iii) SGLT1- and sweet taste receptor-co-expressing cells (Yasumatsu et al. 2020). Whether SGLT1 downstream signaling converges with the canonical signaling pathway has not been investigated. Functional K_{ATP} channels downstream of GLUTs are present in mouse taste cells (Yee et al. 2011), and electrophysiological studies revealed that ~20% of the total outward current of mouse fungiform taste cells is attributed to K_{ATP} channels (Yee et al. 2011). Expression of VRAC has not been investigated in taste cells yet, and the expression of VDCC in type II taste cells is still controversial; while most studies suggest that type II taste cells are devoid of VDCCs (Clapp et al. 2006; DeFazio et al. 2006), a subpopulation of type II cells was shown to respond to KCl depolarization and to bitter stimulation (Medler et al. 2003; Hacker et al. 2008). In summary, while taste cells show principal components for a sweet taste sensation pathway independent of the canonical sweet taste receptor (Figure 3), it remains elusive, if these cells can properly respond to enhanced Glucose levels by metabolically induced cell depolarization and Ca^{2+} signaling. Moreover, it should be stressed that this alternative pathway has only been investigated in rodents so far.

1.6.3 Taste cell-expressed Brush Border enzymes may hydrolyze disaccharides

In the context of metabolism-induced sugar sensing, it is of note that GLUTs and SGLT1 can shuttle only monosaccharides. Thus, to permit sugar-mediated cell depolarization, starch has to be first decomposed to oligo- and disaccharides. This occurs by Amylases of the saliva and pancreas. Further, “Brush Border” enzymes, such as Maltase-glucoamylase (MGAM), Sucrase-isomaltase (SIS), Lactase (LCT) and Trehalase (TREH), on the apical membrane of enterocytes generate monosaccharides, which can then be absorbed by GLUTs and SGLT1 (Robayo-Torres et al. 2006; Sukumaran et al. 2016). Interestingly, Brush Border enzymes, such as α-Glucosidases, MGAM and SIS, are also present on mouse taste type II and III cells (Merigo et al. 2009; Sukumaran et al. 2016), and addition of antagonists of these enzymes diminished taste nerve responses selectively to disaccharides (Sukumaran et al. 2016). Furthermore, T1R3-knockout mice responded to monosaccharides and to disaccharides (Damak et al. 2003). In summary, these data are compatible with a metabolic activation of taste cells via GLUT- and/or SGLT1-mediated uptake of di- and monosaccharides (Figure 3).

1.7 The sweet taste receptor-independent pathway may mediate cephalic phase Insulin release

Oral food intake induces a biphasic Insulin response. The first wave of Insulin is released prior food absorption and the subsequent rise in blood Glucose (Just et al. 2008). This initial Insulin release, referred to as cephalic phase Insulin release (CPIR), prepares the body for ingestion, digestion and nutrient storage (Smeets et al. 2010). It starts 2 min after oral food intake and peaks after 4 min (Powley 2000; Zafra et al. 2006). CPIR is then followed by a second, delayed and prolonged Insulin response (Fischer et al. 1972; Hommel and Fischer 1977). CPIR occurs selectively upon oral exposure to sweet substances, but not to other taste modalities (Just et al. 2008; Dušková et al. 2013). In human, most authors agree that nutritive sugars induce CPIR (Tonosaki et al. 2007; Just et al. 2008; Shinozaki et al. 2008; Dušková et al. 2013; Dhillon et al. 2017), while few studies could not record CPIR upon Sucrose and Glucose exposure (Teff et al. 1995; Abdallah et al. 1997). If artificial sweeteners elicit CPIR has remained elusive (Abdallah et al. 1997; Dušková et al. 2013; Dhillon et al. 2017; Glendinning et al. 2017; Han et al. 2019), and currently no conclusion can be made due to species differences, ambiguous and vague description of experimental parameters, such as pre-stimulation conditions, concentration and duration of the application (for detailed discussion see von Molitor et al. 2020c). As T1R3-knockout mice showed normal CPIR and Glucose tolerance (Simon et al. 2014; Glendinning et al. 2015), while loss/inhibition or activation of K_{ATP} channels diminished or enhanced CPIR respectively (Glendinning et al. 2017), it was proposed, that CPIR may be triggered via the sweet taste receptor-independent pathway. However, these experiments were conducted in global knockout mice (Seino et al. 2000; Seghers et al. 2000; Seino et al.

2016), leaving the possibility of developmental compensation mechanisms. As deletion of P2RX and CALHM1 did not impair CPIR (Glendinning et al. 2017), the sweet taste receptor-independent pathway may not use purinergic transmission. Instead, the hormone Glucagon-like Peptide-1 (GLP-1) has been proposed to be critical for CPIR (Kokrashvili et al. 2014).

1.8 GLP-1 released from taste cells may exert an endocrine action on target tissues

Interestingly, taste cells synthetize not only GLP-1 but also several other hormones typically present in enteroendocrine cells, such as Glucagon, Somatostatin and Ghrelin (Kokrashvili et al. 2014). However, so far only GLP-1 has been shown to play a role in the sweet-sensitive pathway. GLP-1 is mainly synthetized and released from intestinal enteroendocrine L-cells of the gut epithelium after cleavage of Pro-glucagon by Pro-hormone Convertase 1/3 (Habib et al. 2013). Upon oral ingestion of carbohydrates and fat-rich food, GLP-1 is released into the blood stream (Theodorakis et al. 2006) to control fasting plasma Glucagon, potentiate pancreatic Insulin release, influence motoric mechanisms of gastric-emptying and to inhibit short-term food intake (Davis and Sandoval 2020). Although also sweet taste receptor-dependent GLP-1 release has been documented in L-cells (Seino et al. 2016), GLP-1 release occurs most likely in a T1R3-independent mechanism. Accordingly, it was not affected by the murine sweet taste receptor inhibitor Gurmarin nor TRPM5 inhibitors (Saltiel et al. 2017), while antagonists and knockout mice of SGLT1 (Gribble et al. 2003; Glendinning et al. 2017) as well as K_{ATP} channels showed major impacts (Reimann et al. 2008; Seino et al. 2016). Once in the blood stream, GLP-1 might exert an endocrine action on target tissues, such as the pancreas and the brain (Figure 4), by interacting with its cognate receptor GLP-1-R (Holst 2007). However, also paracrine effects might be relevant in the case of GLP-1 function on pancreatic β-cells, since GLP-1 is here locally released from pancreatic α-cells (Chambers et al. 2017). In the taste bud, GLP-1 expression was documented in rodent type II and type III cells of circumvallate papillae (Shin et al. 2008; Kokrashvili et al. 2014), and GLP-1 release from these cells occurs exclusively upon oral sweet stimulation (Martin et al. 2012; Kokrashvili et al. 2014; Takai et al. 2015). Further, GLP-1-R was detected in intragemmal nerve fibers (Shin et al. 2008; Takai et al. 2015), and GLP-1-R-knockout resulted in reduced behavioral attraction and diminished chorda tympani and glossopharyngeal nerve responses to sweet compounds (Shin et al. 2008; Martin et al. 2012; Takai et al. 2015), proposing local GLP-1 signal transmission from taste cells to the nerve (Takai et al. 2015). Additionally, GLP-1 secreted from taste cells, has been shown to contribute to systemic circulating GLP-1 that rises during the cephalic phase, even in the absence of T1R3 (Kokrashvili et al. 2014), and it may stimulate pancreatic β-cells (Campos et al. 1994), neurons of the brain (Göke et al. 1995) and vagal efferents (Nakabayashi et al. 1996). After intraperitoneal and intravenous Glucose stimulation, but not upon oral Glucose intake, GLP-1-R conditional knockout in β-cells showed impaired Glucose

tolerance in mice (Smith et al. 2014). Accordingly, stimulation of non-pancreatic GLP-1-R by GLP-1, released upon oral Glucose application, is essential to control Glucose tolerance by linking brain, gut and taste systems (Figure 4). Regarding a potential effect of artificial sweeteners on GLP-1 release, the evidence is unclear and needs further investigation (for discussion see von Molitor et al. 2020c). It is also unknown, if the canonical and alternative sweet pathways co-exist in the same cell or whether they are separated in different cell subpopulations (von Molitor et al. 2020c). Since GLUTs, SGLT1, K_{ATP}, T1R3 and GLP-1 were found to be expressed in the same cell (Takai et al. 2015) and since both, ATP- and GLP-1-mediated pathways are involved in sweet sensation, these pathways may interact synergistically.

1.9 The sweet taste receptor-independent pathway may be differently decoded in the central nervous system than the canonical pathway

To sense flavor, induce palatability (hedonic value) and recognize the energy content (metabolic value), the gustatory system uses parallel processing (Spector and Travers 2005). Upon oral stimulation of taste cells, gustatory information converges at higher levels, where it is combined with other sensory modalities (Spector and Travers 2005). In the nucleus of the solitary tract (NTS) not only gustatory fibers are integrated (Corson and Erisir 2013), but also gut afferents and somatosensory fibers from the face, mouth and tongue converge there (Bradley 2006).

The NTS is modulated by the amygdala, gustatory cortex and hypothalamus (Figure 4, Smith and Lemon 2007) and is a crucial node where gustatory information are channeled: it controls upper gustatory centers and induces physiological reflexes, such as salivation, mastication and CPIR (Spector and Travers 2005; Roper 2009). Inputs from gustatory nerves, processed in the NTS, result in different outputs: gustatory information and hedonic values are decoded via the thalamic-cortical pathway, while the CPIR response may utilize reflex circuitries between the NTS and the dorsal nucleus of the vagus nerve (DMNX) (Roper 2009). Indeed, a short reflex loop exists between gustatory fibers and vagal efferents (Powley 2000) via direct or indirect NTS-mediated inputs in the DMNX (Corson and Erisir 2013). In this perspective, the canonical and alternative sweet transduction pathway might be differentially represented and channeled in the NTS. Accordingly, inputs from the alternative pathway may stimulate NTS/DMNX reflex circuitries to induce CPIR (Tonosaki et al. 2007; Zaidi et al. 2008). This idea is further supported as chorda tympani dissection abolished sweet taste-mediated CPIR in rats (Tonosaki et al. 2007), and chorda tympani fibers project to diverse areas of the NTS including the central subdivision, which sends axons not only to the parabrachial nucleus but also to lateral/ventral subdivisions and the reticular formation that mediates reflex functions (Zaidi et al. 2008). Further, although T1R3-knockout mice showed greatly diminished neuronal activity

in the NTS upon lingual sugar application, residual responses, mainly to monosaccharides, could still be observed (Lemon and Margolskee 2009). To verify if this if this residual response is linked to the alternative circuit, tracing experiments in sweet taste receptor deficient mice are required (Matsumoto et al. 2009).

There is also functional and anatomical evidence for preferential representation of the alternative pathway on the posterior tongue since i) sweet taste receptor deletion affects glossopharyngeal nerves to a smaller degree (von Molitor et al. 2020c), and ii) gustducin/T1R3 co-expression is reduced in circumvallate papillae (Hoon et al. 1999; Max et al. 2001; Montmayeur et al. 2001), but iii) GLP-1/TRPM5 co-expression is increased (Shin et al. 2008; Kokrashvili et al. 2014), suggesting that circumvallate papillae input via the glossopharyngeal nerve might convey the sugar energy content to induce pre-digestive reflexes.

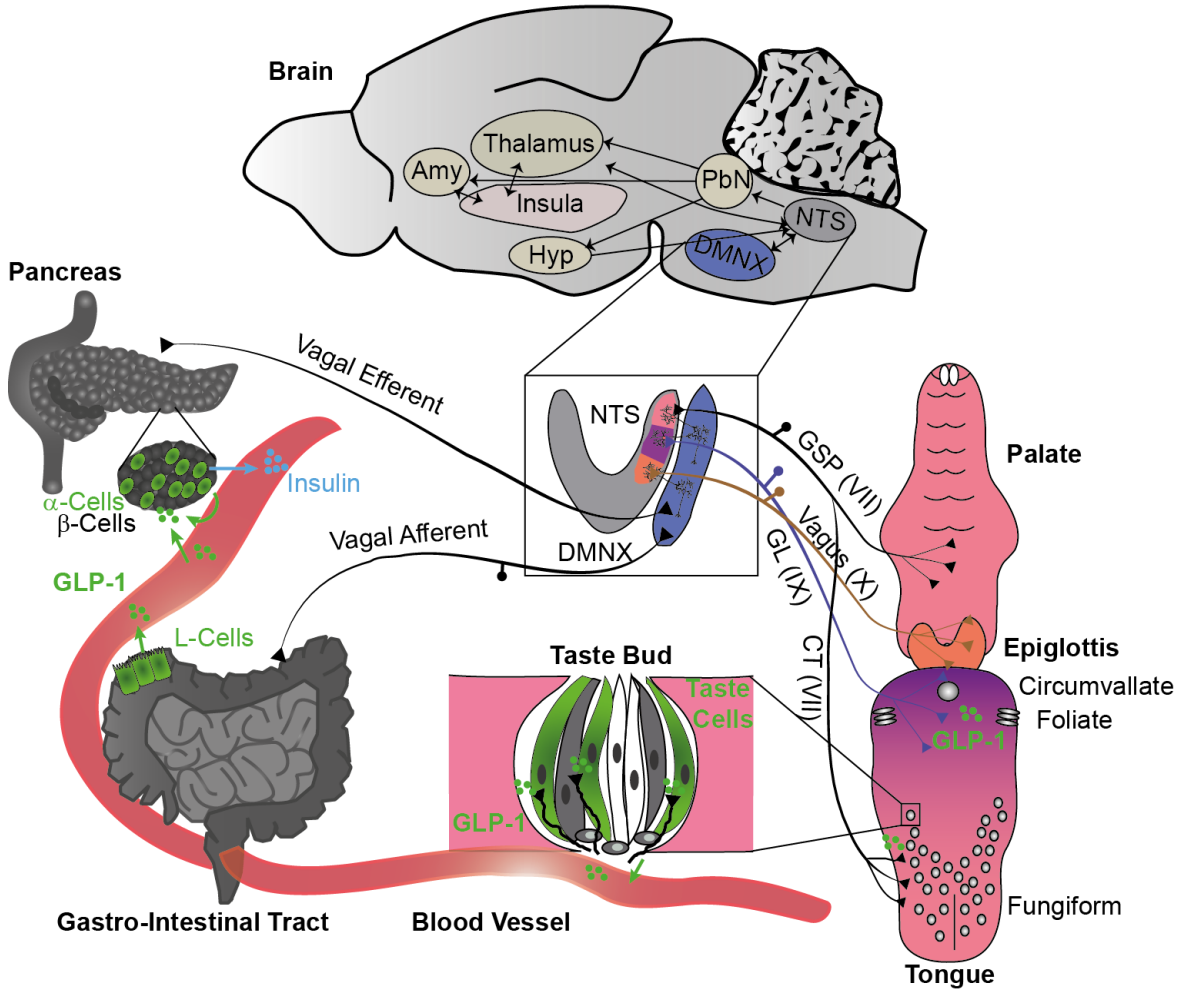

Figure 4: The alternative sweet pathway activates NTS/DMNX-reflexes. Sweet compounds may induce taste cells to secrete GLP-1, which stimulates sensory fibers, thereby, activating specific circuitries in the NTS/DMNX complex to mediate pancreatic pre-ingestive Insulin release (CPIR). To exert systemic effects, GLP-1 may also be released into the blood stream. Besides this metabolic response, the alternative pathway may be involved in sending gustatory information to upper brain centers. Schematic representation in the mouse. Abbreviations: Hyp: hypothalamus, Amy: amygdala, PbN: parabrachial nucleus, GL: glossopharyngeal nerve, CT: chorda tympani nerve, GSP: great superficial petrosal. Figure adapted from von Molitor et al. 2020c.

1.10 The sweet taste receptor-independent pathway may prepare the body for digestion

Food consumption induces a specific taste quality, a hedonic and metabolic value (von Molitor et al. 2020c). Since Sucrose responses were not impaired in a “two-response operant procedure” of T1R3-knockout mice, in which mice were reinforced with water for correct and punished with a mild shock for incorrect responses, the alternative pathway might contribute to distinguish taste modalities (Delay et al. 2006). Further, as T1R3-knockout mice exhibited CPIR but were not attracted to Glucose and Sucrose, it was proposed that the sweet taste receptor-independent pathway does not mediate a significant taste sensation but rather a metabolic response (Glendinning et al. 2015). Accordingly, the hedonic value would require T1R2/T1R3 (Glendinning et al. 2015), while the metabolic value would be mediated via GLUTs and K_{ATP} channels (Glendinning et al. 2017). However, activation of T2R, expressed in sweet-sensitive cells, elicited attraction (Zhao et al. 2003), wherefore it cannot be excluded that signaling molecules of the alternative pathway, which are co-expressed with T1R3 (Takai et al. 2015), contribute in sending sensory information to the central nervous system. Consequently, GLP-1-R-knockout mice showed diminished sensitivity and behavioral responses to sweet compounds (Shin et al. 2008; Takai et al. 2015), proposing GLP-1 contribution in decoding the hedonic value of sweet stimuli. Since K_{ATP}-knockout mice showed unaltered sugar attraction (Glendinning et al. 2017), the functional link between K_{ATP} channels and GLP-1 secretion in taste cells is, however, still speculative. Additionally, sweet attraction may be mediated by postingestive mechanisms, specifically decoded in the dorsal insula (Oliveira-Maia et al. 2012) and dorsal striatum (Tellez et al. 2016). Such attraction might refer to the function of Glucose as an energy fuel and/or on communication between gastro-intestinal tract and NTS via vagal efferents.

Summarizing the anatomical and functional information of diverse mouse models, the canonical pathway, thus, appears to be predominantly important for the hedonic value, while the alternative pathway may serve to report the energy content of food and to prepare the body for digestion (for further discussion see von Molitor et al. 2020c). Therefore, a complex network of interactions at many levels between taste cells, gastro-intestinal tract, pancreas, vagus nerve and brain is used. Additionally, the alternative pathway may be important for ingestion and digestion of food and energy homeostasis. In particular, it might contribute to several functions, including:

- modulation of gustatory nerve fiber activity patterns in response to sweet stimuli (Travers and Norgren 1995)
- activation of NTS/DMNX reflexes responsible for CPIR (Powley 2000; Roper 2009)
- endocrine activation of GLP-1-R in other organs (Kokrashvili et al. 2014; Takai et al. 2015)

- regulation of sweet taste receptor expression (Young et al. 2013; Laffitte et al. 2014)
- affecting sensory processing in higher brain centers (Smith and Lemon 2007)
- inducing taste cell renewal and regeneration in a food-dependent manner in accordance to its trophic action (Koehler et al. 2015)
- controlling caloric sugar intake, as T1R2- and T1R3-knockout mice have surprisingly normal body weight, chow and water intake (Treesukosol et al. 2011)

Table 3 summarizes the main findings of the alternative pathway, its signaling molecules and their functions. As most experiments are based on analogies to cells in other organs, such as gastro-intestinal tract and pancreas, many hypotheses remain rather vague.

Table 3: Overview of signaling molecules involved in the alternative pathway. Brief-access test are palatability preference tests, in which taste solutions are presented for a short duration to animals after water deprivation, and the number of licks is counted. Discrimination tests detect gustatory orosensation, in which animals are trained to distinguish taste qualities by reinforcement for correct and punishment for wrong responses. Symbols mean: ✓= necessary, X= not necessary, - = not tested. Abbreviations: CT: chorda tympani nerve, GL: glossopharyngeal nerve. Table adapted and modified from von Molitor et al. 2020c.

Signaling molecule	Brief-access	Discrimination	CPIR	GLP-1 release	CT response	GL response	Source
T1R3	✓	✓	X	X	✓	✓	Zhao et al. 2003; Damak et al. 2003; Delay et al. 2006; Treesukosol and Spector 2012; Geraedts et al. 2012; Kokrashvili et al. 2014; Glendinning et al. 2015
TRPM5	✓	✓	-	-	✓	✓	Zhao et al. 2003; Talavera et al. 2005; Damak et al. 2006; Eddy et al. 2012; Ren et al. 2014
Gustducin	X	-	-	-	✓	✓	Wong et al. 1996; He et al. 2002; Ruiz et al. 2003; Danilova et al. 2006; Sclafani et al. 2007
PLCβ2	✓	-	-	-	✓	✓	Zhang et al. 2003; Dotson et al. 2005
SGLT1	✓	✓	X	-	✓	✓	Glendinning et al. 2017; Yasumatsu et al. 2020
K_{ATP}	X	-	✓	-	-	-	Glendinning et al. 2017
CALHM	-	-	X	-	-	-	Glendinning et al. 2017
GLP-1-R	✓	-	-	-	✓	✓	Shin et al. 2008; Martin et al. 2010; Takai et al. 2015
P2XR2/ P2XR3	✓	-	X	-	✓	✓	Finger et al. 2005; Hallock et al. 2009; Glendinning et al. 2017

1.11 Sweet taste signaling is not restricted to the oral cavity

Sweet taste receptors are expressed in multiple extraoral tissues including respiratory tract (Lee and Cohen 2014), liver (Taniguchi 2004), testis (Gong et al. 2016), heart (Wauson et al. 2012) and bladder (Elliott et al. 2011) among others (Laffitte et al. 2014). Most of these tissues express not only sweet taste receptors and canonical downstream molecules but also GLUTs and K_{ATP} channels (Table 4). Similar to taste cells, many cells in these organs, such as enteroendocrine cells, are polarized with apical microvilli and they are capable of releasing neuromodulators (Young 2011). Due to the lack of a human taste cell line, cell lines derived

from these organs natively expressing taste receptors and downstream signaling molecules have been employed to screen for new taste receptor agonists/antagonists (Riedel et al. 2017). In pancreatic β-cells, the stomach and esophagus, T1R3-homomeric receptors instead of classical T1R2/T1R3-heterodimers were found. These were proposed to increase ATP production by promoting mitochondrial metabolism (Nakagawa et al. 2014).

Additional to taste sensation, taste receptors have been reported to play a role in the innate immune response. Accordingly, during infections of the human upper airway, gram negative bacteria secrete bitter noxious substances, which are agonists of the bitter receptor T2R38 (Lee et al. 2012). Chemosensory cells, which are discrete non-ciliated cells of the nasal respiratory epithelium (Yamamoto and Ishimaru 2013; Maina et al. 2018), were shown to express bitter T2R and T1Rs in human (Lee and Cohen 2014), gustducin in rats (Finger et al. 2003) and TRPM5 in mice (Lin et al. 2008). Thus, upon T2R38 stimulation PLCβ2 may mediate an increase in intracellular Ca^{2+}, which spreads to adjacent ciliated cells via gap junctions to induce the release of anti-microbial peptides, killing pathogenic microbes (Finger et al. 2003; Lee and Cohen 2014). Stimulation of the sweet taste receptor within the same cell inhibits this defense pathway (Lee and Cohen 2014, 2015). Thus, when the concentration of Glucose in airway mucus decreases due to bacterial proliferation, the tonic activity of T1R2/T1R3 is interrupted and increases the immune response of T2R (Maina et al. 2018).

This far-reaching expression of the sweet taste receptor indicates the importance of understanding the downstream signaling mechanisms and the subsequent actions in the body. Sweet compounds may induce potential health risks via their metabolic effects, such as stimulating the release of gut or pancreatic hormones, altering Glucose absorption and controlling brain processing (Laffitte et al. 2014). Further, the T1R3-homomeric structure in some tissues may offer new and unexpected binding options (Medina et al. 2014). In addition, for its complex involvement in body and Glucose homeostasis the sweet-sensitive pathway is becoming a new interesting drug target (Laffitte et al. 2014). For example, the speculation that GLP-1 secreted from taste cells may mediate CPIR and Glucose tolerance if food is consumed orally, while intestinal GLP-1 is relevant during gastro-intestinal food digestion (Chambers et al. 2017; Svendsen et al. 2018), may give hope that controlling GLP-1 signaling in the tongue might be favorable to glycaemia regulation or even the treatment of diabetes (von Molitor et al. 2020c). Further, in chronic rhinosinusitis, an airway infection, T1R2/T1R3 agonists may serve as a potential treatment in combination with T2R antagonists (Maina et al. 2018).

Table 4: Overview of sweet taste signaling molecules expressed in the gastro-intestinal tract.

Organ	T1R2	T1R3	T2R	Gustducin	PLCβ2	TRPM5	GLUT/ SGLT1	K_{ATP}	Species	Source
Esophagus		✓		low		low			human	Young et al. 2009
Stomach	✓	✓	✓	✓	✓	✓	✓	✓	mouse	Hass et al. 2007; Kaske et al. 2007; Bezençon et al. 2008; Hass et al. 2010; Widmayer et al. 2011; Janssen et al. 2011; Sakata et al. 2012
Intestine	✓	✓		✓	low	✓			human	Jang et al. 2007; Zhang et al. 2009; Bezençon et al. 2008
	✓	✓	✓	✓			✓		mouse	Dyer et al. 2005; Margolskee et al. 2007; Janssen et al. 2011
							✓	✓	rat	Kuhre et al. 2015
Colon		✓	✓	✓					human	Taniguchi 2004; Rozengurt 2006
	✓	✓		low	✓	✓	✓	✓	mouse	Bezençon et al. 2008; Reimann et al. 2008
							low		rat	Peng et al. 2015
Pancreas		✓				✓	✓	✓	human	Prawitt et al. 2003; Taniguchi 2004
	✓	✓		✓		✓	✓	✓	mouse	Prawitt et al. 2003; Colsoul et al. 2010; Nakagawa et al. 2014
							✓	✓	rat	Cook and Hales 1984; Inagaki et al. 1995; Vos et al. 1995

1.12 The lack of adequate test systems calls for the development of new taste models

To find a conclusion of the hypothesized functions and systemic roles of the alternative sweet signaling pathway, further studies are needed. One major question is, if the alternative pathway exists in humans and plays a similar role as it does in rodents (von Molitor et al. 2020c). So far, while the occurrence of CPIR in humans could be observed due to the easily accessible measure of blood Glucose and Insulin levels, the involvement of specific signaling components of the alternative sweet taste pathway, such as GLUTs/ SGLT1, K_{ATP} channels or VRAC, have not been studied due to a limited availability of biological samples (von Molitor et al. 2020c).

Human *in vivo* studies are still paramount to evaluate the ability to taste a certain stimulus and determine its quality (Reed and McDaniel 2006; Aleman et al. 2016). In intensity tests, participants hierarchically rank test solutions according to their sweetness in relation to a standard (Reed and McDaniel 2006). In quality tests, the taste modality is determined (Galindo-Cuspinera et al. 2006; Zhang et al. 2009), and detection threshold tests aim to analyze at what concentration taste can still be distinguish or recognized (Reed and McDaniel 2006; Zhang et al. 2009). Alternatively, sweet taste can be analyzed using hedonic assessment (Reed and

McDaniel 2006), where people are asked to rate how pleasant the compound is (Kampov-Polevoy et al. 1997), and if it is preferred over another one (Reed and McDaniel 2006; Liem and Mennella 2002). However, more sophisticated mechanistic studies on human sweet taste processing fail due to lacking human genetic models. Thus, only experiments with the sweet taste inhibitor Lactisol (Schweiger et al. 2020), the blue food dye Robert's Brilliant Blue FCF133 to label human tongue papillae (Shahbake et al. 2005; Zhang et al. 2009) and genome studies from human blood samples (Keskitalo et al. 2007) can be designed.

One of the very rare approaches to yield human taste data are *in vitro* taste studies that use human fungiform papillae, which can be donated since they regenerate (Ozdener et al. 2011; Ozdener et al. 2012). Therefore, ~6 taste papillae can be isolated with curved spring micro-scissors from the dorsal surface of the anterior tongue, enzymatically digested, minced and grown on Collagen-coated dishes. For long-term maintenance a media using Iscove's Modified Dulbecco's medium, containing 10% fetal bovine serum, a 1:5 ratio of MCDB 153, 10 ng/ml Insulin and a triple cocktail of antibiotics has been established on rat primary taste cells (Ozdener et al. 2006; Ozdener and Rawson 2013). Most of these isolated human taste cells resembled type II cells that were positive for PLCβ2 and gustducin and responded to bitter, sweet and umami tastants with intracellular Ca^{2+} transients. In addition, cells positive for the type III cell marker NCAM and the type I cell marker GLAST were detected at a lower abundance (Ozdener et al. 2011). However, the life span of isolated papillae or their dissociated cells is limited (Chaudhari and Roper 2010; Roper and Chaudhari 2017) and only few *in vitro* experiments can be conducted (Ozdener and Rawson 2013). Further, the heterogeneity of donors may lead to variable results since taste is dependent on age (Moore et al. 1982; Ng et al. 2004; Petty et al. 2020), genetic variances (Eriksson et al. 2019), sex (Than et al. 1994; Fushan et al. 2010) or diseases (Ng et al. 2004; Young et al. 2013). To overcome these problems, epithelial cells derived from human taste buds were immortalized, yielding a cell line called HTC-8, which is bitter-sensitive but does not possess all molecules of the canonical signal cascade (Chapter 1.14, Hochheimer et al. 2014). Thus, taste research still faces a basic struggle of a missing human-based test system, both *in vivo* and *in vitro*.

To find a remedy, recombinant HEK293-based expression systems have been used, in which human taste receptors and their associated downstream signaling molecules are expressed to screen novel taste compounds (Figure 5, for review see von Molitor et al. 2020b). These are advantageous for the screening of large compound libraries, but since they miss the native biological background, they are neither suitable for studying signaling cascades nor complex interactions of cells within taste buds (von Molitor et al. 2020b). Accordingly, these topics could only be addressed using dissociated primary taste cells (Kinnamon and Roper 1988; Kolesnikov and Margolskee 1995), taste buds (Cummings et al. 1996; Huang et al. 2008; Hevezi et al. 2009) and tongue slices (Caicedo et al. 2002; Dando and Roper 2012) from

diverse animals, such as apes (Hevezi et al. 2009), mouse (Baryshnikov et al. 2003; DeFazio et al. 2006), rat (Striem et al. 1989; Abaffy et al. 2003), frog (Avenet and Lindemann 1987; Fujiyama et al. 1994), pig (Naim et al. 1991) and cows (Kurihara and Koyama 1972). Acute isolation procedures, however, may influence cell behavior and they can be used only for a few hours (von Molitor et al. 2020b). Further, interspecies differences question the transferability of animal data to humans. E.g. frogs express 49 bitter T2R, while cows express only 18, dogs 15, chicken 3 (Go 2006) and domestic cats are deficient of the sweet taste receptor (Li et al. 2006). The sweet taste inhibitors Gurmarin (Imoto et al. 1991) and Lactisol (Winnig et al. 2005) are specific to mouse and human, respectively, indicating also structural interspecies differences of the receptors (Sigoillot et al. 2012). Further, taste bud shapes have been reported as oval, spindle-like or melon-like in in human, pigs and horses, respectively (Kikut-Ligaj and Trzcielińska-Lorych 2015). As an alternative, the isolation and immortalization of rodent or human tongue progenitor cells may be promising to gain functional taste cells. Indeed, progenitors from mouse taste buds differentiated into all taste cell types in organoids (Ren et al. 2014; Aihara et al. 2015; Ren et al. 2017; Ren et al. 2020). The knowledge of how to direct this differentiation is, though, still missing.

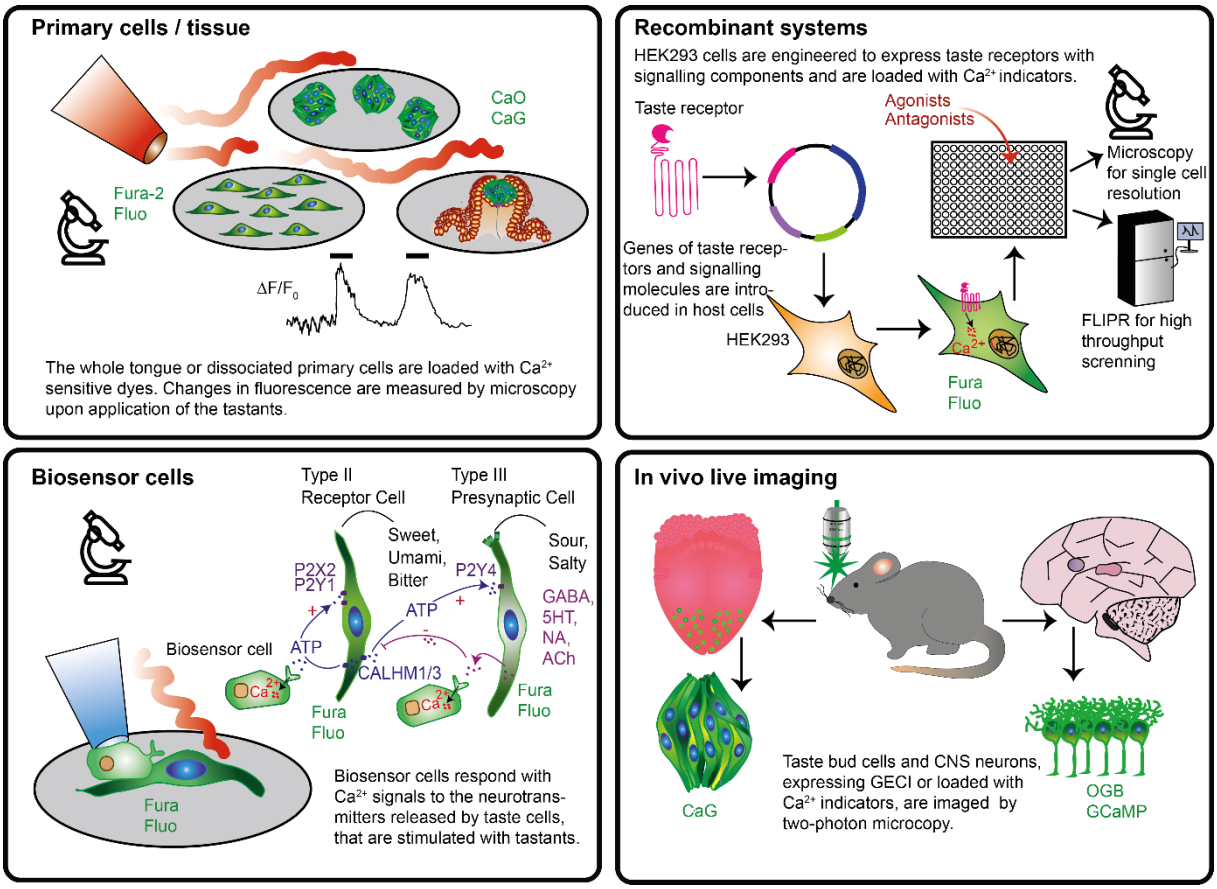

Figure 5: Schematic overview of the four major test systems used to investigate taste signaling. Frequently applied molecular optical biosensors use green fluorescence indicators and are depicted with green letters, curly red lines indicate local application of tastants. Abbreviations: CaG: Calcium Green, CaO: Calcium Orange. Figure adapted from von Molitor et al. 20202b.

1.13 Molecular sensors to study sweet taste signaling

At the cellular level, two major parameters have been measured to study taste: voltage and Ca^{2+} changes. Indeed, upon gustatory stimulation of taste cells, intercellular Ca^{2+} concentrations rise and the information is conveyed to neurons in the central nervous system. Accordingly, an alphabet of voltage and Ca^{2+} changes is used from the brain to the tongue to decipher modalities and sensitivities of tastants. Based on this knowledge, different types of biosensors for fundamental and applied research have been constructed (for additional information see von Molitor et al. 2020b).

The optical biosensors Fura and Fluo allow the recording of intracellular Ca^{2+} changes. They are ratiometric fluorescent dyes that shift their excitation spectra upon Ca^{2+} binding. Thus, the ratio of the emissions directly correlates to the amount of intracellular Ca^{2+} (Bootman et al. 2013). Mostly, Fura and Fluo have been applied to recombinant HEK293 cells expressing taste receptors (Figure 5). In combination with high-content fluorescent-imaging plate readers (FLIPR) this allowed the screening of large compound libraries and to accurately determine dose-response curves and kinetics of the receptor activation (Bufe et al. 2002; Kuhn et al. 2004; Galindo-Cuspinera et al. 2006). Additionally, single wavelength indicators, such as Calcium Green or Calcium Orange, have been used in taste research (Figure 5, Dando and Roper 2009). They do not shift their excitation or emission spectra upon changes in intracellular Ca^{2+} concentrations and, therefore, allow for more combinations with other fluorophores without spectral overlap and reduced imaging intervals in live cell imaging experiments (von Molitor et al. 2020b). To address intercellular communication within taste buds, biosensor cells expressing specific neurotransmitter/hormone receptors have been loaded with fluorescent Ca^{2+}-sensitive dyes and positioned adjacent to taste cells/tissue (Figure 5). However, problems with synthetic Ca^{2+} sensors may arise since they may not always enter the cells of interest and may compartmentalize e.g. in the endoplasmic reticulum (Whitaker 2010). In contrast, the usage of genetically encoded Ca^{2+} indicators (GECIs) allows cell type and subcellular targeting specificity, but they have barely been used in taste research as cell transduction requires some days, which does not fit into the short life span of isolated primary taste cells (von Molitor et al. 2020b). However, in mice, neurons expressing genetically encoded biosensors were employed to monitor brain activity patterns upon gustatory stimulation (Figure 5, Barretto et al. 2015).

In addition to Ca^{2+} changes, voltage alterations have been studied to investigate sweet and bitter gustatory mechanisms. Therefore, patch-clamp recordings are commonly used although they target only single cells. For a higher throughput voltage-sensitive dyes may be applied. However, voltage-sensitive dyes are not common in the field of taste research, and it is not known, how voltage changes are transduced in Ca^{2+} signals, neurotransmitter release and communication with the afferent fibers (von Molitor et al. 2020b).

1.14 Human fungiform papillae-derived taste cells resemble type II bitter-sensitive cells

With the aim to find an unlimited cell source that natively expresses sweet taste receptors and associated signaling molecules, Hochheimer et al. isolated cells from human fungiform papillae with a Collagenase cocktail and immortalized them to achieve a stable cell line that they called HTC-8 (Hochheimer et al. 2014). HTC-8 cells proliferated in monolayer culture with a cell division rate of 0.45 d^{-1}, which allowed long-term cultivation of over 25 passages without morphological changes (Figure 6A, Hochheimer et al. 2014). To investigate the differentiation status of HTC-8 cells, the expression of cytokeratins (KRT) was examined. Epithelial KRTs are intermediate filament proteins comprising a family of more than 20 different members, which are up- and downregulated in various stages of differentiation. Since taste cells are also of epithelial origin, KRTs have been used to determine their differentiation status (Asano-Miyoshi et al. 2008). Proliferating progenitors reside below the taste bud in the basal layer of the epithelium and have been reported to express KRT14 and KRT5 in rat (Asano-Miyoshi et al. 2008). In the process of differentiation, KRT14-positive cells then migrate towards the apical surface where they are incorporated into the taste bud and subsequently start to express KRT8 (Asano-Miyoshi et al. 2008), which heteropolymerizes with the other differentiation markers KRT18 or KRT19 (Zhang et al. 1995; Zhang and Oakley 1996). Gene analysis of HTC-8 cells by RT-PCR proved the expression of KRT8 and KRT19 in addition of the pluripotency gene OCT4 and the taste progenitor marker genes LGR5 and BMI1. These data and the fact that HTC-8 cells were isolated from a pool of only partly differentiated mitotic progenitor cells (Hochheimer et al. 2014) suggest that HTC-8 cells may express factors involved in stem cell maintenance.

HTC-8 cells express also genes associated with mature taste cells (Table 5) as further characterization by RT-PCR revealed expression of 13 out of ~25 known human T2R bitter receptors (Hochheimer et al. 2014). Additionally, an incomplete set of genes associated to sour and salty taste was found (Table 5). However, T1R receptors for sweet or umami taste were absent, suggesting that these cells rather resemble type II bitter-sensitive receptor cells (Hochheimer et al. 2014). Indeed, when HTC-8 cells were loaded with Fluo4, Ca^{2+} transients in response to bitter substances, such as Salicine and Saccharin, were observed, but not to sweet compounds. Intriguingly, the main components of the canonical bitter pathway, such as gustducin, PLCβ2 and TRPM5, have not been detected in HTC-8 cells. Instead, other family members of these missing molecules have been amplified in RT-PCR and may substitute their function (Table 5, Hochheimer et al. 2014). E.g, HTC-8 cells expressed TRPM4 instead of TRPM5 (Hochheimer et al. 2014), and it was speculated, that TRPM4, in the absence of TRPM5, may be involved in the transduction of taste stimuli (Talavera et al. 2008).

Table 5: HTC-8 cell gene expression analysis. HTC-8 cells were grown in monolayer culture and gene expression was analyzed by RT-PCR. Data are adapted from Hochheimer et al. 2014.

Category	Group	Genes expressed
intragemmal and perigemmal marker	cytokeratins	KRT8, 18
	plucripotency	OCT4, LGR5, BMI1, PTCH1
type I cell marker	NTPDase-1	ENTPD1
	ENaC	SCNN1B, SCNN1D
type II cell marker	bitter receptors	TAS2R4, 10, 14, 16, 19, 20, 30, 31, 38, 39, 43, 45, 50
	fatty acid receptor	GPR120
	Gα protein subunits	GNAT2 (transducin), GNA11 ($G\alpha_{11}$), GNA12 ($G\alpha_{12}$), GNA13 ($G\alpha_{13}$), GNAQ ($G\alpha_{q}$), GNAI1 ($G\alpha_{i}$), GNAS ($G\alpha_{s}$)
	Gβ subunits	GNB1, GNB3
	downstream signaling molecules of the canonical pathway	PLCβ3, PLCD4, IP3R3, TRPM4
	Phosphodiesterases	PDE1A
	Adenyl Cyclases	ADCY3, 4, 5, 6, 7, 9
	Protein Kinases	PRKACA, PRKACB, PRKAR1A, PRKAR1B, PRKAR2A, PRKAR2B,
	K^+ channels	KCNJ8,14
type III cell marker	SNAP25	SNAP25
neurotransmitter receptors	ATP-release channels	PANX1, CAHLM2
	ATP-sensitive channels	P2XR7, P2YR12
	Serotonin receptor	5HT2B
Ca^{2+} signaling	Ca^{2+} channels	ORAI1,3, STIM1, TRPV1, TRPA1
	VDCCs	CACNA1G (type T)

In addition to HTC-8 cells, diverse human progenitor cell lines (HTP) were isolated and generated in analogy to HTC-8 cells (Riedel et al. 2016). Quantitative mRNA expression analysis of HTP cells revealed increased levels of the progenitor markers KRT14, SOX9 and LGR6, which were not evident in HTC-8 cells (Figure 6B). Thus, HTP cells might rather have the potential to differentiate into all the different taste cell types upon treatment with an appropriate, but still unknown, differentiation cocktail. Addition of 5% extra FCS already led to morphological and functional changes: HTP cells became more spindle shaped, similar to HTC-8 cells, and Ca^{2+} immobilization was detected in response to the bitter substances Saccharin and Denatonium Benzoate (Figure 6A, C). However, again, no response to sweet stimuli was detected (Riedel et al. 2016).

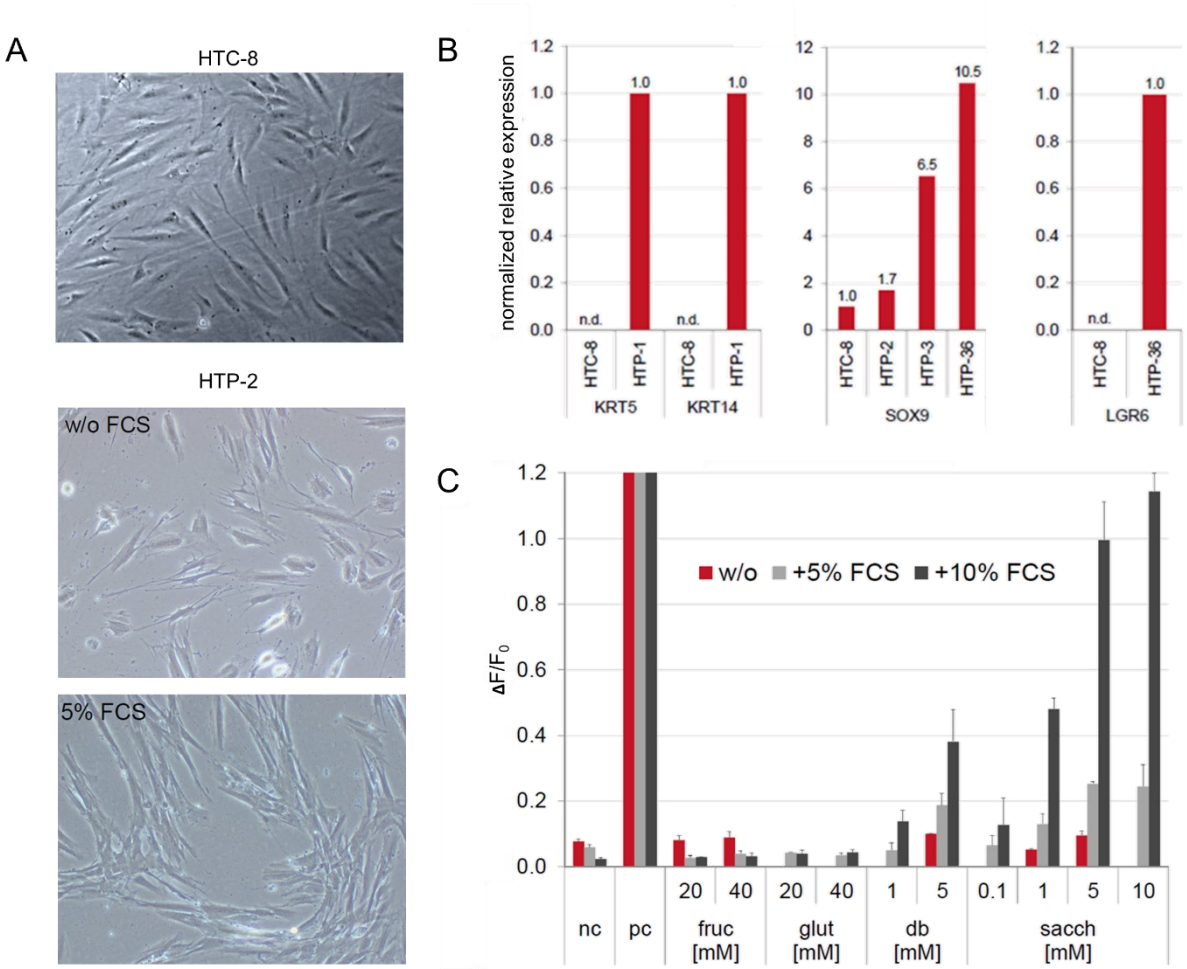

Figure 6: Isolated cells from human lingual epithelium respond to bitter stimuli. A) Brightfield images of HTC-8 and HTP-2 cells. Addition of 5% FCS into HTP culture media induced morphological changes. B) Quantitative mRNA expression analysis of progenitor markers. Gene expression analysis revealed expression of KRT5, KRT14, SOX9 and LGR6 in HTP-1, HTP-2 and HTP-36 cells, respectively, which were not detectable in HTC-8 cells. The amount of each cDNA was standardized to the housekeeping gene Topoisomerase 1 and expressed as $2^{-\Delta\Delta Ct}$ (y-axis). n.d. means not detected. C) Upon addition of 5% extra FCS, HTP-2 cells became bitter-sensitive. Ca^{2+} transients were recorded in response to Denatonium Benzoate (db) and Saccharin (sacch). No response was observed to Fructose (fruc) nor Glutamate (glut). Ionomycin was used as a positive control (pc), negative controls (nc) were in control buffer. To monitor cytoplasmic Ca^{2+} changes, cells were loaded with Fluo4, stimulated with test compounds and variations in fluorescence (excitation 488nm, emission 530nm) were recorded with a plate reader and normalized to the background fluorescence [$\Delta F/F_0 = (F - F_0)/F_0$]. Figure adapted from Riedel et al. 2016.

1.15 The potential of 3D cell cultures

So far, HTC-8 and HTP cells were cultured only as monolayer in 2D to allow easy plate reader recordings of Ca^{2+} changes. However, this may come with remarkable limitations, such as cell flattening, aberrant division rates and changes in phenotype (Baker and Chen 2012; Knight and Przyborski 2015), possibly leading to the inability to express T1Rs. Thus, it might be of interest to grow these cells in three-dimensional systems which might better resemble the architecture of a functional tissue (Breslin and O'Driscoll 2013). For example, complex tissues show a rich extracellular matrix which permits cell-cell as well as cell-matrix interactions (Figure 7) that support intracellular signaling, proliferation, polarization and differentiation of cells (Baker and Chen 2012; Knight and Przyborski 2015; Breslin and O'Driscoll 2013). Over

recent years, various three-dimensional cell culture models and technologies have been developed to obtain or preserve the natural morphology and structure of cells as it is in tissues (Knight and Przyborski 2015). However, models for taste cells mimicking the architecture of taste buds are still in the fledging stage.

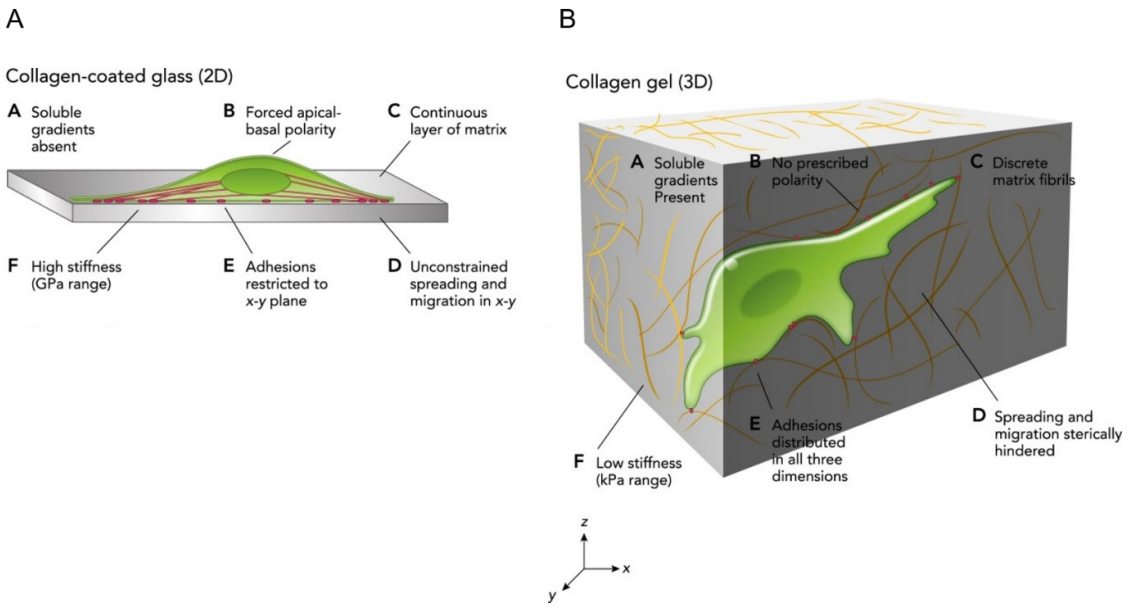

Figure 7: 3D conditions provide more physiological conditions than 2D monolayer cultures. Cells grown as monolayer on a flat surface cannot interact with surrounding cells and the extracellular matrix. Physiological cues are, thus, better resembled in 3D systems. Figure adapted from Duval et al. 2017.

3D culture models can be broadly categorized as scaffold-free or scaffold-based culture systems. Scaffold-free 3D cultures primarily refer to spheroids generated by cellular self-assembly into spherical structures, which are characteristically sized 100–500 µm, and produce their own extracellular matrix components (Klicks et al. 2017; Knight and Przyborski 2015). Low cost, ease of formation and high reproducibility are main advantages of spheroids, which make them suitable for screening processes (Klicks et al. 2017). Spheroids can be generated with different methods: i) by suspending cells in a droplet of medium, referred to hanging drop technique, ii) by modifying vessel surfaces to prevent cellular attachment, referred to forced-floating, or iii) by keeping the cell suspension in motion by stirring, referred to agitation method (Breslin and O'Driscoll 2013). Another, more complex type of spherical 3D cultures are organoids. They contain stem cells or induced pluripotent cells, are capable of self-renewal and by self-organization within the three-dimensional environment, they are able to mimic cellular structures and the function of the tissue they originate from (Gilazieva et al. 2020). So far, spheroids have not been generated with primary taste cells nor with recombinant taste-like cell lines. However, organoids based on mouse LGR5-positive progenitor cells are the major 3D model used in the field of taste research. These models have been shown to contain differentiated mature taste cells expressing diverse taste receptors (Ren et al. 2014; Aihara et al. 2015; Ren et al. 2017; Ren et al. 2020).

To guide or support the three-dimensional cell growth a variety of natural and synthetic scaffolds is available that aim to mimic the porosity, permeability and mechanical stability of the extracellular matrix (Ravi et al. 2015). Accordingly, the scaffold matrix provides a biologically active environment to promote proliferation, differentiation and secretion of signaling molecules (Breslin and O'Driscoll 2013; Ravi et al. 2015). Natural scaffolds, based on components of the extracellular matrix (Knight and Przyborski 2015; Ravi et al. 2015), are biocompatible, biodegradable and have ordinary cell adhesion sites (Knight and Przyborski 2015). Synthetic scaffolds contain a defined chemical composition for increased reproducibility and tunable properties. As they lack natural adhesion sides, cell attractive and repulsive areas can be generated (Knight and Przyborski 2015; Klicks et al. 2017). Coating with cell adhesion facilitating components, such as Collagen, Fibronectin, Poly-L-lysine or Poly-L-ornithine has resulted in limited success in enhancing taste cell attachment, viability and functionality, probably because single extracellular matrix components are insufficient functional (Ozdener et al. 2006; Lee et al. 2018). Accordingly, taste cells have not been cultured on these scaffold-based systems yet (Ozdener et al. 2006; Lee et al. 2018). However, taste cells isolated from tongue tissue have been successfully grown on a highly functional decellularized porcine tongue which was reconstituted into a Collagen hydrogel platform (Lee et al. 2018). Nonetheless, such a system is not suitable for the production of multiple similar biological replicates because the supply of scaffold material is rather limited, and already differentiated primary cells were used which precludes cell expansion and limits reproducibility.

For years, cells were loaded on scaffolds via the bottom-down method, where cells are homogenously applied to the scaffold without control of their distribution leading to potential failure to organize correctly and form an extracellular matrix. Newer approaches, therefore, use the bottom-up method, which aims to position cells and biomaterials brick by brick via micro- and nano-technologies (Mandrycky et al. 2016). By applying this bioprinting technique, a taste bud-like environment could be created by printing epithelia cells in a proper scaffold to support the generation of artificial taste buds. HTC-8 cells or even HTP progenitor cells that, upon differentiation may give rise to mature taste cells organized in a three-dimensional structure, could be printed in such an environment. Such an approach requires, however, quite large cell numbers, wherefore, it may be only feasible with a stably proliferating cell line.

To generate more complex systems resembling instead of cell-cell also tissue-tissue interactions, microfluidic devices and organ-on-a-chip approaches have been developed. In such chip devices, cell culture chambers are connected via micro-vessels to allow the culture of cell types from multiple organs. This permits the study of dynamic mechanical cues and chemical cell signaling networks among organs (Huh et al. 2011). Further, share stress, tension and compression, which are crucial for cell function, are resembled (Bhatia and Ingber 2014). Such systems might be particularly of interest to study the interplay between taste buds,

the brain and gastro-intestinal tract. The small volume of the culture chambers and micro-vessels might allow the exchange of signaling molecules, such as neurotransmitters and hormones, among pancreatic, intestinal, brain and taste cultures. However, main limitations of these systems are high costs and demanding skills due to the rather complex assembly and operation (Klicks et al. 2017).

1.16 3D cell culture in practice

With this variety of methods, multiple tissue specific 3D cultures have been established to study different biological questions. Depending on the purpose of the study, complexity is not always preferred. While microfluidic devices might help to mimic the interaction between different organs, more simple and cost effective models as spheroids might be favored for the screening of new compound libraries (van der Valk et al. 2010). Moreover, consistency across cell-based assays is limited by the use of animal-derived products, used for culturing and surface coting. To decrease inherent product variability, there is growing interest in animal-free products, such as Alginate, Chitin, foam or microcarriers, recombinant Collagen and plant decellularized scaffolds (Justice et al. 2009; Campuzano and Pelling 2019).

Furthermore, also technical readouts in 3D cell culture systems are challenging. In particular, as protocols can often not simply be adapted from 2D, a lack of standardized and robust protocols for the acquisition and analysis of 3D data from 3D cultures still suspend them from mainstream drug screening processes (Duval et al. 2017). However, new concepts thwart these limitations. For instance, the quality of immunofluorescence stainings has been improved with optical clearing protocols, that aim for reduced light scattering and opacity by matching the refractive index between the probe and the surrounding medium, to increase penetration depth (Smyrek and Stelzer 2017; Nürnberg et al. 2020). Classically, PFA-fixed 3D samples are embedded in paraffin or a freezing media and are sectioned with a cryostat or cryotome to gain 2D slices. However, generation of slices is time consuming and suffers from a loss of information (Nürnberg et al. 2020). Further, slides can only resemble a single section of the spheroid, which might not be representative for the whole structure due to a potential heterologous marker distribution. 3D reconstruction is cumbersome and losses of tissue sections encompass only partially analyzed samples (Nürnberg et al. 2020). Accordingly, optical clearing protocols are of major interest to enable fluorescence imaging deep into tissues. Alternatively to classical imaging with PBS or Mowiol, protocols using optical clearing reagents, such as ClearT2, CytoVista, ScaleS and Glycerol, have been used (Nürnberg et al. 2020). Depending on the cell type their performance differs and the most adequate protocol is, thus, cell line specific (Nürnberg et al. 2020).

Optical clearing, is not compatible with all assay formats, e.g. it hinders live specimen acquisition. Currently, confocal and light sheet microscopy (LSFM) are the most appropriate choices to visualize 3D cell cultures at high resolution. Particularly, LSFM meets many requirements for time lapse 3D imaging of live samples larger than 100 µm (Huisken et al. 2004). Further, it permits non-destructive optical sectioning of whole specimens as they are illuminated perpendicular to the detection pathway which generates a sheet of light (Baumgart and Kubitscheck 2012). High penetration in complex living tissues, an excellent dynamic range and extremely fast image recording due to the acquisition of millions of pixels simultaneously, thus, revolutionized 3D imaging (Pampaloni et al. 2015a).

To mimic salivary motion and monitor cellular responses to specific treatments under dynamic conditions, mostly isolated taste buds (Cummings et al. 1996; Huang et al. 2008) or dissociated cells (Kinnamon and Roper 1988; Kolesnikov and Margolskee 1995) attaching to the imaging chamber surface were stimulated with gustatory solutions by bath perfusion. However, monitoring the behavior of 3D cell samples in dynamic flow conditions that do not attach to the chamber surface, such as spheroids, has been problematic, since perfusion leads to their movement out of focus. Thus, gustatory compounds were often added by bulk application (Kuhn et al. 2004; Hochheimer et al. 2014; Behrens et al. 2017), which may cause abrupt changes in the microenvironment and cells may respond with artefacts. To overcome this obstacle, three-dimensional samples were dissembled prior analysis to gain adherent single cells growing as monolayer cultures (Ren et al. 2014), which stresses cells and may also influence their behavior. Thus, adequate perfusion systems for small non-adherent samples are still missing.

1.17 Aim of this study

Investigation of sweet taste signal transduction has started in the 70s and revealed the involvement of the cAMP/PKA pathway (Kurihara and Koyama 1972; Avenet and Lindemann 1987; Tonosaki and Funakoshi 1988). In the 90s, gustducin was discovered (McLaughlin et al. 1992; McLaughlin et al. 1993) and finally, in 2010, the sweet taste receptor (Kitagawa et al. 2001; Max et al. 2001; Bachmanov et al. 2001; Montmayeur et al. 2001; Nelson et al. 2001; Li et al. 2002). The following 10 years were characterized by intensive studies to reveal the canonical sweet, bitter and umami pathway, wherefore mainly bitter-mediated signaling was investigated. Thus, many assumptions true for bitter transduction were transferred to sweet taste signaling, even if there was only weak or contradictory evidence, leading to some confusion in the field. Nonetheless, it became common in literature that bitter, sweet and umami taste modalities are transduced via canonical PLCβ2/IP3 signaling and a simplified interpretation of taste coding in the taste bud was put forward: one signaling mechanism and one cell type (Gilbertson et al. 2000; Caicedo et al. 2002). This cast shadow on the cAMP/PKA

signaling in sugar-mediated responses. Further, it became soon clear that taste signaling was much more complex, given that knockout animals for T1R2/T1R3 (Zhao et al. 2003; Damak et al. 2003) and downstream signaling molecules (for details see von Molitor et al. 2020c) revealed residual responses to caloric sugars but not to artificial sweeteners (Damak et al. 2003). Accordingly, still many questions about sweet taste signalling do not have a clear answer and some findings propose the existence of alternative mechanisms. Thus, with a deep literature research this work first aimed to review and discuss i) the role of the canonical signaling pathway in sweet taste-mediated responses, ii) the existence of a parallel sweet taste receptor-independent pathway, its downstream signaling molecules and physiological role in preparing the body for digestion, and iii) the existence of selectively or generally responsive taste cells.

As most knowledge about sweet taste transduction was obtained from lingual preparations of animals due to the absence of a sweet-sensitive cell line, interspecies differences (Go 2006) question the transferability of these results to human. Moreover, human sample retrieval goes along with ethical concerns (Riedel et al. 2017), wherefore particularly human data on taste are limited. Thus, an adequate system to study taste signaling, screen for agonists/antagonists of the sweet taste receptor or to investigate the communication of taste cells within the taste bud or with other organs is missing. Recently, taste cells derived from human fungiform papillae (HTC-8) have been shown to respond to bitter flavors in monolayer culture (Hochheimer et al. 2014). The inability to sense sweetness might be caused by an unphysiological surrounding, since monolayer cultures cannot resemble the complex *in vivo* environment (Duval et al. 2017). Thus, with the use of this human-derived taste cell line this work aimed i) to establish adequate 3D culture models and characterize them via the three-dimensional visualization of marker distribution with the use of a suitable optical clearing protocol, ii) to establish a perfused live cell assay which allows the functional investigation of taste cultures, and iii) to quantitatively analyze responses upon bitter and sweet compound application and assign these results to the reviewed open questions in the field of taste cell physiology.

2 Methods

2.1 Cell culture media

HTC-8 cells were produced by immortalizing lingual cells isolated from human fungiform taste papillae according to Hochheimer et al. 2014 and kindly provided from BRAIN AG. HTC-8 cell culture media used 335 ml Basal Iscove's medium (Biochrom, F0465), 100 ml MCDB 153 Basal medium (Biochrom, F8105), 10% Fetal Calf Serum (FCS) (Biochrom, S0615), 4 mM L-Glutamin (PAN Biotech, P04-80100), 1% antibiotic/antimycotic (Sigma-Aldrich, A5955), 10 µg/ml Insulin (Sigma-Aldrich, I91077C-5g) and 2.5 µg/ml Gentamycin (Biochrom, A2712). Cells were maintained at 37 °C and 5% CO_2. HTC-8 cells expressing the genetically encoded Ca^{2+} sensor G-GECO were generated according to von Molitor et al. 2020a and kindly provided by BRAIN AG. The Ca^{2+} sensor G-GECO consists of a GCaMP protein connected to a calmodulin Ca^{2+} binding domain as well as a peptide domain (M13). Upon receptor stimulation and intracellular Ca^{2+} increase, Ca^{2+} binds to the calmodulin domain which in turn interacts with M13 resulting in fluorescence increase (Figure 8, Zhao et al. 2011; Lindenburg and Merkx 2012). The G-GECO signal can be detected at an emission of 500-550 nm upon excitation at 480 nm. For HTC-8-G-GECO culture, 0.3 µg/ml Puromycin (A11138-03, GIBCO) were added for G-GECO selection.

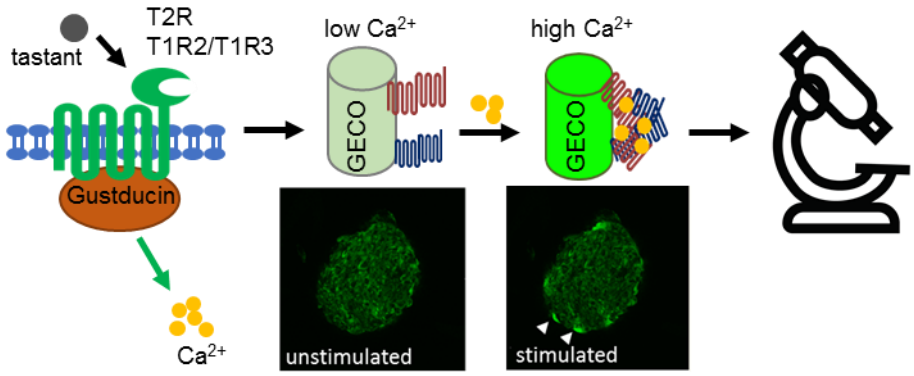

Figure 8: Stable transduction with the Ca^{2+} sensor G-GECO allows recording of gustatory Ca^{2+} responses in HTC-8 spheroids. Upon tastant binding to a bitter or sweet taste receptor, Ca^{2+} is released from stores. This intracellular Ca^{2+} increase can be detected with the genetically encoded Ca^{2+} sensor G-GECO. G-GECO is a single GFP sensor that is dim in the absence of Ca^{2+} and becomes bright when Ca^{2+} binds (Zhao et al. 2011). Fluorescence changes can be detected with the microscope or a plate reader.

LGR5 and its homologs such as LGR6 are hallmarks for adult stem cells in multiple tissues and it was shown that LGR5-positive mouse taste cells resemble taste progenitor cells that when grown as organoids differentiated in all three taste cell types (Ren et al. 2014; Aihara et al. 2015; Ren et al. 2017; Ren et al. 2020). Thus, despite HTC-8 cells, also the progenitor taste cell line HTP-76 was isolated from a human biopsy containing taste buds and immortalized with a comparable procedure used to gain HTC-8 cells (confidential). HTP-76 cells were kindly

provided from BRAIN AG and maintained in human oral epithelial cell growth medium (Pelobiotech, PB-MH-341-7499) with supplements (confidential). The medium was light protected and prewarmed at room temperature. HTP-76 cells were cultured at 34 °C and 5% CO_2 to keep them in their progenitor state, for differentiation experiments, the temperature was increased to 37 °C.

2.2 Cell culture and expansion

For cell expansion, HTC-8 cells were washed with Phosphate Buffered Saline (PBS) without $CaCl_2$ (Sigma Aldrich, D8537) and incubated with ATE-Trypsin (Sigma Aldrich, 59418C) for ~2 min at 37 °C. After cell detachment, Trypsin was inhibited by diluting with culture medium and $0.5x10^6$ cells were transferred in a T75 flask. Media was exchanged every 2-3 days till cells reached ~80-90% confluence. For cryopreservation of cells ($1x10^6$ cells/vial) in liquid nitrogen, HTC-8 media was supplemented with extra 5% FCS and 5% Dimethylsulfoxid (DMSO) (Carl Roth, A994.1).

To grow HTP-76 cells, T25 flasks were coated with 1 µg/cm^2 rh Vitronectin (Fisher Scientific, 15134499) for 1 h at room temperature. The solution was removed prior usage. After cells reached ~90% confluence, they were spitted in a ratio of 1:2. Therefore, cells were washed with PBS without $CaCl_2$ and detached using Acutase (Sigma Aldrich, A6964) at 35 °C for ~2 min. The reaction was stopped with medium. Cells were centrifuged at 500xg for 5 min to eliminate Acutase in the supernatant and transferred to a new flask with fresh medium. The medium was exchanged every other day. For cryopreservation in liquid nitrogen, $1x10^6$ cells were resuspended in 1 ml BamBanker (Wako, 302-1468).

2.3 Generation of 3D taste cultures

For the generation of 3D cultures cells were either grown as spheroids or cultured in scaffold Dynarray chips from 300 MICRONS. For both 3D cultures, 0.5 $x10^3$ cells per spheroid or per Dynarray cavity were used. As HTP-76 cells did not form spheroids by themselves, they were grown in co-culture with HTC-8 cells. Co-cultures used $0.25x10^3$ HTP-76 and $0.25x10^3$ HTC-8-G-GECO cells, in order to discriminate between cells based on G-GECO fluorescence. Co-cultures were maintained at 37 °C in HTP-76 medium. 3D culture development over time was documented with brightfield microscopy and images were taken with an Axiovert 25 (Carl Zeiss Microscopy GmbH, Jena, Germany).

2.3.1 Spheroids

Spheroids were generated using 96-well ultra-low attachment U-shaped plates (Greiner, 650970), which prevent cell attachment to the plastic, thus, favoring cell aggregation. Spheroids in 96-well plates were prepared by plating 0.5 x10^3 cells/well in 150 µl medium and subsequent centrifugation for 5 min at 500xg to favor cell-cell contacts. Spheroids formed overnight and were cultured for 5–7 days in the same medium. HTP-76 spheroids were generated by the addition of 5% Basement Membrane Extract (BME) (Pathclear, 3432-005-01) or 3% Matrigel (R&D systems biotechne, 3432-005-0).

2.3.2 Dynarray chips

The original Dynarray chip was made of a 2x2 cm transparent Polycarbonate foil that contained a 634-cavity array, of which each array has a diameter and depth of 300 µm, respectively (Wuchter et al. 2016). To favor media exchange, the Polycarbonate foil of the Dynarray chip contains 3 µm pores (Giselbrecht et al. 2008). In this work, circular Dynarray chips were used, with a diameter of ~5.5 mm containing 196 cavities (Figure 12A). To sterilize the chips and remove the air in cavities, they were washed in increasing isopropanol concentrations (30, 50, 70, 100%) and finally with PBS without $CaCl_2$. As cells do not attach to the Polycarbonate surface, chips were coated with a solution of 30 µg/ml Collagen (from rat tail tendon; Roche, 11179179001, stock solution 1mg/ml) overnight at 4 °C. On the next day, Dynarray chips were washed with PBS without $CaCl_2$ before cells were added. Detached cells from T75 flasks were centrifuged and resuspended in ~80 µl medium poured on the chip. Cells in the droplet were allowed to adhere to the Dynarray chip surface in the incubator for 4 h before the chip was transferred in a 6-well plate with ~4 ml medium. Dynarray chip cultures were cultured statically for 5–7 days.

2.4 Immunostaining protocols

For the characterization of 3D taste cultures, they were stained with the antibodies and dyes listed in Table 6. Samples were stained either as whole mount (WS) or after slicing with the cryostat (Leica Biosystems, Nussloch, Germany) or vibratome (VT 1000S Leica, Nussloch Germany) to generate 2D samples on slides.

Table 6: Antibodies and dyes used for immunostainings. Antibody (AB) and dye dilutions are indicated for 2D samples (sample slices or cells on slides) and 3D whole mount (WM) stainings.

	AB	Marker for	Dilution 2D	Dilution WM	Species	Supplier
1 AB	Ki67	proliferation	1:300	1:300	rabbit, polyclonal	Merck, AB9260
	Cleaved Caspase 3	apoptosis	1:300	1:400	rabbit, polyclonal	Cell Signaling, 9661
	GM130	Golgi apparatus	1:400	1:400	mouse, monoclonal	BD Bioscience, 610822
	KRT20	mature taste cells	1:25	1:25	mouse, monoclonal	Dako/Agilent, M701929-2
	KRT8	mature taste cells	1:80		rat, polyclonal	DSHB, Toma1
	KRT14	basal cells	1:300	1:400	mouse, monoclonal	Merck, MAB3232
	KRT14	basal cells	1:300	1:400	rabbit polyclonal	Thermo Fischer PA5-16722
	T2R38	bitter receptor 38	1:400		rabbit, polyclonal	Biozol, bs-8650R
	T2R16	bitter receptor 16	1:400		rabbit, polyclonal	Biozol, bs-11616R
	T1R3	sweet taste receptor R3	1:200		rabbit, polyclonal	Sigma Aldrich, SAB4503300
	T1R3	sweet taste receptor R3	1:200		rabbit, polyclonal	LS Bio, A5060
	T1R2	sweet taste receptor R2	1:200		rabbit, polyclonal	LS Bio, A2007
	PLCβ2	Phospholipase Cβ2	1:25		mouse, polyclonal	Santa Cruz, 515912
	Gi 1-2-3	GPCR subunit	1:25		mouse polyclonal	Santa Cruz, 136478
2 AB	Alexa Fluor 647		1:1000	1:800	goat anti-rabbit	Invitrogen, A21246
	Alexa Fluor 647		1:1000	1:800	donkey anti-mouse	Invitrogen, A31571
	Alexa Fluor 488		1:1000	1:800	donkey anti-rabbit	Invitrogen, A21206
	Alexa Fluor 488		1:1000	1:800	goat anti-mouse	Invitrogen, A11001
	Alexa Fluor 488		1:1000	1:800	donkey ant-rat	Invitrogen, A21208
Dyes	Draq5	nuclei	1:1000	1:600		Thermo Fischer, 62522
	DAPI	nuclei	1:1000	1:500		Sigma Aldrich, D9542
	WGA 488	cell membrane	1:200	1:200		Biotium, 29022
	UEA-1	taste cell membrane	1:200			Vector Laboratories, FL-1061
	Phalloidin TRITC	actin filaments	1:1000	1:800		Sigma Aldrich, P19951

2.4.1 Immunostaining of slices

For antibody testing, slices of paraffin embedded human circumvallate papillae and HEK293 cells grown on cover slips overexpressing T1R2/T1R3 were provided from BRAIN AG. Additionally, mouse tongues were fixed with 4% Paraformaldehyde (PFA) (Carol Roth 335.3) in PBS (137 mM NaCl, 2.7 mM KCl, 10 mM Na_2HPO_4 x 2 H_2O, 2 mM KH_2PO_4, pH 7.4) overnight after dissection. PFA was then extensively washed off, tongues were dehydrated in increasing Sucrose concentrations (15% and 30%) (Carl Roth, 4621.1) and frozen at -80 °C in a freezing media (Leica, FSC 22 Clear). Afterwards, tongues were sectioned (10 µm) with the CM-1950 cryostat (Leica Biosystems, Nussloch, Germany). Similarly, Dynarray chips were sectioned (15 µm thick) with a vibratome (VT 1000S Leica, Nussloch Germany) upon fixation with PFA for 45 min, washing with PBS and embedding in 2% Agarose (Carl Roth, 3810).

For immunostaining, samples were permeabilized with 0.1% Triton X-100 (Carl Roth, 3051.4) in PBS to allow antibody penetration, blocked with 3% Bovine Serum Albumin (BSA) (Carl Roth, 8076.3) in PBS for 2 h at room temperature and stained with the appropriate first antibody (Table 6) overnight at 4 °C. Antibodies were diluted in 3% BSA solution. Negative controls did not contain antibodies. The next day, samples were washed 3x5 min with PBS before the secondary antibody and/or dyes were added for 2 h at room temperature. After washing 5x5 min with PBS, slides were mounted with Mowiol (Sigma Aldrich, 81381) and imaged with the inverted Leica SP8 confocal microscope (Leica Microsystems CMS, Mannheim, Germany) equipped with a HC PL APO 20x/0.75 IMM CORR objective at a resolution of 1024x1024pixels, a 2x line average and a gain between 600 and 750 V, to avoid signal overexposure.

2.4.2 Immunostaining of whole mount 3D samples

For whole mount stainings, spheroids and Dynarray chips were fixed 45 min with 4% PFA at 37 °C. After PFA washout (3x5 min PBS), samples were quenched with 0.5 M Glycine (Carl Roth, 3908.3) in PBS for 1 h at 37 °C. Samples were then incubated 10 min in permeabilization buffer (2% Triton X-100 in PBS), 30 min at 37 °C in penetration buffer (0.2% Triton X-100, 0.3 M Glycine, 20% DMSO in PBS) and 2 h in blocking buffer at 37 °C (0.2% Triton X-100, 1% BSA, 10% DMSO in PBS). Subsequently, samples were incubated over night with a primary antibody (Table 6) diluted in antibody buffer (0.2% Tween 20 (Sigma Aldrich, P9416), 10 µg/ml Heparin (Heparin sodium salt from porcine intestinal mucosa, Sigma-Aldrich, H3149-250KU), 1% BSA, 5% DMSO in PBS) overnight at 37 °C. The next day, samples were washed 5x5 min in washing buffer (0.2% Tween 20, 10 µg/mL Heparin, 1% BSA) before the secondary antibody and nuclear dyes were added (Table 6) and incubated overnight at 37 °C. Spheroids were then washed (5x5 min in washing buffer) and optically cleared using the following optical clearing protocols for at least 24 h at room temperature. For ScaleS different blocking and antibody dyes were used (Chapter 2.5.4). All steps were done while shaking.

2.5 Optical clearing protocols

Light penetration depth into biological samples is limited to 50-70 µm due to refractive index (RI) mismatches at biological tissue interfaces between tissue components, such as proteins, water and lipids (Nürnberg et al. 2020). Thus, optical tissue clearing methods aiming to reduce RI mismatches have been developed to allow deeper penetration. As the protocol efficiency varies among cell types, ClearT2, Glycerol and ScaleS protocols were tested on HTC-8 spheroids. For comparison of clearing efficiency, HTC-8 spheroids made of $0.6x10^3$ cells were used and cultured until they reached a diameter of ~300 µm. Subsequently, spheroids were PFA-fixed, stained with the nuclei marker DAPI and Draq5 and the anti-Ki67 antibody to label proliferating cells as described in Chapter 2.4.2. Spheroids were then optically cleared with the diverse protocols for refractive index matching as described in Nürnberg et al. 2020. PBS and Mowiol were used as comparison controls. For imaging, spheroids were transferred in 18-well flat µ-slides (ibidi, 81826) in the respective clearing media and imaged with the inverted Leica SP8 confocal microscope (Leica Microsystems CMS, Mannheim). Images were acquired at a resolution of 1024x1024 pixels, a 2x line average and a z-step size of 1.5 µm.

2.5.1 ClearT2

ClearT2 is based on a detergent-free hyperhydrating protocol that uses a gradual increasing Polyethyleneglycol concentration (ClearT2). The protocol was adapted from Dingle et al. 2015 and conducted according to Nürnberg et al. 2020. Briefly, stained spheroids were incubated for 10 min at room temperature in a solution of 25% Formamide (Sigma Aldrich, 47671) with 10% Polyethyleneglycol 800 (PEG) (Sigma Aldrich, P5413), then 5 min in 50% Formamide with 20% PEG and subsequently in fresh 50% Formamide with 20% PEG for 60 min.

2.5.2 CytoViasta

After staining, spheroids were cleared with the commercially available CytoVista Tissue Clearing Reagent from Invitrogen (V11315).

2.5.3 Glycerol

To gain 88% Glycerol solution, Glycerol (Carl Roth, 3783.2) was diluted in ddH_20 and the refractive index was adjusted to RI = 1.459 with a refractometer (Carl Zeiss, Jena, Germany).

2.5.4 ScaleS

The ScaleS protocol uses a combination of delipidation, maintenance of the aqueous environment and Urea-mediated tissue hydration. This causes partially denaturation and hydration of high refractive index proteins (Hama et al. 2011). The original protocol from Hama

et al. 2011 was modified according to Nürnberg et al. 2020. Prior staining, spheroids were incubated in S0 adaption solution (20% D-Sorbitol (Sigma Aldrich, 1077581000), 5% (w/v) Glycerol, 3% (v/v) DMSO in PBS, pH 7.2 at 37 °C) to prevent sample floating. The following days, spheroids were incubated for 24 h in SA2 solution (10% (w/v) Glycerol, 4 M Urea (Sigma Aldrich, 1084871000), 0.1% (w/v) Triton X-100 in ddH_2O, pH 7.7), then in B4(0) solution (8 M Urea in ddH_2O, pH 8.4) and last in SA2 overnight at 37 °C, respectively. On day 4, spheroids were transferred for 6 h in PBS at room temperature and blocked in ScaleS blocking solution (2.5% (w/v) BSA, 0.05% (w/v) Tween 20, 0.1% (w/v) Triton X-100 in PBS, pH 7.4) for 24 h at 37°C. On day 5, the primary antibody (Table 6) was added in fresh AbScale solution (0.33 M Urea, 0.1% (w/v) Triton X-100 in PBS, pH 7.4) for 24 h at 37 °C, and samples were washed afterwards two times for 2 h with AbScale solution before the secondary antibody (Table 6) was applied in AbScale solution overnight at 37 °C. On day 7, spheroids were washed in AbScale for 6 h at room temperature and reblocked 2x2 h in ScaleS blocking solution. This was followed by sample refixation in 4% PFA for 1 h at room temperature. Afterwards, spheroids were washed in PBS overnight at 4 °C and finally incubated in ScaleS4 solution (40% (w/v) D-Sorbitol, 10% (w/v) Glycerol, 4 M Urea, 15% DMSO in ddH_2O, pH 8.1) overnight at room temperature.

2.5.5 Evaluation of clearing protocols

To evaluate clearing efficiencies data were analyzed as described in Nürnberg et al. 2020 with ImageJ and Microsoft Excel 2013. Clearing and fixation induced shrinkage or swelling of spheroids was evaluated by measuring spheroid diameters twice in a perpendicular angle on maximum z-projections made from image stacks. The decay of the fluorescence signal through the spheroid depth (z) was determined by placing the same circular (r = 50 µm) region of interest (ROI) in the spheroid center where the signal starts to decrease first and measuring the mean signal intensity for each optical section with the z-axis profile function from ImageJ. Depth values were normalized to pre-fixation spheroid diameters and multiplied with the percentage change of volume to calculate the normalized depth. To analyze signal-to-noise-ratios (SNR) fluorescence intensities from background and nuclei were assessed in the same circular ROI used for the signal decay analysis which was processed with a median filter radius (r = 1). Next, a threshold range was manually applied to cover background areas in upper spheroid regions and a binary mask was generated. To analyze mean background intensity and standard deviation, ROIs created from binary masks were used. The signal intensity of nuclear dyes was evaluated with an automated thresholding tool on each optical section, and images were transformed into binary masks, which were applied to measure signal intensities from original stacks. The signal-to-noise-ratio was calculated for each optical section by dividing the mean intensity signal µ by the standard deviation of the background intensity σ

(SNR = $\mu_{Signal}/\sigma_{Background}$). The rose criteria was defined according to Rose stating that an SNR < 5 is necessary to be able to distinguish image features correctly with a probability of 3δ (Burgess 1999). For 3D nuclei segmentation images were pre-processed according to Nürnberg et al. 2020 and nuclei were quantified according to the algorithm of Schmitz et al. 2017 which uses 3D seeded watershed for segmentation.

2.6 Live cell imaging protocols

To assess whether spheroids are sensible to specific taste solutions, live imaging Ca^{2+} experiments were conducted as described in von Molitor et al. 2020a. Perfused live cell imaging setups were established for confocal and LSFM microscopy.

2.6.1 Perfused confocal live cell imaging

After 5-7 days of culture, HTC-8-G-GECO cells were collected, washed with PBS and transferred in µ-slide III 3D perfusion slides (ibidi, 80376) for Ca^{2+} microscopic live cell measurements. To avoid spheroid movement out of focus during perfusion experiments, spheroids were covered with Gelatine nonwoven CL130 Scaffolene pads (high density – crosslinked, 130 g/m^2) from Freudenberg for stabilization. With a classical hole puncher, pads were perforated to a circle of ~ 25 mm^2. Scaffolene got transparent upon liquid contact which makes it permissive to fluorescence imaging. Ibidi slides were then sealed and the chambers were flooded with imaging control buffer (118 mM NaCl, 4.7 mM KCl, 4.2 mM $NaHCO_3$, 1.2 mM KH_2PO_4, 1.2 mM $MgSO_4$ and 1.3 mM $CaCl_2$, pH 7.4). Next, slides were connected to a self-made gravity mediated perfusion system which consisted of 50 ml syringe buffer reservoirs linked via Luer 3-way valves and y-adapters through tubes to the slide (Figure 14A). The perfusion flow had a mean speed of 1.3 ml/min, which exchanged the whole solution in the well in 5–15 s. Prior starting the perfusion, spheroids were first imaged statically in control buffer for 4.2 min. Start of the perfusion did not produce unspecific responses to sheer stress. Spheroids were then stimulated with different gustatory compounds listed in Table 7 and as indicated in the figures by dashed lines. Experiments ended with a washing step with control buffer. Taste compounds were dissolved in control buffer and by adjusting the concentration of NaCl, osmolality was corrected to 272.5 mOSM. Buffer osmolarities were measured prior usage with the Osmomat 030 (Gonotec, Berlin, Germany). In Ca^{2+}-free buffers, residual Ca^{2+} was chelated with 10 mM EGTA (AppliChem, A0878). Images were taken every 5 s from 3 z-planes with the inverted SP8 confocal microscope (Leica Microsystems CMS, Mannheim, Germany) at 700 Hz scan frequency with 1024x1024 pixel resolution and a 2x line average. G-GECO fluorescence was excited at 488 nm with 1% laser intensity and detected at an emission window of 493–739 nm. Stacks were recorded at about 20–40 µm spheroid depth.

Table 7: Compounds used for HTC-8-G-GECO stimulation. [1)] freshly prepared on the experimental day, [2)] light protected

Compound	Concentration	Supplier
Acesulfame K	40 mM	Supelco, LC26461V
ATP disodium salt	10 µM, 1 mM	Roche, 10127531001
D(+)-Cellobiose	40 mM	Merck, 219458
D(-)-Glucose	40 mM	Carl Roth, HN06.3
D(-)-Fructose	40 mM	Carl Roth, 4981.2
D(+)-Sucrose	5, 10, 20, 40, 80 mM	Carl Roth, 4621.1
D-(-)-Lactose	40 mM	Carl Roth, 6868.1
D(-)-Salicine	20 mM	Carl Roth, 7192.2
Sodium Saccharin	0.1, 0.2, 0.5, 10, 20, 40 mM	Sigma Aldrich, 9259
Sodium Gluconate	20 mM	Sigma Aldrich, S2054
Sulforhodamine B sodium salt[1,2]	10, 100 µM	Sigma Aldrich, 1402
Suramin sodium salt[1]	100 µM	Sigma Aldrich, S2671
KCl	50 mM	Carl Roth, 6781.1

The fluorescence dye Sulforhodamine B was used to prove compound penetration into the spheroid core. Therefore, Sulforhodamine B and G-GECO fluorescence were acquired simultaneously with an adapted microscopy protocol. For G-GECO the excitation was at 488 nm with 1.2% laser intensity and an emission window of 493–540 nm, for Sulforhodamine B the excitation was 555 nm with 0.7% laser intensity and an emission window of 600–727 nm. Images were acquired every 3.7 s.

2.6.2 Perfused LSFM live cell imaging

To gain whole 3D spheroid information during live cell imaging, experiments with LSFM were performed with a modified perfusion setup, as described in von Molitor et al. 2020a. Spheroids were mounted with 0.5% low melting Agarose (SeaPlaque GTG Agarose, Camberx Bio Science Rockland) dissolved in control buffer in a glass capillary (U-shaped capillaries 20x1.5 mm, Hilgenberg). The capillary's ends were attached to a µ-dish 35 mm glass bottom dish (ibidi, 1158) with Agarose drops. The confocal gravity mediated perfusion system was used, however, tubes had to be attached with thin wires to the dish and as the system was not closed, a pump was necessary for the outflow (Figure 18A). The mean perfusion speed was 3.5 ml/min and it took 3.5-5 min to exchange the whole buffer in the dish. For LSFM imaging the Leica TCS SP8 DLS vertical turn light sheet microscope (Leica Microsystems CMS, Mannheim, Germany) with a 5 mm wide water corrected mirror and Leica HC APO L 10x/0.3 W objective was used. The excitation and emission wavelengths were adapted from the confocal imaging setup, however, the emission was acquired with a GFP bandpass filter. Z-stacks of over 80–90 µm spheroid depth were taken with an optical sectioning distance of 3.7 µm, an acquisition frequency of 0.2 Hz and a 2x line average.

2.6.3 Evaluation of live cell imaging experiments

The ImageJ software was used to analyze Ca^{2+} transients in spheroids. Data were analyzed in three different modes: i) in the whole spheroid, ii) in four concentric rings and iii) in single cells according their position in the rings. Whole spheroid fluorescence signals were segmented with the thresholding function. To obtain the four concentric rings, termed R1-R4, from the spheroids rim to the center, the erosion function was applied 30 times. Next, the mean fluorescence was measured over time in the segmented areas and then normalized to the mean signal 30 s before stimulation (F_0). The function of fluorescence change $\Delta F/F_0 = (F - F_0)/F$ was then plotted over the experiment time. In a last step, single cells were selected during the stimulated time interval in the rings. Therefore, circular ROIs were manually positioned in the center of each cell, focusing first on highly responding cells (bright cells) and then on cells with a lower response. In the two outer rings (R1, R2) 15 cells, in R3 10 cells and in R4 4 cells were selected. Only selective responses were included in the analysis which were defined as the following i) $\Delta F/F_0$ > 2x standard deviation (SD) in F_0, ii) $\Delta F/F_0$ > 1% and iii) $\Delta F/F_0$ during stimulation > $\Delta F/F_0$ in control solution (spontaneous Ca^{2+} transients). The peak intensity was determined as maximum $\Delta F/F_0$ within the stimulation window. To calculate dose-response curves, peak intensities were plotted versus log agonist concentrations and the half-maximal effective concentration (EC_{50}) was determined applying non-linear regression by fitting the curve with GraphPad Prism 8 according to the equation f(x) = A/[1 + 10^(LogEC_{50}-x)^H]. A and EC_{50} are the magnitude of the saturated and half-maximal concentration, while x stands for the agonist concentration and H for the Hill coefficient. Kinetics of the transients were characterized as following: “time to peak” (T_{peak}) was defined as the time needed to reach the maximum amplitude from the time of stimulation and “time to slope” (T_{slope}) as the time needed from the stimulation to the onset, which corresponds to the time point, where the slope of $\Delta F/F_0$ gets positive. The time interval from the onset to the maximum intensity was defined as “time from slope to peak” ($T_{slope\text{-}peak}$). The parameters were determined with Microsoft Excel 2013. T_{peak}, T_{slope} and $T_{slope\text{-}peak}$ are depicted on an exemplary Ca^{2+} response in Figure 9.

LSFM data were analyzed on whole spheroid level. To corrected for bleaching, the exponential bleaching correction ImageJ plugin was utilized and spheroids were subsequently thresholded along their z-axis (spheroid depth). The penetration depth of confocal microscopy and LSFM was assessed on unstimulated spheroids with the z-axis profile command which displays the G-GECO mean fluorescence as a function of the z-axis.

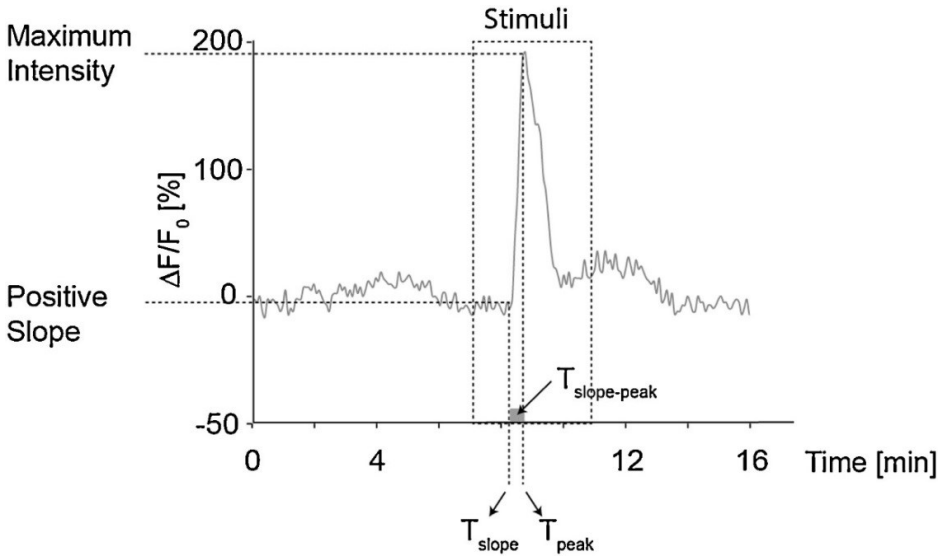

Figure 9: Determination of kinetic characteristics of Ca^{2+} transients. The maximum intensity (F) was calculated with the formula $\Delta F/F_0 = (F - F_0)/F$ with F_0 defining the mean signal intensity 30 s before stimulation. "Time to peak" (T_{peak}) describes the time interval from the beginning of the stimulation to reach the time point of the maximum intensity. "Time to slope" (T_{slope}) is the time interval defined from the start of the stimulation to reach the time point where the slope of $\Delta F/F_0$ gets positive. "Time from slope to peak" ($T_{slope-peak}$) is assigned to the interval indicated by the grey box between T_{slope} and T_{peak}. Figure adapted from von Molitor et al. 2020a.

2.7 Transcriptome analysis of spheroids

RNA sequencing experiments were carried out from BRAIN AG to evaluate spheroids transcriptomes on mRNA level abundancy. For RNA isolation, spheroids were collected from one entire 96-well U-bottom dish after 6 days of culture and RNA was isolated with the QuantiFluor RNA System Kit (Promega, E3311). The RNA content and purity were determined with the NanoDrop ND-1000 spectrophotometer (peQLaB, Dresden, Germany). The TruSeq RNA Library Prep Kit v2 from Illumina, with an input amount of 500 ng of total RNA, was used for library preparation. Prepared libraries were sequenced with a 2x150 bp read length with the HiSeq 3000/4000 SBS Kit and an Illumina Hiseq 4000 sequencer. Subsequently, using Hisat2, (2.0.4) the adapter trimmed, demultiplexed and quality filtered reads were aligned to the hg19 reference genome and transcriptome according to Kim et al. 2015. Prior sorting and indexed with SAMtools, Hisat2 output files (SAM) were converted to the BAM format (Li et al. 2009). Cufflinks (2.1.1) was used to quantify the transcript abundancies displayed in fragments per kilobase of exon per million fragments mapped (FPKM). Results were interpreted as the following:

<1 = no expression

1 - 10 = low expression

10 - 100 = normal expression

100 - 1000 = high expression

>1000 = very high expression

2.8 Statistics and software

ImageJ was used to edit and analyzed fluorescence images. LSFM image stacks were fused with the local entropy function of Leica Application Suite X (LAS X, Version 3.1.5.16308) and deconvolved with the Classic Maximum Likelihood estimation algorithm with Huygens Essential Software (Version 18.04). Quantitative data were obtained using Microsoft Excel 2013 and GraphPad Prism 8. Subsequently, figures were then set into the Adobe Illustrator composite. Normality and homoscedasticity of data were measured by Kolmogorov-Smirnov test and F-test, respectively. Statistics used one-way ANOVA, two-way ANOVA or Student t-test. P-values are indicated as: * < 0.05, ** < 0.01, *** < 0.001 and **** < 0.0001.

3 Results

Since HTC-8 cells derived from human fungiform papillae were previously shown to only express bitter receptors (Hochheimer et al. 2014), this project aimed to investigate HTC-8 cell behavior in a three-dimensional environment and their potential to generate sweet-sensitive cells. Accordingly, HTC-8 cells were grown as spheroids or in Dynarray chips to better resemble physiological conditions. 3D cultures were then tested for their functional responses to diverse taste compounds with the established perfused Ca^{2+} live cell assays.

3.1 Establishment of an optical clearing protocol for HTC-8 3D cultures

To characterize 3D taste cultures and prove their validity, their cell type and protein marker distribution was evaluated using immunostainings. Classically, 3D samples are physical sectioned to gain slices which is cumbersome and often defective. Thus, 3D samples in this work were optically cleared with different methods, such as ClearT2, CytoVista, ScaleS and Glycerol according to Nürnberg et al. 2020 to reduce light scattering and allow higher light penetration deep into the sample.

Orthogonal volume projections for spheroids stained with the nuclei dyes DAPI and Draq5 and the proliferation marker Ki67 revealed improved imaging depths upon clearing with ScaleS and Glycerol (Figure 10A). The DAPI signal intensity had the highest stability in Glycerol and CytoVista, whereas fluorescence intensities for Ki67 and Draq5 did not vary strongly among the tested clearing protocols. While most reagents did not affect spheroid sizes, CytoVista caused a significant shrinkage while ScaleS induced swelling (Figure 10A-C). Intriguingly, also PFA-fixation resulted in a significant spheroid size reduction. The decay of the nuclei signal was determined as a function of spheroid depth. In the top cell layers brightness values were the highest for all protocols, followed by exponential signal reduction (Figure 10D, E). The 50% and 90% signal decay depths were improved for Glycerol, CytoVista and ScaleS (Table 8, Table 9). Accordingly, Draq5 signals could be still detected in ~308 µm spheroid depth using ScaleS, while DAPI was only stable till ~265 µm using the Glycerol protocol. As for the signal intensity, highest signal-to-noise-ratios (SNR) with rapid declines were observed from upper to lower spheroid parts (Figure 10F, G). The depth for reaching the rose criterion (SNR > 5), upon which image features cannot be distinguished accurately anymore, was the largest in CyotVista for DAPI and in Glycerol for Draq5 (Table 8, Table 9). Last, the efficiencies of the nuclei segmentation were compared for the different clearing methods: this revealed highly variable results (Figure 10H). With Glycerol segmentation figures were most closely to the number of seeded cells, i.e. $0.6x10^3$ cells per spheroid. Accordingly, depending on the evaluation criteria, CytoViasta, ScaleS and Glycerol protocols are best suitable to optically clear HTC-8 spheroids. For further analysis, Glycerol was chosen as optical clearing reagent

as: i) it reveled best segmentation results, ii) displayed superior signal stability for DAPI, iii) can be self-made with low costs, and iv) due to the fast protocol, is time effective.

Table 8: DAPI fluorescence penetration and SNR in depth for HTC-8 spheroids. ~300 µm sized HTC-8 spheroids were PFA-fixed, stained with DAPI, optically cleared and imaged with confocal microscopy. The 50% and 90% signal loss in spheroid depth and SNR < 5 were calculated for n ≥ 7 spheroids. Maximum values are highlighted. Table adapted and modified from Nürnberg et al. 2020.

	Absolute depth [µm]			Normalized depth [µm]		
	50% signal loss	90% signal loss	SNR < 5	50% signal loss	90% signal loss	SNR < 5
PBS	45.0	112.5	45.0	52.5	131.2	52.5
Mowiol	51.0	168.0	40.5	56.8	187.0	45.1
ClearT2	43.5	--	42.0	52.5	--	50.6
CytoVista	63.0	145.5	79.5	**96.7**	223.3	**122.0**
ScaleS	**85.5**	**259.5**	**88.5**	84.5	256.6	87.5
Glycerol	**84.0**	**264.0**	**85.5**	84.5	**265.4**	86.0

Table 9: Draq5 fluorescence penetration and SNR in depth for HTC-8 spheroids. ~300 µm sized HTC-8 spheroids were PFA-fixed, stained with Draq5, optically cleared and imaged with confocal microscopy. The 50% and 90% signal loss in spheroid depth and SNR < 5 were calculated for n ≥ 7 spheroids. Maximum values are highlighted. Table adapted and modified from Nürnberg et al. 2020.

	Absolute depth [µm]			Normalized depth [µm]		
	50% signal loss	90% signal loss	SNR < 5	50% signal loss	90% signal loss	SNR < 5
PBS	46.5	124.5	64.5	54.2	145.2	75.2
Mowiol	58.5	184.5	102.0	65.1	205.4	113.5
ClearT2	52.5	150.0	96.0	63.3	180.9	115.8
CytoVista	75.0	162.0	129.0	**115.1**	248.6	198.0
ScaleS	81.0	**312.0**	162.0	80.1	**308.5**	160.2
Glycerol	**85.5**	276.0	**232.5**	86.0	277.5	**233.7**

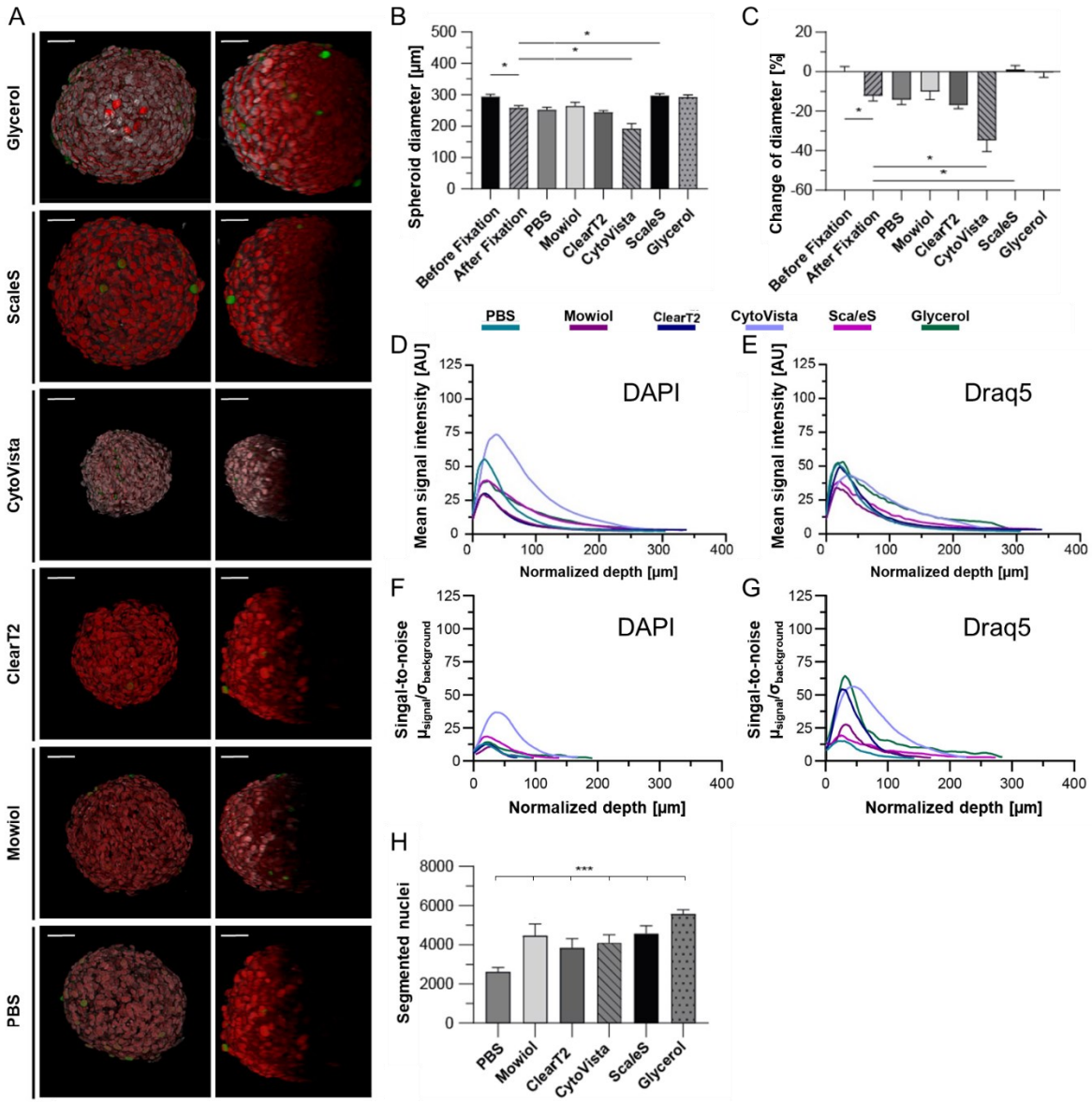

Figure 10: Comparison of different optical clearing methods for HTC-8 spheroid immunostainings. HTC-8 spheroids of $0.6x10^3$ cells were cultured until a diameter of ~300 µm, PFA-fixed, immunostained and optically cleared. A) Representative top (left row) and orthogonal views (right row) of HTC-8 spheroids stained with anti-Ki67 (green) and the nuclear dyes DAPI (grey) and Draq5 (red). Images show 3D volume projections of merged channels. Scale bars: 50 µm. B) Average spheroid diameters were measured from brightfield images before and after fixation and from confocal images after immunostaining and clearing. C) Changes of spheroid diameters normalized to the pre-fixation values. Graphs depict mean +SD for n ≥ 7 spheroids. D, E) DAPI and Draq5 fluorescence mean intensity measurement over spheroid depth. To compensate for volume changes of spheroids induced by clearing protocols, values were normalized according to the degree of spheroid swelling or shrinkage. Graphs depict mean intensities for n ≥ 7 spheroids. F, G) Graphs show mean signal-to-noise-ratios of DAPI and Draq5 for n ≥ 7 spheroids as a function of normalized spheroid depth. H) Quantitative analysis of Draq5 ladled nuclei. Plots show mean +SD. For each condition n ≥ 7 spheroids were evaluated. Figure adapted and modified from Nürnberg et al. 2020.

3.2 Characterization of HTC-8 3D cultures

In this work, two different 3D culture models were compared, spheroids and Dynarray chips, both promoting the growth of spherical structures similar to the native structure of lingual taste buds. Spheroids were generated from $0.5x10^3$ HTC-8 cells and prepared using ultralow attachment plates which promote cell aggregation (Figure 11A). Over time spheroid diameters decreased from 410 µm (d1), to 300 µm (d6) and 270 µm (d10) (Figure 11A, B). The most prominent size reduction was observed between day 1-5, afterwards diameters were relatively stable (Figure 11B), and accordingly spheroids aged between 5 and 7 days were used in this work for functional assessment and characterization. As no loose cells were observed around spheroids, the shrinkage was probably due to increased spheroid compactness rather than to a loss of apoptotic cells (Figure 11A). Next, spheroids were harvested, PFA-fixed and stained with anti-Ki67, anti-Cleaved Caspase 3 and anti-Gm130 to detect proliferation, apoptosis and Golgi apparatus orientation, respectively. Nuclei were stained with DAPI and membranes with wheat germ agglutinin (WGA) to visualize cell morphologies. The marker distribution within the spheroid structure was analyzed with confocal microscopy upon optical clearing with Glycerol. Reconstruction of 3D projections of several z-planes (Figure 11C) showed that proliferating cells were mainly localized in the periphery, while apoptotic cells were found throughout the whole spheroid. Remarkably enlarged Golgi apparatus were observed in elongated cells on the spheroid rim. In contrast, in the spheroid center, cells were rounder and smaller and contained uniformly small Golgi apparatus. Accordingly, the 3D spheroid environment already contributed to emerge different cell morphologies and proliferating activities according to the cells position within the spheroid.

Alternatively, HTC-8 cells were cultured in Dynarray chips containing 196 cavities (Figure 12A). In each cavity $0.5x10^3$ HTC-8 cells were seeded, according to the seeding number of spheroids. HTC-8 cells first filled cavities and on later time points (d5) started to grow between cavities on the polymer foil. To allow nutrition supply, chips have small wholes which are visible as dark dots. Characterization of Dynarray chip cultures, stained with anti-Cleaved Caspase 3 and anti-Ki67, revealed most apoptotic and proliferating cells on the chip/cavity surface (Figure 12B). Cell morphologies, apparent by endogenous G-GECO fluorescence, revealed elongated cells throughout the whole chip, while spheroids contained elongated cells only at the spheroid rim. Cells with enlarged Golgi apparatus were again observed on the chip surface (Figure 12C). Dynarray chips, thus, offer an additional suitable 3D model for the cultivation of HTC-8 cells.

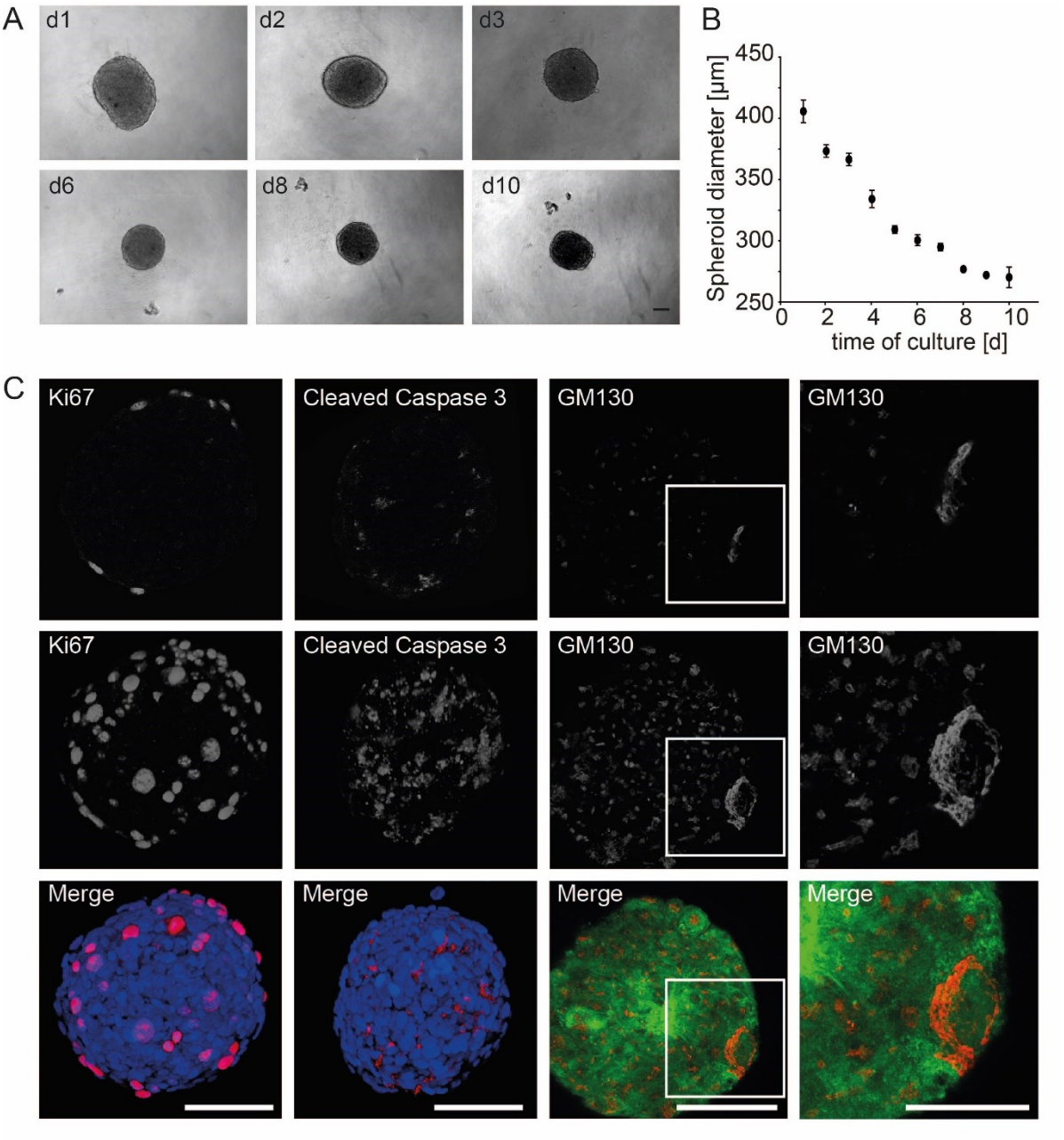

Figure 11: Characterization of HTC-8 spheroids. Spheroids were formed from 0.5x10^3 HTC-8 cells using ultra low attachment plates. A) Brightfield images of HTC-8 spheroids on selected time points of culture (d = days in culture). Scale bar: 100 µm. B) Spheroid sizes were monitored over time by measuring spheroid diameters with ImageJ. Bar shows mean ± SEM of at least n ≥ 5 spheroids. C) Immunostaining of HTC-8 spheroids cultured for 6 days stained with anti-Ki67, anti-Cleaved Caspase 3 and anti-GM130 antibodies (all red). Nuclei were stained with DAPI (blue) and plasma membranes with WGA (green). The first row shows a single z-plane in the middle of the spheroid, lower rows show 3D projections of several z-planes over ~100 µm depth of spheroids cleared with Glycerol. The right panel shows a magnification of the indicated region. Scale bars: 100 µm. Panel C is adapted and modified from von Molitor et al. 2020a.

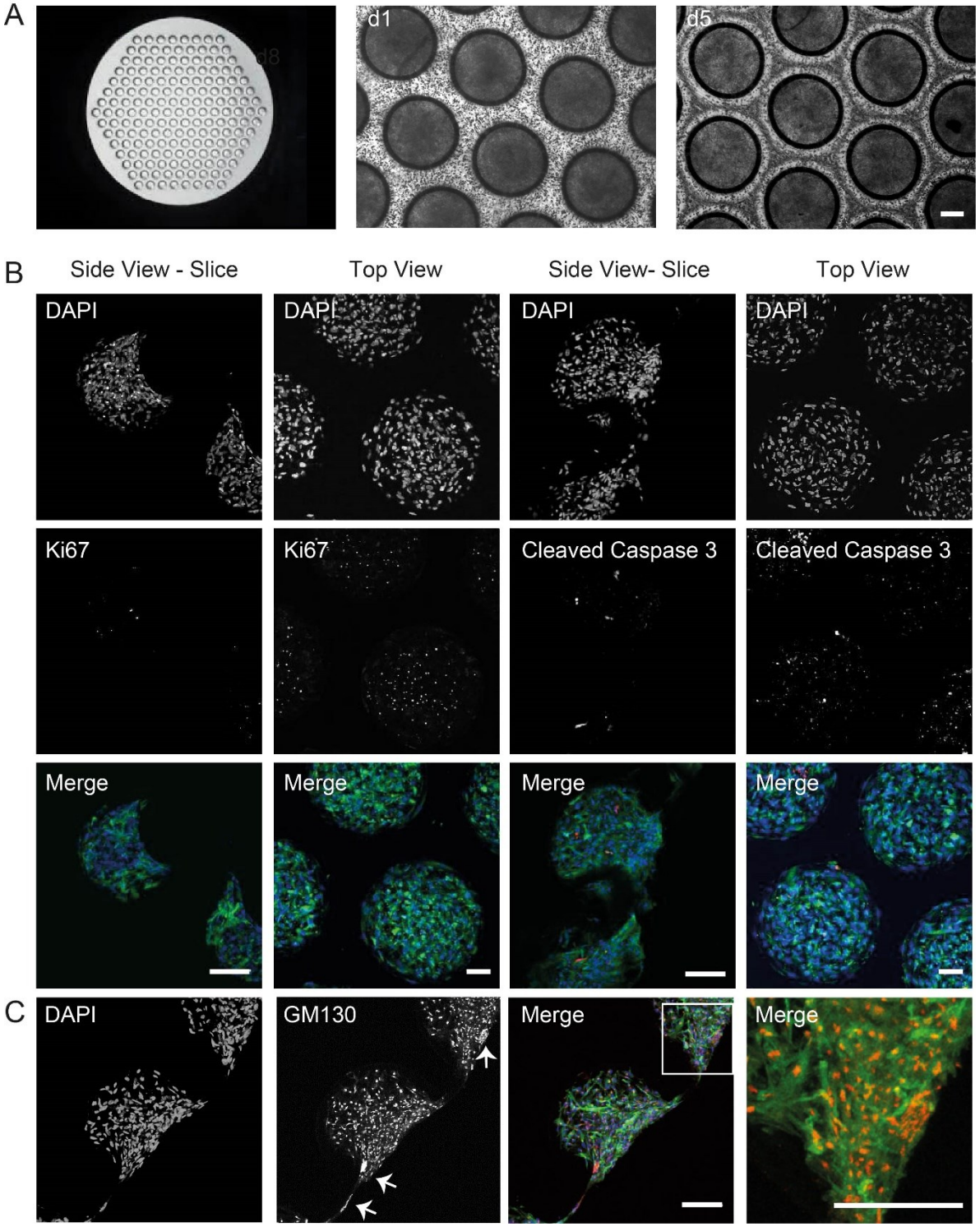

Figure 12: Characterization of HTC-8 cells grown in Dynarray chips. A) The first image shows an example of a 196-well Dynarray chip. Image adapted from www.300microns.com. Each cavity was filled with $0.5x10^3$ HTC-8-G-GECO cells and cultured for 5 days (d). B, C) For immunostaining, cultures were PFA-fixed and stained with anti-Ki67, anti-Cleaved Caspase 3 and anti-GM130 (all red). Nuclei were labelled with DAPI (blue). Green fluorescence of endogenous G-GECO shows cell morphologies. Side views are confocal images of slices generated with the vibratome, top views are images from whole mount samples cleared with Glycerol. C) Arrows indicate enlarged Golgi apparatus. The right panel shows a magnification of the indicated region. Scale bars: 100 µm.

3.3 The lack of reliable antibodies urges the need of a functional Ca^{2+} assay to study gustatory responses of HTC-8 spheroids

Previously, HTC-8 cells have been shown in 2D plate reader-based experiments to respond to bitter compounds, and using RT-PCR analysis revealed expression of corresponding bitter receptors (Bufe et al. 2002; Hochheimer et al. 2014). As initial spheroid (Figure 11C) and Dynarray chip (Figure 12C) characterization revealed different cell morphologies and enlarged Golgi apparatus on the spheroid rim, it was of major interest how T2R expression is distributed within the spheroids. However, the selected antibodies for T2R16 and T2R38 failed to detect a clear signal in HTC-8 spheroids. A possible reason could be the rather low receptor concentration of individual T2R, since several isoforms are expressed in HTC-8 cells (Hochheimer et al. 2014) or unspecificity of the antibodies. This prompted the analysis of additional taste cell markers including PLCβ2, gustducin, KRT14 (as a maker for precursor cells), KRT8 and KRT20 (as a marker for mature taste cells), as well as the dye Ulex europaeus agglutinin-1 (UEA-1), a type of lectin that binds to α-Fucose and labels rodent taste bud membranes (Yoshimoto et al. 2016). Since this project aimed to detect sweet taste receptors, antibodies for the T1R2 and T1R3 subunits were tested as well. To validate these antibodies and the dye, slices of mouse and human tongues as well as HEK293 and HTC-8 cells overexpressing T1R2 and T1R3 were used as positive controls. However, none of the tested markers displayed robust nor specific results. Although the UEA-1 dye and KRT antibodies resulted in an appropriate staining of native mouse or human taste bud papillae (Figure 13), no staining was detected in HTC-8 spheroids nor in Dynarray chips. T1R antibodies (Table 6) tested in cells overexpressing the respective receptors showed either no result or false positive signals (data not shown). Thus, HTC-8 3D cultures could not be further characterized with immunostainings, and consequently an assay was needed to functionally analyze them (Chapter 3.4). Therefore, gustatory responses were investigated with live cell Ca^{2+} imaging upon stimulation with bitter and sweet compounds, which allowed to determine if HTC-8 cells in 3D cultures are sensitive to these stimuli, and if different responses appear in distinct locations within the samples.

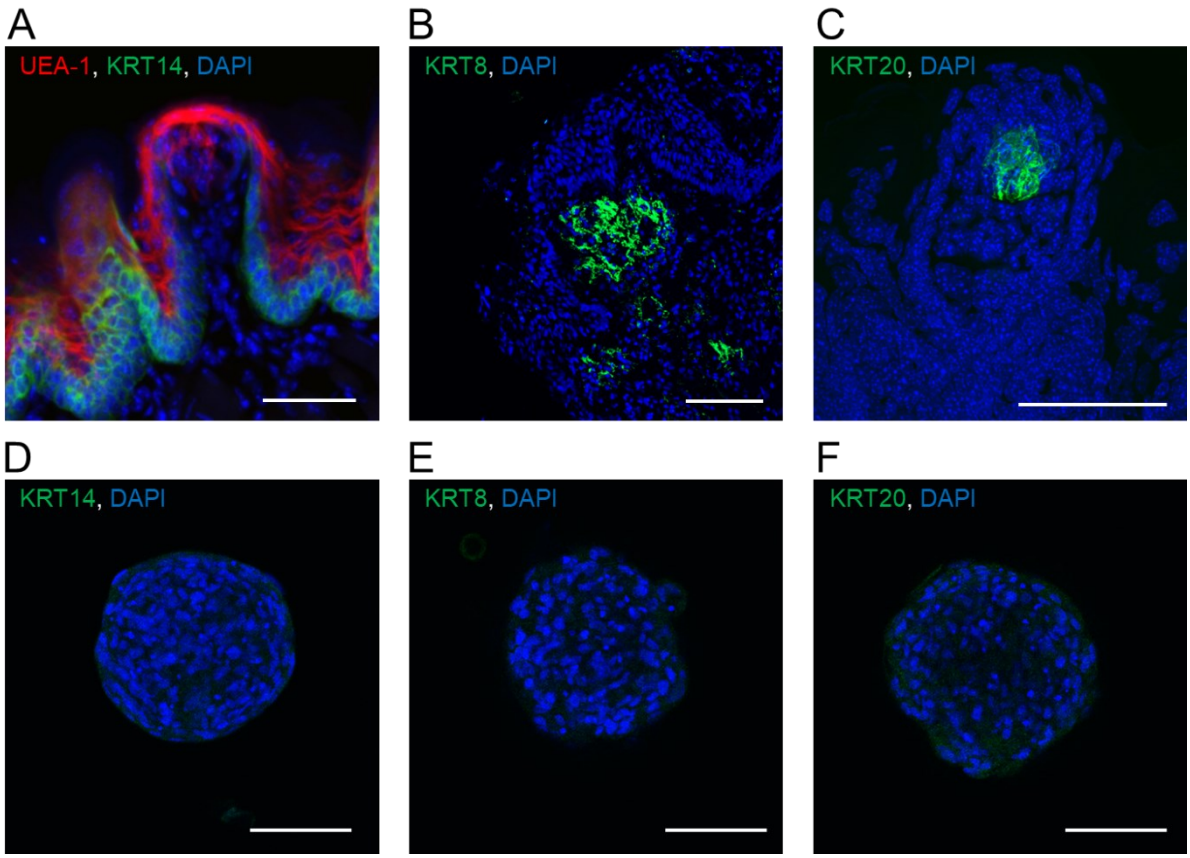

Figure 13: Evaluation of fluorescence taste cell markers. PFA-fixed cryosections of mice tongue or HTC-8 spheroids were stained with UEA-1 dye and anti-KRT antibodies as indicated. A) Mouse taste bud of fungiform papillae, scale bar: 50 µm. B) Human taste bud of foliate papilla, scale bar: 50 µm. C) Human taste bud of circumvallate papillae, scale bar: 100 µm. D-F) Spheroids of $0.5x10^3$ HTC-8 cells cultured for 5 days. Scale bars: 100 µm.

3.4 Development of a perfused live cell imaging setup for confocal microscopy

Previous HTC-8 monolayer cultures were loaded with Fluo4, stimulated by bulk application of gustatory compounds, and fluorescence responses were analyzed in a plate reader (Hochheimer et al. 2014). In contrast, this work used 3D cultures and microscopic live cell imaging to investigate the dynamic processes of signal transduction in HTC-8 spheroids expressing the genetically encoded Ca^{2+} sensor G-GECO (Figure 8). Additionally, flavors were applied by gravity mediated dynamic perfusion to overcome abrupt and fluctuating changes in the cellular microenvironment.

So far, especially spheroids have been precluded from time lapse microscopy upon perfusion, because due to their small size, fragility and round shape, they could not be fixed to the imaging chamber and, thus, moved out of focus. Therefore, a setup that allows sample fixation without destroying the spheroid morphology and integrity, but allowing enough stability to image a defined region over a long time with confocal microscopy at the same time was established (Figure 14A). The final setup used µ-slide III 3D perfusion slides (ibidi) as imaging chambers for spheroids and Dynarray chip cultures. Once positioned in the small chamber

(volume 60 µl), samples were covered with CL130 Scaffolene pads (Freudenberg) which enclosed the samples like a mesh and hold them in place when perfused (Figure 14B-D). Scaffolene is generated in a rotary spinning process from Collagen and upon contact with fluids became transparent but remained dimensionally stable (Figure 14C). As buffer reservoirs syringes were used and connected to the microfluidic chamber via tubes, y-adapters and Luer locks (Figure 14A).

To test the validity of this system, the bitter compound Salicine (20 mM), already known to induce Ca^{2+} responses in HTC-8 monolayer culture (Hochheimer et al. 2014), was applied. Dynarray chip cultures and spheroids responded with a similarly consistent Salicine-induced rise in G-GECO fluorescence, while in control buffer and upon starting the perfusion (4.2 min) signals stayed at baseline level (Figure 14E-H). Only some slight and occasional spontaneous Ca^{2+} transients were observed at single cell level when the perfusion was activated (Figure 14G, H), but this did not affect the whole sample mean fluorescence (Figure 14E, F). Cells in spheroids responded faster than those in Dynarray chips, probably because spheroids are directly exposed to compounds, while in Dynarray chips compounds had to diffuse into the cave structure and through the pores to reach the cells. For osmolarity control, spheroids were perfused with Gluconate (20 mM) which led to no change in fluorescence (Figure 14F, H). Accordingly, whole image analysis of 3D HTC-8-G-GECO samples revealed only specific responses upon Salicine stimulation.

In summary, results from immunostainings and functional Ca^{2+} responses were comparable for HTC-8-G-GECO cells grown as spheroids and in Dynarray chips. Both models may, thus, serve as potential 3D taste model. As the generation of spheroids is more time and cost effective, they were chosen as model for further experiments.

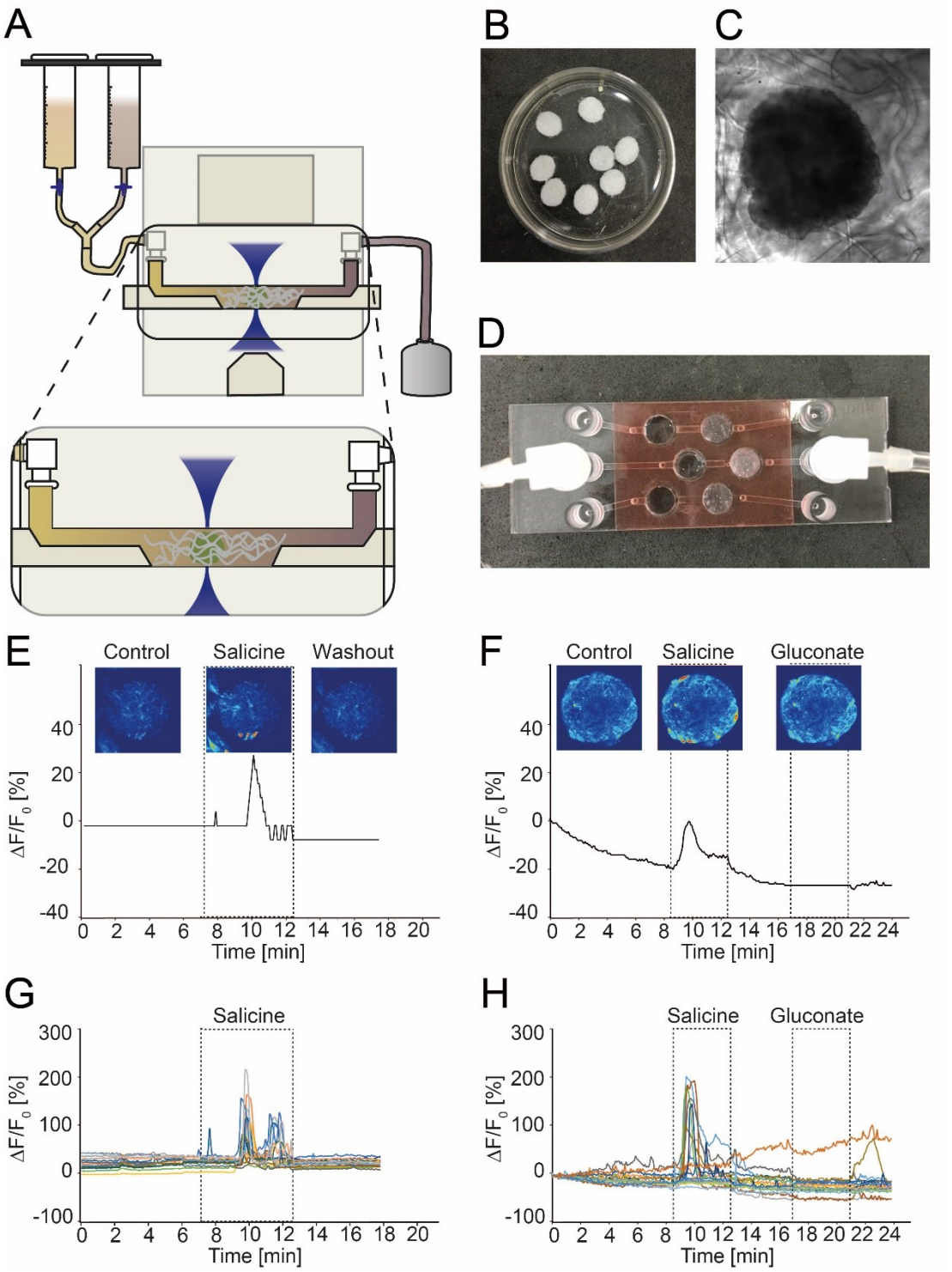

Figure 14: Perfused live cell imaging setup for confocal microscopy to study the Salicine bitter response. A) Scheme of the confocal live cell imaging setup. Syringes served as buffers reservoirs and were connected to microfluidic slides (ibidi) with tubes, y-adapters and Luer locks. The perfusion was gravity mediated. B) CL130 Scaffolene pads (Freudenberg) produced with a whole puncher perfectly fitted in the perfusion chambers. C) Brightfield image of a spheroid embedded in the Scaffolene mesh. D) µ-slide III 3D perfusion slide connected to tubes. Only the second of the two reservoirs was filled with spheroids and Scaffolene. E-H) Representative Ca^{2+} responses of HTC-8-G-GECO cells cultured for 5-7 days in Dynarray chips (E, G) or as spheroids (F, H). The mean fluorescence intensity of the whole cavity (E) and the whole spheroid (F) was plotted versus time and translated as color code with blue corresponding to low and red to high $[Ca^{2+}]$cyt. The perfusion was started after 4.2 min and Salicine (20 mM) and Gluconate (20 mM) were applied as indicated by the dashed boxes. G, H) Single cell responses of the same Dynarray and spheroid shown in (E) and (F), respectively. Figure adapted and modified from von Molitor et al. 2020a.

3.5 Analysis of Saccharin-induced Ca2+ transients in HTC-8-G-GECO spheroids

In the next step, it was tested whether HTC-8-G-GECO spheroids respond also to other bitter substances such as Saccharin. Stimulating HTC-8-G-GECO spheroids with increasing Saccharin concentrations resulted in a transient elevation of cytosolic Ca^{2+} concentrations in a dose-dependent fashion with an EC_{50} of 1.8 mM (Figure 15A, B). When extracellular Ca^{2+} was omitted, no response was observed (Figure 15C). These results are consistent with Saccharin responses already described in HTC-8 monolayer culture (Hochheimer et al. 2014) and suggest that Saccharin-mediated Ca^{2+} transients require extracellular Ca^{2+}, but do not relay on Ca^{2+} release from intracellular stores.

Consistent to the application of Salicine (Figure 14F, H), also Saccharin (Figure 15D) stimulation led to larger Ca^{2+} elevations on the spheroid rim than in the core, which accommodated to the observation that cells on the spheroid periphery had a different morphology with a larger size and Golgi apparatus (Figure 11C). This prompted the addition of spatial information to the quantitative analysis. With an ImageJ macro one spheroid z-plane image was divided in four concentric regions, termed R1-R4 from the border of the spheroid to the core (Figure 15D, lower row). Dose-response curves were determined for each individual ring. The outer ring displayed higher sensitivity and potency, while inner rings had progressively increasing EC_{50} values moving towards the spheroid center: 1.06, 1.50, 1.67, 1.46 mM, respectively (Figure 15E). The differences between the responses of the four rings were evident for all tested Saccharin concentrations (Figure 15F–H). In outer rings (R1, R2), the Ca^{2+} transients were not only higher but also started to respond simultaneously earlier than inner rings (R3, R4).

To better characterize these observations, kinetics of the mean fluorescence amplitudes were quantified more precisely (Figure 15I–L). When spheroids were stimulated with an exemplarily concentration of 5 mM Saccharin, R1 responded with a significantly earlier (T_{peak}) (Figure 15J) and higher fluorescence peak (Figure 15I) that had a faster onset (T_{slope}) (Figure 15K) compared to fluorescence peaks of inner rings. In contrast, the time period from the onset to the peak was identical in all regions (Figure 15L).

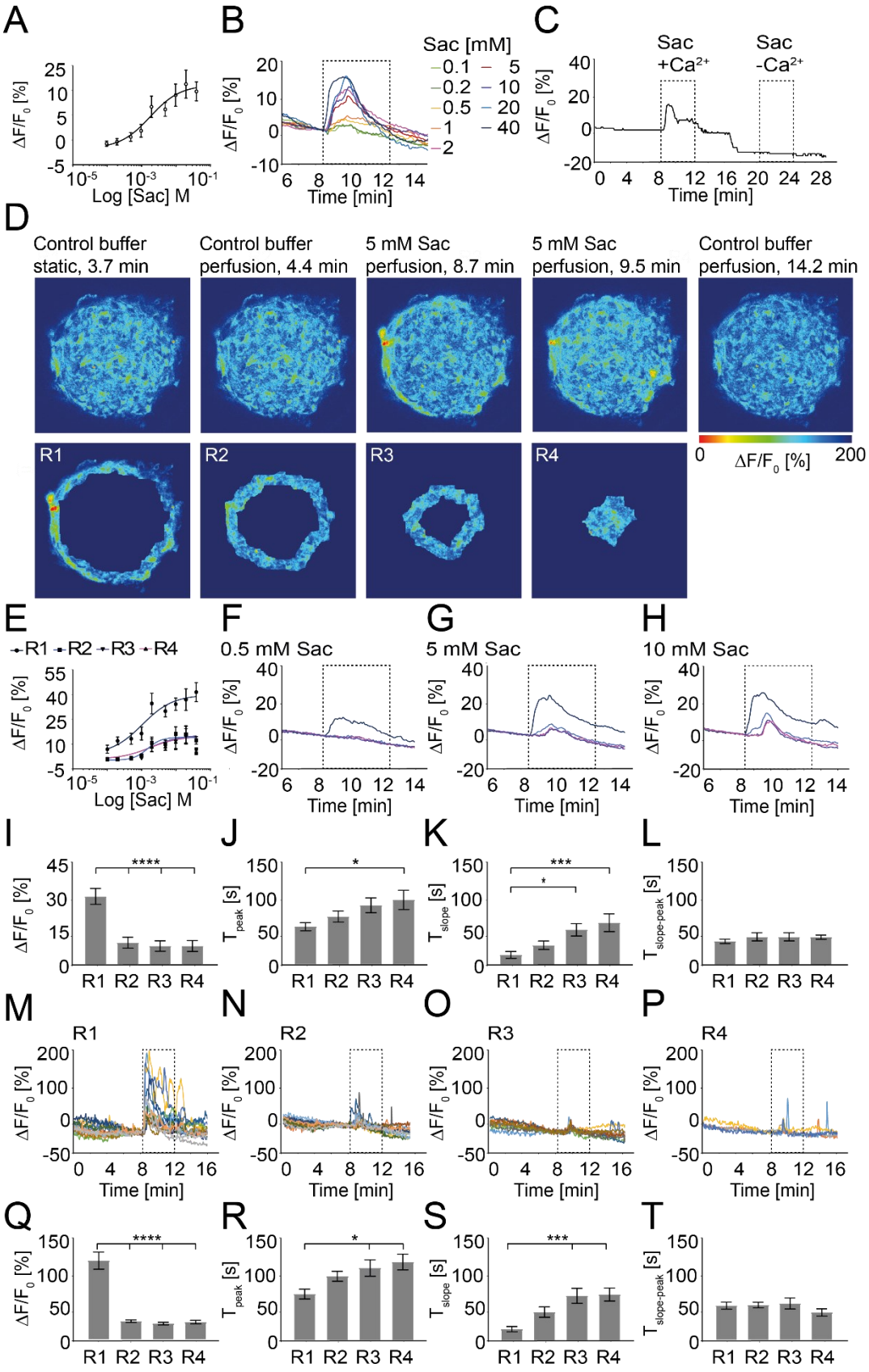

Figure 15: Characterization of the Saccharin response in HTC-8-G-GECO spheroids. HTC-8-G-GECO cells were cultured as spheroids for 5-7 days and perfused with either control solution or Saccharin (Sac). Resulting Ca^{2+} transients were recorded with live cell confocal imaging of G-GECO fluorescence. Saccharin stimulation is depicted by dashed lines. A) Saccharin dose-response curve of maximum fluorescence intensity calculated from whole spheroid responses: EC_{50} = 1.8 mM. B) Time course of the mean fluorescence measured in the whole

spheroid area upon stimulation with increasing Saccharin concentrations of n ≥ 5 spheroids. Error bars were left out for clarity. C) The Saccharin response was absent upon external Ca^{2+} depletion. D) Confocal images of a representative time course experiment upon Saccharin (5 mM) stimulation. For the analysis, spheroids were divided in four concentric rings (R1-R4, upper row), and single cells were selected in the rings as ROIs. G-GECO fluorescence intensity was translated as color code with blue corresponding to low (0% $\Delta F/F_0$) and red to high $[Ca^{2+}]_{cyt}$ (200% $\Delta F/F_0$). E) Dose-response curve for Saccharin in the four concentric rings. EC_{50}: R1 = 1.06 mM, R2 = 1.50 mM, R3 = 1.67 mM and R4 = 1.46 mM. F-H) Mean responses to 0.5, 5 and 10 mM Saccharin application in the four rings: R1: dark blue, R2: light blue, R3: purple, R4: pink. Error bars were left out for clarity. I-L) Quantitative ring fluorescence analysis upon stimulation with 5 mM Saccharin of maximum intensity (I), time to peak (J), time to slope (K) and time slope to peak (L) as a function of the concentric rings. Graphs show mean ± SEM of n ≥ 5 spheroids. M-P) Representative cell traces of individual cells to 5 mM Saccharin selected as ROIs in the four rings. Q-T) Quantitative single cell fluorescence analysis of maximum intensity (Q), time to peak (R), time to slope (S) and time slope to peak (T) as a function of the different rings. Bars show mean ± SEM of n ≥ 5 spheroids. Statistics used one-way ANOVA with multiple comparison. Figure adapted and modified from von Molitor et al. 2020a.

Next, a second macro was applied which permitted the analysis of individual cells selected in the four concentric rings instead of analyzing the bulk response of all cells. Panels M-P of Figure 15 depict these individual cell traces upon application of 5 mM Saccharin. Single cell analysis confirmed the quantitative ring analysis as the amplitude and time courses (T_{peak}, T_{slope}, $T_{slope\text{-}peak}$) of evoked Ca^{2+} transients depended on the cell position within the spheroid. Again, Ca^{2+} transients with larger amplitudes were recorded in cells of R1, while cells selected in inner rings evoked lower peaks (Figure 15Q) and delayed responses (T_{peak}, T_{slope}) (Figure 15R, S). However, the time from the onset to the peak ($T_{slope\text{-}peak}$) was comparable in all cells independent of their position (Figure 15T) suggesting that HTC-8-G-GECO cells may us a common signaling mechanism in all the spheroid regions that propagates from the spheroid periphery (R1) to the center (R4).

3.6 Analysis of ATP-induced Ca^{2+} transients in HTC-8-G-GECO spheroids

In response to gustatory stimulation, taste cells release neurotransmitters for intercellular communication. One of the principal neurotransmitters of the taste bud is ATP which is released from type II cells to convey information to afferent nerve fibers, but also to induce autocrine and paracrine feedback onto type II and type III cells, respectively (Huang et al. 2007; Huang et al. 2009; Kinnamon and Finger 2013). ATP-dependent signaling has been reported to induce intracellular Ca^{2+} release upon binding of ATP to either P2RX2 or P2RY1 purinergic receptors on type II or P2YR4 on type III cells (Baryshnikov et al. 2003; Huang et al. 2009; Dando and Roper 2009). To address if ATP is involved in the Saccharin response of HTC-8-G-GECO spheroids, fluorescence changes were evaluated upon perfusion with 1 mM ATP which corresponds to a saturating concentration in rodent taste cells (Kim et al. 2000; Baryshnikov et al. 2003; Fedorov et al. 2007). Comparison of ATP-evoked transients to a treatment with 20 mM Saccharin revealed Ca^{2+} transients with fairly diverse onset kinetics (Figure 16A-C). Indeed, ATP responses were shorter ($T_{slope\text{-}peak}$) (Figure 16G) as peaks were reached faster (T_{peak}) (Figure 16E) in all spheroid regions. Onset (T_{slope}) (Figure 16F) and maximum amplitudes (Figure 16D) of ATP responses were, tough, similar to those of the

Saccharin response, and also ATP-evoked Ca^{2+} transients increased from the spheroid rim to the center. Further, analysis of individual HTC-8-G-GECO cell responses showed that most cells responded to both stimuli, ATP and Saccharin (Figure 16C).

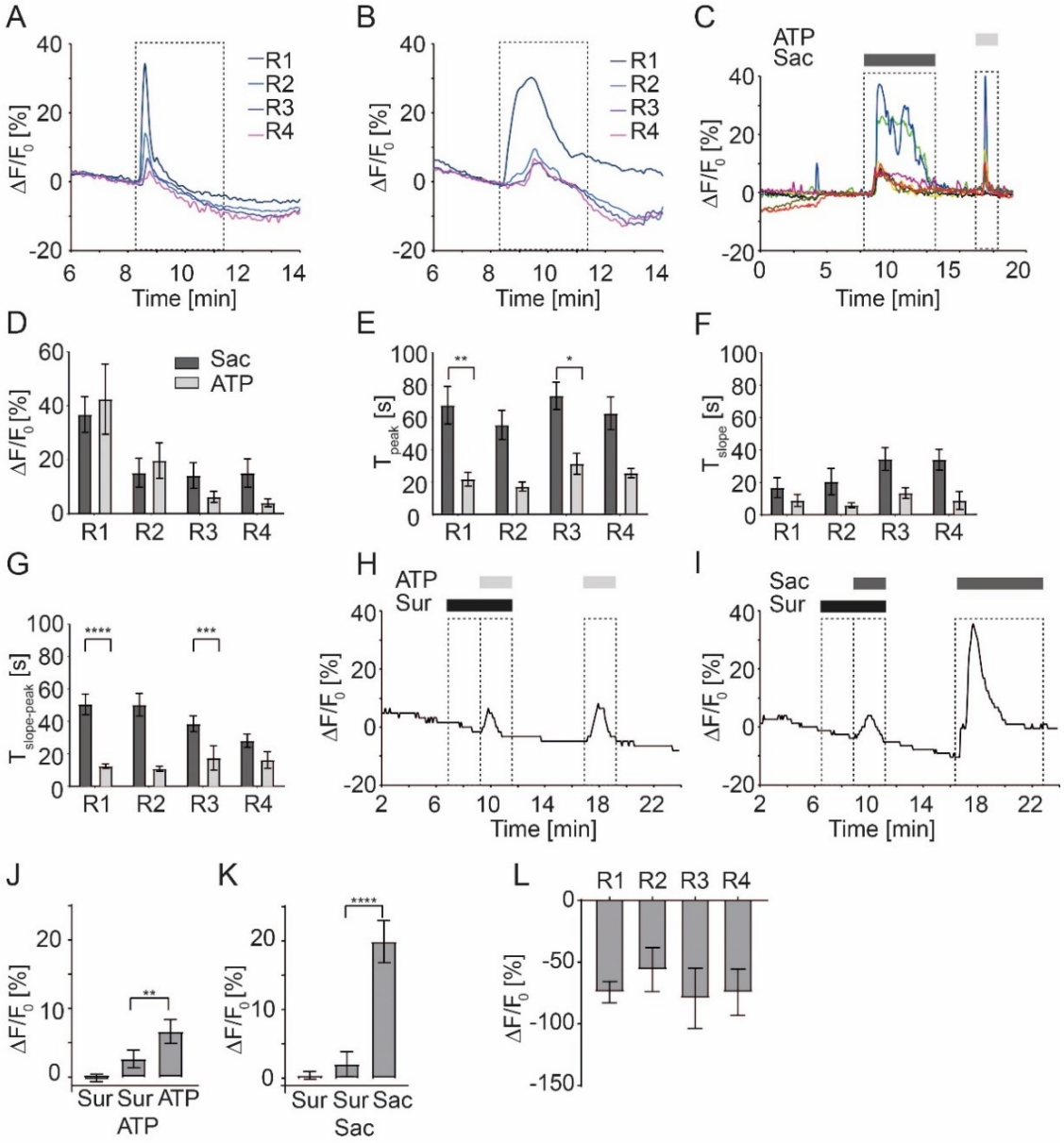

Figure 16: The Saccharin response requires ATP. HTC-8-G-GECO cells were cultured as spheroids for 5-7 days, stimulated with ATP and/or Saccharin (Sac) as indicated and subsequent Ca^{2+} responses were analyzed with confocal live imaging. A, B) Time course of mean G-GECO fluorescence changes in the four spheroid rings (R1-R4) upon perfusion with 1 mM ATP (A) and 20 mM Saccharin (B). Error bars were left out for clarity. C) Representative single cell traces of a spheroid stimulated first with ATP (1 mM) and then with Saccharin (10 mM). The majority of cells respond to both stimuli. D–G) Quantitative analysis of maximum intensity (D), time to peak (E), time to slope (F) and time slope to peak (G) measured with the ring analysis upon 1 mM ATP or 20 mM Saccharin stimulation. Bars show mean ± SEM of n ≥ 5 spheroids. Statics were performed using two-way ANOVA with multiple comparison. H–L) The purinergic antagonist Suramin reduced Ca^{2+} transients triggered by ATP or Saccharin. H, I) Representative whole spheroid traces upon addition of 10 µM ATP (H) or 2 mM Saccharin (I) with and without 100 µM Suramin (Sur). Quantitative whole spheroid G-GECO fluorescence analysis revealed that Suramin significantly inhibits ATP (J) and Saccharin (K) responses without inducing a response itself. Bars show mean ± SEM of n ≥ 5 spheroids. L) Quantitative analysis of the reduction of Saccharin-induced Ca^{2+} transients by Suramin in the different rings. Bars show mean ± SEM of n ≥ 5 spheroids. Statistics were performed using one-way ANOVA with multiple comparison. Figure adapted and modified from von Molitor et al. 2020a.

The purinergic P2 antagonist Suramin was used to unravel the role of intercellular purinergic communication in Saccharin responses. Since Suramin, at high concentrations, has been described to modulate receptor-G-protein coupling (Lehmann et al. 2002), a lower Suramin concentration (100 µM) was used in combination with a non-saturating concentration of ATP (10 µM) or Saccharin (2 mM). Spheroids were first perfused with Suramin alone, which induced no G-GECO fluorescence changes (Figure 16J, K), and then in combination with either ATP (Figure 16H, J) or Saccharin (Figure 16I, K). Both, ATP and Saccharin responses were significantly reduced in the presence of Suramin in whole spheroid analysis. As the relative inhibition of the Saccharin response was equivalent in all rings (Figure 16L), it can be proposed that ATP plays an essential role and is involved in bitter responses equally in all spheroid regions. In the outer rims, ATP possibly functions as an autocrine signal that enhances the taste responses in the cells, while in the inner rings it may act in a paracrine manner to amplify bitter responses and support their trafficking towards the center.

3.7 Compound diffusion into HTC-8-G-GECO spheroids induced a delay in Ca^{2+} transients

To verify whether the responses observed in the spheroid core were caused by either i) signal transmission from outer to inner regions, or ii) via compound diffusion into the spheroid, the red fluorescent dye Sulforhodamine B was added as a tracer. Similarly to ATP and Saccharin, also Sulforhodamine B carries negative charges and is small enough to pass through the intercellular space (Polat et al. 2011). When Sulforhodamine B perfusion was applied, a red fluorescence signal was detected, fist in the perfusion medium and the Scaffolene fibers, and then in the spheroid (Figure 17A) where it constantly raised. In the outer ring the Sulforhodamine B fluorescence signal developed faster (T_{sope}) (Figure 17D, E) but in inner rings fluorescence signals reached similar (100 µM) or even higher (10 µM) peaks compared to the rim (Figure 17F). In contrast to Ca^{2+} transients, Sulforhodamine B accumulated in the spheroid core and continued to rise over time without reaching a plateau. Combining the information of the mean spheroid radius (r = 110.48 ± 4.06 µm) with the time interval between the signal onset on the border and in the core (T_{slope}(R4) - T_{slope}(R1) = 10.3 ± 1.47 s), a diffusion coefficient of $1x10^{-5}$ cm^2/s was calculated for Sulforhodamine B in HTC-8-G-GECO spheroids. Accordingly, small negatively charged molecules can diffuse through several cell layers into the spheroid core and accumulate there. After washout, Sulforhodamine B fluorescence signals decreased to control levels, first in outer and subsequently in inner regions (Figure 17F).

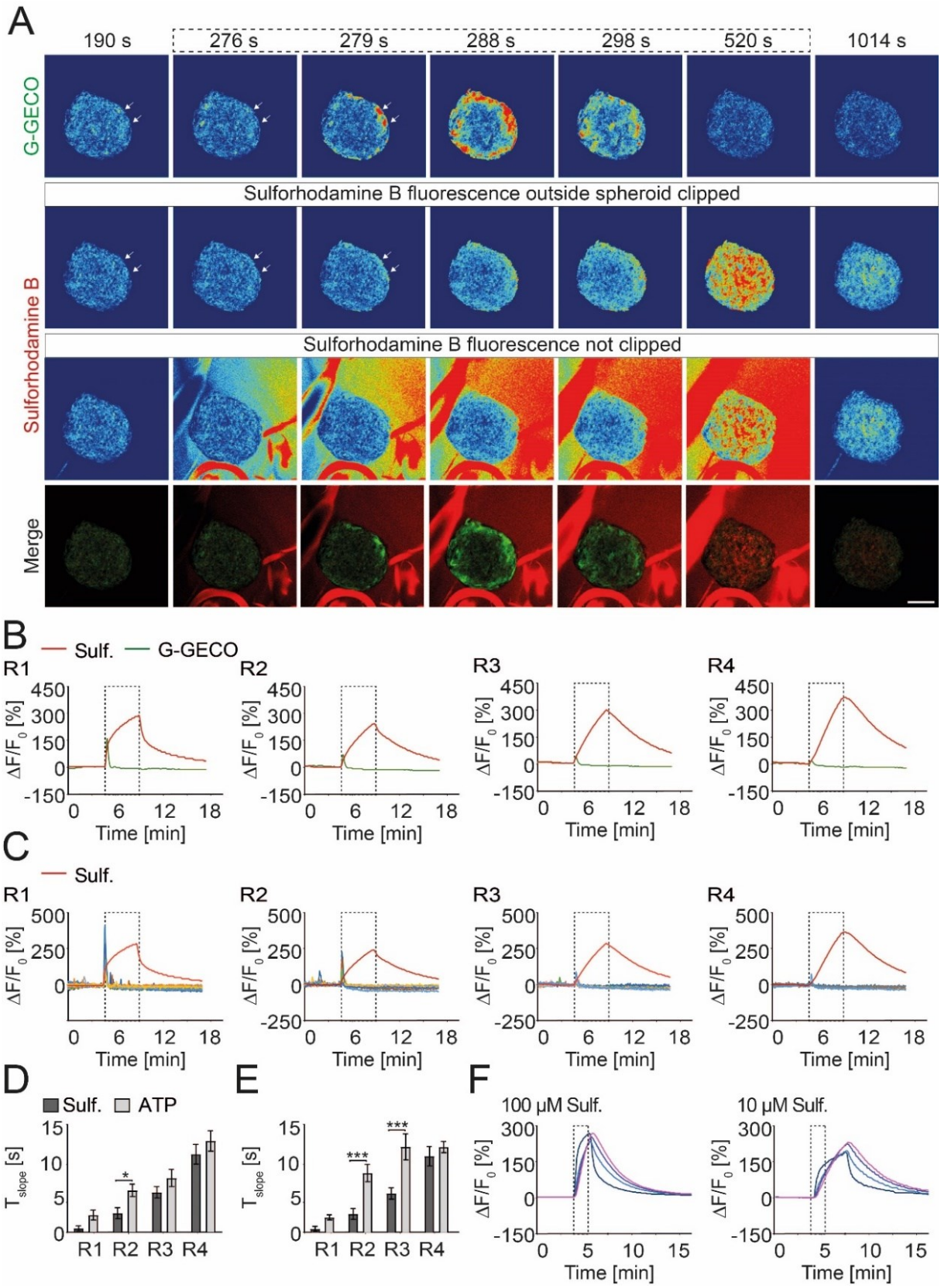

Figure 17: Negatively charged compounds can propagate into spheroid cores. HTC-8-G-GECO spheroids were cultured for 5-7 days and perfused with either 1 mM ATP or 10 µM Sulforhodamine B (Sulf.) as indicated by dashed boxes. A) Confocal images of a representative experiment showing G-GECO and Sulforhodamine B signals at selected time points. Rainbow colors correspond to the fluorescence intensity, blue corresponds to $\Delta F/F_0$ = 0% and red to $\Delta F/F_0$ = 200% for G-GECO and = 350% for Sulforhodamine B. For better visualization, Sulforhodamine B images are shown either with background fluorescence (third line) or upon removal of fluorescence signals outside

the spheroid (second line panels). Merged images of G-GECO (green) and Sulforhodamine B (red) fluorescence are shown in bottom panels. Scale bar: 100 µm. B, C) Traces of ATP-induced Ca^{2+} signals and Sulforhodamine B kinetics of the experiment shown in (A) using ring (B) or single cell analysis (C). D, E) Quantitative comparison of time to slope between Sulforhodamine B and G-GECO signals using ring (D) or single cell analysis (E). Bars show mean ± SEM of n = 12 spheroids. Statistics used one-way ANOVA with multiple comparison. F) Mean traces of whole spheroid fluorescence changes in the four concentric rings (R1: dark blue, R2: light blue, R3: purple, R4: pink) upon addition of 100 µM (n = 5 spheroids) and 10 µM (n = 6 spheroids) Sulforhodamine B. Error bars were left out for clarity. Figure adapted and modified from von Molitor et al. 2020a.

To correlate the time resolution of the ATP-induced Ca^{2+} transients with the Sulforhodamine B diffusion, Sulforhodamine B and G-GECO fluorescence were recorded simultaneously. Both signal intensities started to rise in R1 and propagated to inner rings (Figure 17A-C). In the depicted representative experiment (Figure 17A), the Sulforhodamine B signal started to increase first at 276 s, while the onset of the G-GECO response to ATP was 3 s delayed (Figure 17A). Analysis of the responses in all four rings confirmed that both signals progressed with a phase shift (T_{slope}(G-GECO) - T_{slope}(Sulforhodamine B)) that ranged from 1.85 ± 0.49 s in R1 to 5.07 ± 1.81 s in R4. However, the signals travelled at the same velocity towards the spheroid core, as the Sulforhodamine B signal was always a few seconds faster than the G-GECO signal (Figure 17D, E). Notably, the kinetic profiles differed as the Sulforhodamine B fluorescence developed slowly and gradually, while G-GECO Ca^{2+} transients reached their maximum quickly and returned to baseline within a few seconds.

In summary, these observations suggest that the reduced Ca^{2+} amplitudes in inner rings of HTC-8-G-GECO spheroids upon gustatory stimulation are not due to limited compound diffusion. Conversely, compound diffusion kinetics were mirroring the delayed onset of Ca^{2+} responses towards the spheroid center.

3.8 Development of a perfused live cell imaging setup for LSFM

So far, taste induced Ca^{2+} transients were analyzed with confocal microscopy which uses a laser that illuminates only a specific point and a pinhole that excludes out of focus signals. Images are, thus, created in a focal plane by scanning point by point in a raster pattern (Cang et al. 2007), which improves the signal-to-noise-ratio but comes with the price of limited time resolution. Thus, only three spheroid layers could be imaged in a 5 s time interval which is insufficient to describe the whole spheroid response and record the velocity of Ca^{2+} transients. On account of this, the established live cell imaging setup was adjusted for LSFM (Figure 18A). In LSFM, a sheet of light instead of a point illuminates the whole focal plane of the sample from the side (Lehmann et al. 2002). This allowed the acquisition of more than 30 z-planes of HTC-8-G-GECO spheroids (10 times more than with the confocal acquisition) over a z-distance of 80-100 µm every 5 s, when using a slice interval of 3 µm at a stack rate of 0.2 Hz. To compare the stability of the fluorescence signal in spheroid depth between LSFM and confocal microscopy, the intensity of the mean G-GECO fluorescence signal was analyzed in

unstimulated spheroids as a function of z-depth. For LSFM, the signal intensity was well retained over 80 µm in depth, whereas with confocal microscopy the signal severely decayed already after 20 µm (Figure 18B). Thus, LSFM allowed to image 1/3 of the whole 3D structure without losing spatial and temporal resolution.

Since the vertical turn Leica TCS SP8 DLS LSFM uses laser scanning illumination perpendicular to the detection pathway, the sample had to be placed between the two LSFM mirrors, therefore, the ibidi perfusion slide could not be used, and the live cell imaging setup had to be modified accordingly (Figure 18A). Spheroids were mounted with low melting Agarose in an open U-shaped glass capillary which was retained in a µ-bottom glass petri dish filled with imaging buffer. In this way, the LSFM mirrors could be positioned around the capillary submerged in the solution. To exchange the solution, tubes were fixed with thin wires at opposite sides of the dish. Additionally, the open system needed a pump for the outflow, in order to balance the gravity mediated inflow and to avoid overflow.

The functionality of the new setup was evaluated by recording changes in G-GECO fluorescence upon perfusion with ATP (1 mM). Although the well-known LSFM shadowing effect produced striping artifacts on images (Mayer et al. 2018), as spheroids contained regions that attenuated light and reduced illumination, ATP-evoked fluorescence transients could be observed and analyzed also in spheroid depth (Figure 18C). Notably, ATP-induced fluorescence peaks were much higher at upper spheroid layers, whereas fluorescence peaks at equatorial layers were smaller (Figure 18D) and corresponded to the results obtained with confocal microscopy (Figure 18C, D lower rows). The onset of Ca^{2+} transients to the ATP stimulation was delayed compared to confocal experiments as i) it took much longer to exchange the solution in the LSFM imaging chamber, which contained 2 ml instead of the 60 ul in the µ-slide III 3D perfusion slides, and ii) compounds had to diffuse through the Agarose barrier to reach the spheroids. Thus, the LSFM live cell imaging setup needs further improvements in regard to perfusion volume and sample stabilization.

Nonetheless, the newly established LSFM live cell imaging setup allowed the acquisition of Ca^{2+} dynamics in three dimensions, which is of importance, when cells do not respond homogenously within the 3D samples or when the 3D samples are not homogenous in shape and cell type composition. Implementation of such approaches can be advantageous for the screening of new flavors in a taste bud-like 3D structure but also to study taste signaling.

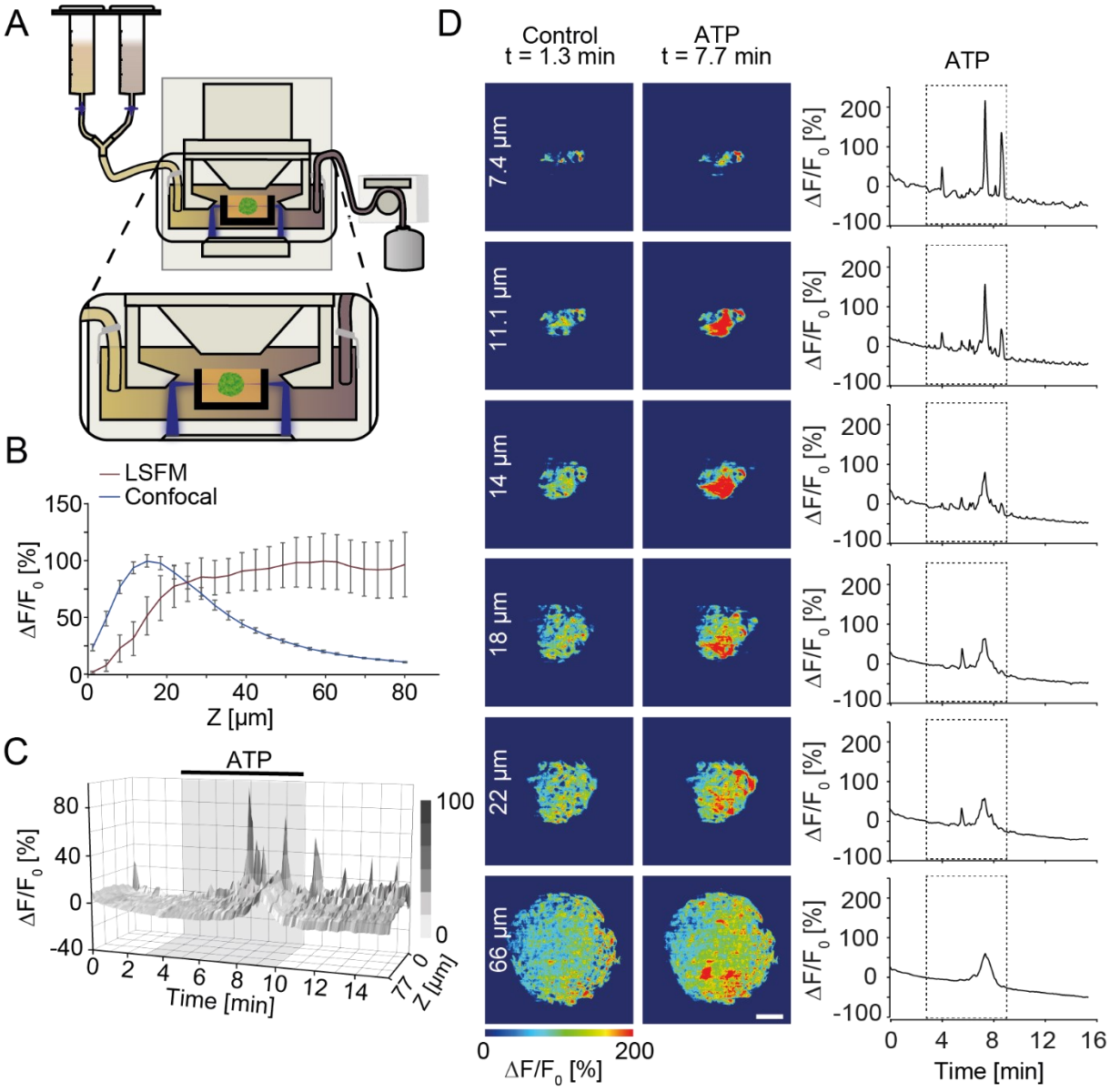

Figure 18: A perfused live cell imaging setup for LSFM. Schematic drawing of the LSFM live imaging setup. Syringes were connected via tubes, y-adapters and Luer locks to a 3.5 cm glass bottom petri dish. Tubes for in- and outflow were attached with wires. The inflow was gravity mediated, while a pump was used for the outflow. An open U-shaped glass capillary was fixed in the glass bottom dish and LSFM mirrors were positioned around. Spheroids were mounted with low melting Agarose in the glass capillary. B) Signal stability over spheroid depth of unstimulated G-GECO fluorescence for confocal (n = 8 spheroids) and LSFM (n = 4 spheroids) acquisition with 3.7 µm z-steps. Data show mean ± SEM. C) Mean ATP-induced (1 mM) Ca^{2+} transients plotted over time and spheroid depth (z) (n = 4 spheroids). Bleaching was corrected with the exponential function in ImageJ. The black bar shows the stimulation interval. D) Representative images of an HTC-8-G-GECO spheroid at different z-planes in control buffer or upon stimulation with ATP (1 mM). The color code represents G-GECO fluorescence intensity, blue corresponds to low (0% $\Delta F/F_0$) and red to high (200% $\Delta F/F_0$) [Ca^{2+}]cyt. Scale bar: 100 µm. On the right, the corresponding plots of Ca^{2+} transients are shown as a function of time. The stimulation window is indicated by dashed boxes. Figure adapted and modified from von Molitor et al. 2020a.

3.9 HTC-8-G-GECO cells responded to sugars only in 3D culture

So far, HTC-8-G-GECO spheroids have only been shown to respond to bitter compounds. However, the observed morphological differences between cells of the outer and core regions (Figure 11C) suggest that the 3D environment of spheroids may has induced changes in the expression profiles of HTC-8-G-GECO cells compared to monolayer culture. According to these observations, one may speculate that HTC-8-G-GECO spheroids might express, besides T2R, also T1R taste receptors. Indeed, upon stimulation with the nutritive sugars Fructose, Glucose and Sucrose an increase in HTC-8-G-GECO fluorescence was observed in the outer spheroid ring, while no/little responses occurred in inner regions (R2-R4) (Figure 19A-C). In contrast to Ca^{2+} transients evoked by the bitter compounds Salicine and Saccharin (compare Figure 14F, and Figure 15), which revealed a sharp peak, responses to sugars showed wider peaks with also a sharp increase but a prolonged signal decay. Only the kinetics of Sucrose-evoked Ca^{2+} transients were comparable to those of bitter compounds. Intriguingly, the unsweet sugar Cellobiose (Figure 19D) and the less sweet ranked sugar Lactose (Figure 19E) revealed comparable intensity levels, while the non-caloric artificial sweetener Acesulfame K induced no Ca^{2+} transients (Figure 19F, G).

To verify whether these sweet responses occurred only in the 3D environment of spheroids, Sucrose and Salicine stimulation was tested and compared in monolayer HTC-8-G-GECO cultures (Figure 19H), spheroids (Figure 19K) and ~12 h monolayer cultures generated from trypsinized spheroids (Figure 19N). Analyzing the single cell traces, it was evaluated whether the cells responded either specifically to Sucrose, Salicine or to both stimuli. Indeed, HTC-8-G-GECO cells responded only to Sucrose when cultured as spheroids (Figure 19L) or upon its dissociation (Figure 19O), while in permanent monolayer culture only selective responses to Salicine were observed (Figure 19I). The proportion of cells sensitive to sugars was, thus, affected by the culturing protocol. Moreover, HTC-8-G-GECO cells grown in monolayer cultures from spheroids were roundish (Figure 19P), while HTC-8-G-GECO cells are usually rather elongated and stretched when kept as monolayer (Figure 19J). Thus, these results indicate that the 3D environment has not only changed the morphologies of HTC-8-G-GECO cells but also their functionality profiles.

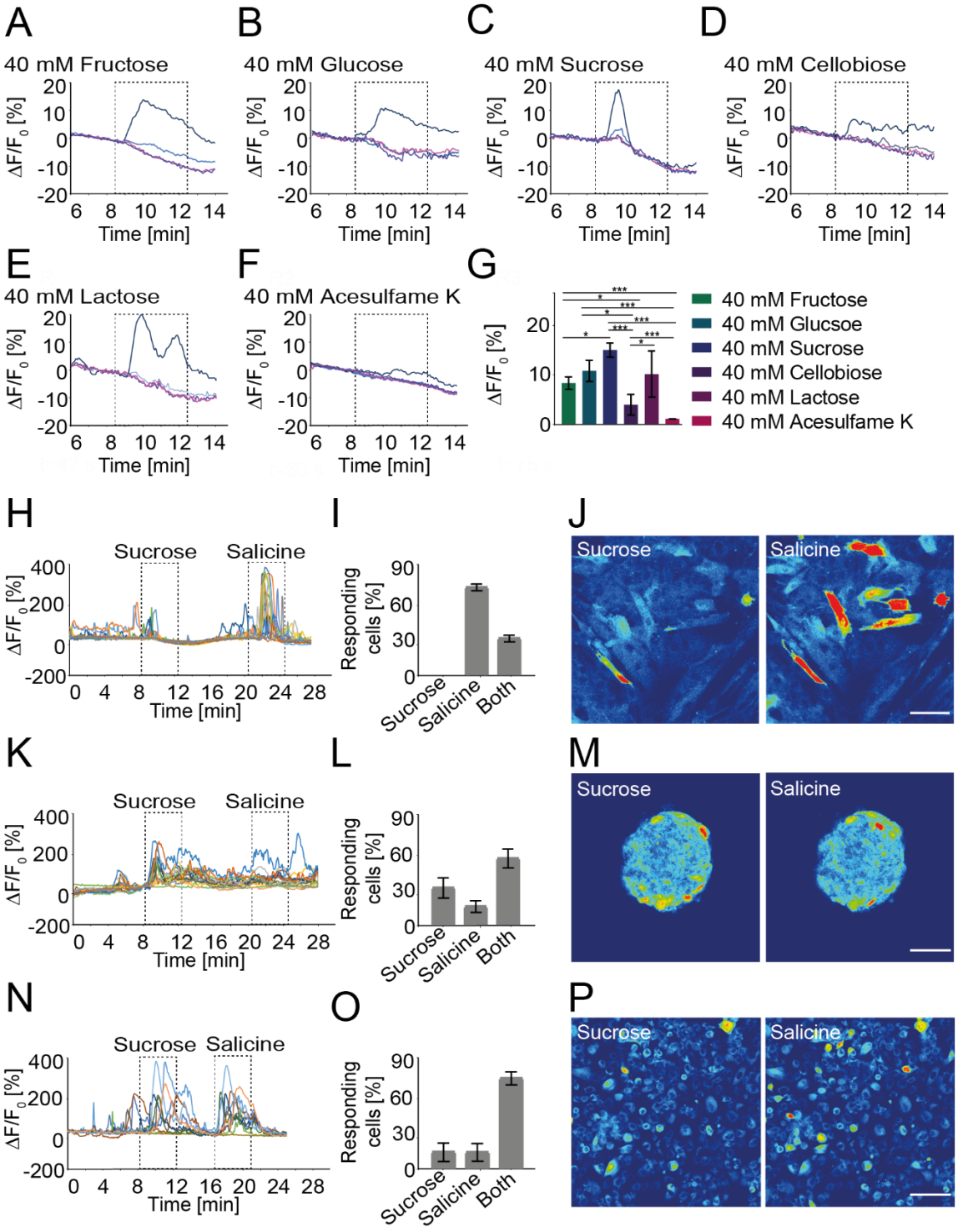

Figure 19: HTC-8-G-GECO spheroids respond to sweet stimuli upon 3D culture. HTC-8-G-GECO cells were cultured as spheroids for 5-7 days, and gustatory Ca^{2+} responses were analyzed with confocal live imaging. Dashed lines indicate stimulation intervals. A-F) Time courses of mean G-GECO fluorescence changes in the four spheroid rings (R1: dark blue, R2: light blue, R3: purple, R4: pink) upon perfusion with 40 mM sweet solutions as indicated of n ≥ 4 spheroids. Error bars were left out for clarity. G) Quantitative whole spheroid analysis of mean maximum intensity levels to the sweet compounds shown in (A-F). Bars show mean ± SEM of n ≥ 4 spheroids. Statistics used one-way ANOVA with multiple comparison. H-P) Comparison of Salicine (20 mM) and Sucrose (20 mM) responses of HTC-8-G-GECO cells grown as permanent monolayer (H-J), spheroids (K-M) or as monolayer (12 h) from trypsinized spheroids (N-P). H, K, N) Representative cell traces of individual cells. I, L, O) Bars show percentage of cells responding either specifically to Sucrose, Salicine or both stimuli (n ≥ 3 experiments). J, M, P) Representative confocal images taken during stimulation intervals. The color code represents G-GECO fluorescence intensity, blue corresponds to low and red to high $[Ca^{2+}]_{cyt}$. Scale bars: 100 µm.

3.10 Analysis of Sucrose-induced Ca^{2+} transients in HTC-8-G-GECO spheroids

Sucrose-induced Ca^{2+} transients of HTC-8-G-GECO spheroids were further characterized to compare their kinetics to those of the bitter responses. Sucrose stimulation led to robust transient elevations of cytoplasmic Ca^{2+} in a dose-dependent manner with an EC_{50} of 24.73 mM (Figure 20A, B). As for Saccharin, no response was detected in the absence of extracellular Ca^{2+} suggesting that also Sucrose responses relay on extracellular Ca^{2+} influx (Figure 20C).

Regarding regional differences, also Sucrose stimulation led to a larger Ca^{2+} increase on the spheroid rim (Figure 20D). Analyzing the data with the ImageJ ring macro confirmed higher sensitivity in the first ring, with an EC_{50} of 28.96 mM, while in R2-R4 Sucrose elicited very few small Ca^{2+} transients. This difference between the responses of the four rings was evident for all Sucrose concentrations tested (Figure 20J). As responses in R2-R4 were almost undetectable, exact fluoresce intensity numbers could not be determined for every concentration in each sample with the ring analysis. Dose-response curves of the inner rings, thus, suffer from a limited amount of available data, wherefore EC_{50} values could not be properly determined here. Thus, to characterize the kinetics of Ca^{2+} transients in the individual four rings, a plateau Sucrose concentration was used. 40 mM Sucrose evoked a significantly higher fluorescence peak in R1 compared to inner rings as observed in the Saccharin response. At difference, ring analysis revealed that all spheroid regions started to respond (T_{slope}) (Figure 20K) and reach their peak (T_{peak}) (Figure 20J) simultaneously when stimulated with Sucrose. Again, single cell analysis (Figure 20Q-P) confirmed the ring analysis. As responses in R4 could be hardly separated from the baseline activity, the kinetics of single cell responses (T_{peak}, T_{slope}, $T_{slope\text{-}peak}$) could not be determined. Likewise, in Saccharin-evoked Ca^{2+} transients, the duration ($T_{slope\text{-}peak}$) of the Sucrose response was similar in all spheroid regions (Figure 20L, T). Accordingly, also Sucrose-induced Ca^{2+} signals may underlie the same or similar signaling mechanism independent from the cells position within the spheroid. In contrast to Saccharin, the signal onset of Sucrose-induced Ca^{2+} transients was not delayed in inner regions. However, Sulforhodamine B experiments suggested that compounds require a defined period to diffuse into the spheroid core. The observed differences may have three possible explanations: i) the time intervals used (5 s) may be too long to resolve the propagation of Sucrose-induced Ca^{2+} transients, ii) Sucrose diffuses faster than Saccharin, or iii) the Sucrose response uses a different signaling mechanism. Indeed, direct comparison of Sucrose and Saccharin kinetics revealed that the Saccharin response in the first ring started earlier (Figure 20W), reached the peak faster (Figure 20V) and had a shorter duration (Figure 20X), tough Sucrose and Saccharin transients did not differ significantly in their maximum intensity levels (Figure 20U).

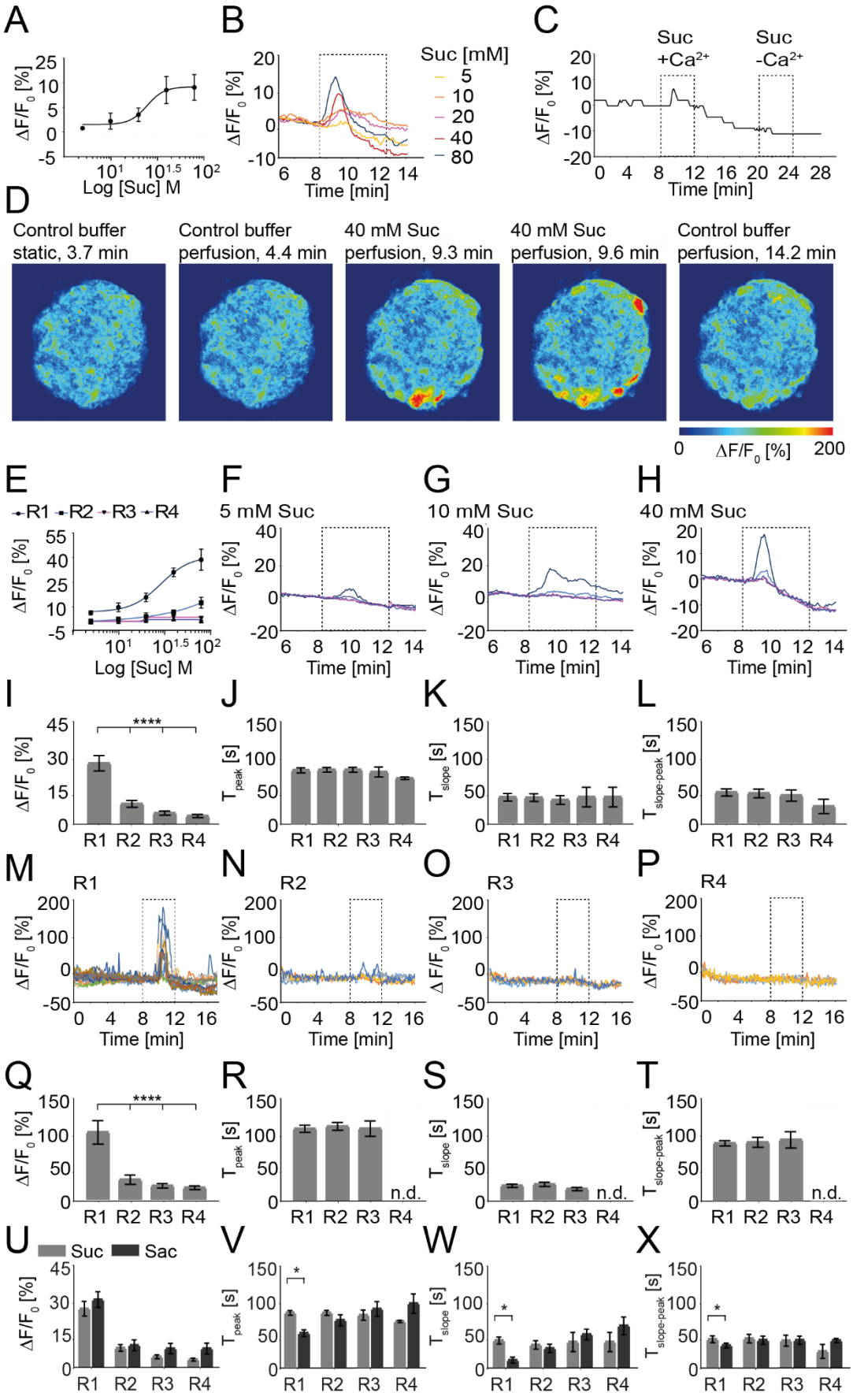

Figure 20: Characterization of Ca^{2+} responses to Sucrose in HTC-8-G-GECO spheroids. HTC-8-G-GECO cells were cultured as spheroids for 5-7 days and perfused with Sucrose (Suc) as indicated by dashed lines. Ca^{2+} transients were recorded with confocal live cell imaging. A) Sucrose dose-response curve of maximum

fluorescence intensity calculated from whole spheroid analysis; EC_{50} = 24.7 mM. B) Mean traces of whole spheroid responses to increasing Sucrose concentrations of n ≥ 5 spheroids. Error bars were left out for clarity. C) The Sucrose (40 mM) response was absent upon external Ca^{2+} depletion. D) Confocal images of a representative experiment upon Sucrose (40 mM) stimulation. The color code represents G-GECO fluorescence intensity, blue corresponds to low (0% $\Delta F/F_0$) and red to high (200% $\Delta F/F_0$) $[Ca^{2+}]_{cyt}$. E) Dose-response curve for Sucrose of the four concentric rings. EC_{50} values could not be determined for R2-R4. EC_{50} for R1 = 28.96 mM. F-H) Mean intensity traces in the four concentric rings (R1: dark blue, R2: light blue, R3: purple, R4: pink) to 5, 10 and 40 mM Sucrose. Error bars were left out for clarity. I-L) Quantitative ring fluorescence analysis upon Sucrose (40 mM) stimulation: maximum intensity (I), time to peak (J), time to slope (K) and time slope to peak (L) are shown for the responses of the four concentric rings. Graphs show mean ± SEM of n ≥ 5 spheroids. M-P) Representative traces of individual cells in response to 40 mM Sucrose. Q-T) Quantitative single cell analysis of maximum intensity (Q), time to peak (R), time to slope (S) and time slope to peak (T) in the four rings. In panels (R-S) data for R4 could not be detected (n.d.) as Ca^{2+} transients were not high enough. Data show mean ± SEM of n ≥ 5 spheroids. U-X) Quantitative comparison of maximum intensity (U), time to peak (V), time to slope (W) and time slope to peak (X) measured with the ring analysis upon 40 mM Sucrose or 5 mM Saccharin (Sac) stimulation. Data show mean ± SEM of n ≥ 5 spheroids. Statistics used two-way ANOVA with multiple comparison.

3.11 Analysis of KCl-induced Ca^{2+} transients in HTC-8-G-GECO spheroids

Type III cells are characterized by SNAP25 expression which is a t-SNARE protein involved in vesicle fusion with the membrane to release neurotransmitters (Yang et al. 2000). Since HTC-8 cells have been previously described to express SNAP25 in monolayer culture (Hochheimer et al. 2014), and SNAP25-positive mouse taste cells responded to KCl depolarization (DeFazio et al. 2006), it was tested if also HTC-8-G-GECO spheroids respond to KCl depolarization with Ca^{2+} transients.

Indeed, analysis of the four concentric regions revealed, that cells on the periphery (R1) responded with significantly larger Ca^{2+} transients, while Ca^{2+} responses in inner rings were hardly detectable (R2-R4) (Figure 21A, B, F). In all spheroid regions, Ca^{2+} transients started (T_{slope}) concurrently (Figure 21D) and also the peaks (T_{peak}) were reached simultaneously (Figure 21C). This result is at difference with Sulforhodamine B that required a certain time to diffuse into the spheroid center. However, a positively charged ion like K^+ may diffuse much faster than a small negatively charged molecule. Alternatively, the time interval (5 s) used for image acquisition could be too long to resolve a temporal delay due to diffusion. The time between the onset and the peak ($T_{slope\text{-}peak}$) was similar in all concentric regions (Figure 21E), suggesting that KCl-mediated Ca^{2+} signals occur with a similar signaling mechanism in the whole spheroid.

Notably, quantitative cell analysis revealed that 90% of responding cells elicited Ca^{2+} transients to KCl and Fructose stimulation (Figure 21H, I). Single cell traces further confirmed that individual cells were sensitive to Fructose, Salicine and KCl (Figure 21G, H). However, this is in contrast with SNAP25-positive mouse type III cells, which specifically responded only to KCl depolarization but not gustatory stimulation (DeFazio et al. 2006). Thus, these data suggest that HTC-8-G-GECO cells share characteristics of both, type II and type III cells when grown as spheroid. Fitting these observations, a subpopulation of type III cells positive for

SNAP25 and responding to bitter and sweet stimulation via PLCβ3 and Ca^{2+} release from stores was previously described in mice (Banik et al. 2020). Accordingly, some HTC-8-G-GECO cells within the spheroid may resemble such broadly responding cells. Fewer cells within the spheroid responded to only a specific stimulus and may represent tightly tuned cells.

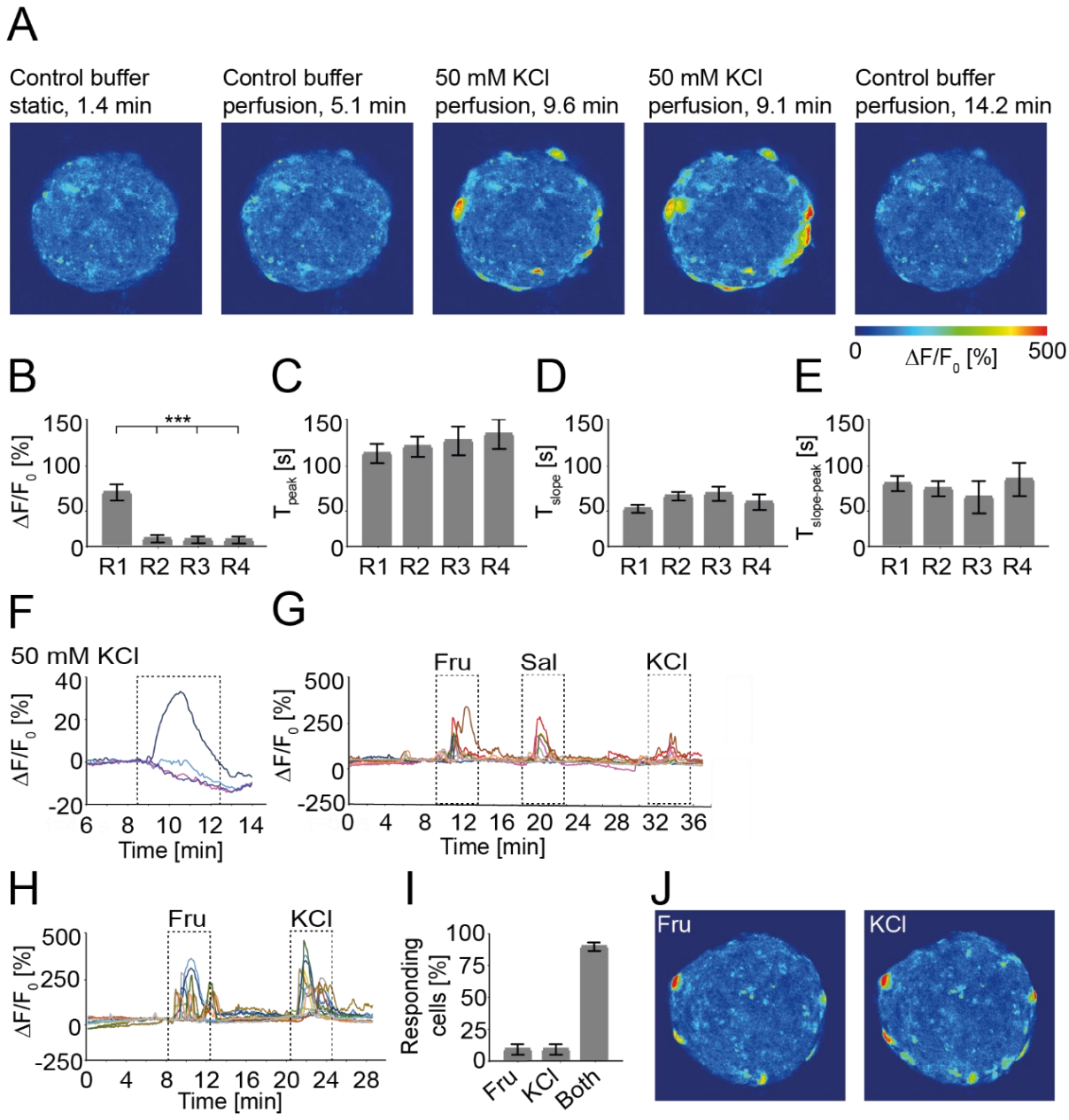

Figure 21: Characterization of Ca^{2+} responses to KCl depolarization in HTC-8-G-GECO spheroids. HTC-8-G-GECO cells were cultured as spheroids for 5-7 days. Ca^{2+} transients were recorded with confocal live cell imaging upon spheroid perfusion with 50 mM KCl. A) Exemplary HTC-8-G-GECO spheroid responding to KCl. The color code represents G-GECO fluorescence intensity, blue corresponds to low (0% $\Delta F/F_0$) and red to high (500% $\Delta F/F_0$) $[Ca^{2+}]_{cyt}$. B-E) Quantitative ring fluorescence analysis upon KCl stimulation: maximum intensity (B), time to peak (C), time to slope (D) and time slope to peak are shown for responses of the four concentric regions (R1-R4). Graphs show mean ± SEM of n ≥ 4 spheroids. Statistics used one-way ANOVA with multiple comparison. F) Mean traces of ring responses (R1: dark blue, R2: light blue, R3: purple, R4: pink) to KCl of n ≥ 4 spheroids. Error bars were left out for clarity. G, H) Representative traces of single cells showing that HTC-8-G-GECO cells in spheroids respond to Fructose (40 mM), Salicine (40 mM) and KCl (50 mM). I) Bars show percentage of cells responding to either only Fructose, KCl or both stimuli (n ≥ 3 experiments). J) Representative images of the experiment depicted in (H) during the stimulation window.

3.12 Progenitor cells as a promising source to gain sweet-sensitive cells

In vivo, taste cell progenitors give rise to mature taste cells of three different types. Although HTC-8 cells express a pool of stem cell maintenance markers (LGR5, OCT4, BMI1) and may be only partly differentiated (Hochheimer et al. 2014), their differentiation profile is probably already primed towards type II bitter-sensitive cells. An alternative source for the generation of sweet-sensitive taste cells could be the human taste progenitor cell line HTP-76, which was also obtained from human fungiform papillae, but via a procedure that selected only progenitors (confidential), positive for the stem cell marker SOX9 and LGR6 (Riedel et al. 2016). HTP-76 cells already differ from HTC-8 cells by shape; while HTC-8 cells are elongated and spindle formed, HTP-76 cells have a rather roundish morphology (Figure 22A). Being in an undifferentiated state, HTP cells might be able to specifically differentiate into sweet-sensitive type II cells. The knowledge of how to direct this differentiation is, though, still missing. As HTP-76 cells were so far only grown as monolayer, again, the introduction of a third dimension might natively induce the expression of T1Rs. Therefore, spheroids and Dynarray cultures based on the cell line HTP-76 were tested as potential 3D models.

HTP-76 cells were unable to form spheroids by themselves and the addition of promoting additives, such as BME or matrigel led to bulky cell aggregates which did not include all cells. Instead, co-cultures with HTC-8-G-GECO cells revealed roundish spheroids already on d1 (Figure 22B) which, however, developed buddings on later culture stages (d4). Subsequent immunostaining with Phalloidin, which labels F-actin, showed that these buddings were formed by HTP-76 cells, whereas HTC-8-G-GECO cells formed the inner core (Figure 22C). Conversely, in Dynarray chips coated with Collagen HTP-76 cells grew as monoculture (Figure 23A) and in co-cultures with HTC-8-G-GECO cells. In co-culture, HTP-76 cells filled the core of the cavity and were enwrapped by HTC-8-G-GECO cells (Figure 23B). Accordingly, the cellular distribution in Dynarray chips may rather resemble that in native taste buds, where progenitor cells reside below mature taste cells which are in contact with the saliva at the taste pore (Figure 1). Further, immunostaining with anti-Cleaved Caspase 3 and anti-Ki67 revealed few apoptotic and some proliferating cells throughout the chip, respectively (Figure 23C). Similar to monolayer culture (Riedel et al. 2016), HTP-76 cells expressed also in Dynarray chip cultures the progenitor marker KRT14, while KRT20, an indicator for differentiation was still absent (Figure 23C). If HTP-76 cells express T1R2/T1R3 was not determined so far, due to lack of reliable antibodies and of G-GECO expression, required for live cell imaging. Possible alternatives to investigate the presence of sweet taste receptors in HTP-76 cells would be i) to use chemical Ca^{2+}-sensitive fluorescence dyes, ii) RNA sequencing or iii) *in situ* hybridization.

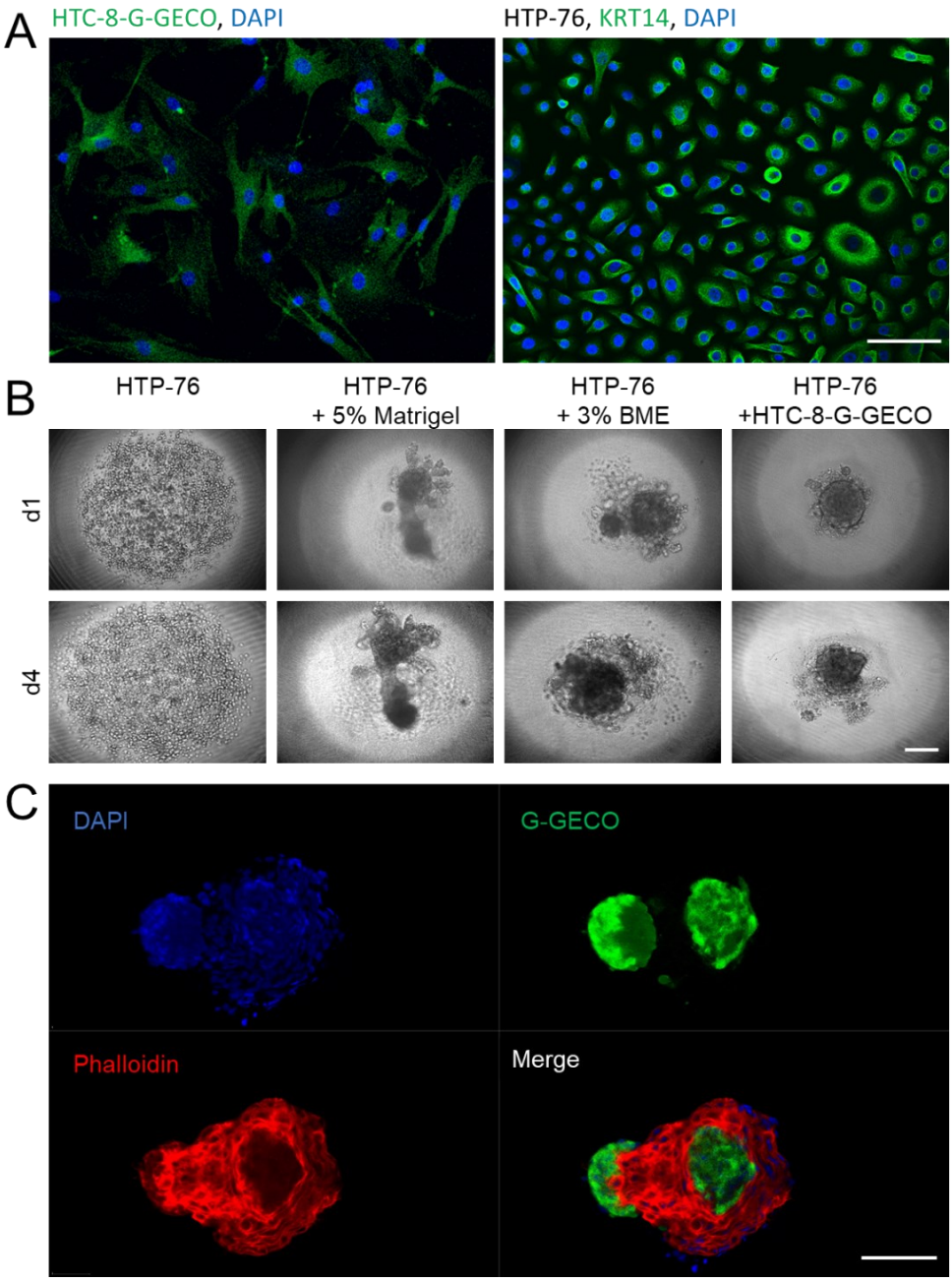

Figure 22: Characterization of HTP-76 progenitor spheroids. A) While HTC-8-G-GECO cells have an elongated morphology, HTP-76 cells are smaller and rounder. Nuclei were stained with DAPI and HTP-76 cell bodies with anti-KRT14, while HTC-8 cells expressed endogenous G-GECO. Scale bar: 100 µm. B) $0.5x10^3$ HTP-76 cells were cultured for 4 days in different conditions as indicated to form spheroids. Scale bar: 200 µm. C) 3D view of an HTP-76/HTC-8-G-GECO ($0.25x10^3$ cells of each type) spheroid co-culture cleared with Glycerol. Nuclei were stained with DAPI and actin filaments with Phalloidin. Scala bar: 100 µm.

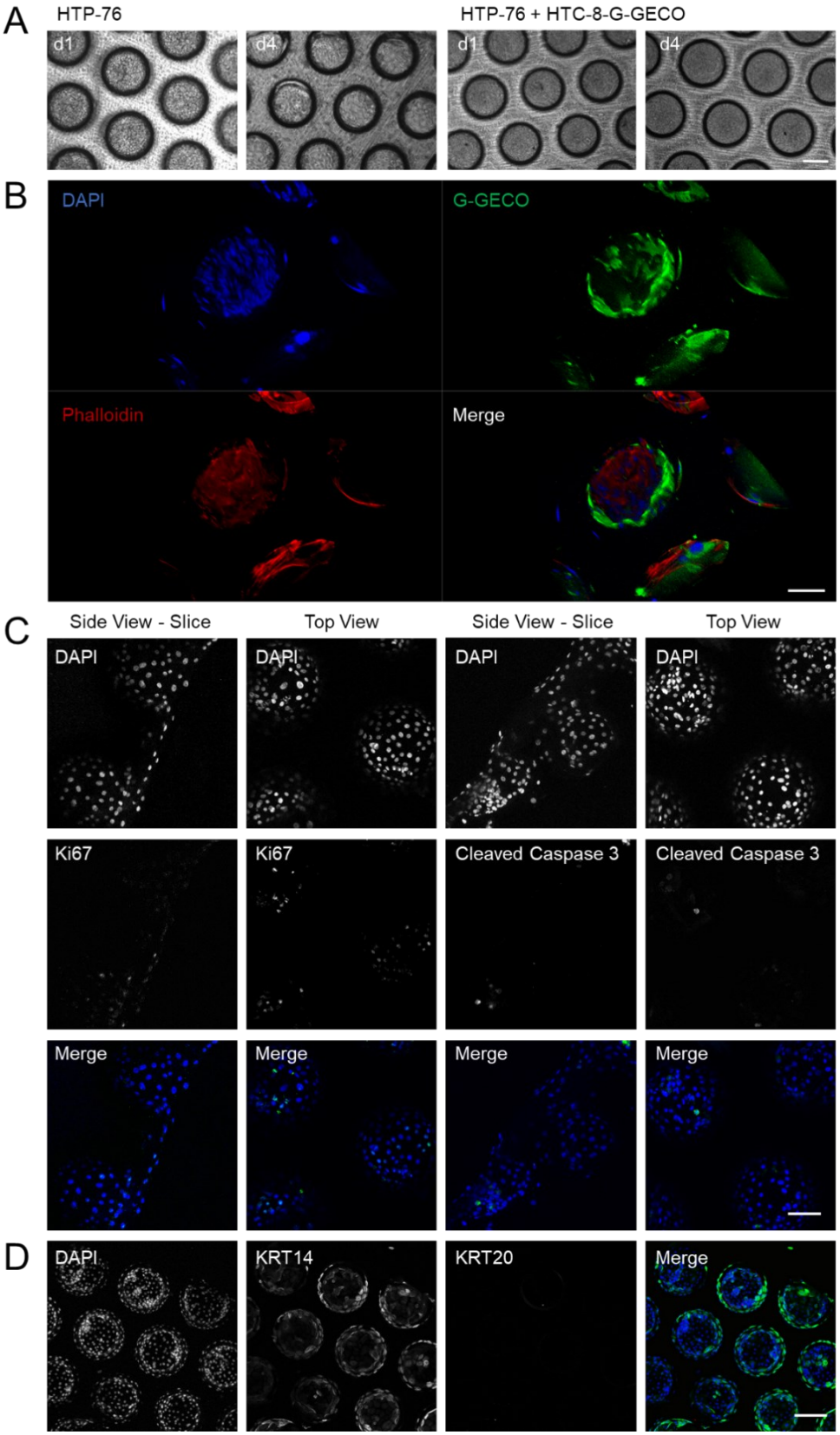

Figure 23: Characterization of HTP-76 progenitor cells grown in Dynarray chips. A) HTP-76 were either grown as monoculture ($0.5x10^3$ cells) or HTP-76/HTC-8-G-GECO co-culture ($0.25x10^3$ cells of each type) in Dynarray cavities for 4 days (d). Scale bar: 200 µm. B) 3D view of an HTP-76/HTC-8-G-GECO co-culture in a Dynarray cavity. Nuclei were stained with DAPI. Actin filaments, to indicate cell bodies, were stained with Phalloidin. Scale bar: 100 µm. C-D) HTP-76 monocultures stained with anti-Ki67 (C), anti-Cleaved Caspase 3 (C) anti-KRT14 and antiKRT20 (D) (all green). Nuclei were labelled with DAPI (blue). Side views are confocal images of slices generated with the vibratome, top views are images from whole mount samples cleared with Glycerol. Scale bar: 100 µm.

4 Discussion

Sugar, once a luxury product, has sneaked in virtually all food sources over the world, thereby, creating severe health issues (Borges et al. 2017; Pepino 2015; Bray and Popkin 2014). To maintain the pleasure of sweet food and simultaneously avoid the negative sequelae of sugar consumption, artificial sweeteners without calories have become popular substitutes. Although initially denoted as safe, recent studies have shown that daily intake of artificial sweeteners can lead to metabolic syndrome, type II diabetes or cancer (Nettleton et al. 2009; Ardalan et al. 2017). Reasons for this might be the expression of sweet taste receptors and downstream signaling molecules in multiple extraoral tissues (Yamamoto and Ishimaru 2013; Laffitte et al. 2014). Thus, understanding taste signaling is not only fundamental to shed light on taste perception but may also provide a basis for translational research to identify new therapeutic drugs against metabolic dysfunctions (Laffitte et al. 2014). Further, trawling through literature brought evidence that sweet taste may be transduced also in the absence of T1R2/T1R3 receptors (Damak et al. 2003) via a parallel alternative sweet signaling mechanism (von Molitor et al. 2020c). Due to the complexity of taste signaling, species specificity of sweet taste perception and the difficulty to perform adequate studies in human (Riedel et al. 2017), there are still many open questions in understanding the whole extent of sweet taste signaling and even primary mechanisms are not fully revealed. This calls for novel, more physiological models to analyze human sweet taste processing. Therefore, the experimental part of this study was based on isolated and immortalized cells from human fungiform papillae (HTC-8) (Hochheimer et al. 2014). HTC-8 cells were grown as spheroids or Dynarray chips to mimic the cellular organization of taste buds. These 3D models are inexpensive, allow the generation of replicates and promote a more physiological environment in which cells may communicate and compounds have to diffuse through cell layers to reach their target. To study gustatory responses in these cultures, HTC-8 cells expressing the Ca^{2+} sensor G-GECO were used and time course experiments were performed upon perfusion with taste compounds. HTC-8 spheroids responded to bitter substances with faster and shorter Ca^{2+} transients than to sugars, while no amplitudes were detected upon addition of the artificial sweetener Acesulfame K. According to these kinetic differences, bitter and sweet responses might be mediated by distinct signaling pathways, which could correlate to the canonical and alternative pathway, respectively. Since individual HTC-8 cells simultaneously responded to KCl, sweet and bitter or only specifically to one of these modalities, spheroids might contain broadly tuned and tightly tuned cells. Additionally, ATP-mediated positive feedback in the generation of compound-evoked Ca^{2+} transients was suggested by the effects of the purinergic antagonist Suramin which reduced Ca^{2+} responses to ATP and Saccharin. Thus, the established taste model in combination with the live cell imaging setup contributed to study human taste physiology and may be implemented in the screening for sugar alternatives.

4.1 Optical clearing with Glycerol allows penetration deep into HTC-8 spheroids

Usually, immunostaining analysis of mouse taste buds is performed on thin (~ 5 µm) sections generated with a cryotome. However, since taste papillae are usually sized 15-32 μm^3 (Whitehead et al. 1999), many structural information are lost with this approach. To overcome this hurdle, FocusClear™ was used to optically clear whole mouse tongues. This increased light transmission across optical sections by 4.2 fold on average and allowed to record stable fluorescence signals up to 75 µm in depth (Hua et al. 2013). At 150 µm signals were totally vanished (Hua et al. 2013). HTC-8 spheroids in this work were optically cleared with Glycerol. This revealed 50% signal loss at 85 µm and 90% signal loss at 276 µm depth. Besides FocusClear™ no other clearing reagent has been tested on lingual tissues or taste cells so far.

As inherent characteristics of cell lines influence clearing effects, the best optical clearing protocol for each individual cell type has to be evaluated (Nürnberg et al. 2020). Indeed, due to different properties, vessels in mouse tongue tissue scraped from their surrounding tissue, wherefore they were apparent for additional 75 µm (Hua et al. 2013). Thus, to find the best suitable clearing reagent for HTC-8 spheroids, ClearT2, ScaleS and Glycerol were compared in terms of fluorescence signal stability and signal-to-noise-ratio (SNR). Maximum intensity and SNR values were superior for Draq5 compared to DAPI in all clearing protocols, though SNR for DAPI also decayed at an admissible spheroid depth below the Rose criteria. Thus, DAPI has been used in most protocols to stain nuclei as it allowed the combination with dyes and/or Alexa Fluor 647, which is an advantage in HTC-8 cells expressing endogenous green (488 nm) G-GECO fluorescence.

While ClearT2 and Glycerol preserved spheroid sizes, CytoVista led to a significant shrinkage, probably due to its dehydration property (Pan et al. 2016), while the hyperhydrating ScaleS protocol led to increased volumes (Nürnberg et al. 2020). Depending on the biological question, these effects can sometimes be desired (Nürnberg et al. 2020). On the one side, small samples sizes reduce image acquisition times and data amounts (Pan et al. 2016), but this may come with the price of losing spatial information and issues during automated segmentation (Nürnberg et al. 2020). On the other side, increased sample sizes may allow the recording of densely packed structures below the optical resolution limit (Chen et al. 2015). Commonly, volume preservation of samples is desired for reasons of quantification, reproducibility and structural integrity (Nürnberg et al. 2020). As Glycerol is inexpensive, can be self-made, did not induce volume changes and revealed stable fluorescence signals deep into samples, it was chosen as optical clearing agent for HTC-8 spheroids.

4.2 Spheroids and Dynarray chips are feasible models to generate *in vitro* taste bud-like structures

As isolated LGR5- or LGR6-positive murine progenitor cells were capable to generate spherical organoids containing all the different taste cell types (Ren et al. 2014; Aihara et al. 2015; Ren et al. 2017; Ren et al. 2020), HTC-8 cells were also cultured as spheroids with the hope to induce sweet taste receptor expression. In addition, HTC-8 cells were cultured in Dynarray chips, which may in contrast to spheroids support and/or guide cell assembly to taste bud-like structures, due to their roundish cavities. Further, Dynarray chips are open on top to allow media exchange similarly to taste buds embedded in the tongue. In both 3D culture models, HTC-8 cells grew as compact cell aggregates. Immunostaining of spheroids revealed more proliferative cells on the rim, and in accordance with this, proliferative cells in Dynarray chips were located at the surface, where they are in contact with the surrounding media. This observation is in agreement with a BrdU staining of murine taste organoids showing that proliferation occurred preferentially in the outer cell layers (Aihara et al. 2015), while in another publication BrdU-positive cells were scattered within the organoids (Ren et al. 2014). BrdU-positive cells in mouse taste buds represented undifferentiated proliferating progenitors, positive for the stem cell marker SOX2 (Ren et al. 2014).

Of notice was also an enlarged Golgi apparatus in peripheral but not inner cells in HTC-8 spheroids. Analogously, in Dynarray chip cultures, HTC-8 cells with an enlarged Golgi apparatus were mainly present at the surface contacting the medium. A prominent Golgi apparatus, extending away from the nucleus in apical and basal regions has also been reported in differentiated rat type II cells. In accordance with the results of this work, the enlarged Golgi apparatus was described only in a few taste cells (Pumplin and Getschman 2000). In other cell types, enlarged Golgi apparatus have been reported as a marker for differentiation. For example in mature osteocytes the Golgi apparatus occupied ~30% of the total surface, whereas in undifferentiated cells only ~7% of the area were occupied (Kasap et al. 2011). In secretory cells, such as mammary epithelial cells or pancreatic cells, which have similarities with taste cells, immense Golgi apparatus could be observed during development (Munger 1958; Emerman et al. 1979). Thus, cells with enlarged Golgi apparatus in HTC-8 3D cultures could be cells in a status that more closely resembles differentiated taste cells.

In murine progenitor-derived organoids, T1R expression occurred after three days in culture (Aihara et al. 2015), thus, HTC-8-G-GECO 3D cultures were also cultured for 5-7 days in this work, which referred to a time point, where spheroid sizes remained relatively stable. To obtain information on T1R expression in HTC-8-G-GECO 3D models, different T1R antibodies (Table 6) were tested on native mouse/human papillae and HEK293 cells expressing recombinant T1R (data not shown) since most of these antibodies have not been characterized in publications. Previous reports have used antibodies produced from Santa Cruz for

immunostaining of T1R and its downstream signaling molecules (Aihara et al. 2015; Takai et al. 2015; Gaillard et al. 2015; Takai et al. 2019) which are, however, no longer available. Since then, no other reliable antibodies were introduced to the market, which is why most authors used T1R3-GFP (Yee et al. 2011; Sukumaran et al. 2016; Ren et al. 2017), PLCβ2-GFP (DeFazio et al. 2006; Dando and Roper 2012) or TRPM5-GFP (Clapp et al. 2006) transgenic mice to visualize defined taste cell types. Unluckily, the antibodies tested in this work did not produce reliable results. Although the anti-KRT8 antibody (Ren et al. 2014; Gaillard et al. 2015) and UEA-1 dye (Yoshimoto et al. 2016) were previously used to label differentiated taste cells in murine taste organoids and papillae, and a staining was observed on slices of mouse papillae in this work as well, no successful staining was achieved in HTC-8 cultures. This was probably not due to the staining protocol, as it was successful for other antibodies, and rather due to the absence of these markers in HTC-8 spheroids (Supplementary Table 19). Thus, since HTC-8 spheroids could not be characterized with immunostaining, live cell assays have been applied to determine their functional responses to gustatory compounds.

4.3 Perfused live cell imaging systems mimic the physiological application of compounds and allow the analysis of acute gustatory responses

Current recordings (Avenet and Lindemann 1987; Medler et al. 2003; Clapp et al. 2006; DeFazio et al. 2006) and the change in fluorescence of Ca^{2+}-sensitive dyes (Akabas et al. 1988; Ren et al. 2014) have been used as major readouts to expand the knowledge on taste signaling. Since most studies used primary cells, which have a limited life span of ~10 days *in vivo* and of 7 passages *in vitro* (Ozdener and Rawson 2013), genetically encoded Ca^{2+} sensors have not been largely used (von Molitor et al. 2020b). However, HTC-8 cells are stably proliferating and, therefore, could be genetically modified to stably express the Ca^{2+} sensor G-GECO. This allowed not only the recoding and subsequent quantitative analysis of gustatory-induced Ca^{2+} transients, but also to identify HTC-8 cell morphologies.

Under physiological conditions, taste cells are exposed to gustatory compounds through the saliva flow, and in drug cytotoxicity studies continuous perfusion has been found to be necessary to establish steady state concentrations and drug profiles (Abberger et al. 2006). However, under perfusion conditions, samples have to be stabilized without damage. As no optimal solution has been found so far, gustatory responses of taste organoids were studied mainly on cells upon organoid dissociation and subsequent monolayer culture to allow attachment to the perfusion chamber (Ren et al. 2014). Alternatively, organoids were stimulated within a bulk addition of test compounds, which neither allows the application of multiple compounds in succession nor the acquisition of kinetic information (Akabas et al. 1988; Kuhn et al. 2004; Meyerhof et al. 2010; Hochheimer et al. 2014). Thus, continuous and cautiously controlled perfusion conditions are a main prerequisite for the precise investigation

of substance-mediated cellular signaling to evade undesired artefact-like effects by sudden bulk addition that can mask, hamper or modify compound-induced activity (Li and Cui 2014). Therefore, new microfluidic devises are constantly developed to allow perfusion-mediated analysis of compound-induced cellular responses in 3D cell culture systems. However, most of these microfluidic devices are highly complex, involve different cell compartments, need special knowledge and cleanrooms for fabrication, which makes them inadequate for routine screening experiments (Faustino et al. 2016). Further, these systems are not applicable to perform high resolution microscopy as they are primarily made of Polydimethylsiloxane (PDMS) or similar polymers, which are not light transparent. While PDMS has a n_D of ~1.43, microscopy immersion objectives have mostly a limited operational range with a predefined refractive index of typically $n_D = 1.523$. Accordingly, there is a need for simple, commercially available perfusion systems in combination with feasible 3D cultures (Faustino et al. 2016).

The here established live cell imaging system was tested on two different 3D cultures: spheroids and Dynarray chips. Both methods allow fast and easy handling, are inexpensive and permit the generation of multiple replicates in one experimental trial. Using the µ-slide III perfusion slides made of optical quality polymer and glass, data could be generated with single cell resolution within these 3D samples. The major challenge to obtain high quality confocal recordings in perfusion condition with these floating and fragile 3D structures was, thus, to keep them in place without impairing their structure. The solution was the use of Scaffolene Collagen meshes which proved to be sufficiently transparent and soft upon wetting to allow damage-free positioning of spheroids and Dynarray chips. Scaffolene permitted light penetration without increasing background signals, and as they are provided sterile, they are a promising scaffold to generate 3D cultures that can be directly used for live imaging or plate reader analysis. The µ-slide III 3D perfusion slides can be closed and connected to a pumping system. Thus, the setup is not limited to endpoint measurements, and the closed system can be transferred from the incubator to the microscope permitting long-term imaging studies, e.g. on spheroid formation. Future, using both wells of the µ-slide III 3D perfusion slides in a circuit may provide a system that allows studying CPIR or GLP-1 release by the cultivation of taste spheroids in one chamber and cultivation of gastro-intestinal-derived spheroids in the other well. Such a model may give first ideas on whether GLP-1 is released from human taste cells. So far, this has only been addressed in rodents.

To improve the temporal resolution of the live cell imaging setup, which would allow to acquire multiple z-planes instead of only three, the live cell imaging setup was transferred to LSFM. In contrast to previously published live cell imaging experiments with LSFM, which required a highly complex imaging chamber (Pampaloni et al. 2014; Patra et al. 2014; Pampaloni et al. 2015b), the system of this work can be setup simply in every lab and is inexpensive. To position and stabilize spheroids, it uses a U-shaped glass capillary and Agarose for embedding.

Improvements to keep sterility, media temperature, humidity and pH constant are, however, necessary to maintain cellular health during prolonged experiment times. Further, alternative mounting materials such as Alginate hydrogels should be tested since Agarose has been shown to influence intracellular Ca^{2+} signaling in chondrocytes as a consequence of mechanical compression (Roberts et al. 2001). A major disadvantage of the present LSFM live cell imaging setup is the huge volume of the recording chamber, which expands drug diffusion times and, thereby, compromises the temporal resolution of compound-induced response measurements. Accordingly, future adjustments are necessary.

To test the established perfused live cell imaging setup as potential assays to study taste signaling, HTC-8-G-GECO spheroids and Dynarray cultures were first stimulated with the bitter compound Salicine. Subsequent analysis of both models revealed highest Ca^{2+} transients in cells on the boarder, whereas in the center, HTC-8-G-GECO cells responded with smaller Ca^{2+} transients. Further, no transients were observed upon starting the perfusion nor upon stimulation with Gluconate, which was applied for osmolarity control. Accordingly, these systems allowed high resolution recordings that can be quantitatively analyzed even at a single cell level. Thus, they may be implemented to study cellular responses and intercellular communication. Since they can be multiplexed, they provide more data in a shorter time than human *in vivo* studies. Considering that 3D models are of increasing importance for disease models, this setup is suitable to image acute drug responses in complex 3D structures and can be applied to different fields of pharmacological research.

4.4 Sweet and bitter responses follow different kinetics in HTC-8-G-GECO spheroids

Saccharin bitter taste is transduced predominantly via the high affinity T2R43, T2R44 (also called T2R31) and the low affinity T2R8 (Kuhn et al. 2004; Pronin et al. 2007). T2R43 and T2R44 were expressed in HTC-8 monolayer culture, whereas T2R8 was not detected (Hochheimer et al. 2014). As stimulation with Saccharin induced specific Ca^{2+} transients in HTC-8-G-GECO spheroids, it is likely that these receptors are also present in 3D cultures. Remarkably, the positioning of individual cells did not only show morphological differences, such as stretched cell bodies and enlarged Golgi apparatus on the rim, but also a similar functional stratification. Accordingly, from the spheroid border to the core, Ca^{2+} amplitudes upon Saccharin stimulation declined, the onset of the responses (T_{slope}) became longer and EC_{50} values increased. EC_{50} values in the outer region, determined with the ring analysis, corresponded to previously published EC_{50} values of 1.1-1.17 mM in monolayer HEK293 cell cultures overexpressing T2R43 or T2R44 (Kuhn et al. 2004; Meyerhof et al. 2010). Reasons for these regional function differences could be that: i) cells on the spheroid rim may express more receptors and represent rather mature type II cells, ii) the expression of T2R44 and T2R43 in HTC-8-G-GECO cells may increase from the spheroid core to the periphery, given

that T2R43 displays a higher EC_{50} (1.7 mM) than T2R44 (1.1 mM) (Kuhn et al. 2004), or that iii) the diffusion of Saccharin through several cell layers may dilute its concentration. To address the latter hypothesis, experiments with Sulforhodamine B perfusion showed that a dye with comparable size and charge as ATP can diffuse and accumulate in the spheroid core at a similar velocity or even faster than the propagation of the Ca^{2+} transients. Thus, in regard to the Ca^{2+} waves travelling from outer to inner cell layers, these data suggest that i) the postponement between Ca^{2+} and Sulforhodamine B signals may correspond to the period required by ATP to bind to its receptors and induce intracellular signaling, ii) the diffusion of ATP through several cell layers of the spheroid may progressively delay the onset of Ca^{2+} responses when moving towards the spheroid center, or that iii) signal propagation may be the result of cell-cell communication via a purinergic paracrine mechanism. In summary, the Sulforhodamine B experiments showed that a small compound can diffuse into the spheroid core and accumulate there. Therefore, the gradually decreasing amplitudes of Ca^{2+} responses are not caused by a limited availability of the agonist in deeper cell layers. Accordingly, these data further support the idea of possible intrinsic differences in cellular phenotypes depending on the cell localization within the spheroid.

Interestingly, upon 3D culture, HTC-8-G-GECO cells started to respond also to sugars, which was not apparent in monolayer culture. Both, sweet and bitter substances showed decreasing peak intensities of Ca^{2+} responses from the spheroid periphery to the center. However, at difference, Saccharin bitter compound-induced Ca^{2+} transients in the three inner rings were still measurable with the ring analysis, while Sucrose-induced Ca^{2+} transients were very low to almost undetectable. Moreover, for Sucrose, the signal started to rise in all rings concurrently, while for Saccharin, it was delayed in inner rings. Since Sulforhodamine B also needed time to penetrate and accumulate in the core, the simultaneously appearing Ca^{2+} transients upon Sucrose stimulation were probably caused by elongated time intervals used for confocal image acquisition, which averted to display delayed starting times. Alternatively, it may refer to diverse intracellular signaling mechanisms or intercellular communication. Further, cells may have different spatial activity, e.g. cells in the first ring may have used a rather slow metabolic mechanism in which Glucose is internalized via GLUTs and metabolized, which has been proposed to take up to a minute (Nakagawa et al. 2015), while inner rings may have used the canonical T1R2/T1R3 downstream signaling cascade, which is faster but appears simultaneously due to delayed compound diffusion into the spheroid core. Such a distribution of internal sweet taste receptor expression in organoids was previously reported in mouse taste organoids (Aihara et al. 2015). Due to the almost complete absence of Ca^{2+} transients in the spheroid core, EC_{50} values for Sucrose could only be determined for the whole spheroid (24.7 mM) and in the first ring (28.96 mM), where most Ca^{2+} transients occurred. In literature, EC_{50} values measured in human for Sucrose sensitivity vary largely (Table 10) as they are

dependent on age (Moore et al. 1982; Petty et al. 2020), fungiform papillae density (Zhang et al. 2009), menstrual cycle (Than et al. 1994), ethnic background (Fushan et al. 2010), gender (Than et al. 1994; Fushan et al. 2010), smoking (Pepino 2015) or assay design (Aleman et al. 2016). Moreover, threshold levels may differ according to the pathway activated. For example, if Sucrose rather binds to the sweet taste receptor or is digested and internalized via GLUTs. Indeed, also the alternative pathway may contribute to sweet taste discrimination (Chapter 1.10, Delay et al. 2006; Yamamoto and Ishimaru 2013) and may have a completely different dose-response curve.

Table 10: Sucrose EC_{50} levels in humans. Sweetness intensity wase ranked with gradual values.

EC_{50} (mM)	Source
5.5	Low et al. 2017
6-20	Zhang et al. 2009
7-12	Pepino and Mennella 2007
12-36	Richter and Campbell 1939
25-27	Than et al. 1994
44	Heath et al. 2006
47	Aleman et al. 2016

4.5 Saccharin has sweet and bitter taste

Interestingly, Saccharin tastes bitter or sweet depending on its concentration (Behrens et al. 2017). Concentration intensity curves for the perception in humans showed that at low concentrations Saccharin sweetness increases reaching a plateau at 2-6 mM. Beyond these concentrations, sweet perception decreases, while bitterness becomes the dominant taste (Moskowitz and Klarman 1975; Galindo-Cuspinera et al. 2006). Notably, the dose-response curve measured in HTC-8-G-GECO spheroids showed that the intensity of Ca^{2+} transients at 2 mM was slightly above the curve and had the highest variability (highest SEM at 2 mM, Figure 15A, E). This reminds the concentration intensity curves in humans (Behrens et al. 2017), suggesting that Saccharin may mediate sweet and bitter responses also in HTC-8-G-GECO spheroids. This hypothesis was corroborated by the observation that only HTC-8-G-GECO spheroids responded to sugars, while stimulation of monolayer cultures with sweet compounds did not result in specific Ca^{2+} transients (Hochheimer et al. 2014).

With respect to the underlying biology, two pathways can be activated upon Saccharin application in rodents; i) the cAMP/PKA cascade (Nakashima and Ninomiya 1999) and ii) PLCβ2/IP3 signaling (Bernhardt et al. 1996; Nakashima and Ninomiya 1998, 1999). While the cAMP pathway may be more relevant between 3 and 20 mM (Nakashima and Ninomiya 1999), the IP3 pathway was proposed to prevail at concentrations beyond 20 mM (Bernhardt et al. 1996; Nakashima and Ninomiya 1998, 1999). If this is the case, then the sweet pathway would utilize cAMP-mediated signaling, and the bitter pathway rather the IP3-mediated signaling. A direct prove is, however, still missing, since taste quality and signaling have never

been determined and correlated in the very same study, meaning that either the taste quality or signaling was investigated. Thus, the exact turning points of signaling cascades and taste qualities have not been identified and linked. To investigate this idea, optical cAMP sensors could be applied. In previous studies, cAMP was measured with enzyme immunoassays on lysate extract from tongue epithelia, however, newer molecular cAMP biosensors may allow the simultaneous acquisition of Ca^{2+} and cAMP in the same cell (von Molitor et al. 2020b).

4.6 Bitter compounds may activate the canonical pathway in HTC-8-G-GECO spheroids

The results of the live cell imaging experiments indicated that the spheroid culture led to cells with different behavior and activity profiles that were not observed in monolayer culture. For further fundamental research and implementation in industrial screening, the underlying signaling mechanisms have to be understood. First insights could be derived from a preliminary transcriptome analysis of HTC-8-G-GECO spheroids that was conducted and evaluated by the cooperation partner BRAIN AG (Supplementary Table 15-19). Since these data are only based on a single run, further replicates are necessary to corroborate these findings (Chapter 4.11). In the following, the results of these expression data will be discussed in the light of the live cell imaging done in this work and will be set into context with literature. For a better overview, results are illustrated in Figure 24 and summarized in Table 12.

In literature, there is agreement that in vertebrates, bitter, sweet and umami gustatory compounds bind to corresponding G-protein coupled taste receptors and activate the canonical taste pathway. In brief, this includes taste receptors, G-proteins like gustducin, PLCβ2 and TRPM5. Additionally, sweet taste could be transduced via AC-mediated cAMP production and subsequent activation of PKA to inhibit VDKC and induce cell depolarization (Avenet et al. 1988; Striem et al. 1989). The transcriptome analysis showed that HTC-8-G-GECO spheroids expressed several but not all expected canonical pathway components at a detectable level, but for many, alternative candidates were found. The following description is sorted according to the major levels of the canonical taste signaling pathway.

4.6.1 Taste receptor mRNA levels of HTC-8-G-GECO spheroids might be below the detection limit of transcriptome analysis

Although Ca^{2+} transients were specifically observed during bitter and sweet tastant stimulation intervals within the live cell imaging experiments, transcriptome analysis could not reveal high expression of taste receptors. While T1R2 was not detectable, T1R3 revealed an expression value of 0.18 (Supplementary Table 15), though only values ≥1 were rated as “expressed” in this work. In mouse fungiform papillae, qPCR data on T1R3 expression, relative to the house keeping gene Glycerinaldehyd-3-phosphat-dehydrogenase (GAPDH), revealed a value of $1506x10^{-5}$, which was higher than that for T1R2, which was $0.21x10^{-5}$ relative to GAPDH

(Choi et al. 2016). These data suggest a rather low expression of the sweet taste receptor even in native tissue. In a previous mouse taste organoid study, mRNA sequence data were collected over a period of 14 days. Interestingly, vales ≥1 for the sweet taste receptor were only observed beyond 10 days of culture (Table 11, Ren et al. 2017), whereas in this study, spheroids were cultured only for 5-7 days. Accordingly, prolonged culture periods for HTC-8-G-GECO spheroids might have also resulted in higher expression of sweet taste receptors.

Table 11: Comparison of transcriptomic data of mouse taste cell organoids and HTC8-8-G-GECO spheroids. Grey rows show transcriptome data from Ren et al. 2017 (n = 1) and white rows from HTC-8-G-GECO spheroids (n = 1). First timepoint where expression levels exceed the threshold of 1 are highlighted. – means not measured, and n.d. not detectable. Ren et al. obtained transcriptome analysis on LGR5-positive mouse taste progenitor cell organoids on different days of culture (d).

Gene	d2	d4	d6	d8	d10	d12	d14
TAS1R2	0.202050	0.042681	0.150388	0.337488	0.406516	**1.326948**	3.827242
	-	-	n.d.	-	-	-	-
TAS1R3	0.104850	0.615244	0.027871	0.225979	0.678652	**1.384480**	2.078111
	-	-	0.178202	-	-	-	-
TAS2R16	n.d.	n.d.	n.d.	n.d.	n.d.	0.139821	0.313309
	-	-	n.d.	-	-	-	-
TAS2R8	0.030387	n.d.	n.d.	0.654922	0.739343	**2.755914**	4.904194
	-	-	n.d.	-	-	-	-
GNAT3	1.832019	0.414071	**2.140376**	22.08206	23.34530	58.11854	85.70332
			n.d.				
PLCβ2	0.956556	0.229991	0.902990	**3.273437**	6.113130	13.30839	20.34059
	-	-	n.d.	-	-	-	-
TRPM5	0.394523	0.135511	0.700865	**2.882704**	3.453291	10.70301	15.84846
	-	-	n.d.	-	-	-	-

Along with this, neither the Saccharin nor Salicine T2R receptors were detected in the mRNA sequencing screen of HTC-8-G-GECO spheroids. However, also T2R are natively expressed at a very low abundance (qPCR, < 0.01 relative to β-actin in mouse circumvallate and foliate papillae) (Lossow et al. 2016), possibly since several T2R isoforms exist (Hochheimer et al. 2014). Since Saccharin and Salicine receptors were reported in HTC-8 monolayer cultures (Hochheimer et al. 2014), it can again well be that their mRNA has been diluted (Chapter 4.11). Moreover, many T2Rs could also not be detected in the previous mRNA sequencing screen of mouse progenitor taste organoids (Table 11, Ren et al. 2017). Accordingly, T2R mRNA levels may be below the detection limit of the transcriptome analysis. Since i) there is no alternative pathway known to canonical bitter taste signaling, ii) the live cell imaging data obtained with Salicine and Saccharin resulted in Ca^{2+} transients within the stimulation interval, and iii) only few cells within the spheroid responded with Ca^{2+} elevations upon stimulation, one may presume that T2R could be expressed in these few responding cells in HTC-8-G-GECO spheroids.

4.6.2 Diverse G-proteins may transmit gustatory signals in HTC-8-G-GECO spheroids

Heterotrimeric G-proteins are the intracellular partners of taste receptors. Conformational change of the taste receptor, upon ligand binding, results in the exchange from GDP to GTP at the Gα subunit and the dissociation of Gβγ. Subsequently GTP-bound Gα and the liberated Gβγ interact with downstream proteins (McCudden et al. 2005). In the human genome, G-proteins are encoded by 16 Gα genes assigned to different Gα families, in particular: $G\alpha_{(s/olf)}$, $G\alpha_{(i\text{-}1/i\text{-}2/i\text{-}3/o/t\text{-}rod/t\text{-}cone/gust/z)}$, $G\alpha_{(q/11/14/16)}$ and $G\alpha_{(12/13)}$ (McCudden et al. 2005). In general, $G\alpha_s$ stimulates AC to increase intracellular cAMP levels, whereas $G\alpha_i$ inhibits AC. The $G\alpha_q$ family activates PLC and generates IP3 (McCudden et al. 2005).

mRNA analysis in HTC-8-G-GECO spheroids revealed that neither gustducin nor transducin (Supplementary Table 15), which rescued bitter signaling in Gα-knockout mice (He et al. 2002), was expressed. However, in the previous mRNA sequence screen of mouse progenitor organoids they were detected in contrast to taste receptors (Table 11, Ren et al. 2017). Further, gustducin was expressed 20% higher (~0.05 relative to β-actin in mouse circumvallate and foliate papillae) in a qPCR study than T2R37, which resulted in the highest expression of all T2R (qPCR, ~0.01 relative to β-actin in mouse circumvallate and foliate papillae) in native mouse taste tissue (Lossow et al. 2016). Thus, gustducin and transducin are probably not involved in HTC-8-G-GECO spheroid signal transmission. $G\alpha_{i\text{-}2}$, $G\alpha_{i\text{-}3}$ and $G\alpha_s$ which have been emphasized as the dominant species in rodent taste buds, as their expression appeared to be even higher than that of $G\alpha_{gustducin}$ (Kusakabe et al. 2000), were expressed in HTC-8-G-GECO spheroids (Supplementary Table 15). $G\alpha_{i\text{-}2}$, $G\alpha_{i\text{-}3}$ and/or $G\alpha_s$ may activate AC, with which they are co-expressed in some taste cells (Kusakabe et al. 1998; Kusakabe et al. 2000). In addition, HTC-8-G-GECO spheroids contained mRNA for $G\alpha_q$ and $G\alpha_{11\text{-}13}$ (Supplementary Table 15), though $G\alpha_{12}$ and $G\alpha_{13}$ were so far not attributed to taste cells, but $G\alpha_{11}$ and $G\alpha_q$ are involved in PLC activation (Kusakabe et al. 1998). $G\alpha_{15}$, detected by immunostaining in rat taste buds (Kusakabe et al. 1998), was not present in HTC-8-G-GECO spheroids.

The Gβγ subunit has guanine nucleotide dissociation inhibitor activity and facilitates binding of Gαβγ heterotrimers to GPCRs. Additionally, Gβγ can activate further effector molecules, such as kinases and small G-proteins (McCudden et al. 2005). In taste cells, predominantly the $G\beta_3\gamma_{13}$ subunit (Huang et al. 1999; Rössler et al. 2000) mediates IP3 generation (Hwang et al. 1990; Spielman et al. 1994). However, also $G\beta_1$ is expressed in 80% of mouse type II cells, and $G\beta_1\gamma_{13}$ may mediate bitter responses (Huang et al. 1999). HTC-8-G-GECO spheroids did not express $G\beta_3\gamma_{13}$, but $G\beta_1$, $G\beta_2$ and $G\gamma_2$ were detected in the mRNA screen (Supplementary Table 15). Since heterologous $G\beta_1\gamma_2$ and $G\beta_1\gamma_{13}$ expression in COS-7 cells resulted in comparable enhancements of IP3, which was significantly higher in comparison to that of other $G\beta_1\gamma$ pairs, $G\beta_1\gamma_2$ may be very similar to $G\beta_1\gamma_{13}$ and used by HTC-8-G-GECO spheorids to mediate taste responses (Figure 24, Table 12).

4.6.3 PLCβ3 and PLCδ4 may activate TRPM in HTC-8-G-GECO spheroids

In canonical taste signaling, the IP3-hydrolyzing enzyme PLCβ2 is the first downstream molecule to be activated (Rössler et al. 1998; Miyoshi et al. 2001; Yan et al. 2001; Zhang et al. 2003). Besides PLCβ five additional PLC classes exist in mammals: PLC-β, PLC-γ, PLC-δ, PLC-ε and PLC-ζ. PLCβ is the most abundant isoenzyme and can be activated either via $G\alpha_q$ or via Gβγ of stimulated G_i family members (McCudden et al. 2005). Instead of PLCβ2, HTC-8-G-GECO spheroids expressed PLCβ3 and PLCδ4 (Supplementary Table 15). PLCβ3 has been shown to mediate Ca^{2+} release from stores upon bitter and sweet stimulation in mouse taste cells (Hacker et al. 2008; Banik et al. 2020), and PLCδ4 has been described to stimulate TRPM8 in sensory neurons via IP3 production (Yudin and Rohacs 2015). Accordingly, PLCβ3 and PLCδ4 could substitute the activity of the absent PLCβ2 in HTC-8-G-GECO spheroids and may induce Ca^{2+} release from stores to activate downstream TRPM (Figure 24, Table 12).

4.6.4 TRPM4 may induce unconventional ATP release in HTC-8-G-GECO spheroids

Type II cells are devoid of conventional synapses and, thus, activate TRPM5 to cause cell depolarization (Pérez et al. 2002; Liu and Liman 2003) and subsequent ATP release via CALHM1/3 (Finger et al. 2005; Taruno et al. 2013). However, TRPM5 mRNA was not abundant in HTC-8-G-GECO spheroids but, therefore, they expressed TRPM4 (Supplementary Table 15). TRPM4 is equivalently required in mice taste cells as its deletion, similarly to TRPM5, impacted the sensitivity to bitter, sweet and umami stimuli (Banik et al. 2018). Further, TRPM4 expression was confirmed in all mouse taste papillae (Liu et al. 2011b). Accordingly, HTC-8-G-GECO spheroids might be able to activate the PLC/IP3-dependent cascade upon gustatory stimulation, though substituting signaling molecules of the canonical pathway might be utilized (Figure 24, Table 12).

4.6.5 Ca^{2+}-sensitive ACs may mediate cAMP synthesis in HTC-8-G-GECO spheroids

Sugars as well as Saccharin were shown to stimulate an additional pathway downstream the sweet taste receptor in which AC increases cAMP levels to allow PKA-mediated inhibition of K^+ conductance resulting in cell depolarization (Avenet and Lindemann 1987; Striem et al. 1989; Striem et al. 1991; Naim et al. 1991). Mammal AC isoforms can be either transmembrane (ACs1–9) or soluble in the cytoplasm (AC, AC10) (Halls and Cooper 2017). They can be actively stimulated via $G\alpha_s$ or inhibited via $G\alpha_{i/o}$, while indirect regulation may occur upon stimulation of certain signaling pathways. For example, Ca^{2+}, released as a consequence of intracellular signaling, can bind to calmodulin to activate/inhibit ACs (Halls and Cooper 2017).

In HTC-8-G-GECO spheroids the transmembrane ACs 3, 4, 5, 6, 7, 9 were noted in the mRNA screen at different expression levels (Supplementary Table 15). This is in accordance with a previous study showing that AC4, 6, 8 were constantly present in mouse circumvallate papillae

taste buds, while AC2, 5, 9 were found only occasionally (Abaffy et al. 2003). However, in rodent taste buds, AC3 and AC7 were not detected (Abaffy et al. 2003), which is at difference with HTC-8-G-GECO spheroids. Of the detected ACs in HTC-8-G-GECO spheorids, AC5 and AC6 are inhibited by Ca^{2+} (Katsushika et al. 1992), while AC8 belongs to the Ca^{2+}-sensitive ACs (Cali et al. 1994; Trubey et al. 2006), which may be responsible for tastant-evoked cAMP synthesis as a secondary consequence of cytoplasmic Ca^{2+} elevation (Trubey et al. 2006). Further, 66% of AC8-positive cells co-stained for gustducin in rat taste cells (Abaffy et al. 2003).

4.6.6 Cell depolarization via cAMP/PKA-mediated signaling may not prevail in HTC-8-G-GECO spheroids

AC-generated cAMP induces taste cell depolarization via PKA-mediated phosphorylation of K^+ outward channels (Avenet and Lindemann 1987; Striem et al. 1991). PKAs have so far not been exactly determined in mammal taste cells, and only PRKACA and PARKACB have been mapped specifically to taste transduction in the axolotl (Kohli et al. 2020). PRKACA and PRKACB mRNA transcripts were also abundant in HTC-8-G-GECO spheroids (Supplementary Table 15). However, since mRNA sequencing did not result in a hit of any outward rectifying K^+ channel in HTC-8-G-GECO spheroids, this pathway may not prevail, although in rat taste buds a variety of outward rectifying K^+ channels has been reported, including members from each of the three subfamilies: KCNA, KCNB and KCNC (Liu et al. 2005). Electrophysiological and molecular biological assays suggested that the VDKC KCNA5, which is characterized by a very rapid activation and slow deactivation, is the major functional outward rectifying K^+ channel in the anterior rat tongue (Liu et al. 2005).

4.6.7 PDEs may generate permissive conditions for PLC downstream signaling in HTC-8-G-GECO spheroids

In taste cells, PDE1A keeps cAMP levels low to abate PKA activity and subsequently create permissive conditions for PLC signaling (Margolskee 1993; Gilbertson et al. 2000). In regard to this hypothesis, mRNA transcripts of PDE1A, 6D, 8A, 9A were present in HTC-8-G-GECO spheroids (Supplementary Table 15), though only PDE1A has been described in the context of taste transduction (Margolskee 2002). Intriguingly, precisely this PDE seemed to be expressed at a low level in HTC-8-G-GECO spheroids compared to the other PDEs detected. The detected PDEs in HTC-8-G-GECO spheroids may, nonetheless, contribute to temporally and spatially constrain the PKA signal generated by cAMP (Figure 24, Table 12).

Additionally, PDEs may hydrolyze cAMP to activate cAMP-suppressible CNGs, to induce cell depolarization and allow Ca^{2+} influx (Kolesnikov and Margolskee 1995; Misaka et al. 1997). In human type II cells, CNGs are encoded by CNGA4 (Nordström et al. 2004) which was, however, not expressed in HTC-8-G-GECO spheroids. Thus, this pathway may not be utilized.

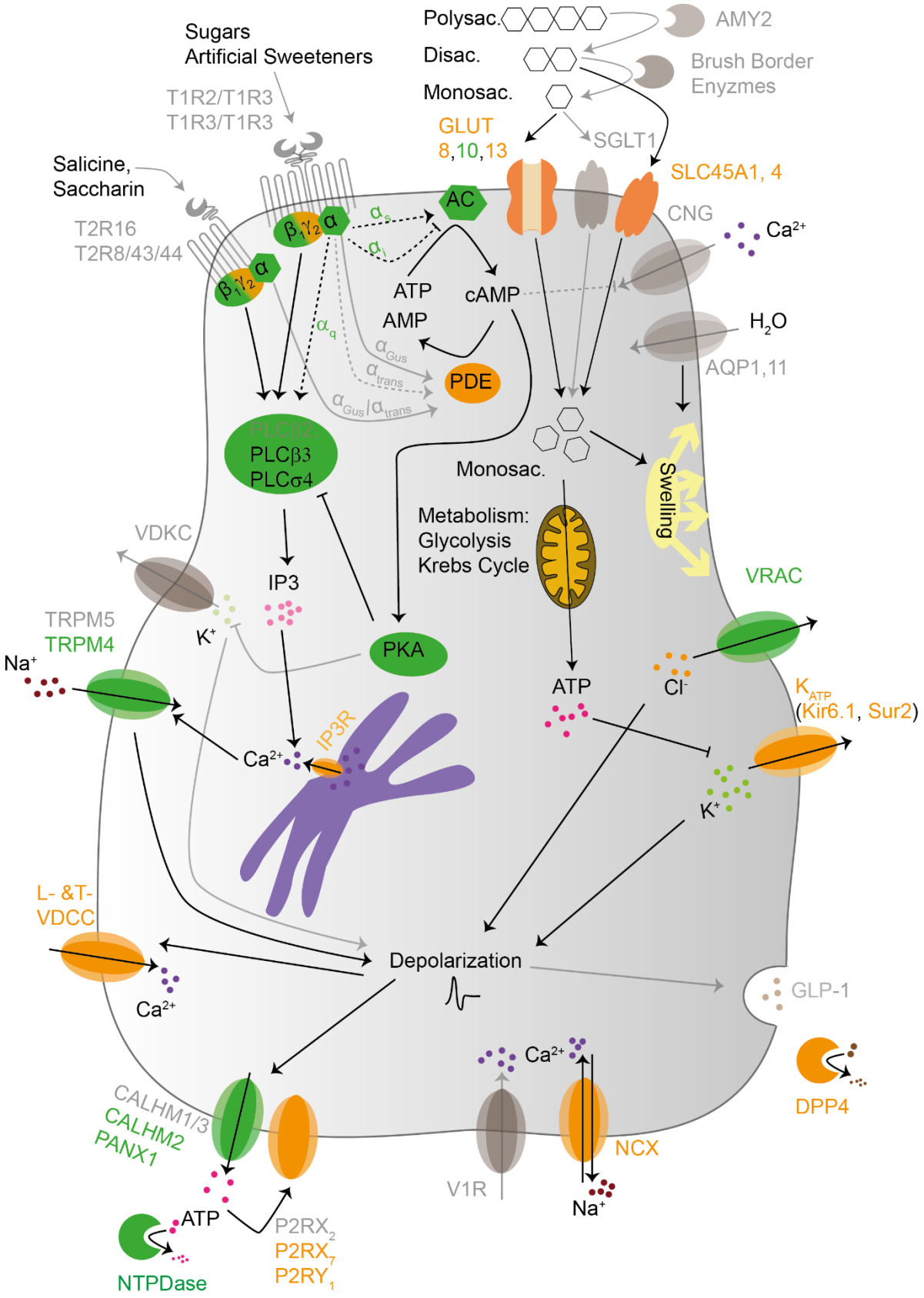

Figure 24: Possible bitter and sweet pathways in HTC-8-G-GECO cells. Signaling molecules of the canonical and the alternative pathway are colored according to their mRNA expression levels: orange: 1-10 = low expression; green <10 = intermediate to high expression. Signaling molecules not detected are grey/transparent. Data are preliminary and are based on the mRNA sequence analysis of only one 96-well plate of HTC-8-G-GECO spheroids. Quantitative data are listed in Supplementary Table 15-19.

Table 12: Taste signaling molecules that may be utilized by HTC-8-G-GECO spheroids to transduce bitter and sweet taste. Expected molecules have been described in literature. Expressed and substituting molecules were determined in the transcriptome analysis of HTC-8-G-GECO spheroids. Symbols of the last row mean: ✓ a certain molecule was present or a family member was expressed that could substitute the function according to literature, ? a family member was expressed but from literature it is not clear if it can substitute the function, X neither the molecule nor a family member was expressed, * a different, not related molecule has been proposed.

Group	Expected	Expressed	Substituted by	Signaling
Canonical taste signaling				
Taste receptors	T1R2	no	GLUT8, 10, 13	✓
	T1R3	no	GLUT8, 10, 13	✓
	T2R8 (Saccharin)	no		X
	T2R16 (Salicine)	no		X
	T2R31/44 (Saccharin)	no		X
	T2R43 (Saccharin)	no		X
G-proteins	gustducin	no	$G\alpha_{i-2}$, $G\alpha_{i-3}$, $G\alpha_s$, $G\alpha_{11}$, $G\alpha_q$	✓
	transducin	no	$G\alpha_{i-2}$, $G\alpha_{i-3}$, $G\alpha_s$, $G\alpha_{11}$, $G\alpha_q$	✓
	β_3	no	β_2, β_1	✓
	γ_{13}	no	γ_2	✓
PLC	PLCβ2	no	PLCβ3, PLCδ4	✓
TRPM	TRPM5	no	TRPM4	✓
AC	AC2, 4, 5, 6, 8, 9	AC4, 5, 6, 9	AC3, 7	✓
PKA	PRKACA, PRKACB	yes		✓
VDKC	KCNA5	no		X
PDE	PDE1A	yes	PDE6D, 8A, 9A	✓
Alternative sweet taste pathway				
GLUT	GLUT1, 2-5, 8-10, 13	GLUT8, 10, 13		✓
SGLT	SGLT1	no		X
K_{ATP}	Kir6.1	yes		✓
	SUR1	no	SUR2	✓
Brush Boarder enzymes	AMY	no	SLC45A*	✓
	SIS	no	GANC, SLC45A*	✓
	TREH	no	SLC45A*	✓
	LCT	no	SLC45A*	✓
VRAC	LRRC8A	yes		✓
AQP	AQP7, 8	no	AQP1, 11 (low)	✓
Purinergic signaling				
ATP release	PANX1	yes		✓
	CALHM1/3	no	CALHM2	?
Purinergic receptors	P2YR1	yes		✓
	P2XR2	no	P2XR7	✓
Ca^{2+} channels				
VDCC	T-type	yes		✓
	L-type	yes		✓
Store operated	ORAI1	yes		✓
	ORAI3	yes		✓
	STIM1	yes		✓
Vanilloid receptor	VR1	low		X
Na^+/Ca^{2+} channel	NCX	yes		✓

4.6.8 Canonical taste signaling may reach beyond gustudcin-PLCβ2-TRPM5 signaling

In summary, from the live cell imaging experiments and the transcriptome analysis of HTC-8-G-GECO spheroids, a pathway similar to the PLCβ2-IP3-TRPM5 cascade may exist that uses substituting family member molecules instead of gustducin, PLCβ2 and TRPM5 (Figure 24, Table 12). These family members may support each other (Banik et al. 2018) or may be expressed in different cell subtypes (Hacker et al. 2008). E.g. TRPM4 and TRPM5 may functionally couple to generate a response, since ~90% of TRPM5 positive mouse taste cells co-expressed TRPM4 (Banik et al. 2018), whereas PLCβ3 signaling was present specifically in type III cells, but PLCβ2 signaling was restricted to type II cells (Hacker et al. 2008; Banik et al. 2020). Thus, there is still much to learn to better understand the roles of these substituting family members. Further, these consumptions again show that even the primary canonical signal pathway is not fully revealed and that a network beyond gustducin, PLCβ2 and TRPM5 may contribute. HTC-8-G-GECO spheroids may have used this canonical pathway with substituting family members to transduce Saccharin and Salicine bitter taste. Whether sweet taste uses this pathway as well has to be tested by the application of the sweet taste inhibitor Lactisol. However, the additionally tested artificial sweetener Acesulfame K did not mediate Ca^{2+} transients, suggesting that HTC-8-G-GECO spheroids could not sense sweet taste via the canonical pathway. Since neither VDKCs nor CNGs have been noted in the mRNA sequencing screen of HTC-8-G-GECO spheroids, the cAMP/PKA pathway may not prevail.

4.7 Sugars may activate the sweet taste receptor-independent pathway in HTC-8-G-GECO spheroids

Sweetness levels in humans are classically determined in a ratio to Sucrose (Moskowitz 1970; Hobbs 2009). Accordingly, Sucrose is ranked as 100, followed by Glucose (74-80) and Lactose (40), while Acesulfame K and Fructose have been ranked with 200 and 150-170, respectively (Hobbs 2009). HTC-8-G-GECO spheroids could not mirror these sweetness levels, and Lactose stimulation resulted even in the highest Ca^{2+} transients. In regard to the assumed absence of T1R2 and extremely low expression of T1R3, but upregulation of GLUT8, 10, 13 in HTC-8-G-GECO spheroids compared to monolayer cultures (Supplementary Table 18), the observed sugar-mediated Ca^{2+} transients might be the result of sugar internalization, metabolism and subsequent cell depolarization rather than downstream signaling of the sweet taste receptor. Indeed, GLUT8 and GLUT10 are sensitive to Glucose and Galactose, respectively, and GLUT8 transports additionally Fructose (Table 2). Further evidence for this idea comes from a study conducted in murine β-cells which also contain signaling molecules of the canonical and alternative pathway (Yamamoto and Ishimaru 2013). Upon stimulation of β-cells with 25 mM Glucose, two Ca^{2+} peaks occurred, a first rapid sharp peak and a prolonged delayed one (Nakagawa et al. 2015). The sharp first peak was dependent on T1R3 since it

was abolished in T1R3-knockout animals, while the broad second peak relied on Glucose metabolism since it was absent when using a non-metabolizable Glucose analogous (Nakagawa et al. 2015). Sugar-mediated Ca^{2+} transients in HTC-8-G-GECO spheroids resembled rather the kinetics of the second peak observed in β-cells since in contrast to HTC-8-G-GECO bitter responses, Ca^{2+} transients of sugars showed broader peaks that started earlier, which might be attributed to Glucose metabolism. This hypothesis is further supported by the observation that i) the artificial sweetener Acesulfame K, which is not a GLUT substrate, did not induce Ca^{2+} elevations in HTC-8-G-GECO spheroids, and ii) also T1R3-knockout mice could not detect artificial sweeteners but sugars (Damak et al. 2003). Thus, HTC-8-G-GECO spheroids may have rather used the metabolic alternative pathway to sense sugars.

4.7.1 The SLC45 family may allow disaccharide entry in HTC-8-G-GECO spheroids

As only monosaccharides are GLUT substrates, disaccharides need to be digested. Therefore, Brush Border enzymes are expressed on mouse taste type II and III cells (Sukumaran et al. 2016). Accordingly, hydrolysis of the unsweet sugars Lactose and Cellobiose would lead to the generation of Glucose and Galactose, which are both substrates of GLUTs. While Brush Border enzymes were absent in HTC-8-G-GECO spheroids, α-Glucosidase C (GANC), which is also present on mouse taste cells (Sukumaran et al. 2016), was expressed (Supplementary Table 18). GANC is able to release Glucose from oligosaccharides and may be involved in the Glycogen metabolism (Gabriško 2020). It co-localizes with actin filaments, is present in the nucleoplasm and cytoplasm but its physiological function is still unknown. Since cells already have specific Glycogen metabolizing enzymes, GANC may also process Glucose-containing sugar substrates (Gabriško 2020). Under neutral pH, GANC hydrolyzes low molecular-weight substrates with α-1,4-glycosidic linkages, such as Maltose, to release Glucose (Martiniuk and Hirschhorn 1981). However, it is not known whether also α-1,2-glycosidic linkages as in Sucrose can be cleaved. Instead, Lactose and Cellobiose contain β-1,4-glycosidic linkages.

An alternative route for disaccharide entry was discovered in fruit fly. Indeed, a Sucrose transporter (SCRT) has been identified in *Drosophila melanogaster* (Meyer et al. 2011). It displays the highest degree of amino acid identity with the human solute carrier family 45 number A2 (SLC45A2), followed by the other three members (Meyer et al. 2011). SLC45A1 is activated during hyperglycemia and may be involved in Glucose homeostasis in the brain (Vitavska and Wieczorek 2013; Bartölke et al. 2014). SLC45A2 may be responsible for the melanin synthesis in skin and hair. SLC45A3 has been detected in skin, in eyes during prostate cancer and in kidney, where it may transport Sucrose as an osmolyte (Vitavska and Wieczorek 2013; Bartölke et al. 2014). SLC45A4 seems to be ubiquitously expressed, though recent data suggest a role in nutrition of spermatozoa (Vitavska and Wieczorek 2017). Indeed, SLC45A4-mediated uptake of radiolabeled Sucrose was shown in mammalian cells and has been

reported to be H^+-dependent (Vitavska and Wieczorek 2017). Moreover, SLC45A carriers have been described to transport monosaccharides, such as Glucose or Fructose (Bartölke et al. 2014; Vitavska and Wieczorek 2017), which are subsequently metabolized during glycolysis (Morioka et al. 2018). Transcriptome analysis of HTC-8-G-GECO spheroids revealed expression of SLC45A1, 3, 4 (Supplementary Table 18). Accordingly, alternatively to GLUTs, mono- and disaccharides could have been taken up via SLC45A transporters and their subsequent metabolism may have resulted in osmotic swelling and VRAC activation or downstream K_{ATP} channel activation (Figure 24, Table 12). Lactose or Cellobiose uptake via these transporters has not been studied so far.

In another study, it was found that CHO and HEK293 cells can survive in serum-free protein-free culture medium using Sucrose, Lactose or Maltose as sugar source (Leong et al. 2017). Although a Maltose transporter is not known to exist, cells grown with Maltose started to stably proliferate as Maltose was internalized without prior hydrolysis from the medium (Leong et al. 2017). Accordingly, there is a chance that also other unknown transporters for disaccharides may exist. Further, Hyaluronidase which increases muscular absorption of Sucrose (Sund and Schou 1965), has been detected in human saliva (Chauency et al. 1954) and was expressed at a low level in HTC-8-G-GECO spheroids.

4.7.2 K_{ATP} channels may act downstream of GLUTs in HTC-8-G-GECO spheroids

Upon sugar uptake via GLUTs in type II cells and subsequent metabolism, increased ATP concentrations may inhibit downstream K_{ATP} channels to mediate cell depolarization (Yee et al. 2011) similar to what is described in β-cells (Seino et al. 2000; Yamamoto and Ishimaru 2013). K_{ATP} channels are large tetrameric channels (Babenko et al. 1998) expressed in multiple tissues and contain two structural subunits: an inwardly rectifying potassium channel subunit (Kir6.x), which forms the pore, and a sulfonylurea receptor (SUR_X), which functions as regulatory subunit (Seino 2003). There are two Kir6.x (Kir6.1, Kir6.2) and three SUR (SUR1, SUR2A, SUR2B) forms that occur in diverse combinations to form K_{ATP} channels (Table 13, Inagaki et al. 1995; Inagaki et al. 1996; Isomoto et al. 1996; Yamada et al. 1997; Seino 2003). SUR/Kir6.2 combinations have a high conductance of ~70 pS and can be inhibited by micromolar ATP concentrations (Babenko et al. 1998; Li et al. 2016), while Sur/Kir6.1 combinations are characterized by a lower ~33 pS conductance and can be stimulated with nucleoside diphosphates (NDPs) in the presence of Mg^{2+} (Yamada et al. 1997). Although some studies claim that Kir6.1 can be blocked by physiological ATP concentrations (Beech et al. 1993; Yamada et al. 1997), treatment with the metabolic inhibitor Na-azide, which reduces intracellular ATP, revealed enhanced K_{ATP} channel activity for all combinations with different sensitivities in oocytes (Table 13, Li et al. 2016), and in another study Kir6.1 and Kir6.2, expressed in COS-7 cells with SUR2, showed a comparable ATP sensitivity (Kono et al. 2000).

Table 13: Possible K_{ATP} channel combinations in tissues. SUR and Kir6.x subunits can assemble to various combinations (Inagaki et al. 1995; Inagaki et al. 1996; Isomoto et al. 1996; Yamada et al. 1997; Seino 2003; Yee et al. 2011). ATP sensitivity (1-6, from low to high) was tested with the metabolic inhibitor Na-azide (Li et al. 2016).

K_{ATP} channel	Tissue	ATP sensitivity
SUR1/Kir6.1	taste cells	6
SUR1/Kir6.2	ß-cells	4
SUR2A/Kir6.1	*unknown *in vivo*	*not tested
SUR2A/Kir6.2	cardiac, skeletal muscle cells	2
SUR2B/Kir6.1	vascular smooth muscle cells, colon, gastric myocytest	3
SUR2B/Kir6.2	non-vascular smooth muscle cells	5

In mouse circumvallate papillae, SUR1/Kir6.1 are the main K_{ATP} forming subunits (Yee et al. 2011), but also SUR2A was detected. In contrast, SUR2B and Kir6.2 were expressed only in non-taste tissue (Yee et al. 2011). In another study, SUR1 was reported to be uniquely expressed in rat fungiform papillae, whereas neither SUR1 nor SUR2 were found in circumvallate papillae (Liu et al. 2011a). In HTC-8-G-GECO spheroids mRNA levels for Kir6.1 and SUR2 were abundant (Supplementary Table 18). As SUR2A and SUR2B are splice variants (Seino 2003), it cannot be concluded which of them or if both subunits are present. SUR2A/Kir6.1 channels are relatively unexplored and their functionality has not been proved *in vivo*. This combination was, therefore, rather tested in heterologous expression systems and was proposed as taurine-sensitive K_{ATP} channel (Brochiero et al. 2002). SUR2B/Kir6.1 channels are natively expressed (Table 13). Thus, SUR2B/Kir6.1 channels downstream of GLUTs may depolarize HTC-8-G-GECO spheroids upon sugar entry.

4.7.3 Osmotic sensing may transduce sugars sweet taste in HTC-8-G-GECO spheroids

As introduced earlier, an alternative mode for sugar-induced cellular depolarization could be via osmotic swelling-mediated compensatory Cl^- efflux through VRAC (Best et al. 2010). For the swelling upon Glucose entry via GLUTs or SGLT1, water influx could involve aquaporins (Matsumura et al. 2007; Best et al. 2010; Louchami et al. 2012). Of these, AQP1, 2, 5 were found to mediate this cell swelling in rat taste buds (Watson et al. 2007). In HTC-8-G-GECO spheroids these aquaporins were also present, although they were expressed at a very low abundance below the threshold value of 1 (Supplementary Table 18). As HTC-8-G-GECO spheroids expressed also the leucine-rich repeat-containing protein LRRC8A, which is a main component of VRAC, this pathway may be active upon sugar stimulation (Figure 24, Table 12).

4.7.4 HTC-8-G-GECO spheroids may not release GLP-1

Upon activation of the alternative pathway, it was proposed that taste cells may release GLP-1 to initiate CPIR (von Molitor et al. 2020c). GLP-1 is released after cleavage of Pro-glucagon by Pro-hormone Convertase 1/3 exclusively upon oral sweet stimulation (Martin et al. 2012; Kokrashvili et al. 2014; Takai et al. 2015). In HTC-8-G-GECO spheroids, Pro-glucagon and

Pro-hormone Convertase 1/3 mRNA levels were absent (Supplementary Table 18), suggesting that spheroids were not able to produce and secrete GLP-1. However, Dipeptidyl-peptidase 4 (DDP4), which digests GLP-1, was abundant which is in contrast with previous results of mouse circumvallate papillae were DDP4 was not detected (Shin et al. 2008).

4.7.5 The sugar-mediated response of HTC-8-G-GECO spheroids may be mediated by signaling molecules linked to metabolic sensing

In summary, functional imaging studies showed that culturing HTC-8-G-GECO cells in a 3D environment changed their phenotype and physiology. Indeed, specific responses to sweet compounds were observed in spheroids and spheroid-derived monolayer cultures but not in permanent monolayer cultures. Interestingly, in the preliminary mRNA sequencing screen, rather GLUTs instead of the sweet taste receptor were detected. Accordingly, sugars sweet taste in HTC-8-G-GECO spheroids may be mediated via the alternative pathway. As for the canonical signaling pathway, again, not all signaling molecules of the alternative pathway could be detected, however, they may have been substituted by family members (Figure 24, Table 12). Additionally, unrelated molecules such as SCRT could be involved. To make a final conclusion if HTC-8-G-GECO spheroids use the canonical, the alternative or both signaling pathways, additional live cell experiments with sugars in the presence of the sweet taste inhibitor Lactisol (Schweiger et al. 2020), the SUR inhibitor Glibenclamide (Yamada et al. 1997; Sim et al. 2002), the glycolysis inhibitor 2-Deoxyglucose (Bartölke et al. 2014), the SLC45A inhibitor Carbonyl Cyanide m-Chlorophenyl-hydrazone (CCCP) (Bartölke et al. 2014), the VRAC inhibitor 4-(2-Butyl-6,7-dichloro-2-cyclopentyl-indan-1-on-5-yl) oxobutyric acid (DCPIB) (Han et al. 2014) or non-metabolizable sugar substitutes (Nakagawa et al. 2015; Yasumatsu et al. 2020) should be conducted.

4.8 Possible ways for Ca^{2+} entry in HTC-8-G-GECO spheroids

It is generally accepted that bitter and sweet taste perception induce Ca^{2+} release from internal stores (Roper and Chaudhari 2017; Chaudhari and Roper 2010). However, perfusion experiments with Ca^{2+}-free buffers did not result in Ca^{2+} responses to Saccharin nor Sucrose in HTC-8-G-GECO spheroids, suggesting that Saccharin and Sucrose responses did not relay on intracellular Ca^{2+} stores. Fittingly, Saccharin-induced Ca^{2+} responses in HTC-8 monolayer cultures were reported to induce cell depolarization and subsequent intracellular Ca^{2+} release without the involvement of PLC (Hochheimer et al. 2014). Moreover, Glucose-evoked Ca^{2+} peaks in murine β-cells mediated by GLUT, required Ca^{2} influx (Nakagawa et al. 2015).

While it is generally believed that VDCCs are not expressed in type II taste cells (Clapp et al. 2006; DeFazio et al. 2006), functional L- and T-type channels were reported to be involved in the Saccharin (Béhé et al. 1990) and Sucrose (Nakagawa et al. 2015) response in mice.

Further, VDCCs expression has been shown in some type II cells which may represent a small subpopulation (Béhé et al. 1990; Medler et al. 2003; Hacker et al. 2008). As mRNA sequencing data of HTC-8-G-GECO spheroids revealed expression of T- and L-type VDCCs (Supplementary Table 17), the contribution of VDCCs in compound-mediated Ca^{2+} entry cannot be excluded.

Additional mechanisms are also possible. The store operated Ca^{2+} channels ORAI1 and ORAI3 which are controlled by the endoplasmic reticulum Ca^{2+} depletion sensing stromal interaction molecule-1 (STIM1) are responsible for Ca^{2+} entry upon store depletion (Dramane et al. 2012; Abdoul-Azize et al. 2014). ORAI1 and ORAI3 are present in CD36-positive cells (Dramane et al. 2012) and CD36 is expressed in some type II and type III cells in mouse taste buds (Gilbertson and Khan 2014). As ORAI1, 3 and STIM1 mRNA was detected within the mRNA sequencing screen (Supplementary Table 17), HTC-8-G-GECO spheroids may utilize a similar mechanism to refill stores. Additionally Ca^{2+} influx may be mediated via activation of vanilloid receptors (VR1s), which were shown to be involved in the Saccharin-mediated metallic taste and Ca^{2+} entry (Riera et al. 2007; Hochheimer et al. 2014). In HTC-8 monolayer cultures VR1 is expressed, however, its expression was significantly reduced in spheroids even below the threshold level of 1 (Supplementary Table 17). Na^{+}/Ca^{2+} exchangers (NCX) in mouse type II cells have been proposed to contribute to the termination of Ca^{2+}-evoked signals of VDCCs but not to Ca^{2+} responses that depended on the Ca^{2+} release from stores (Szebenyi et al. 2010). Since NCXs were expressed in HTC-8-G-GECO spheroids, they may play a similar role there. This Ca^{2+} entry requiring mechanism is, however, discrepant from the classical mechanism proposed in native taste cells, which implies intracellular Ca^{2+} release (Chaudhari and Roper 2010; Roper and Chaudhari 2017).

4.9 Purinergic intercellular signaling may boost and/or transmit taste responses in HTC-8-G-GECO spheroids

In the taste bud, ATP is released from type II cells via an atypical mechanism involving pannexin 1 and CALHM1/3 to exert, besides P2YR4 paracrine type III stimulation, also an autocrine positive feedback via P2XR2 and P2YR1 (Huang et al. 2007; Romanov et al. 2007; Huang et al. 2009). Stimulation of HTC-8-G-GECO spheroids with ATP revealed robust Ca^{2+} transients with a fast onset and offset. Consistent to bitter and sweet responses, also ATP mediated faster and stronger responses in cells located in the spheroid periphery compared to cells in the core. In accordance to this, ATP-induced Ca^{2+} transients occurred predominantly in cells located in the outer part of mouse taste buds (Hayato et al. 2007). To address, whether HTC-8-G-GECO spheroids were potentially able to release ATP, the transcriptome data for the candidate protein families CALHM and pannexin were screened.

4.9.1 HTC-8-G-GECO spheroids express CALHM2 instead of CALHM1/3

In HTC-8-G-GECO spheroids, only CALHM2 was expressed (Supplementary Table 16). However, in mouse fungiform and circumvallate papillae usually all family members of CALHM (CALHM1-3) are expressed in comparable amounts and co-localize with the type II cell marker TRPM5 (Moyer et al. 2009). While CALHM1 is necessary for ATP release (Taruno et al. 2013), CALHM3 contributes as a pore-forming subunit to the hexameric complex in taste cells (Ma et al. 2018). CALHM3 cannot induce ionic currents if expressed alone (Ma et al. 2018), but heterologous expression of only CALHM1 in non-taste cells allowed ATP permeability (Taruno et al. 2013; Siebert et al. 2013). Surprisingly, knockout of either one subunit in mice reduced responses to gustatory stimuli (Ma et al. 2012; Taruno et al. 2013; Ma et al. 2018), although in CALHM3-knockout mice CALHM1 expression was not downregulated (Ma et al. 2018). Thus, both subunits seem to be necessary to mediate ATP release *in vivo*. In taste cells, a function for CALHM2 has not been described so far, and combinations of CALHM1/2 resulted in comparable currents to CALHM1 alone in oocytes (Ma et al. 2018b). Further, similar to CALHM3, CALHM2 alone most likely cannot from functional channels (Ma et al. 2018). Thus, it remains unclear, whether HTC-8-G-GECO cells can release ATP via such channels.

4.9.2 ATP may be released via pannexin 1 in HTC-8-G-GECO spheroids

Besides CALHM1/3, also pannexin 1 is present in mouse type II cells and was proposed to mediate ATP release, since it was antagonized by Carbenoxolone (Huang et al. 2007; Romanov et al. 2007; Dando and Roper 2009; Murata et al. 2010). However, this antagonist is only moderately specific and other studies could not confirm the inhibitory effect even when Carbenoxolone was used at high concentrations (Romanov et al. 2007; Romanov et al. 2008). Further, knockout of pannexin 1 in mice did not impact ATP release nor gustatory responses (Romanov et al. 2012; Vandenbeuch et al. 2015; Tordoff et al. 2015), questioning its role as ATP release channel. However, pannexin 1 may have been utilized to release ATP in HTC-8-G-GECO spheroids since i) transcriptome analysis revealed high pannexin 1 expression levels (Supplementary Table 16), ii) only CALHM2 instead of the highly ATP-permeable CALHM1/3 channel was expressed, and iii) addition of the purinergic inhibitor Suramin significantly reduced ATP as well as Saccharin-mediated Ca^{2+} transients.

4.9.3 Purinergic signaling may utilize P2RX7 and P2RY1 in HTC-8-G-GECO spheroids

For ATP-dependent signal transduction, one would expect the presence of purinergic receptors. While in HTC-8 monolayer culture, P2RY4, P2RY12 and P2RX2 were not detected (Hochheimer et al. 2014), HTC-8-G-GECO spheroids showed expression of P2RX7 and P2RY1 (Supplementary Table 16). In mouse fungiform papillae, P2RX7 mediates autocrine and paracrine stimulation of type II and type III cells, respectively (Hayato et al. 2007). Since

P2RX7 is also involved in apoptosis in different cell types and taste cells are constantly regenerated, P2RX7 could trigger apoptosis in HTC-8-G-GECO spheroids as well and may play a role in taste bud renewal (Beidler and Smallman 1965; Schulze-Lohoff et al. 1998). When mouse type II cells were stimulated with P2RX and P2RY agonists, only P2RY agonists affected Ca^{2+} levels, indicating that rather P2RY modulates taste cell responses (Kim et al. 2000). P2RY12, which was detected in monolayer HTC-8 culture (Hochheimer et al. 2014), is not expressed in taste buds and was rather found in non-taste lingual epithelia in mice (Bystrova et al. 2006; Hayato et al. 2007). On the contrary, P2RY1 that natively mediates positive autocrine feedback onto type II cells (Huang et al. 2007; Romanov et al. 2007; Huang et al. 2009) was expressed in HTC-8-G-GECO spheroids (Supplementary). Thus, purinergic signaling within HTC-8-G-GECO spheroids most likely occurred either due to P2RX7 or P2YR1 stimulation. This hypothesis is further supported since application of the P2RX and P2RY antagonist Suramin, significantly reduced Saccharin-mediated Ca^{2+} transients indicating that purinergic intercellular communication is critical to magnify and convey bitter signaling in HTC-8-G-GECO spheroids. As Suramin inhibited the Saccharin response in all spheroid rings equally, ATP may exert rather an autocrine modulation. Further, NTPDase-1, expressed in HTC-8-G-GECO spheroids (Supplementary Table 16), may enzymatically degrade ATP in the spheroid microenvironment and contribute together with purinergic receptor desensitization to the fast offset of Ca^{2+} transients (Hayato et al. 2007; Hochheimer et al. 2014).

4.9.4 3D microenvironments and LSFM may be advantageous to study intercellular signaling

In flat monolayer cultures, the aspect of intercellular communication may be underestimated as cells cannot optimally interact with each other since released substances are diluted in the large media volume. Conversely, ATP released from Saccharin-stimulated HTC-8-G-GECO cells may readily find its receptors in 3D cultures where cells are in close contact, which may be important for signal amplification and diffusion. Thus, to better address such more complex physiological questions in a 3D context, LSFM may be superior to confocal microscopy. Further, LSFM may be beneficial to study signaling mechanisms not compartmentalized to a specific region that extend through several cell layers into diverse directions via intercellular communication. This may be particularly relevant when 3D cultures do not have a regular spherical shape or when they contain different cell types, such as in co-cultures or organoids.

The LSFM experiments of spheroids stimulated with ATP showed oscillation-like, repetitive Ca^{2+} transient with declining peaks over time in the whole spheroid analysis, which was different from the single and fast Ca^{2+} responses observed in the confocal setup. A possible explanation for the reduced response amplitudes and the rapid decay of the signal, even in presence of ATP, could be the desensitization of P2Rs (Hayato et al. 2007). The presence of

repetitive transients in LSFM experiments might be caused by i) the increased exposure time, ii) the prolonged exchange times of buffers, iii) the embedding in Agarose, which likely impeded ATP diffusion and modified the surrounding milieu allowing the congregation of released molecules but also degradation products, and iv) the different spheroid regions imaged. Indeed, these repetitive transients were mainly observed in the outer z-planes, which were not recorded with confocal microscopy due to the limited time resolution.

4.10 HTC-8-G-GECO spheroids may contain tightly and broadly tuned cells

Gustation in the taste bud has been described to follow labelled lines. This implies that diverse taste modalities use different signaling pathways in distinct cell types (Gilbertson et al. 2000; Caicedo et al. 2002). Indeed, in native mouse taste cells, T1R and T2R are expressed in distinct type II cell subpopulations (Nelson et al. 2001). Yet, other publications showed that some individual taste cells respond at the same time to different gustatory stimuli (Table 14). Thus, in the taste bud there may be “tightly tuned” cells, specifically responding to only one taste modality, and “broadly tuned” cells, responding to several modalities (Keiichi and Masaya 1984; Gilbertson et al. 2001; Banik et al. 2020). Interestingly, some cells in HTC-8-G-GECO spheroids were also sensitive to both, sweet and bitter stimulation.

Table 14: Overview of studies that have reported the presence of broadly tuned taste cells. Abbreviations: BT: broadly tuned cells, CV: circumvallate papillae, FF: fungiform papillae, F: foliate papillae.

BT responsiveness	Percentage of BT	Papillae	Species	Source
sweet, bitter, umami, sour, salty	~85	FF	rat	Kimura and Beidler 1961; Sato and Beidler 1997; Sato and Beidler 1982,
sweet, bitter, poorly to salty, sour	~70	FF	mouse	Keiichi and Masaya 1984
sweet, bitter, umami, sour, salty	nearly all cells responded at least to two modalities	FF	rat	Ozeki 1971; Ozeki and Sato 1972
sweet, bitter, umami, sour, salty	one modality: 27% two modalities: 25 % thee modalities: 34% four modalities: 14%	anterior soft palates	rat	Gilbertson et al. 2001
sweet, salty, sour, bitter	~40	CV	mouse	Caicedo et al. 2002
KCl, bitter	~70	CV, F	mouse	Hacker et al. 2008
sweet, bitter, umami, sour, salty	~70	CV, F, FF	mouse	Banik et al. 2018

The board tuning of cells may be the result of i) an overlap in the transduction mechanisms of diverse downstream components of sweet, bitter and umami (Gilbertson et al. 2000) or ii) the expression of multiple signaling cascades in one taste cell (Herness and Gilbertson 1999). According to the later hypothesis, HTC-8-G-GECO double responding cells may express components of the canonical bitter pathway and the alternative sweet pathway. So far, GLUT

and T1R3 co-expression was shown in mouse taste cells (Yee et al. 2011), however the co-expression of GLUTs with T2R has not been investigated yet. In mouse taste cells, broadly tuned cells were positive for the type III cell marker GAD67 and SNAP25 and responded to sweet, bitter and umami via a PLCβ3/IP3-mediated pathway to release Ca^{2+} from the stores (Banik et al. 2020). In accordance to this, transcriptome analysis of HTC-8-G-GECO spheroids revealed also expression of type III cell markers, such as SNP25, VDCC or PLCβ3, and type II cell markers including Gα-proteins, TRPM4, IP3-R and pannexin 1.

In general, broad tuning might allow greater flexibility of conveying gustatory information and potentially may allow finer discrimination (Gilbertson et al. 2001; Banik et al. 2020). However, how or where the information of tightly and broadly tuned cells converge, and how the signals are processed, is still unclear (Chandrashekar et al. 2006). To convey information, these cell populations may either communicate with each other or they might send diverse signals to the gustatory nerve endings (Banik et al. 2020). Remarkably, knockout of either IP3-R, which induces the inability to process bitter stimuli in type II cells, or knockout of PLCβ3, which impacts bitter transduction in broadly tuned type III cells, resulted in severely diminished behavioral responses to the bitter compound Quinine, suggesting that the input of both cell populations is necessary to activate neurons in the NTS (Banik et al. 2020). Two currents of thought differently describe decoding of gustation (Bradbury 2004; Chandrashekar et al. 2006). Conferring to the “labelled line” theory, diverse taste modalities use diverse signaling pathways in different cell types and also signal to dedicated nerves and neurons up to the brain (Wang et al. 2018). In this theory, the role of broadly responding cells remains unclear (Banik et al. 2020). On the contrary, the “cross coding” theory proposes that it is the pattern of activities of a cell network that encodes a specific taste (Gilbertson et al. 2001; Bradbury 2004). In this scenario, broadly tuned cells would allow to encode information with activity patterns and increase the information amount that is transmitted (Banik et al. 2020). Since broadly and tightly tuned cells are present in taste buds and probably also in HTC-8-G-GECO spheroids, both decoding systems may be valid (Banik et al. 2020). Indeed, in cat (Pfaffmann 1941) and rat (Breza et al. 2010) some chorda tympani fibers responded specifically to one tastant, while others were sensitive to multiple tastants according to tightly and broadly tuned taste cells.

4.11 Further perspectives

Despite the variety of methods applied to study HTC-8 spheroids, including immunostaining, live cell imaging and gene expression analysis, it could not be concluded how exactly Ca^{2+} responses to sweet and bitter stimuli are generated. The discrepancies of the live cell imaging experiments, which suggested positive responses to sweet and bitter stimuli, with the transcriptome analysis may have several reasons. A first reason might be that the expression levels of candidate molecules was below the detection limit of RNA transcriptome analysis

(Chapter 4.6.1, Ren et al. 2017). Even though the percentage of cells responding was not quantified due to the analysis of only one z-plane and a lack of automatic cell segmentation, it could be clearly observed that only a small percentage of cells responded within the spheroid, and that these cells were mainly located on the spheroid border. The small number of responding cells in correlation to the total cell number in the spheroid may has diluted candidate mRNAs. Additionally, only few copies of the molecules may have been expressed per cell. Further, increased cell passage numbers may have led to a loss of candidate protein expression, as after 25 passages, Ca^{2+} responses were getting progressively weaker in comparison to those of earlier cell passages. Moreover, mRNA expression data were based on only one mRNA sequencing screen, therefore, it has to be considered that mRNA expression data are not definitive and additional replicates need to be performed. Since HTC-8-G-GECO spheroids were disassembled prior mRNA preparation, mRNA transcripts might have decayed during this procedure and the relative expression values could be biased. Indeed, in microarray-based studies on human colon cancer tissues, a prolonged time interval of 60 min from tissue harvest to RNA isolation affected expression profiles in ~70% of the studied genes (Huang et al. 2001). In another analysis, increased RNA extraction periods led only in 8% to transcript loss, however, the relative expression levels were dramatically altered (Gallego et al. 2014). The process of mRNA degradation in HTC-8-G-GECO spheroids might account especially for cells at the spheroid periphery, which were mostly responding to gustatory stimulation, but have also been exposed to higher stress than cells in the core.

Advanced techniques, such as single cell sequencing, would allow to specifically analyze the genome and transcriptome of responding HTC-8-G-GECO cells (Sukumaran et al. 2017). Indeed, single cell analysis was previously used to analyze the transcriptome of individual type II and type III taste cells of mouse circumvallate papillae. In this study, type II cells were identified by endogenous T1R3-GFP expression and type III cells upon live cell imaging experiments with KCl (Sukumaran et al. 2017). However, for this single cell analysis, circumvallate papillae were dissociated and cultured as monolayer prior analysis (Sukumaran et al. 2017), which leads to a loss of spatial information and might stress cells, thereby, influencing their behavior. To isolate specific single cells from heterogeneous tissues and to maintain spatial information, laser micro-dissection may be used (Frumkin et al. 2008) though, this complex technique requires expertise and it would be difficult to re-identify responding cells based on live cell imaging experiments, especially those not located on the spheroid periphery. Nonetheless, even single cell sequencing from randomized cells may help to understand the heterogeneity of cell populations within the spheroid.

The absence of reliable antibodies also precludes flow cytometry cell sorting. However, trypsinized cells from spheroids might be sorted based on their G-GECO signals in response to gustatory stimulation. But also with this technique spatial information are lost.

As an alternative, specific cell populations might be identified via fluorescence *in situ* hybridization (FISH). FISH uses short labelled single-stranded DNA sequences to hybridize to their complementary nucleotide target sequences in fixed cells (Markaki et al. 2013). Indeed, also for FISH, advanced protocols for 3D samples have been established, which were subsequently analyzed with super-resolution structured illumination microscopy (Markaki et al. 2012; Markaki et al. 2013). Moreover, FISH has been shown to be stable upon optical clearing of mouse brains with CLARITY (Chung et al. 2013), suggesting that FISH can also be examined with confocal microscopy upon clearing with Glycerol.

4.12 Outlook: HTP-76 cells as a potential unlimited cell source to study taste cell differentiation

Due to the extraoral sweet taste receptor expression, understanding sweet taste signaling is not only important to improve the nutritional value of food, but may also help to develop strategies for the treatment of diabetes and obesity (von Molitor et al. 2020c). Further, it is not only T1R2/T1R3 that mediates sweet taste but there is increasing evidence for the involvement of the sweet taste receptor-independent pathway. Accordingly, a cell line that can sense sugars with both pathways could be of major interest as it more closely reflects the *in vivo* situation. Even if HTC-8 cells may be already primed towards bitter sensitivity (Hochheimer et al. 2014), they became sweet-sensitive when cultured in 3D. However, not all classical singling molecules of the canonical pathway were expressed, wherefore it has to be debated if HTC-8 spheroids can reliably reflect the behavior of human sweet- and bitter-sensitive taste cells. Further, HTC-8 cells do not possess all progenitor markers anymore (Riedel et al. 2016), which may impede their differentiation. Instead, SOX9- and LGR6-expressing HTP cells may resemble more progenitor-like cells (Riedel et al. 2016) that can be rather differentiated to express components of both, the canonical and the alternative sweet pathway.

In a previous publication, LGR5- and LGR6-positive primary mouse taste cells, indeed grew as organoids containing all different taste cell types, including type II cells expressing sweet taste receptors (Ren et al. 2014; Aihara et al. 2015; Ren et al. 2017; Ren et al. 2020) and GLUTs (Takai et al. 2019). Thus, it was tested if HTP-76 cells could be suitable to generate 3D cultures. For spheroid generation a co-culture with HTC-8-G-GECO cells was required, in which HTC-8-G-GECO cells formed the core spheroid and HTP-76 cells grew as buddings. A similar structure was observed in mouse progenitor cell organoids, where mature cells grew in the center and stem cells, positive for SOX9 and BrdU, as buddings (Aihara et al. 2015). In contrast, in Dynarray co-cultures, HTP-76 cells filled the core of the cavity and HTC-8-G-GECO cells grew on top, which resembles the distribution of progenitors and mature taste cells in native taste buds. Although the knowledge of how to drive the differentiation to mature type II cells is missing, diverse pathways have been proposed to play a role in taste cell differentiation.

Sonic hedgehog (Shh) is a key signaling molecule involved in cell growth and differentiation in multiple tissues and binds to patched 1 (Ptc). While Shh is expressed in basal taste cells, Ptc expression occurs in epithelial cells on the basal sides outside of the taste bud, adjacent to Shh-expressing cell clusters (Miura et al. 2001). With this, KRT5 and KRT14-expressing progenitor cells have also been described to reside at the basement membrane outside taste buds (Gaillard et al. 2015; Asano-Miyoshi et al. 2008; Okubo et al. 2009) and to produce post-mitotic daughter cells that either differentiate into keratinocytes (Miura et al. 2006), or enter the taste buds and start to transiently express Shh upon SOX2 stimulation (Okubo et al. 2006). Type IV progenitor cells, thus, express KRT5/14, SOX2 and Trp63 (p63), which belongs to the p53 transcription factor family, and could be critical for tongue development since Trp63-deficient embryos had a thinner tongue epithelial layer (Mills et al. 1999). Using genetic lineage tracing in mice further revealed, that Shh-positive cells may give rise to all three taste cell types (Castillo et al. 2014). Accordingly, Shh signaling has been shown to control the development and maintenance of taste organs in mice (Liu et al. 2013). Further, most Shh-positive cells differentiated to type I cells, followed by type II and type III cells, which reflects the relative proportions of these cell types in taste buds (Miura et al. 2014). Thus, Shh may regulate taste bud regeneration (Miura and Barlow 2010). Moreover, in multiple studies it was found that taste bud innervation is required for taste cell maintenance since denervation led to the relapse of taste buds. With this, also Shh and Ptc expression was lost, suggesting that their expression is nerve-dependent (Miura et al. 2006). Though all these studies proposed a role for Shh in taste cell differentiation *in vivo*, addition of Shh into the media did not affect differentiation in mouse progenitor cell organoids (Ren et al. 2014) but promoted proliferation (Ren et al. 2017).

As Shh signaling, also Wnt/β-catenin signaling is involved in progenitor cell fate decisions, required for embryonic taste bud development and taste cell turnover (Gaillard and Barlow 2011). Since β-catenin induced excess clusters of Shh-positive cells, Wnt signaling appears to act upstream of Shh (Gaillard et al. 2015). In mice, activation of Wnt/β-catenin drives first the proliferation of progenitors and then the differentiation of mainly type I cells in fungiform and circumvallate papillae, with a smaller amount of type II cells, but does not produce type III cells. This might be caused by graded levels of β-catenin signaling, which determine the specific cell fate in a concentration-dependent manner: i) high levels may promote type I cell differentiation, ii) moderate levels type II cell differentiation, and iii) high- and mid-levels preclude type III cell formation (Gaillard et al. 2015). Moreover, Wnt agonists have been shown to induce long-term salivary gland stem cell expansion (Maimets et al. 2016). Further, removal of Wnt3a reduced mouse progenitor cell organoid sizes (Aihara et al. 2015; Ren et al. 2017) and led to the absence of T1R2 and the type III cell marker SNAP25 (Aihara et al. 2015). To augment Wnt signaling, R-spondins interact with LGR5/LGR6. Accordingly, addition of R-spondin led to a substantial growth in progenitor mouse taste cell organoids (Ren et al. 2014).

Further, Noggin, which inhibits bone morphogenetic proteins (BMP), substantially increased the number of papillae *in vivo* (Zhou et al. 2006), and progenitor mouse taste cell organoids grew larger in presence of Noggin, with significantly more mature taste cells of all three types (Aihara et al. 2015; Ren et al. 2017).

Likewise, a role for Notch signaling has been proposed to function in cell lineage decisions in mice (Seta et al. 2003). Blocking Notch signaling accelerated the differentiation of mature taste cells and altered cell fate determination in progenitor mouse taste cell organoids (Ren et al. 2017; Ren et al. 2020). Further, inhibition of Notch modulated multiple signaling pathways including upregulation of Wnt (Ren et al. 2020).

Moreover, T1R was not expressed in the absence of the epidermal growth factor (EGF) (Aihara et al. 2015), and it was found that Insulin may be an important regulator of taste cell proliferation via activation of the mTOR pathway (Takai et al. 2019). Indeed, inhibition of mTOR and depletion of Insulin led to larger organoids but with less mature taste cells (Takai et al. 2019).

Thus, a variety of signaling pathways has been proposed to mediate taste cell differentiation. Besides Insulin, which was proposed to inhibit differentiation, none of these signaling factors was added in HTP-76 nor HTC-8 media. Since progenitor cell organoids from neonatal mice generated more taste receptor cells than progenitors from adults, and since they showed massive transcriptional differences, the age of HTC-8 and HTP-76 donors might further influence their potential as appropriate cell line (Ren et al. 2020). Besides the addition of differentiation promoting signals, also more physiological conditions may trigger cell polarization and differentiation. Accordingly, perfusion of stem cell cultures has supported osteoblast (Altmann et al. 2014) or retina cell (Rieke et al. 2008) differentiation. Shear fluid may also mimic saliva motion on the tongue, thereby supporting HTC-8 and HTP-76 cell differentiation. This is, indeed, feasible with Dynarray chips, since they can be used with dynamic medium exchange when incorporated in perfusion reactors.

4.13 Conclusion

In the present work human lingual cells derived from human fungiform papillae were grown as spheroids and in Dynarray chips to mimic a 3D environment similar to that of taste buds. These 3D taste cell cultures responded to KCl depolarization, bitter substances and nutritive sugars and utilized ATP for intercellular communication. Thus, this approach could be of large interest because i) it used a stably proliferating cell line of human origin, ii) HTC-8 cells may be broadly responding cells sensitive to sweet and bitter compounds, and iii) 3D taste bud-like structures are easy and inexpensive to generate. Although gustducin, PLCβ2 and TRPM5 are always described as “the players” of canonical taste signaling, results obtained from HTC-8-G-GECO spheroids suggested that multiple additional family members may contribute. Further, HTC-8-

G-GECO spheroids contained signaling components of the sweet taste receptor-independent pathway. In industry HTC-8-G-GECO spheroids might appreciate higher acceptance than previously used heterologous expression systems since only native human taste cells may reproduce the complexity of the human taste response. In contrast to human *in vivo* studies, HTC-8-G-GECO spheroids further offer the great potential to multiplex and compounds can be applied irrespectively of their potential toxicity. Thus, studies with HTC-8-G-GECO spheroids may save precious time and cost. Further, they may be implemented to study sweet taste singling and to screen for new sugar substitutes. Additionally, cultivation with other organ spheroids in microfluidic devices may allow to mimic whole-body responses upon application of new test molecules that have so far not been addressed in human.

5 References

Abaffy, T.; Trubey, K.; Chaudhari, N. (2003): Adenylyl cyclase expression and modulation of cAMP in rat taste cells. In *Am J Physiol, Cell Physiol* 284 (6), C1420-8.

Abberger, T.; Jennings, P.; Mirlach, A. et al. (2006): Application of a population balance model to a perfusion in vitro toxicity system. In *Toxicol In Vitro* 20 (7), pp. 1213–1224.

Abdallah, L.; Chabert, M.; Louis-Sylvestre, J. (1997): Cephalic phase responses to sweet taste. In *Am J Clin Nutr* 65 (3), pp. 737–743.

Abdoul-Azize, S.; Selvakumar, S.; Sadou, H. et al. (2014): Ca2+ signaling in taste bud cells and spontaneous preference for fat: unresolved roles of CD36 and GPR120. In *Biochimie* 96, pp. 8–13.

Adler, E.; Hoon, M.; Mueller, K. et al. (2000): A Novel Family of Mammalian Taste Receptors. In *Cell* 100 (6), pp. 693–702.

Aihara, E.; Mahe, M.; Schumacher, M. et al. (2015): Characterization of stem/progenitor cell cycle using murine circumvallate papilla taste bud organoid. In *Sci Rep* 5, p. 17185.

Akabas, M.; Dodd, J.; Al-Awqati, Q. (1988): A bitter substance induces a rise in intracellular calcium in a subpopulation of rat taste cells. In *Science* 242 (4881), pp. 1047–1050.

Aleman, M.; Marconi, L.; Nguyen, N. et al. (2016): The Influence of Assay Design, Blinding, and Gymnema sylvestre on Sucrose Detection by Humans. In *J Undergrad Neurosci Educ* 15 (1), A18-23.

Altmann, B.; Löchner, A.; Swain, M. et al. (2014): Differences in morphogenesis of 3D cultured primary human osteoblasts under static and microfluidic growth conditions. In *Biomaterials* 35 (10), pp. 3208–3219.

Ardalan, M.; Tabibi, H.; Ebrahimzadeh Attari, V.; Malek Mahdavi, A. (2017): Nephrotoxic Effect of Aspartame as an Artificial Sweetener: a Brief Review. In *Iran J Kidney Dis* 11 (5), pp. 339-343.

Asano-Miyoshi, M.; Abe, K.; Emori, Y. (2000): Co-expression of calcium signaling components in vertebrate taste bud cells. In *Neuroscience Letters* 283 (1), pp. 61–64.

Asano-Miyoshi, M.; Hamamichi, R.; Emori, Y. (2008): Cytokeratin 14 is expressed in immature cells in rat taste buds. In *J Mol Histol* 39 (2), pp. 193–199.

Ashcroft, F.; Harrison, D.; Ashcroft, S. (1984): Glucose induces closure of single potassium channels in isolated rat pancreatic beta-cells. In *Nature* 312 (5993), pp. 446–448.

Avenet, P.; Hofmann, F.; Lindemann, B. (1988): Transduction in taste receptor cells requires cAMP-dependent protein kinase. In *Nature* 331 (6154), pp. 351–354.

Avenet, P.; Lindemann, B. (1987): Patch-clamp study of isolated taste receptor cells of the frog. In *J Membr Biol* 97 (3), pp. 223–240.

Babenko, A.; Aguilar-Bryan, L.; Bryan, J. (1998): A view of sur/KIR6.X, KATP channels. In *Annual review of physiology* 60, pp. 667–687.

Bachmanov, A.; Bosak, N.; Floriano, W. et al. (2011): Genetics of sweet taste preferences. In *Flavour Fragr J* 26 (4), pp. 286–294.

Bachmanov, A.; Li, X.; Reed, D. et al. (2001): Positional cloning of the mouse saccharin preference (Sac) locus. In *Chem Senses* 26 (7), pp. 925–933.

Bachmanov, A.; Reed, D.; Ninomiya, Y. et al. (1997): Sucrose consumption in mice: major influence of two genetic loci affecting peripheral sensory responses. In *Mamm Genome* 8 (8), pp. 545–548.

Baker, B.; Chen, C. (2012): Deconstructing the third dimension: how 3D culture microenvironments alter cellular cues. In *J Cell Sci* 125 (Pt 13), pp. 3015–3024.

Banik; Debarghya; Benfey, E. et al. (2020): A subset of broadly responsive Type III taste cells contribute to the detection of bitter, sweet and umami stimuli. In *PLoS Genet* 16 (8), e1008925.

Banik, D.; Martin, L.; Freichel, M. et al. (2018): TRPM4 and TRPM5 are both required for normal signaling in taste receptor cells. In *Proc Natl Acad Sci U S A* 115 (4), E772-E781.

Barlow, L. (2015): Progress and renewal in gustation: new insights into taste bud development. In *Development* 142 (21), pp. 3620–3629.

Barretto, R.; Gillis-Smith, S.; Chandrashekar, J. et al. (2015): The neural representation of taste quality at the periphery. In *Nature* 517 (7534), pp. 373–376.

Bartölke, R.; Heinisch, J.; Wieczorek, H.; Vitavska, O. (2014): Proton-associated sucrose transport of mammalian solute carrier family 45: an analysis in Saccharomyces cerevisiae. In *Biochem J* 464 (2), pp. 193–201.

Baryshnikov, S.; Rogachevskaja, O.; Kolesnikov, S. (2003): Calcium signaling mediated by P2Y receptors in mouse taste cells. In *J Neurophysiol* 90 (5), pp. 3283–3294.

Baumgart, E.; Kubitscheck, U. (2012): Scanned light sheet microscopy with confocal slit detection. In *Opt Express* 20 (19), pp. 21805–21814.

Beauchamp, G. (2016): Why do we like sweet taste: A bitter tale? In *Physiol Behav* 164 (Pt B), pp. 432–437.

Beauchamp, G.; Mennella, J. (2011): Flavor perception in human infants: development and functional significance. In *Digestion*, pp. 1–6.

Beech, D.; Zhang, H.; Nakao, K.; Bolton, T. (1993): K channel activation by nucleotide diphosphates and its inhibition by glibenclamide in vascular smooth muscle cells. In *Br J Pharmacol* 110 (2), pp. 573–582.

Béhé, P.; DeSimone, J.; Avenet, P.; Lindemann, B. (1990): Membrane currents in taste cells of the rat fungiform papilla. Evidence for two types of Ca currents and inhibition of K currents by saccharin. In *J Gen Physiol* 96 (5), pp. 1061–1084.

Behrens, M.; Blank, K.; Meyerhof, W. (2017): Blends of Non-caloric Sweeteners Saccharin and Cyclamate Show Reduced Off-Taste due to TAS2R Bitter Receptor Inhibition. In *Cell Chem Biol* 24 (10), 1199-1204.e2.

Behrens, M.; Meyerhof, W.; Hellfritsch, C.; Hofmann, T. (2011): Sweet and umami taste: natural products, their chemosensory targets, and beyond. In *Angew Chem Int Ed Engl* 50 (10), pp. 2220–2242.

Beidler, L.; Smallman, R. (1965): Renewal of cells within taste buds. In *J Cell Biol* 27 (2), pp. 263–272.

Belpoggi, F.; Soffritti, M.; Padovani, M. et al. (2006): Results of long-term carcinogenicity bioassay on Sprague-Dawley rats exposed to aspartame administered in feed. In *Ann N Y Acad Sci* 1076, pp. 559–577.

Bernhardt, S.; Naim, M.; Zehavi, U.; Lindemann, B. (1996): Changes in IP3 and cytosolic Ca2+ in response to sugars and non-sugar sweeteners in transduction of sweet taste in the rat. In *J Physiol (Lond)* 490 (Pt 2), pp. 325–336.

Best, L.; Brown, P.; Sener, A.; Malaisse, W. (2010): Electrical activity in pancreatic islet cells: The VRAC hypothesis. In *Islets* 2 (2), pp. 59–64.

Bezençon, C.; Fürholz, A.; Raymond, F. et al. (2008): Murine intestinal cells expressing Trpm5 are mostly brush cells and express markers of neuronal and inflammatory cells. In *J Comp Neurol* 509 (5), pp. 514–525.

Bhatia, S.; Ingber, D. (2014): Microfluidic organs-on-chips. In *Nat Biotechnol* 32 (8), pp. 760-772.

Bootman, M.; Rietdorf, K.; Collins, T. et al. (2013): Ca2+-sensitive fluorescent dyes and intracellular Ca2+ imaging. In *Cold Spring Harb Protoc* 2013 (2), pp. 83–99.

Borges, M.; Louzada, M.; Sá, T. de et al. (2017): Artificially Sweetened Beverages and the Response to the Global Obesity Crisis. In *PLoS Med* 14 (1), e1002195.

Bradbury, J. (2004): Taste perception: cracking the code. In *PLoS Biol* 2 (3), E64.

Bradley, Robert M. (2006): The role of the nucleus of the solitary tract in gustatory processing: CRC Press.

Bray, G.; Popkin, B. (2014): Dietary sugar and body weight: have we reached a crisis in the epidemic of obesity and diabetes?: health be damned! Pour on the sugar. In *Diabetes Care* 37 (4), pp. 950–956.

Breslin, P.; Huang, L. (2006): Human taste: peripheral anatomy, taste transduction, and coding. In *Adv Otorhinolaryngol* 63, pp. 152–190.

Breslin, S.; O'Driscoll, L. (2013): Three-dimensional cell culture: the missing link in drug discovery. In *Drug Discov Today* 18 (5-6), pp. 240–249.

Breza, J.; Nikonov, A.; Contreras, R. (2010): Response latency to lingual taste stimulation distinguishes neuron types within the geniculate ganglion. In *J Neurophysiol* 103 (4), pp. 1771-1784.

Brochiero, E.; Wallendorf, B.; Gagnon, D. et al. (2002): Cloning of rabbit Kir6.1, SUR2A, and SUR2B: possible candidates for a renal K(ATP) channel. In *Am J Physiol Renal Physiol* 282 (2), F289-300.

Bufe, B.; Hofmann, T.; Krautwurst, D. et al. (2002): The human TAS2R16 receptor mediates bitter taste in response to beta-glucopyranosides. In *Nat Genet* 32 (3), pp. 397–401.

Burgess, A. (1999): The Rose model, revisited. In *J Opt Soc Am A Opt Image Sci Vis* 16 (3), pp. 633–646.

Bystrova, M.; Yatzenko, Y.; Fedorov, I. et al. (2006): P2Y isoforms operative in mouse taste cells. In *Cell Tissue Res* 323 (3), pp. 377–382.

Caicedo, A.; Kim, K.-N.; Roper, S. (2002): Individual mouse taste cells respond to multiple chemical stimuli. In *J Physiol (Lond)* 544 (2), pp. 501–509.

Caicedo, A.; Pereira, E.; Margolskee, R.; Roper, S. (2003): Role of the G-Protein Subunit α-Gustducin in Taste Cell Responses to Bitter Stimuli. In *J Neurosci* 23 (30), pp. 9947–9952.

Cali, J.; Zwaagstra, J.; Mons, N. et al. (1994): Type VIII adenylyl cyclase. A Ca2+/calmodulin-stimulated enzyme expressed in discrete regions of rat brain. In *Journal of Biological Chemistry* 269 (16), pp. 12190–12195.

Campos, R.; Lee, Y.; Drucker, D. (1994): Divergent tissue-specific and developmental expression of receptors for glucagon and glucagon-like peptide-1 in the mouse. In *Endocrinology* 134 (5), pp. 2156–2164.

Campuzano, S.; Pelling, A. (2019): Scaffolds for 3D Cell Culture and Cellular Agriculture Applications Derived From Non-animal Sources. In *Front. Sustain. Food Syst.* 3.

Cang, H.; Xu, C.; Montiel, D.; Yang, H. (2007): Guiding a confocal microscope by single fluorescent nanoparticles. In *Opt Lett* 32 (18), pp. 2729–2731.

Castillo, D.; Seidel, K.; Salcedo, E. et al. (2014): Induction of ectopic taste buds by SHH reveals the competency and plasticity of adult lingual epithelium. In *Development* 141 (15), pp. 2993-3002.

Chambers, A.; Sorrell, J.; Haller, A. et al. (2017): The Role of Pancreatic Preproglucagon in Glucose Homeostasis in Mice. In *Cell Metab* 25 (4), 927-934.e3.

Chandrashekar, J.; Hoon, M.; Ryba, N.; Zuker, C. (2006): The receptors and cells for mammalian taste. In *Nature* 444 (7117), pp. 288–294.

Chandrashekar, J.; Mueller, K.; Hoon, M. et al. (2000): T2Rs Function as Bitter Taste Receptors. In *Cell* 100 (6), pp. 703–711.

Chaudhari, N.; Landin, A.; Roper, S. (2000): A metabotropic glutamate receptor variant functions as a taste receptor. In *Nat Neurosci* 3 (2), pp. 113–119.

Chaudhari, N.; Roper, S. (2010): The cell biology of taste. In *J Cell Biol* 190 (3), pp. 285–296.

Chauency, H.; Lionwtti, F.; Winer, R.; Lisanti, V. (1954): Enzymes of human saliva. I. The determination, distribution, and origin of whole saliva enzymes. In *J Dent Res* 33 (3), pp. 321-334.

Chen, F.; Tillberg, P.; Boyden, E. (2015): Optical imaging. Expansion microscopy. In *Science* 347 (6221), pp. 543–548.

Choi, H.-J.; Cho, Y.-K.; Chung, K.-M.; Kim, K.-N. (2016): Differential expression of taste receptors in tongue papillae of DBA mouse. In *International Journal of Oral Biology* 41 (1), pp. 25–32.

Chung, K.; Wallace, J.; Kim, S.-Y. et al. (2013): Structural and molecular interrogation of intact biological systems. In *Nature* 497 (7449), pp. 332–337.

Clapp, T.; Medler, K.; Damak, S. et al. (2006): Mouse taste cells with G protein-coupled taste receptors lack voltage-gated calcium channels and SNAP-25. In *BMC Biol* 4, p. 7.

Clapp, T.; Stone, L.; Margolskee, R.; Kinnamon, S. (2001): Immunocytochemical evidence for co-expression of Type III IP3 receptor with signaling components of bitter taste transduction. In *BMC Neurosci* 2, p. 6.

Clapp, T.; Yang, R.; Stoick, C. et al. (2004): Morphologic characterization of rat taste receptor cells that express components of the phospholipase C signaling pathway. In *J Comp Neurol* 468 (3), pp. 311–321.

Clark, J. (1998): Taste and flavour: their importance in food choice and acceptance. In *Proc Nutr Soc* 57 (4), pp. 639–643.

Colsoul, B.; Schraenen, A.; Lemaire, K. et al. (2010): Loss of high-frequency glucose-induced Ca2+ oscillations in pancreatic islets correlates with impaired glucose tolerance in Trpm5-/- mice. In *Proc Natl Acad Sci U S A* 107 (11), pp. 5208–5213.

Cook, D.; Hales, C. (1984): Intracellular ATP directly blocks K+ channels in pancreatic B-cells. In *Nature* 311 (5983), pp. 271–273.

Corson, J.; Erisir, A. (2013): Monosynaptic convergence of chorda tympani and glossopharyngeal afferents onto ascending relay neurons in the nucleus of the solitary tract: A high-resolution confocal and correlative electron microscopy approach. In *J Comp Neurol* 521 (13), pp. 2907–2926.

Cummings, D.; Overduin, J. (2007): Gastrointestinal regulation of food intake. In *J Clin Invest* 117 (1), pp. 13–23.

Cummings, T.; Daniels, C.; Kinnamon, S. (1996): Sweet taste transduction in hamster: sweeteners and cyclic nucleotides depolarize taste cells by reducing a K+ current. In *J Neurophysiol* 75 (3), pp. 1256–1263.

Damak, S.; Rong, M.; Yasumatsu, K. et al. (2003): Detection of sweet and umami taste in the absence of taste receptor T1r3. In *Science* 301 (5634), pp. 850–853.

Damak, S.; Rong, M.; Yasumatsu, K. et al. (2006): Trpm5 null mice respond to bitter, sweet, and umami compounds. In *Chem Senses* 31 (3), pp. 253–264.

Dando, R.; Roper, S. (2009): Cell-to-cell communication in intact taste buds through ATP signalling from pannexin 1 gap junction hemichannels. In *J Physiol (Lond)* 587 (Pt 24), pp. 5899–5906.

Dando, R.; Roper, S. (2012): Acetylcholine is released from taste cells, enhancing taste signalling. In *J Physiol (Lond)* 590 (13), pp. 3009–3017.

Danilova, V.; Damak, S.; Margolskee, R.; Hellekant, G. (2006): Taste responses to sweet stimuli in alpha-gustducin knockout and wild-type mice. In *Chem Senses* 31 (6), pp. 573–580.

Davis, E.; Sandoval, D. (2020): Glucagon-Like Peptide-1: Actions and Influence on Pancreatic Hormone Function. In *Compr Physiol* 10 (2), pp. 577–595.

Dawson, P.; Mychaleckyj, J.; Fossey, S. et al. (2001): Sequence and functional analysis of GLUT10: a glucose transporter in the Type 2 diabetes-linked region of chromosome 20q12-13.1. In *Mol Genet Metab* 74 (1-2), pp. 186–199.

DeFazio, R.; Dvoryanchikov, G.; Maruyama, Y. et al. (2006): Separate populations of receptor cells and presynaptic cells in mouse taste buds. In *J Neurosci* 26 (15), pp. 3971–3980.

Delay, E.; Hernandez, N.; Bromley, K.; Margolskee, R. (2006): Sucrose and monosodium glutamate taste thresholds and discrimination ability of T1R3 knockout mice. In *Chem Senses* 31 (4), pp. 351–357.

Dhillon, J.; Lee, J.; Mattes, R. (2017): The Cephalic Phase Insulin Response to Nutritive and Low-Calorie Sweeteners in Solid and Beverage Form. In *Physiol Behav* 181, pp. 100–109.

Di Pizio, A.; Niv, M. (2014): Computational Studies of Smell and Taste Receptors. In *Isr. J. Chem.* 54 (8-9), pp. 1205–1218.

Dingle, Y.-T.; Boutin, M.; Chirila, A. et al. (2015): Three-Dimensional Neural Spheroid Culture: An In Vitro Model for Cortical Studies. In *Tissue Eng Part C Methods* 21 (12), pp. 1274–1283.

Doblado, M.; Moley, K. (2009): Facilitative glucose transporter 9, a unique hexose and urate transporter. In *Am J Physiol Endocrinol Metab* 297 (4), E831-5.

Dotson, C.; Roper, S.; Spector, A. (2005): PLCβ2-Independent Behavioral Avoidance of Prototypical Bitter-Tasting Ligands. In *Chem Senses* 30 (7), pp. 593–600.

Douard, V.; Ferraris, R. (2008): Regulation of the fructose transporter GLUT5 in health and disease. In *Am J Physiol Endocrinol Metab* 295 (2), E227-37.

Dramane, G.; Abdoul-Azize, S.; Hichami, A. et al. (2012): STIM1 regulates calcium signaling in taste bud cells and preference for fat in mice. In *J Clin Invest* 122 (6), pp. 2267–2282.

DuBois, G. (2016): Molecular mechanism of sweetness sensation. In *Physiol Behav* 164 (Pt B), pp. 453–463.

Dušková, M.; Macourek, M.; Šrámková, M. et al. (2013): The role of taste in cephalic phase of insulin secretion. In *Prague Med Rep* 114 (4), pp. 222–230.

Duval, K.; Grover, H.; Han, L.-H. et al. (2017): Modeling Physiological Events in 2D vs. 3D Cell Culture. In *Physiology (Bethesda)* 32 (4), pp. 266–277.

Dyer, J.; Salmon, K.; Zibrik, L.; Shirazi-Beechey, S. (2005): Expression of sweet taste receptors of the T1R family in the intestinal tract and enteroendocrine cells. In *Biochem Soc Trans* 33 (Pt 1), pp. 302–305.

Eddy, M.; Eschle, B.; Peterson, D. et al. (2012): A conditioned aversion study of sucrose and SC45647 taste in TRPM5 knockout mice. In *Chem Senses* 37 (5), pp. 391–401.

Elliott, R.; Kapoor, S.; Tincello, D. (2011): Expression and distribution of the sweet taste receptor isoforms T1R2 and T1R3 in human and rat bladders. In *J Urol* 186 (6), pp. 2455-2462.

Emerman, J.; Burwen, S.; Pitelka, D. (1979): Substrate properties influencing ultrastructural differentiation of mammary epithelial cells in culture. In *Tissue and Cell* 11 (1), pp. 109–119.

Eriksson, L.; Esberg, A.; Haworth, S. et al. (2019): Allelic Variation in Taste Genes Is Associated with Taste and Diet Preferences and Dental Caries. In *Nutrients* 11 (7).

Faustino, V.; Catarino, S.; Lima, R.; Minas, G. (2016): Biomedical microfluidic devices by using low-cost fabrication techniques: A review. In *J Biomech* 49 (11), pp. 2280–2292.

Fedorov, I.; Rogachevskaja, O.; Kolesnikov, S. (2007): Modeling P2Y receptor-Ca2+ response coupling in taste cells. In *Biochim Biophys Acta* 1768 (7), pp. 1727–1740.

Finger, T.; Böttger, B.; Hansen, A. et al. (2003): Solitary chemoreceptor cells in the nasal cavity serve as sentinels of respiration. In *Proceedings of the National Academy of Sciences* 100 (15), pp. 8981–8986.

Finger, T.; Danilova, V.; Barrows, J. et al. (2005): ATP signaling is crucial for communication from taste buds to gustatory nerves. In *Science* 310 (5753), pp. 1495–1499.

Fischer, U.; Hommel, H.; Ziegler, M.; Michael, R. (1972): The mechanism of insulin secretion after oral glucose administration. I. Multiphasic course of insulin mobilization after oral administration of glucose in conscious dogs. Differences to the behaviour after intravenous administration. In *Diabetologia* 8 (2), pp. 104–110.

Fredriksson, R.; Lagerström, M.; Lundin, L.-G.; Schiöth, H. (2003): The G-protein-coupled receptors in the human genome form five main families. Phylogenetic analysis, paralogon groups, and fingerprints. In *Mol Pharmacol* 63 (6), pp. 1256–1272.

Frumkin, D.; Wasserstrom, A.; Itzkovitz, S. et al. (2008): Amplification of multiple genomic loci from single cells isolated by laser micro-dissection of tissues. In *BMC Biotechnol* 8 (1), p. 17.

Fujiyama, R.; Miyamoto, T.; Sato, T. (1994): Differential distribution of two Ca(2+)-dependent and -independent K+ channels throughout receptive and basolateral membranes of bullfrog taste cells. In *Pflugers Arch* 429 (2), pp. 285–290.

Fuller, J. (1974): Single-locus control of saccharin preference in mice. In *J Hered* 65 (1), pp. 33–36.

Fushan, A.; Simons, C.; Slack, J.; Drayna, D. (2010): Association between common variation in genes encoding sweet taste signaling components and human sucrose perception. In *Chem Senses* 35 (7), pp. 579–592.

Gabriško, M. (2020): The in silico characterization of neutral alpha-glucosidase C (GANC) and its evolution from GANAB. In *Gene* 726, p. 144192.

Gaillard, D.; Barlow, L. (2011): Taste bud cells of adult mice are responsive to Wnt/β-catenin signaling: implications for the renewal of mature taste cells. In *Genesis* 49 (4), pp. 295–306.

Gaillard, D.; Xu, M.; Liu, F. et al. (2015): β-Catenin Signaling Biases Multipotent Lingual Epithelial Progenitors to Differentiate and Acquire Specific Taste Cell Fates. In *PLoS Genet* 11 (5), e1005208.

Galindo-Cuspinera, V.; Winnig, M.; Bufe, B. et al. (2006): A TAS1R receptor-based explanation of sweet 'water-taste'. In *Nature* 441 (7091), pp. 354–357.

Gallego; Romero, I.; Pai, A. et al. (2014): RNA-seq: impact of RNA degradation on transcript quantification. In *BMC Biol* 12, p. 42.

Geraedts, M.; Takahashi, T.; Vigues, S. et al. (2012): Transformation of postingestive glucose responses after deletion of sweet taste receptor subunits or gastric bypass surgery. In *Am J Physiol Endocrinol Metab* 303 (4), E464-74.

Gilazieva, Z.; Ponomarev, A.; Rutland, C. et al. (2020): Promising Applications of Tumor Spheroids and Organoids for Personalized Medicine. In *Cancers* 12 (10).

Gilbertson, T.; Boughter, J.; Zhang, H.; Smith, D. (2001): Distribution of Gustatory Sensitivities in Rat Taste Cells: Whole-Cell Responses to Apical Chemical Stimulation. In *J Neurosci* 21 (13), pp. 4931–4941.

Gilbertson, T.; Damak, S.; Margolskee, R. (2000): The molecular physiology of taste transduction. In *Current Opinion in Neurobiology* 10 (4), pp. 519–527.

Gilbertson, T.; Khan, N. (2014): Cell signaling mechanisms of oro-gustatory detection of dietary fat: advances and challenges. In *Prog Lipid Res* 53, pp. 82–92.

Giselbrecht, S.; Gottwald, E.; Truckenmueller, R. et al. (2008): Microfabrication of chip-sized scaffolds for three-dimensional cell cultivation. In *J Vis Exp* (15).

Glendinning, J.; Frim, Y.; Hochman, A. et al. (2017): Glucose elicits cephalic-phase insulin release in mice by activating KATP channels in taste cells. In *Am J Physiol Regul Integr Comp Physiol* 312 (4), R597-R610.

Glendinning, J.; Stano, S.; Holter, M. et al. (2015): Sugar-induced cephalic-phase insulin release is mediated by a T1r2+T1r3-independent taste transduction pathway in mice. In *Am J Physiol Regul Integr Comp Physiol* 309 (5), R552-60.

Go, Y. (2006): Proceedings of the SMBE Tri-National Young Investigators' Workshop 2005. Lineage-specific expansions and contractions of the bitter taste receptor gene repertoire in vertebrates. In *Mol Biol Evol* 23 (5), pp. 964–972.

Göke, R.; Larsen, P.; Mikkelsen, J.; Sheikh, S. (1995): Distribution of GLP-1 binding sites in the rat brain: evidence that exendin-4 is a ligand of brain GLP-1 binding sites. In *Eur J Neurosci* 7 (11), pp. 2294–2300.

Gong, T.; Wei, Q.; Mao, D.; Shi, F. (2016): Expression patterns of taste receptor type 1 subunit 3 and α-gustducin in the mouse testis during development. In *Acta Histochem* 118 (1), pp. 20–30.

Gribble, F.; Williams, L.; Simpson, A.; Reimann, F. (2003): A novel glucose-sensing mechanism contributing to glucagon-like peptide-1 secretion from the GLUTag cell line. In *Diabetes* 52 (5), pp. 1147–1154.

Gutierrez, R.; Fonseca, E.; Simon, S. (2020): The neuroscience of sugars in taste, gut-reward, feeding circuits, and obesity. In *Cell Mol Life Sci* 77 (18), pp. 3469–3502.

Habib, A.; Richards, P.; Rogers, G. et al. (2013): Co-localisation and secretion of glucagon-like peptide 1 and peptide YY from primary cultured human L cells. In *Diabetologia* 56 (6), pp. 1413–1416.

Hacker, K.; Laskowski, A.; Feng, L. et al. (2008): Evidence for two populations of bitter responsive taste cells in mice. In *J Neurophysiol* 99 (3), pp. 1503–1514.

Hallock, R.; Tatangelo, M.; Barrows, J.; Finger, T. (2009): Residual chemosensory capabilities in double P2X2/P2X3 purinergic receptor null mice: intraoral or postingestive detection? In *Chem Senses* 34 (9), pp. 799–808.

Halls, M.; Cooper, D. (2017): Adenylyl cyclase signalling complexes - Pharmacological challenges and opportunities. In *Pharmacol Ther* 172, pp. 171–180.

Hama, H.; Kurokawa, H.; Kawano, H. et al. (2011): Scale: a chemical approach for fluorescence imaging and reconstruction of transparent mouse brain. In *Nat Neurosci* 14 (11), pp. 1481–1488.

Han, P.; Bagenna, B.; Fu, M. (2019): The sweet taste signalling pathways in the oral cavity and the gastrointestinal tract affect human appetite and food intake: a review. In *International journal of food sciences and nutrition* 70 (2).

Han, Q.; Liu, S.; Li, Z. et al. (2014): DCPIB, a potent volume-regulated anion channel antagonist, attenuates microglia-mediated inflammatory response and neuronal injury following focal cerebral ischemia. In *Brain Research* 1542, pp. 176–185.

Hass, N.; Schwarzenbacher, K.; Breer, H. (2007): A cluster of gustducin-expressing cells in the mouse stomach associated with two distinct populations of enteroendocrine cells. In *Histochem Cell Biol* 128 (5).

Hass, N.; Schwarzenbacher, K.; Breer, H. (2010): T1R3 is expressed in brush cells and ghrelin-producing cells of murine stomach. In *Cell Tissue Res* 339 (3), pp. 493–504.

Hayato, R.; Ohtubo, Y.; Yoshii, K. (2007): Functional expression of ionotropic purinergic receptors on mouse taste bud cells. In *J Physiol (Lond)* 584 (Pt 2), pp. 473–488.

He, W.; Danilova, V.; Zou, S. et al. (2002): Partial rescue of taste responses of alpha-gustducin null mice by transgenic expression of alpha-transducin. In *Chem Senses* 27 (8), pp. 719–727.

Heath, T.; Melichar, J.; Nutt, D.; Donaldson, L. (2006): Human Taste Thresholds Are Modulated by Serotonin and Noradrenaline. In *J Neurosci* 26 (49), pp. 12664–12671.

Hellekant, G.; Ninomiya, Y.; Danilova, V. (1998): Taste in chimpanzees. III: labeled-line coding in sweet taste. In *Physiol Behav* 65 (2), pp. 191–200.

Herness, M.; Gilbertson, T. (1999): Cellular mechanisms of taste transduction. In *Annual review of physiology* 61, pp. 873–900.

Hevezi, P.; Moyer, B.; Lu, M. et al. (2009): Genome-wide analysis of gene expression in primate taste buds reveals links to diverse processes. In *PLoS ONE* 4 (7), e6395.

Hobbs, L. (2009): Chapter 21 - Sweeteners from Starch: Production, Properties and Uses. In James N. BeMiller, Roy Lester Whistler (Eds.): Starch. Chemistry and technology. 3rd ed. London: Academic (Food science and technology), pp. 797–832. Available online at http://www.sciencedirect.com/science/article/pii/B9780127462752000215.

Hochheimer, A.; Krohn, M.; Rudert, K. et al. (2014): Endogenous gustatory responses and gene expression profile of stably proliferating human taste cells isolated from fungiform papillae. In *Chem Senses* 39 (4), pp. 359–377.

Holst, J. (2007): The physiology of glucagon-like peptide 1. In *Physiol Rev* 87 (4), pp. 1409-1439.

Hommel, H.; Fischer, U. (1977): The mechanism of insulin secretion after oral glucose administration V. Portal venous IRI concentration in dogs after ingestion of glucose. In *Diabetologia* 13 (3), pp. 269–272.

Hoon, M.; Adler, E.; Lindemeier, J. et al. (1999): Putative Mammalian Taste Receptors. In *Cell* 96 (4), pp. 541–551.

Hoon, M.; Northup, J.; Margolskee, R.; Ryba, N. (1995): Functional expression of the taste specific G-protein, alpha-gustducin. In *Biochem J* 309 (Pt 2), pp. 629–636.

Horn, F.; Bettler, E.; Oliveira, L. et al. (2003): GPCRDB information system for G protein-coupled receptors. In *Nucleic Acids Res* 31 (1), pp. 294–297.

Hua, T.-E.; Yang, T.-L.; Yang, W.-C. et al. (2013): 3-D neurohistology of transparent tongue in health and injury with optical clearing. In *Front Neuroanat* 7, p. 36.

Huang, A.; Wu, S. (2018): Substance P as a putative efferent transmitter mediates GABAergic inhibition in mouse taste buds. In *Br J Pharmacol* 175 (7), pp. 1039–1053.

Huang, J.; Qi, R.; Quackenbush, J. et al. (2001): Effects of ischemia on gene expression. In *J Surg Res* 99 (2), pp. 222–227.

Huang, L.; Shanker, Y.; Dubauskaite, J. et al. (1999): Ggamma13 colocalizes with gustducin in taste receptor cells and mediates IP3 responses to bitter denatonium. In *Nat Neurosci* 2 (12), pp. 1055–1062.

Huang, S.; Czech, M. (2007): The GLUT4 glucose transporter. In *Cell Metab* 5 (4), pp. 237-252.

Huang, Y.; Dando, R.; Roper, S. (2009): Autocrine and paracrine roles for ATP and serotonin in mouse taste buds. In *J Neurosci* 29 (44), pp. 13909–13918.

Huang, Y.; Maruyama, Y.; Roper, S. (2008): Norepinephrine is coreleased with serotonin in mouse taste buds. In *J Neurosci* 28 (49), pp. 13088–13093.

Huang, Y.; Pereira, E.; Roper, S. (2011): Acid stimulation (sour taste) elicits GABA and serotonin release from mouse taste cells. In *PLoS ONE* 6 (10), e25471.

Huang, Y.-J.; Maruyama, Y.; Dvoryanchikov, G. et al. (2007): The role of pannexin 1 hemichannels in ATP release and cell-cell communication in mouse taste buds. In *Proc Natl Acad Sci U S A* 104 (15), pp. 6436–6441.

Huh, D.; Hamilton, G.; Ingber, D. (2011): From 3D cell culture to organs-on-chips. In *Trends Cell Biol* 21 (12), pp. 745–754.

Huisken, J.; Swoger, J.; Del Bene, F. et al. (2004): Optical sectioning deep inside live embryos by selective plane illumination microscopy. In *Science* 305 (5686), pp. 1007–1009.

Hwang, P.; Verma, A.; Bredt, D.; Snyder, S. (1990): Localization of phosphatidylinositol signaling components in rat taste cells: role in bitter taste transduction. In *Proceedings of the National Academy of Sciences* 87 (19), pp. 7395–7399.

Imoto, T.; Miyasaka, A.; Ishima, R.; Akasaka, K. (1991): A novel peptide isolated from the leaves of Gymnema sylvestre—I. Characterization and its suppressive effect on the neural responses to sweet taste stimuli in the rat. In *Comparative Biochemistry and Physiology Part A: Physiology* 100 (2), pp. 309–314.

Inagaki, N.; Gonoi, T.; Clement, J. et al. (1995): Reconstitution of IKATP: an inward rectifier subunit plus the sulfonylurea receptor. In *Science* 270 (5239), pp. 1166–1170.

Inagaki, N.; Gonoi, T.; Iv, J. et al. (1996): A Family of Sulfonylurea Receptors Determines the Pharmacological Properties of ATP-Sensitive K+ Channels. In *Neuron* 16 (5), pp. 1011–1017.

Isomoto, S.; Kondo, C.; Yamada, M. et al. (1996): A novel sulfonylurea receptor forms with BIR (Kir6.2) a smooth muscle type ATP-sensitive K+ channel. In *Journal of Biological Chemistry* 271 (40), pp. 24321–24324.

Jang, H.-J.; Kokrashvili, Z.; Theodorakis, M. et al. (2007): Gut-expressed gustducin and taste receptors regulate secretion of glucagon-like peptide-1. In *Proceedings of the National Academy of Sciences* 104 (38), pp. 15069–15074.

Janssen, S.; Laermans, J.; Verhulst, P.-J. et al. (2011): Bitter taste receptors and α-gustducin regulate the secretion of ghrelin with functional effects on food intake and gastric emptying. In *Proc Natl Acad Sci U S A* 108 (5), pp. 2094–2099.

Just, T.; Pau, H.; Engel, U.; Hummel, T. (2008): Cephalic phase insulin release in healthy humans after taste stimulation? In *Appetite* 51 (3), pp. 622–627.

Justice, B.; Badr, N.; Felder, R. (2009): 3D cell culture opens new dimensions in cell-based assays. In *Drug Discov Today* 14 (1-2), pp. 102–107.

Kampov-Polevoy, A.; Garbutt, J.; Janowsky, D. (1997): Evidence of preference for a high-concentration sucrose solution in alcoholic men. In *Am J Psychiatry* 154 (2), pp. 269–270.

Karimnamazi, H.; Travers, S.; Travers, J. (2002): Oral and gastric input to the parabrachial nucleus of the rat. In *Brain Research* 957 (2), pp. 193–206.

Kasap, M.; Karaoz, E.; Akpinar, G. et al. (2011): A unique Golgi apparatus distribution may be a marker for osteogenic differentiation of hDP-MSCs. In *Cell Biochem Funct* 29 (6), pp. 489-495.

Kaske, S.; Krasteva, G.; König, P. et al. (2007): TRPM5, a taste-signaling transient receptor potential ion-channel, is a ubiquitous signaling component in chemosensory cells. In *BMC Neurosci* 8, p. 49.

Katsushika, S.; Chen, L.; Kawabe, J. et al. (1992): Cloning and characterization of a sixth adenylyl cyclase isoform: types V and VI constitute a subgroup within the mammalian adenylyl cyclase family. In *Proceedings of the National Academy of Sciences* 89 (18), pp. 8774–8778.

Keiichi, T.; Masaya, F. (1984): Intracellular taste cell responses of mouse. In *Comparative Biochemistry and Physiology Part A: Physiology* 78 (4), pp. 651–656.

Keskitalo, K.; Knaapila, A.; Kallela, M. et al. (2007): Sweet taste preferences are partly genetically determined: identification of a trait locus on chromosome 16. In *Am J Clin Nutr* 86 (1), pp. 55–63.

Kikut-Ligaj, D.; Trzcielińska-Lorych, J. (2015): How taste works: cells, receptors and gustatory perception. In *Cell Mol Biol Lett* 20 (5), pp. 699–716.

Kim, D.; Langmead, B.; Salzberg, S. (2015): HISAT: a fast spliced aligner with low memory requirements. In *Nat Methods* 12 (4), pp. 357–360.

Kim, Y.; Bobkov, Y.; Kolesnikov, S. (2000): Adenosine triphosphate mobilizes cytosolic calcium and modulates ionic currents in mouse taste receptor cells. In *Neuroscience Letters* 290 (3), pp. 165–168.

Kimura, K.; Beidler, L. (1961): Microelectrode study of taste receptors of rat and hamster. In *Journal of cellular and comparative physiology* 58, pp. 131–139.

Kinnamon, S.; Finger, T. (2013): A taste for ATP: neurotransmission in taste buds. In *Front Cell Neurosci* 7, p. 264.

Kinnamon, S.; Roper, S. (1988): Membrane properties of isolated mudpuppy taste cells. In *J Gen Physiol* 91 (3), pp. 351–371.

Kitagawa, M.; Kusakabe, Y.; Miura, H. et al. (2001): Molecular genetic identification of a candidate receptor gene for sweet taste. In *Biochem Biophys Res Commun* 283 (1), pp. 236-242.

Klicks, J.; von Molitor, E.; Ertongur-Fauth, T. et al. (2017): In vitro skin three-dimensional models and their applications. In *JCB* 3 (1), pp. 21–39.

Knight, E.; Przyborski, S. (2015): Advances in 3D cell culture technologies enabling tissue-like structures to be created in vitro. In *J Anat* 227 (6), pp. 746–756.

Koehler, J.; Baggio, L.; Cao, X. et al. (2015): Glucagon-like peptide-1 receptor agonists increase pancreatic mass by induction of protein synthesis. In *Diabetes* 64 (3), pp. 1046–1056.

Kohli, P.; Marazzi, L.; Eastman, D. (2020): Transcriptome analysis of axolotl oropharyngeal explants during taste bud differentiation stages. In *Mech Dev* 161, p. 103597.

Kokrashvili, Z.; Yee, K.; Ilegems, E. et al. (2014): Endocrine Taste Cells. In *Br J Nutr* 111 (01), S23-9.

Kolesnikov, S.; Margolskee, R. (1995): A cyclic-nucleotide-suppressible conductance activated by transducin in taste cells. In *Nature* 376 (6535), pp. 85–88.

Kono, Y.; Horie, M.; Takano, M. et al. (2000): The properties of the Kir6.1-6.2 tandem channel co-expressed with SUR2A. In *Pflugers Arch* 440 (5), pp. 692–698.

Kuhn, C.; Bufe, B.; Winnig, M. et al. (2004): Bitter taste receptors for saccharin and acesulfame K. In *J Neurosci* 24 (45), pp. 10260–10265.

Kuhre, R.; Frost, C.; Svendsen, B.; Holst, J. (2015): Molecular mechanisms of glucose-stimulated GLP-1 secretion from perfused rat small intestine. In *Diabetes* 64 (2), pp. 370–382.

Kurihara, K.; Koyama, N. (1972): High activity of adenyl cyclase in olfactory and gustatory organs. In *Biochem Biophys Res Commun* 48 (1), pp. 30–34.

Kusakabe, Y.; Yamaguchi, E.; Tanemura, K. et al. (1998): Identification of two α-subunit species of GTP-binding proteins, Gα15 and Gαq, expressed in rat taste buds. In *Biochimica et Biophysica Acta (BBA) - Molecular Cell Research* 1403 (3), pp. 265–272.

Kusakabe, Y.; Yasuoka, A.; Asano-Miyoshi, M. et al. (2000): Comprehensive study on G protein alpha-subunits in taste bud cells, with special reference to the occurrence of Galphai2 as a major Galpha species. In *Chem Senses* 25 (5), pp. 525–531.

Laffitte, A.; Neiers, F.; Briand, L. (2014): Functional roles of the sweet taste receptor in oral and extraoral tissues. In *Curr Opin Clin Nutr Metab Care* 17 (4), pp. 379–385.

Lee, J.; Cho, A.-N.; Jin, Y. et al. (2018): Bio-artificial tongue with tongue extracellular matrix and primary taste cells. In *Biomaterials* 151, pp. 24–37.

Lee, R.; Cohen, N. (2014): Bitter and sweet taste receptors in the respiratory epithelium in health and disease. In *J Mol Med (Berl)* 92 (12), pp. 1235–1244.

Lee, R.; Cohen, N. (2015): Taste receptors in innate immunity. In *Cell Mol Life Sci* 72 (2), pp. 217–236.

Lee, R.; Xiong, G.; Kofonow, J. et al. (2012): T2R38 taste receptor polymorphisms underlie susceptibility to upper respiratory infection. In *J Clin Invest* 122 (11), pp. 4145–4159.

Lehmann, N.; Krishna Aradhyam, G.; Fahmy, K. (2002): Suramin affects coupling of rhodopsin to transducin. In *Biophysical Journal* 82 (2), pp. 793–802.

Lemon, C.; Katz, D. (2007): The neural processing of taste. In *BMC Neurosci* 8 Suppl 3, S5.

Lemon, C.; Margolskee, R. (2009): Contribution of the T1r3 taste receptor to the response properties of central gustatory neurons. In *J Neurophysiol* 101 (5), pp. 2459–2471.

Lemon, C.; Smith, D. (2005): Neural representation of bitter taste in the nucleus of the solitary tract. In *J Neurophysiol* 94 (6), pp. 3719–3729.

Leong, D.; Tan, J.; Chin, C. et al. (2017): Evaluation and use of disaccharides as energy source in protein-free mammalian cell cultures. In *Sci Rep* 7, p. 45216.

Li, C.; Cui, W.; Wang, H. (2016): Sensitivity of KATP channels to cellular metabolic disorders and the underlying structural basis. In *Acta Pharmacologica Sinica* 37 (1), pp. 134–142.

Li, H.; Handsaker, B.; Wysoker, A. et al. (2009): The Sequence Alignment/Map format and SAMtools. In *Bioinformatics* 25 (16), pp. 2078–2079.

Li, X.; Li, W.; Wang, H. et al. (2006): Cats Lack a Sweet Taste Receptor. In *J Nutr* 136 (7), 1932S-1934S.

Li, X.; Servant, G.; Tachdjian, C. (2011): The discovery and mechanism of sweet taste enhancers. In *Biomol Concepts* 2 (4), pp. 327–332.

Li, X.; Staszewski, L.; Xu, H. et al. (2002): Human receptors for sweet and umami taste. In *Proc Natl Acad Sci U S A* 99 (7), pp. 4692–4696.

Li, Z.; Cui, Z. (2014): Three-dimensional perfused cell culture. In *Biotechnol Adv* 32 (2), pp. 243–254.

Liem, D.; Mennella, J. (2002): Sweet and sour preferences during childhood: role of early experiences. In *Dev Psychobiol* 41 (4), pp. 388–395.

Lin, W.; Ogura, T.; Margolskee, R. et al. (2008): TRPM5-expressing solitary chemosensory cells respond to odorous irritants. In *J Neurophysiol* 99 (3), pp. 1451–1460.

Lindemann, B. (1999): Receptor seeks ligand: on the way to cloning the molecular receptors for sweet and bitter taste. In *Nat Med* 5 (4), pp. 381–382.

Lindenburg, L.; Merkx, M. (2012): Colorful calcium sensors. In *Chembiochem* 13 (3), pp. 349-351.

Liu, D.; Liman, E. (2003): Intracellular Ca2+ and the phospholipid PIP2 regulate the taste transduction ion channel TRPM5. In *Proc Natl Acad Sci U S A* 100 (25), pp. 15160–15165.

Liu, D.-X.; Liu, X.-M.; Zhou, L.-H. et al. (2011a): Expression of sulfonylurea receptors in rat taste buds. In *Acta Histochem* 113 (4), pp. 489–492.

Liu, H.; Ermilov, A.; Grachtchouk, M. et al. (2013): Multiple Shh signaling centers participate in fungiform papilla and taste bud formation and maintenance. In *Dev Biol* 382 (1), pp. 82–97.

Liu, L.; Hansen, D.; Kim, I.; Gilbertson, T. (2005): Expression and characterization of delayed rectifying K+ channels in anterior rat taste buds. In *Am J Physiol, Cell Physiol* 289 (4), C868-80.

Liu, P.; Shah, B.; Croasdell, S.; Gilbertson, T. (2011b): Transient receptor potential channel type M5 is essential for fat taste. In *J Neurosci* 31 (23), pp. 8634–8642.

Lossow, K.; Hübner, S.; Roudnitzky, N. et al. (2016): Comprehensive Analysis of Mouse Bitter Taste Receptors Reveals Different Molecular Receptive Ranges for Orthologous Receptors in Mice and Humans. In *J Biol Chem* 291 (29), pp. 15358–15377.

Louchami, K.; Best, L.; Brown, P. et al. (2012): A new role for aquaporin 7 in insulin secretion. In *Cell Physiol Biochem* 29 (1-2), pp. 65–74.

Low, J.; McBride, R.; Lacy, K.; Keast, R. (2017): Psychophysical Evaluation of Sweetness Functions Across Multiple Sweeteners. In *Chem Senses* 42 (2), pp. 111–120.

Lush, I. (1989): The genetics of tasting in mice. VI. Saccharin, acesulfame, dulcin and sucrose. In *Genet Res* 53 (2), pp. 95–99.

Ma, Z.; Siebert, A.; Cheung, K.-H. et al. (2012): Calcium homeostasis modulator 1 (CALHM1) is the pore-forming subunit of an ion channel that mediates extracellular Ca2+ regulation of neuronal excitability. In *Proc Natl Acad Sci U S A* 109 (28), E1963-71.

Ma, Z.; Taruno, A.; Ohmoto, M. et al. (2018): CALHM3 Is Essential for Rapid Ion Channel-Mediated Purinergic Neurotransmission of GPCR-Mediated Tastes. In *Neuron* 98 (3), 547-561.e10.

Maimets, M.; Rocchi, C.; Bron, R. et al. (2016): Long-Term In Vitro Expansion of Salivary Gland Stem Cells Driven by Wnt Signals. In *Stem Cell Reports* 6 (1), pp. 150–162.

Maina, I.; Workman, A.; Cohen, N. (2018): The role of bitter and sweet taste receptors in upper airway innate immunity: Recent advances and future directions. In *World J Otorhinolaryngol Head Neck Surg* 4 (3), pp. 200–208.

Mandrycky, C.; Wang, Z.; Kim, K.; Kim, D.-H. (2016): 3D bioprinting for engineering complex tissues. In *Biotechnol Adv* 34 (4), pp. 422–434.

Margolskee, R. (1993): The biochemistry and molecular biology of taste transduction. In *Current Opinion in Neurobiology* 3 (4), pp. 526–531.

Margolskee, R. (2002): Molecular mechanisms of bitter and sweet taste transduction. In *Journal of Biological Chemistry* 277 (1), pp. 1–4.

Margolskee, R.; Dyer, J.; Kokrashvili, Z. et al. (2007): T1R3 and gustducin in gut sense sugars to regulate expression of Na+-glucose cotransporter 1. In *Proceedings of the National Academy of Sciences* 104 (38), pp. 15075–15080.

Markaki, Y.; Smeets, D.; Cremer, M.; Schermelleh, L. (2013): Fluorescence in situ hybridization applications for super-resolution 3D structured illumination microscopy. In : Nanoimaging: Springer, pp. 43–64.

Markaki, Y.; Smeets, D.; Fiedler, S. et al. (2012): The potential of 3D-FISH and super-resolution structured illumination microscopy for studies of 3D nuclear architecture: 3D structured illumination microscopy of defined chromosomal structures visualized by 3D (immuno)-FISH opens new perspectives for studies of nuclear architecture. In *Bioessays* 34 (5), pp. 412–426.

Martin, B.; Shin, Y.-K.; White, C. et al. (2010): Vasoactive intestinal peptide-null mice demonstrate enhanced sweet taste preference, dysglycemia, and reduced taste bud leptin receptor expression. In *Diabetes* 59 (5), pp. 1143–1152.

Martin, C.; Passilly-Degrace, P.; Chevrot, M. et al. (2012): Lipid-mediated release of GLP-1 by mouse taste buds from circumvallate papillae: putative involvement of GPR120 and impact on taste sensitivity. In *J Lipid Res* 53 (11), pp. 2256–2265.

Martiniuk, F.; Hirschhorn, R. (1981): Characterization of neutral isozymes and human α-glucosidase Differences in substrate specificity, molecular weight and electrophoretic mobility. In *Biochimica et Biophysica Acta (BBA) - Enzymology* 658 (2), pp. 248–261.

Matsumoto, I.; Ohmoto, M.; Yasuoka, A. et al. (2009): Genetic tracing of the gustatory neural pathway originating from T1R3-expressing sweet/umami taste receptor cells. In *Ann N Y Acad Sci* 1170.

Matsumura, K.; Chang, B.; Fujimiya, M. et al. (2007): Aquaporin 7 is a beta-cell protein and regulator of intraislet glycerol content and glycerol kinase activity, beta-cell mass, and insulin production and secretion. In *Mol Cell Biol* 27 (17), pp. 6026–6037.

Matsunami, H.; Montmayeur, J.; Buck, L. (2000): A family of candidate taste receptors in human and mouse. In *Nature* 404 (6778), pp. 601–604.

Max, M.; Shanker, Y.; Huang, L. et al. (2001): Tas1r3, encoding a new candidate taste receptor, is allelic to the sweet responsiveness locus Sac. In *Nat Genet* 28 (1), pp. 58–63.

Mayer, J.; Robert-Moreno, A.; Sharpe, J.; Swoger, J. (2018): Attenuation artifacts in light sheet fluorescence microscopy corrected by OPTiSPIM. In *Light Sci Appl* 7, p. 70.

McCudden, C.; Hains, M.; Kimple, R. et al. (2005): G-protein signaling: back to the future. In *Cell Mol Life Sci* 62 (5), pp. 551–577.

McLaughlin, S.; McKinnon, P.; Margolskee, R. (1992): Gustducin is a taste-cell-specific G protein closely related to the transducins. In *Nature* 357 (6379), pp. 563–569.

McLaughlin, S.; McKinnon, P.; Robichon, A. et al. (1993): Gustducin and transducin: a tale of two G proteins. In *Ciba Found Symp* 179, 186-96; discussion 196-200.

Medina, A.; Nakagawa, Y.; Ma, J. et al. (2014): Expression of the glucose-sensing receptor T1R3 in pancreatic islet: changes in the expression levels in various nutritional and metabolic states. In *Endocr J* 61 (8), pp. 797–805.

Medler, K.; Margolskee, R.; Kinnamon, S. (2003): Electrophysiological Characterization of Voltage-Gated Currents in Defined Taste Cell Types of Mice. In *J Neurosci* 23 (7), pp. 2608-2617.

Merigo, F.; Benati, D.; Cecchini, M. et al. (2009): Amylase expression in taste receptor cells of rat circumvallate papillae. In *Cell Tissue Res* 336 (3), pp. 411–421.

Merigo, F.; Benati, D.; Cristofoletti, M. et al. (2011): Glucose transporters are expressed in taste receptor cells. In *J Anat* 219 (2), pp. 243–252.

Meyer, H.; Vitavska, O.; Wieczorek, H. (2011): Identification of an animal sucrose transporter. In *J Cell Sci* 124 (Pt 12), pp. 1984–1991.

Meyerhof, W.; Batram, C.; Kuhn, C. et al. (2010): The molecular receptive ranges of human TAS2R bitter taste receptors. In *Chem Senses* 35 (2), pp. 157–170.

Mills, A.; Zheng, B.; Wang, X. et al. (1999): p63 is a p53 homologue required for limb and epidermal morphogenesis. In *Nature* 398 (6729), pp. 708–713.

Misaka, T.; Kusakabe, Y.; Emori, Y. et al. (1997): Taste buds have a cyclic nucleotide-activated channel, CNGgust. In *Journal of Biological Chemistry* 272 (36), pp. 22623–22629.

Miura, H.; Barlow, L. (2010): Taste bud regeneration and the search for taste progenitor cells. In *Arch Ital Biol* 148 (2), pp. 107–118.

Miura, H.; Kusakabe, Y.; Harada, S. (2006): Cell lineage and differentiation in taste buds. In *Arch Histol Cytol* 69 (4), pp. 209–225.

Miura, H.; Kusakabe, Y.; Sugiyama, C. et al. (2001): Shh and Ptc are associated with taste bud maintenance in the adult mouse. In *Mech Dev* 106 (1-2), pp. 143–145.

Miura, H.; Scott, J.; Harada, S.; Barlow, L. (2014): Sonic hedgehog-expressing basal cells are general post-mitotic precursors of functional taste receptor cells. In *Dev Dyn* 243 (10), pp. 1286–1297.

Miyoshi, M.; Abe, K.; Emori, Y. (2001): IP(3) receptor type 3 and PLCbeta2 are co-expressed with taste receptors T1R and T2R in rat taste bud cells. In *Chem Senses* 26 (3), pp. 259–265.

Montmayeur, J.; Liberles, S.; Matsunami, H.; Buck, L. (2001): A candidate taste receptor gene near a sweet taste locus. In *Nat Neurosci* 4 (5), pp. 492–498.

Moore, L.; Nielsen, C.; Mistretta, C. (1982): Sucrose taste thresholds: age-related differences. In *J Gerontol* 37 (1), pp. 64–69.

Morioka, S.; Perry, J.; Raymond, M. et al. (2018): Efferocytosis induces a novel SLC program to promote glucose uptake and lactate release. In *Nature* 563 (7733), pp. 714–718.

Moskowitz, H. (1970): Ratio scales of sugar sweetness. In *Perception & Psychophysics* 7 (5), pp. 315–320.

Moskowitz, H.; Klarman, L. (1975): The Tastes of Artifical Sweeteners and their Mixtures. In *Chem Senses* 1 (4), pp. 411–421.

Moyer, B.; Hevezi, P.; Gao, N. et al. (2009): Expression of genes encoding multi-transmembrane proteins in specific primate taste cell populations. In *PLoS ONE* 4 (12), e7682.

Munger, B. (1958): A light and electron microscopic study of cellular differentiation in the pancreatic islets of the mouse. In *Am J Anat* 103 (2), pp. 275–311.

Murata, Y.; Yasuo, T.; Yoshida, R. et al. (2010): Action potential-enhanced ATP release from taste cells through hemichannels. In *J Neurophysiol* 104 (2), pp. 896–901.

Naim, M.; Ronen, T.; Striem, B. et al. (1991): Adenylate cyclase responses to sucrose stimulation in membranes of pig circumvallate taste papillae. In *Comparative Biochemistry and Physiology Part B: Comparative Biochemistry* 100 (3), pp. 455–458.

Nakabayashi, H.; Nishizawa, M.; Nakagawa, A. et al. (1996): Vagal hepatopancreatic reflex effect evoked by intraportal appearance of tGLP-1. In *Am J Physiol* 271 (5 Pt 1), E808-13.

Nakagawa, Y.; Nagasawa, M.; Medina, J.; Kojima, I. (2015): Glucose Evokes Rapid Ca2+ and Cyclic AMP Signals by Activating the Cell-Surface Glucose-Sensing Receptor in Pancreatic β-Cells. In *PLoS ONE* 10 (12), e0144053.

Nakagawa, Y.; Ohtsu, Y.; Nagasawa, M. et al. (2014): Glucose promotes its own metabolism by acting on the cell-surface glucose-sensing receptor T1R3. In *Endocr J* 61 (2), pp. 119–131.

Nakashima, K.; Ninomiya, Y. (1998): Increase in inositol 1,4,5-triphosphate levels of the fungiform papilla in response to saccharin and bitter substances in mice. In *Cell Physiol Biochem* 8 (4), pp. 224–230.

Nakashima, K.; Ninomiya, Y. (1999): Transduction for sweet taste of saccharin may involve both inositol 1,4,5-trisphosphate and cAMP pathways in the fungiform taste buds in C57BL mice. In *Cell Physiol Biochem* 9 (2), pp. 90–98.

Nelson, G.; Chandrashekar, J.; Hoon, M. et al. (2002): An amino-acid taste receptor. In *Nature* 416 (6877), pp. 199–202.

Nelson, G.; Hoon, M.; Chandrashekar, J. et al. (2001): Mammalian Sweet Taste Receptors. In *Cell* 106 (3), pp. 381–390.

Nettleton, J.; Lutsey, P.; Wang, Y. et al. (2009): Diet soda intake and risk of incident metabolic syndrome and type 2 diabetes in the Multi-Ethnic Study of Atherosclerosis (MESA). In *Diabetes Care* 32 (4), pp. 688–694.

Ng, K.; Woo, J.; Kwan, M. et al. (2004): Effect of age and disease on taste perception. In *Journal of pain and symptom management* 28 (1), pp. 28–34.

Ninomiya, Yuzo; Mizukoshi, Tsuneyoshi; Higashi, Tetsuichiro; Katsukawa, Hideo; Funakoshi, Masaya (Eds.) (1984): Gustatory neural responses in three different strains of mice (302).

Nordström, K.; Larsson, T.; Larhammar, D. (2004): Extensive duplications of phototransduction genes in early vertebrate evolution correlate with block (chromosome) duplications. In *Genomics* 83 (5), pp. 852–872.

Nürnberg, E.; Vitacolonna, M.; Klicks, J. et al. (2020): Routine Optical Clearing of 3D-Cell Cultures: Simplicity Forward. In *Front Mol Biosci* 7, p. 20.

Ogura, T.; Mackay-Sim, A.; Kinnamon, S. (1997): Bitter Taste Transduction of Denatonium in the Mudpuppy Necturus maculosus. In *J Neurosci* 17 (10), pp. 3580–3587.

Ohla, K.; Yoshida, R.; Roper, S. et al. (2019): Recognizing Taste: Coding Patterns Along the Neural Axis in Mammals. In *Chem Senses* 44 (4), pp. 237–247.

Okubo, T.; Clark, C.; Hogan, B. (2009): Cell lineage mapping of taste bud cells and keratinocytes in the mouse tongue and soft palate. In *Stem Cells* 27 (2), pp. 442–450.

Okubo, T.; Pevny, L.; Hogan, B. (2006): Sox2 is required for development of taste bud sensory cells. In *Genes Dev* 20 (19), pp. 2654–2659.

Oliveira-Maia, A.; Araujo, I. de; Monteiro, C. et al. (2012): The insular cortex controls food preferences independently of taste receptor signaling. In *Front Syst Neurosci* 6, p. 5.

Ootani, S.; Umezaki, T.; Shin, T.; Murata, Y. (1995): Convergence of afferents from the SLN and GPN in cat medullary swallowing neurons. In *Brain Research Bulletin* 37 (4), pp. 397–404.

Oyama, Y.; Yamano, H.; Ohkuma, A. et al. (1999): Carrier-mediated transport systems for glucose in mucosal cells of the human oral cavity. In *J Pharm Sci* 88 (8), pp. 830–834.

Ozdener, H.; Spielman, A.; Rawson, N. (2012): Isolation and culture of human fungiform taste papillae cells. In *JoVE (Journal of Visualized Experiments)* (63), e3730.

Ozdener, H.; Yee, K.; Cao, J. et al. (2006): Characterization and long-term maintenance of rat taste cells in culture. In *Chem Senses* 31 (3), pp. 279–290.

Ozdener, M.; Brand, J.; Spielman, A. et al. (2011): Characterization of human fungiform papillae cells in culture. In *Chem Senses* 36 (7), pp. 601–612.

Ozdener, M.; Rawson, N. (2013): Primary culture of mammalian taste epithelium. In *Methods Mol Biol* 945, pp. 95–107.

Ozeki, M. (1971): Conductance change associated with receptor potentials of gustatory cells in rat. In *J Gen Physiol* 58 (6), pp. 688–699.

Ozeki, M.; Sato, M. (1972): Responses of gustatory cells in the tongue of rat to stimuli representing four taste qualities. In *Comparative Biochemistry and Physiology Part A: Physiology* 41 (2), pp. 391–407.

Pampaloni, F.; Berge, U.; Marmaras, A. et al. (2014): Tissue-culture light sheet fluorescence microscopy (TC-LSFM) allows long-term imaging of three-dimensional cell cultures under controlled conditions. In *Integr Biol (Camb)* 6 (10), pp. 988–998.

Pampaloni, F.; Chang, B.-J.; Stelzer, E. (2015a): Erratum to: light sheet-based fluorescence microscopy (LSFM) for the quantitative imaging of cells and tissues. In *Cell Tissue Res* 362 (1), p. 265.

Pampaloni, F.; Richa, R.; Ansari, N.; Stelzer, E. (2015b): Live spheroid formation recorded with light sheet-based fluorescence microscopy. In *Methods Mol Biol* 1251, pp. 43–57.

Pan, C.; Cai, R.; Quacquarelli, F. et al. (2016): Shrinkage-mediated imaging of entire organs and organisms using uDISCO. In *Nat Methods* 13 (10), pp. 859–867.

Patra, B.; Peng, Y.-S.; Peng, C.-C. et al. (2014): Migration and vascular lumen formation of endothelial cells in cancer cell spheroids of various sizes. In *Biomicrofluidics* 8 (5), p. 52109.

Peng, B.; Zhu, Q.; Zhong, Y. et al. (2015): Chlorogenic Acid Maintains Glucose Homeostasis through Modulating the Expression of SGLT-1, GLUT-2, and PLG in Different Intestinal Segments of Sprague-Dawley Rats Fed a High-Fat Diet. In *Biomed Environ Sci* 28 (12), pp. 894–903.

Pepino, M. (2015): Metabolic effects of non-nutritive sweeteners. In *Physiol Behav* 152 (Pt B), pp. 450–455.

Pepino, M.; Mennella, J. (2007): Effects of Cigarette Smoking and Family History of Alcoholism on Sweet Taste Perception and Food Cravings in Women. In *Alcohol Clin Exp Res* 31 (11), pp. 1891–1899.

Pérez, C.; Huang, L.; Rong, M. et al. (2002): A transient receptor potential channel expressed in taste receptor cells. In *Nat Neurosci* 5 (11), pp. 1169–1176.

Petty, S.; Salame, C.; Mennella, J.; Pepino, M. (2020): Relationship between Sucrose Taste Detection Thresholds and Preferences in Children, Adolescents, and Adults. In *Nutrients* 12 (7).

Pfaffmann, C. (1941): Gustatory afferent impulses. In *Journal of cellular and comparative physiology* 17 (2), pp. 243–258.

Polat, B.; Lin, S.; Mendenhall, J. et al. (2011): Experimental and molecular dynamics investigation into the amphiphilic nature of sulforhodamine B. In *J Phys Chem B* 115 (6), pp. 1394–1402.

Powley, T. (2000): Vagal circuitry mediating cephalic-phase responses to food. In *Appetite* 34 (2), pp. 184–188.

Prawitt, D.; Monteilh-Zoller, M.; Brixel, L. et al. (2003): TRPM5 is a transient Ca2+-activated cation channel responding to rapid changes in Ca2+i. In *Proceedings of the National Academy of Sciences* 100 (25), pp. 15166–15171.

Pronin, A.; Xu, H.; Tang, H. et al. (2007): Specific alleles of bitter receptor genes influence human sensitivity to the bitterness of aloin and saccharin. In *Curr Biol* 17 (16), pp. 1403–1408.

Pumplin, D.; Getschman, E. (2000): Synaptic proteins in rat taste bud cells: Appearance in the Golgi apparatus and relationship to ?-gustducin and the Lewisb and A antigens. In *J Comp Neurol* 427 (2), pp. 171–184.

Ravi, M.; Paramesh, V.; Kaviya, S. et al. (2015): 3D cell culture systems: advantages and applications. In *J Cell Physiol* 230 (1), pp. 16–26.

Reed, D.; McDaniel, A. (2006): The Human Sweet Tooth. In *BMC Oral Health* 6 (Suppl 1), S17.

Reimann, F.; Habib, A.; Tolhurst, G. et al. (2008): Glucose Sensing in L Cells: A Primary Cell Study. In *Cell Metab* 8 (6-3), pp. 532–539.

Ren, W.; Aihara, E.; Lei, W. et al. (2017): Transcriptome analyses of taste organoids reveal multiple pathways involved in taste cell generation. In *Sci Rep* 7 (1), p. 4004.

Ren, W.; Lewandowski, B.; Watson, J. et al. (2014): Single Lgr5- or Lgr6-expressing taste stem/progenitor cells generate taste bud cells ex vivo. In *Proc Natl Acad Sci U S A* 111 (46), pp. 16401–16406.

Ren, W.; Liu, Q.; Zhang, X.; Yu, Y. (2020): Age-related taste cell generation in circumvallate papillae organoids via regulation of multiple signaling pathways. In *Exp Cell Res*, p. 112150.

Richter, C.; Campbell, K. (1939): Sucrose taste thresholds of rats and humans. In *Am J Physiol* 128 (2), pp. 291–297.

Riedel, K.; Pertl, C.; Haack, M. et al. (2016): Association for Chemoreception Sciences (AChemS), 38th Annual Meeting, April 20-23, 2016, Bonita Springs, Florida. In *Chem Senses* 41 (7), e1-e110.

Riedel, K.; Sombroek, D.; Fiedler, B. et al. (2017): Human cell-based taste perception - a bittersweet job for industry. In *Nat Prod Rep* 34 (5), pp. 484–495.

Rieke, M.; Gottwald, E.; Weibezahn, K.-F.; Layer, P. (2008): Tissue reconstruction in 3D-spheroids from rodent retina in a motion-free, bioreactor-based microstructure. In *Lab Chip* 8 (12), pp. 2206–2213.

Riera, C.; Vogel, H.; Simon, S.; Le Coutre, J. (2007): Artificial sweeteners and salts producing a metallic taste sensation activate TRPV1 receptors. In *Am J Physiol Regul Integr Comp Physiol* 293 (2), R626-34.

Robayo-Torres, C.; Quezada-Calvillo, R.; Nichols, B. (2006): Disaccharide digestion: clinical and molecular aspects. In *Clin Gastroenterol Hepatol* 4 (3), pp. 276–287.

Roberts, S.; Knight, M.; Lee, D.; Bader, D. (2001): Mechanical compression influences intracellular Ca2+ signaling in chondrocytes seeded in agarose constructs. In *J Appl Physiol* 90 (4), pp. 1385–1391.

Romanov, R.; Bystrova, M.; Rogachevskaya, O. et al. (2012): The ATP permeability of pannexin 1 channels in a heterologous system and in mammalian taste cells is dispensable. In *J Cell Sci* 125 (Pt 22), pp. 5514–5523.

Romanov, R.; Rogachevskaja, O.; Bystrova, M. et al. (2007): Afferent neurotransmission mediated by hemichannels in mammalian taste cells. In *EMBO J* 26 (3), pp. 657–667.

Romanov, R.; Rogachevskaja, O.; Khokhlov, A.; Kolesnikov, S. (2008): Voltage dependence of ATP secretion in mammalian taste cells. In *J Gen Physiol* 132 (6), pp. 731–744.

Roper, S. (2009): Parallel processing in mammalian taste buds? In *Physiol Behav* 97 (5), pp. 604–608.

Roper, S. (2013): Taste buds as peripheral chemosensory processors. In *Semin Cell Dev Biol* 24 (1), pp. 71–79.

Roper, S.; Chaudhari, N. (2017): Taste buds: cells, signals and synapses. In *Nat Rev Neurosci* 18 (8), pp. 485–497.

Rössler, P.; Boekhoff, I.; Tareilus, E. et al. (2000): G protein betagamma complexes in circumvallate taste cells involved in bitter transduction. In *Chem Senses* 25 (4), pp. 413–421.

Rössler, P.; Kroner, C.; Freitag, J. et al. (1998): Identification of a phospholipase C β subtype in rat taste cells. In *European Journal of Cell Biology* 77 (3), pp. 253–261.

Rozengurt, E. (2006): Taste receptors in the gastrointestinal tract. I. Bitter taste receptors and alpha-gustducin in the mammalian gut. In *Am J Physiol Gastrointest Liver Physiol* 291 (2), G171-7.

Ruiz, C.; Wray, K.; Delay, E. et al. (2003): Behavioral evidence for a role of alpha-gustducin in glutamate taste. In *Chem Senses* 28 (7), pp. 573–579.

Sabino-Silva, R.; Mori, R.; David-Silva, A. et al. (2010): The Na(+)/glucose cotransporters: from genes to therapy. In *Braz J Med Biol Res* 43 (11), pp. 1019–1026.

Sainz, E.; Korley, J.; Battey, J.; Sullivan, S. (2001): Identification of a novel member of the T1R family of putative taste receptors. In *J Neurochem* 77 (3), pp. 896–903.

Sakata, I.; Park, W.-M.; Walker, A. et al. (2012): Glucose-mediated control of ghrelin release from primary cultures of gastric mucosal cells. In *Am J Physiol Endocrinol Metab* 302 (10), E1300-10.

Saltiel, M.; Kuhre, R.; Christiansen, C. et al. (2017): Sweet Taste Receptor Activation in the Gut Is of Limited Importance for Glucose-Stimulated GLP-1 and GIP Secretion. In *Nutrients* 9 (4).

Sato, T.; Beidler, L. (1982): The response characteristics of rat taste cells to four basic taste stimuli. In *Comparative Biochemistry and Physiology Part A: Physiology* 73 (1), pp. 1–10.

Sato, T.; Beidler, L. (1997): Broad tuning of rat taste cells for four basic taste stimuli. In *Chem Senses* 22 (3), pp. 287–293.

Scheepers, A.; Joost, H.-G.; Schürmann, A. (2004): The glucose transporter families SGLT and GLUT: molecular basis of normal and aberrant function. In *JPEN J Parenter Enteral Nutr* 28 (5), pp. 364–371.

Schmidt, S.; Joost, H.-G.; Schürmann, A. (2009): GLUT8, the enigmatic intracellular hexose transporter. In *Am J Physiol Endocrinol Metab* 296 (4), E614-8.

Schmitz, A.; Fischer, S.; Mattheyer, C. et al. (2017): Multiscale image analysis reveals structural heterogeneity of the cell microenvironment in homotypic spheroids. In *Sci Rep* 7, p. 43693.

Schulze-Lohoff, E.; Hugo, C.; Rost, S. et al. (1998): Extracellular ATP causes apoptosis and necrosis of cultured mesangial cells via P2Z/P2X7 receptors. In *Am J Physiol* 275 (6), F962-71.

Schweiger, K.; Grüneis, V.; Treml, J. et al. (2020): Sweet Taste Antagonist Lactisole Administered in Combination with Sucrose, But Not Glucose, Increases Energy Intake and Decreases Peripheral Serotonin in Male Subjects. In *Nutrients* 12 (10).

Sclafani, A.; Zukerman, S.; Glendinning, J.; Margolskee, R. (2007): Fat and carbohydrate preferences in mice: the contribution of alpha-gustducin and Trpm5 taste-signaling proteins. In *Am J Physiol Regul Integr Comp Physiol* 293 (4), R1504-13.

Seghers, V.; Nakazaki, M.; DeMayo, F. et al. (2000): Sur1 knockout mice. A model for K(ATP) channel-independent regulation of insulin secretion. In *J Biol Chem* 275 (13), pp. 9270–9277.

Seino, S. (2003): Physiology and pathophysiology of KATP channels in the pancreas and cardiovascular system. In *Journal of Diabetes and its Complications* 17 (2), pp. 2–5.

Seino, S.; Iwanaga, T.; Nagashima, K.; Miki, T. (2000): Diverse roles of K(ATP) channels learned from Kir6.2 genetically engineered mice. In *Diabetes* 49 (3), pp. 311–318.

Seino, Y.; Maekawa, R.; Ogata, H.; Hayashi, Y. (2016): Carbohydrate-induced secretion of glucose-dependent insulinotropic polypeptide and glucagon-like peptide-1. In *J Diabetes Investig* 7 (Suppl 1), pp. 27–32.

Servant, G.; Tachdjian, C.; Tang, X.-Q. et al. (2010): Positive allosteric modulators of the human sweet taste receptor enhance sweet taste. In *Proc Natl Acad Sci U S A* 107 (10), pp. 4746–4751.

Seta, Y.; Seta, C.; Barlow, L. (2003): Notch-associated gene expression in embryonic and adult taste papillae and taste buds suggests a role in taste cell lineage decisions. In *J Comp Neurol* 464 (1), pp. 49–61.

Shahbake, M.; Hutchinson, I.; Laing, D.; Jinks, A. (2005): Rapid quantitative assessment of fungiform papillae density in the human tongue. In *Brain Research* 1052 (2), pp. 196–201.

Shigemura, N.; Yasumatsu, K.; Yoshida, R. et al. (2005): The role of the dpa locus in mice. In *Chem Senses* 30 Suppl 1, i84-5.

Shin, Y.-K.; Martin, B.; Golden, E. et al. (2008): Modulation of taste sensitivity by GLP-1 signaling. In *J Neurochem* 106 (1), pp. 455–463.

Shindo, Y.; Miura, H.; Carninci, P. et al. (2008): G alpha14 is a candidate mediator of sweet/umami signal transduction in the posterior region of the mouse tongue. In *Biochem Biophys Res Commun* 376 (3), pp. 504–508.

Shinozaki, K.; Shimizu, Y.; Shiina, T. et al. (2008): Relationship between taste-induced physiological reflexes and temperature of sweet taste. In *Physiol Behav* 93 (4-5), pp. 1000-1004.

Siebert, A.; Ma, Z.; Grevet, J. et al. (2013): Structural and functional similarities of calcium homeostasis modulator 1 (CALHM1) ion channel with connexins, pannexins, and innexins. In *J Biol Chem* 288 (9), pp. 6140–6153.

Sigoillot, M.; Brockhoff, A.; Meyerhof, W.; Briand, L. (2012): Sweet-taste-suppressing compounds: current knowledge and perspectives of application. In *Appl Microbiol Biotechnol* 96 (3), pp. 619–630.

Sim, J.; Yang, D.; Kim, Y. et al. (2002): ATP-sensitive K(+) channels composed of Kir6.1 and SUR2B subunits in guinea pig gastric myocytes. In *Am J Physiol Gastrointest Liver Physiol* 282 (1), G137-44.

Simon, B.; Learman, B.; Parlee, S. et al. (2014): Sweet taste receptor deficient mice have decreased adiposity and increased bone mass. In *PLoS ONE* 9 (1), e86454.

Smeets, P.; Erkner, A.; Graaf, C. de (2010): Cephalic phase responses and appetite. In *Nutr Rev* 68 (11), pp. 643–655.

Smith, David V.; Lemon, Christian H. (Eds.) (2007): The Role of the Nucleus of the Solitary Tract in Gustatory Processing: CRC Press/Taylor & Francis.

Smith, E.; An, Z.; Wagner, C. et al. (2014): The role of β-cell GLP-1 signaling in glucose regulation and response to diabetes drugs. In *Cell Metab* 19 (6), pp. 1050–1057.

Smyrek, I.; Stelzer, E. (2017): Quantitative three-dimensional evaluation of immunofluorescence staining for large whole mount spheroids with light sheet microscopy. In *Biomed Opt Express* 8 (2), pp. 484–499.

Spector, A.; Travers, S. (2005): The representation of taste quality in the mammalian nervous system. In *Behav Cogn Neurosci Rev* 4 (3), pp. 143–191.

Spielman, A.; Huque, T.; Nagai, H. et al. (1994): Generation of inositol phosphates in bitter taste transduction. In *Physiol Behav* 56 (6), pp. 1149–1155.

Striem, B.; Naim, M.; Lindemann, B. (1991): Generation of Cyclic AMP in Taste Buds of the Rat Circumvallate Papilla in Response to Sucrose. In *Cell Physiol Biochem* 1 (1), pp. 46–54.

Striem, B.; Pace, U.; Zehavi, U. et al. (1989): Sweet tastants stimulate adenylate cyclase coupled to GTP-binding protein in rat tongue membranes. In *Biochem J* 260 (1), pp. 121–126.

Sukumaran, S.; Lewandowski, B.; Qin, Y. et al. (2017): Whole transcriptome profiling of taste bud cells. In *Sci Rep* 7 (1), p. 7595.

Sukumaran, S.; Yee, K.; Iwata, S. et al. (2016): Taste cell-expressed α-glucosidase enzymes contribute to gustatory responses to disaccharides. In *Proc Natl Acad Sci U S A* 113 (21), pp. 6035–6040.

Sund, R.; Schou, J. (1965): Hyaluronidase as an accelerator of muscular absorption of water and water-soluble compounds. In *Acta Pharmacol Toxicol (Copenh)* 23 (2), pp. 194–204.

Svendsen, B.; Larsen, O.; Gabe, M. et al. (2018): Insulin Secretion Depends on Intra-islet Glucagon Signaling. In *Cell Rep* 25 (5), 1127-1134.e2.

Szebenyi, S.; Laskowski, A.; Medler, K. (2010): Sodium/calcium exchangers selectively regulate calcium signaling in mouse taste receptor cells. In *J Neurophysiol* 104 (1), pp. 529-538.

Takai, S.; Watanabe, Y.; Sanematsu, K. et al. (2019): Effects of insulin signaling on mouse taste cell proliferation. In *PLoS ONE* 14 (11), e0225190.

Takai, S.; Yasumatsu, K.; Inoue, M. et al. (2015): Glucagon-like peptide-1 is specifically involved in sweet taste transmission. In *FASEB J* 29 (6), pp. 2268–2280.

Talavera, K.; Yasumatsu, K.; Voets, T. et al. (2005): Heat activation of TRPM5 underlies thermal sensitivity of sweet taste. In *Nature* 438 (7070), pp. 1022–1025.

Talavera, K.; Yasumatsu, K.; Yoshida, R. et al. (2008): The taste transduction channel TRPM5 is a locus for bitter-sweet taste interactions. In *FASEB J* 22 (5), pp. 1343–1355.

Taniguchi, K. (2004): Expression of the sweet receptor protein, T1R3, in the human liver and pancreas. In *J Vet Med Sci* 66 (11), pp. 1311–1314.

Taruno, A.; Vingtdeux, V.; Ohmoto, M. et al. (2013): CALHM1 ion channel mediates purinergic neurotransmission of sweet, bitter and umami tastes. In *Nature* 495 (7440), pp. 223–226.

Tatzer, E.; Schubert, M.; Timischl, W.; Simbruner, G. (1985): Discrimination of taste and preference for sweet in premature babies. In *Early Human Development* 12 (1), pp. 23–30.

Teff, K.; Devine, J.; Engelman, K. (1995): Sweet taste: Effect on cephalic phase insulin release in men. In *Physiol Behav* 57 (6), pp. 1089–1095.

Tellez, L.; Han, W.; Zhang, X. et al. (2016): Separate circuitries encode the hedonic and nutritional values of sugar. In *Nat Neurosci* 19 (3), pp. 465–470.

Than, T.; Delay, E.; Maier, M. (1994): Sucrose threshold variation during the menstrual cycle. In *Physiol Behav* 56 (2), pp. 237–239.

Theodorakis, M.; Carlson, O.; Michopoulos, S. et al. (2006): Human duodenal enteroendocrine cells: source of both incretin peptides, GLP-1 and GIP. In *Am J Physiol Endocrinol Metab* 290 (3), E550-9.

Thorens, B. (2015): GLUT2, glucose sensing and glucose homeostasis. In *Diabetologia* 58 (2), pp. 221–232.

Tizzano, M.; Dvoryanchikov, G.; Barrows, J. et al. (2008): Expression of Galpha14 in sweet-transducing taste cells of the posterior tongue. In *BMC Neurosci* 9, p. 110.

Tonosaki, K.; Funakoshi, M. (1988): Cyclic nucleotides may mediate taste transduction. In *Nature* 331 (6154), pp. 354–356.

Tonosaki, K.; Hori, Y.; Shimizu, Y.; Tonosaki, K. (2007): Relationships between insulin release and taste. In *Biomed Res* 28 (2), pp. 79–83.

Tordoff, M.; Aleman, T.; Ellis, H. et al. (2015): Normal Taste Acceptance and Preference of PANX1 Knockout Mice. In *Chem Senses* 40 (7), pp. 453–459.

Toyono, T.; Seta, Y.; Kataoka, S. et al. (2011): Differential expression of the glucose transporters in mouse gustatory papillae. In *Cell Tissue Res* 345 (2), pp. 243–252.

Travers, S.; Norgren, R. (1995): Organization of orosensory responses in the nucleus of the solitary tract of rat. In *J Neurophysiol* 73 (6), pp. 2144–2162.

Treesukosol, Y.; Smith, K.; Spector, A. (2011): The functional role of the T1R family of receptors in sweet taste and feeding. In *Physiol Behav* 105 (1), pp. 14–26.

Treesukosol, Y.; Spector, A. (2012): Orosensory detection of sucrose, maltose, and glucose is severely impaired in mice lacking T1R2 or T1R3, but Polycose sensitivity remains relatively normal. In *Am J Physiol Regul Integr Comp Physiol* 303 (2), R218-35.

Trubey, K.; Culpepper, S.; Maruyama, Y. et al. (2006): Tastants evoke cAMP signal in taste buds that is independent of calcium signaling. In *Am J Physiol, Cell Physiol* 291 (2), C237-44.

Uchida, Y.; Sato, T. (1997): Changes in outward K+ currents in response to two types of sweeteners in sweet taste transduction of gerbil taste cells. In *Chem Senses* 22 (2), pp. 163-169.

Usui-Aoki, K.; Matsumoto, K.; Koganezawa, M. et al. (2005): Targeted expression of Ip3 sponge and Ip3 dsRNA impaires sugar taste sensation in Drosophila. In *J Neurogenet* 19 (3-4), pp. 123–141.

van der Valk, J.; Brunner, D.; Smet, K. de et al. (2010): Optimization of chemically defined cell culture media--replacing fetal bovine serum in mammalian in vitro methods. In *Toxicol In Vitro* 24 (4), pp. 1053–1063.

Vandenbeuch, A.; Anderson, C.; Kinnamon, S. (2015): Mice Lacking Pannexin 1 Release ATP and Respond Normally to All Taste Qualities. In *Chem Senses* 40 (7), pp. 461–467.

Vandenbeuch, A.; Clapp, T.; Kinnamon, S. (2008): Amiloride-sensitive channels in type I fungiform taste cells in mouse. In *BMC Neurosci* 9, p. 1.

Vargas, E.; Podder, V.; Carrillo Sepulveda, M. (2020): StatPearls. Physiology, Glucose Transporter Type 4 (GLUT4).

Vitavska, O.; Wieczorek, H. (2013): The SLC45 gene family of putative sugar transporters. In *Mol Aspects Med* 34 (2-3), pp. 655–660.

Vitavska, O.; Wieczorek, H. (2017): Putative role of an SLC45 H+/sugar cotransporter in mammalian spermatozoa. In *Pflugers Arch* 469 (11), pp. 1433–1442.

von Molitor, E.; Nürnberg, E.; Ertongur-Fauth, T. et al. (2020a): Analysis of calcium signaling in live human Tongue cell 3D-Cultures upon tastant perfusion. In *Cell Calcium* 87, p. 102164.

von Molitor, E.; Riedel, K.; Hafner, M. et al. (2020b): Sensing Senses: Optical Biosensors to Study Gustation. In *Sensors (Basel)* 20 (7).

von Molitor, E.; Riedel, K.; Krohn, M. et al. (2020c): An alternative pathway for sweet sensation: possible mechanisms and physiological relevance. In *Pflugers Arch*.

Vos, A. de; Heimberg, H.; Quartier, E. et al. (1995): Human and rat beta cells differ in glucose transporter but not in glucokinase gene expression. In *J Clin Invest* 96 (5), pp. 2489–2495.

Wang, L.; Gillis-Smith, S.; Peng, Y. et al. (2018): The coding of valence and identity in the mammalian taste system. In *Nature* 558 (7708), pp. 127–131.

Wauson, E.; Zaganjor, E.; Lee, A.-Y. et al. (2012): The G protein-coupled taste receptor T1R1/T1R3 regulates mTORC1 and autophagy. In *Mol Cell* 47 (6), pp. 851–862.

Whitaker, M. (2010): Genetically encoded probes for measurement of intracellular calcium. In *Methods Cell Biol* 99, pp. 153–182.

Whitehead, M.; Ganchrow, J.; Ganchrow, D.; Yao, B. (1999): Organization of geniculate and trigeminal ganglion cells innervating single fungiform taste papillae: a study with tetramethylrhodamine dextran amine labeling. In *Neuroscience* 93 (3), pp. 931–941.

Widmayer, P.; Breer, H.; Hass, N. (2011): Candidate chemosensory cells in the porcine stomach. In *Histochem Cell Biol* 136 (1), pp. 37–45.

Winnig, M.; Bufe, B.; Meyerhof, W. (2005): Valine 738 and lysine 735 in the fifth transmembrane domain of rTas1r3 mediate insensitivity towards lactisole of the rat sweet taste receptor. In *BMC Neurosci* 6, p. 22.

Wong, G.; Gannon, K.; Margolskee, R. (1996): Transduction of bitter and sweet taste by gustducin. In *Nature* 381 (6585), pp. 796–800.

Wong, G.; Ruiz-Avila, L.; Margolskee, R. (1999): Directing Gene Expression to Gustducin-Positive Taste Receptor Cells. In *J Neurosci* 19 (14), pp. 5802–5809.

Wright, E.; Loo, D.; Hirayama, B. (2011): Biology of human sodium glucose transporters. In *Physiol Rev* 91 (2), pp. 733–794.

Wuchter, P.; Saffrich, R.; Giselbrecht, S. et al. (2016): Microcavity arrays as an in vitro model system of the bone marrow niche for hematopoietic stem cells. In *Cell Tissue Res* 364 (3), pp. 573–584.

Yamada, M.; Isomoto, S.; Matsumoto, S. et al. (1997): Sulphonylurea receptor 2B and Kir6.1 form a sulphonylurea-sensitive but ATP-insensitive K+ channel. In *J Physiol (Lond)* 499 (Pt 3), pp. 715–720.

Yamamoto, K.; Ishimaru, Y. (2013): Oral and extra-oral taste perception. In *Semin Cell Dev Biol* 24 (3), pp. 240–246.

Yan, W.; Sunavala, G.; Rosenzweig, S. et al. (2001): Bitter taste transduced by PLC-beta(2)-dependent rise in IP(3) and alpha-gustducin-dependent fall in cyclic nucleotides. In *Am J Physiol, Cell Physiol* 280 (4), C742-51.

Yang, R.; Crowley, H.; Rock, M.; Kinnamon, J. (2000): Taste cells with synapses in rat circumvallate papillae display SNAP-25-like immunoreactivity. In *J Comp Neurol* 424 (2), pp. 205–215.

Yasumatsu, K.; Ohkuri, T.; Yoshida, R. et al. (2020): Sodium-glucose cotransporter 1 as a sugar taste sensor in mouse tongue. In *Acta Physiologica* 230 (4).

Yee, C.; Yang, R.; Böttger, B. et al. (2001): "Type III" cells of rat taste buds: immunohistochemical and ultrastructural studies of neuron-specific enolase, protein gene product 9.5, and serotonin. In *J Comp Neurol* 440 (1), pp. 97–108.

Yee, K.; Sukumaran, S.; Kotha, R. et al. (2011): Glucose transporters and ATP-gated K+ (KATP) metabolic sensors are present in type 1 taste receptor 3 (T1r3)-expressing taste cells. In *Proc Natl Acad Sci U S A* 108 (13), pp. 5431–5436.

Yoshimoto, J.; Okada, S.; Kishi, M.; Misaka, T. (2016): Ulex Europaeus Agglutinin-1 Is a Reliable Taste Bud Marker for In Situ Hybridization Analyses. In *J Histochem Cytochem* 64 (3), pp. 205–215.

Young, R. (2011): Sensing via intestinal sweet taste pathways. In *Front Neurosci* 5, p. 23.

Young, R.; Chia, B.; Isaacs, N. et al. (2013): Disordered control of intestinal sweet taste receptor expression and glucose absorption in type 2 diabetes. In *Diabetes* 62 (10), pp. 3532-3541.

Young, R.; Sutherland, K.; Pezos, N. et al. (2009): Expression of taste molecules in the upper gastrointestinal tract in humans with and without type 2 diabetes. In *Gut* 58 (3), pp. 337–346.

Yudin, Y.; Rohacs, T. (2015): The Role of PLCÎ´4 in the Activity of TRPM8 Expressing Sensory Neurons. In *Biophysical Journal* 108 (2), 284a.

Zafra, M.; Molina, F.; Puerto, A. (2006): The neural/cephalic phase reflexes in the physiology of nutrition. In *Neuroscience and biobehavioral reviews* 30 (7).

Zaidi, F.; Todd, K.; Enquist, L.; Whitehead, M. (2008): Types of Taste Circuits Synaptically Linked to a Few Geniculate Ganglion Neurons. In *J Comp Neurol* 511 (6), pp. 753–772.

Zhang, C.; Cotter, M.; Lawton, A. et al. (1995): Keratin 18 is associated with a subset of older taste cells in the rat. In *Differentiation* 59 (3), pp. 155–162.

Zhang, C.; Oakley, B. (1996): The distribution and origin of keratin 20-containing taste buds in rat and human. In *Differentiation* 61 (2), pp. 121–127.

Zhang, G.-H.; Zhang, H.-Y.; Wang, X.-F. et al. (2009): The relationship between fungiform papillae density and detection threshold for sucrose in the young males. In *Chem Senses* 34 (1), pp. 93–99.

Zhang, Y.; Hoon, M.; Chandrashekar, J. et al. (2003): Coding of Sweet, Bitter, and Umami Tastes. In *Cell* 112 (3), pp. 293–301.

Zhao, F.-Q.; Keating, A. (2007): Functional properties and genomics of glucose transporters. In *Curr Genomics* 8 (2), pp. 113–128.

Zhao, G.; Zhang, Y.; Hoon, M. et al. (2003): The Receptors for Mammalian Sweet and Umami Taste. In *Cell* 115 (3), pp. 255–266.

Zhao, Y.; Araki, S.; Wu, J. et al. (2011): An expanded palette of genetically encoded Ca^{2+} indicators. In *Science* 333 (6051), pp. 1888–1891.

Zhou, Y.; Liu, H.-X.; Mistretta, C. (2006): Bone morphogenetic proteins and noggin: inhibiting and inducing fungiform taste papilla development. In *Dev Biol* 297 (1), pp. 198–213.

6 Appendix

6.1 List of abbreviations

AB	Antibody
AC	Adenyl cyclase
Amy	Amygdala
AQ	Aquaporin
ATP	Adenosine triphosphate
BME	Basement membrane extract
BR	Broadly tuned taste cells
BSA	Bovine serum albumin
CALHM	Calcium homeostasis modulator
cAMP	Cyclic adenosine monophosphate
CAR	Ca^{2+} receptor
CNG	Cyclic-nucleotide-suppressible channel
CPIR	Cephalic phase Insulin release
CT	Chorda tympani nerve
DMNX	Dorsal nucleus of vagus nerve
DMSO	Dimethylsulfoxid
Dpa	d-Phenylalanine aversion
DPP4	Dipeptidyl-peptidase 4
EC_{50}	Half maximal effective concentration
FCS	Fetal calf serum
FISH	Fluorescence *in situ* hybridization
FLIPR	Fluorescent-imaging plate reader
GANC	α-Glucosidase C
GAPDH	Glycerinaldehyd-3-phosphat-dehydrogenase
G-GECO	Ca^{2+}-sensitive fluorescence sensor
GL	Glossopharyngeal nerve
GLP-1	Glucagon like peptide-1
GLP-1-R	Glucagon like peptide-1 receptor

GLUT	Glucose transporter
GPCR	G-protein coupled receptor
HTC-8	Human taste cell line-8
HTP-76	Human taste progenitor cell line-76
IP3	Inositol-3-phosphate
IP3-R	Inositol-3-phosphate receptor
KCN	Potassium inwardly-rectifying channel
KRT	Cytokeratin
LCT	Lactase
LRRC8A	Leucine-rich repeat-containing protein 8A
LSFM	Light sheet fluorescence microscopy
MGAM	Maltase-glucoamylase
n.d.	Not detectable
NCX	Sodium-calcium exchanger
NPD	Nucleosidediphosphate
NTS	Nucleus of the solitary tract
PANX	Pannexin
PbN	Parabrachial
PBS	Phosphate buffered saline
PDE	Phosphodiesterase
PDMS	Polydimethylsiloxane
PFA	Paraformaldehyde
PKA	Protein kinase A
PLC	Phospholipase C
Ptc	Patched 1
R1-R4	Concentric rings in the spheroid from border to the center
ROI	Region of interest
Sac	Saccharin
SLC45	Solute carrier family 45
SCRT	Sucrose transporter
SD	Standard deviation
SEM	Standard error of the mean

SGLT	Sodium-driven glucose symporter
Shh	Sonic hedgehog signaling
SIS	Sucrase-isomaltase
SNAP25	Synaptosomal-associated protein, 25kDa
SNR	Signal-to-noise-ratio
STIM	Stromal interaction molecule
SUR	Sulfonylurea receptor
T1R1	Taste receptor type 1 member 1
T1R2	Taste receptor type 1 member 2
T1R3	Taste receptor type 1 member 3
T2R	Taste receptor type 2 (bitter receptor)
T_{peak}	Time interval from the start of the stimulation to reach the peak
$T_{pslope-peak}$	Time interval between T_{slope} and T_{peak}
TREH	Trehalase
TRPM5	Transient receptor potential M5 channel
T_{slope}	Time interval from the start of the stimulation to the time point where the slope of $\Delta F/F_0$ gets positive
VDCC	Voltage-dependent Ca^{2+} channel
VDKC	Voltage-dependent K^+ channel
VR1	Vanilloid receptor 1
VRAC	Volume regulated anion channel
WGA	Wheat germ agglutinin
WM	Whole mount
WS	Whole spheroid

6.2 List of figures

6.3 List of tables

6.4 Supplementary data

Table 15: Total mRNA levels of signaling molecules involved in the canonical sweet pathway. HTC-8 monolayer data are adapted from Hochheimer et al. 2014 and were generated with RT-PCR. – means no data available and n.d. not detectable. The expression profile of HTC-8-G-GECO spheroids was analyzed using RNA transcriptome analysis (preliminary based on one 96-well plate of HTC-8-G-GECO spheroids).

Gene	Gene-ID	Name	monolayer expression	spheroid expression
TAS1R1	80835	Taste receptor type 1, member 1	n.d.	0.127369
TAS1R2	80835	Taste receptor type 1, member 2	n.d.	n.d.
TAS1R3	80835	Taste receptor type 1, member 3	n.d.	0.178202
TAS2R43	259289	Taste receptor type 2, member 43	yes	n.d.
TAS2R44	259290	Taste receptor type 2, member 44	yes	n.d.
TAS2R16	50833	Taste receptor type 2, member 16	yes	n.d.
TAS2R8	50836	Taste receptor type 2, member 8	n.d.	n.d.
GNA11	2767	Guanine nucleotide-binding protein, alpha 11	yes	39.2826
GNA12	2768	Guanine nucleotide-binding protein, alpha 12	yes	33.7985
GNA13	10672	Guanine nucleotide-binding protein, alpha 13	yes	18.8536
GNA14	9630	Guanine nucleotide-binding protein, alpha 14	-	0.0688294
GNA15	2769	Guanine nucleotide-binding protein, alpha 15	-	n.d.
GNAI1	2770	Guanine nucleotide-binding protein, alpha inhibiting activity polypeptide	yes	28.1139
GNAI2	2771	Guanine nucleotide-binding protein, alpha 2	-	208.148
GNAI3	2773	Guanine nucleotide-binding protein, alpha 3	-	16.0283
GNAQ	2776	Guanine nucleotide-binding protein, q polypeptide	yes	10.7886
GNAS	2778	Guanine nucleotide-binding protein, alpha stimulating activity	yes	483.451
GNAT1	2779	Guanine nucleotide-binding protein, alpha transducing activity polypeptide 1 (transducin)	n.d.	n.d.
GNAT2	2780	Guanine nucleotide-binding protein, alpha transducing activity polypeptide 2	yes	0.182286
GNAT3	346562	Guanine nucleotide-binding protein, alpha transducing activity polypeptide 3 (gustducin)	n.d.	n.d.
GNAB1	2782	Guanine nucleotide binding protein, beta polypeptide 1	-	143.5
GNB2	2782	Guanine nucleotide binding protein, beta polypeptide 2	Yes	143.564
GNB3	2784	Guanine nucleotide binding protein, beta polypeptide 3	Yes	0.276436
GNG2	54331	Guanine nucleotide binding protein, gamma 2	-	6.5
GNG13	51764	Guanine nucleotide binding protein, gamma 13	n.d.	n.d.
PLCB2	5330	Phospholipase C, beta 2	n.d.	0.0117849
PLCB3		Phospholipase C, beta 3	-	12.4688
PLCD4	84812	Phospholipase C, delta 4	yes	0.932247
IPR3	3710	Inositol 1,4,5-triphosphate receptor type 3	yes	6.10692
TRPM8	79054	Transient receptor potential channel, subfamily M, member 8	-	n.d.
TRPM5	29850	Transient receptor potential channel, subfamily M, member 5	n.d.	n.d.
TRPM4	54795	Transient receptor potential channel, subfamily M, member 4	yes	20.2525
PRKACA	5566	Protein kinase cAMP-dependent, catalytic, alpha	yes	26.4683

PRKACB	5567	Protein kinase cAMP-dependent, catalytic, beta	yes	7.67641
PRKAR1A	5573	Protein kinase cAMP-dependent, regulatory, type I, alpha	yes	89.6428
PRKAR1B	55575	Protein kinase cAMP-dependent, regulatory, type I, beta	yes	2.25261
PRKAR2A	5576	Protein kinase cAMP-dependent, regulatory, type II, alpha	yes	19.6399
PRKAR2B	5577	Protein kinase cAMP-dependent, regulatory, type II, beta	yes	16.4058
ADCY2	108	Adenylate cyclase 2	-	0.0821962
ADCY3	109	Adenylate cyclase 3	yes	35.9626
ADCY4	196883	Adenylate cyclase 4	yes	11.1271
ADCY5	111	Adenylate cyclase 5	yes	0.575655
ADCY6	112	Adenylate cyclase 6	yes	18.186
ADCY7	113	Adenylate cyclase 7	yes	8.73962
ADCY8	114	Adenylate cyclase 8	-	n.d.
ADCY9	115	Adenylate cyclase 9	yes	36.9145
PDE1A	5136	Phosphodiesterase 1A	yes	1.42567
PDE2A	5138	Phosphodiesterase 2A	-	0.0130996
PDE3B	5140	Phosphodiesterase 2B	-	1.01099
PDE6D	5147	Phosphodiesterase 6D	-	13.0428
PDE8A	5151	Phosphodiesterase 8A	-	4.81881
PDE8B	8622	Phosphodiesterase 8B	-	0.080251
PDE9A	5152	Phosphodiesterase 9A	-	2.18239
KCNA1	3736	Potassium voltage gated channel, shaker related subfamily, member 1	n.d.	n.d.
KCNA2	3737	Potassium voltage gated channel, shaker related subfamily, member 2	n.d.	0.0299735
KCNA3	3738	Potassium voltage gated channel, shaker related subfamily, member 3	n.d.	n.d.
KCNA5	3741	Potassium voltage gated channel, shaker related subfamily, member 5	n.d.	n.d.
KCNA6	3742	Potassium voltage gated channel, shaker related subfamily, member 6	n.d.	n.d.
KCNB1	3745	Potassium voltage gated channel, shab related subfamily, member 1	n.d.	n.d.
KCNB2	9312	Potassium voltage gated channel, shab related subfamily, member 2	n.d.	n.d.
KCNC1	3746	Potassium voltage-gated channel subfamily C member 1	-	0.88208
KCNC2	3747	Potassium voltage-gated channel subfamily C member 2	-	n.d.

Table 16: Total mRNA levels of channels involved in purinergic signal transmission. HTC-8 monolayer data are adapted from Hochheimer et al. 2014 and were generated with RT-PCR. – means no data available and n.d. not detectable. The expression profile of HTC-8-G-GECO spheroids was analyzed using RNA transcriptome analysis (preliminary based on one 96-well plate of HTC-8-G-GECO spheroids).

Gene	Gene-ID	Name	monolayer expression	spheroid expression
CALHM1	255022	Calcium homeostasis modulator 1	n.d.	n.d.
CALHM2	51063	Calcium homeostasis modulator 2	yes	36.6129
CALHM3	119395	Calcium homeostasis modulator 3	n.d.	n.d.
P2RX2	22953	Purinergic receptor P2X, ligand gated ion channel 2	n.d.	n.d.
P2RX3	5024	Purinergic receptor P2X, ligand gated ion channel 3	n.d.	n.d.
P2RX7	5027	Purinergic receptor P2X, ligand gated ion channel 7	yes	1.02846
P2RY1	5028	Purinergic receptor P2Y, G-protein coupled, 1	n.d.	2.83163
P2RY4	5030	Purinergic receptor P2Y, G-protein coupled, 4	n.d.	n.d.
P2RY12	64805	Purinergic receptor P2Y, G-protein coupled, 12	yes	n.d.
PANX1	24145	Pannexin 1	yes	21.7951
ENTPD1	953	Ectonucleoside triphosphate diphosphohydrolase 1 (NTPDase-1)	yes	22.3401

Table 17: Total mRNA levels of channels involved in Ca^{2+} signaling. HTC-8 monolayer data are adapted from Hochheimer et al. 2014 and were generated with RT-PCR. – means no data available and n.d. not detectable. The expression profile of HTC-8-G-GECO spheroids was analyzed using RNA transcriptome analysis (preliminary based on one 96-well plate of HTC-8-G-GECO spheroids).

Gene	Gene-ID	Name	monolayer expression	spheroid expression
CACNA1A	773	Calcium voltage-gated channel subunit alpha1A	n.d.	2.35267
CACNA1B	782	Calcium voltage-gated channel subunit beta 1	yes	0.00554409
CACNA1C	775	Calcium voltage-gated channel, L-type, alpha 1C	n.d.	8.04937
CACNA1D	776	Calcium voltage-gated channel, L-type, alpha 1D	n.d.	0.0138746
CACNA1E	777	Calcium voltage-gated channel, R-type, alpha 1E	n.d.	n.d.
CACNA1F	778	Calcium voltage-gated channel, L-type, alpha 1F	n.d.	n.d.
CACNA1G	8913	Calcium voltage-gated channel, T-type, alpha 1G	n.d.	5.23753
CACNA1H	8912	Calcium voltage-gated channel, T-type, alpha 1H	n.d.	0.125691
CACNA1I	8911	Calcium voltage-gated channel, T-type, alpha 1I	n.d.	n.d.
CACNA1S	779	Calcium voltage-gated channel, T-type, alpha 1S	n.d.	n.d.
TRPV1	7442	Transient receptor potential cation channel, subfamily V, member 5 (VR1)	yes	0.476222
SLC8A1	6546	Solute carrier family 8 member A1 (Na^+/Ca^{2+} Exchanger)	-	2.53927
CASR	846	Calcium sensing receptor	-	n.d.

ORAI1	84876	ORAI calcium release-activated calcium modulator 1	yes	25.9594
ORAI3	93129	ORAI calcium release-activated calcium modulator 3	yes	13.2408
STIM	6786	Stromal activating enhancer	yes	23.0189
CNGA1	1259	Cyclic nucleotide gated channel alpha 1	yes	n.d.
CNGA2	1260	Cyclic nucleotide gated channel alpha 2	n.d.	n.d.
CNGA3	1261	Cyclic nucleotide gated channel alpha 3	n.d.	0.0145708
CNGA4	1262	Cyclic nucleotide gated channel alpha 4	n.d.	n.d.
CNGB1	1258	Cyclic nucleotide gated channel beta 1	n.d.	n.d.
CNGB3	54714	Cyclic nucleotide gated channel beta 3	n.d.	n.d.

Table 18: Total mRNA levels of channels involved in the alternative sweet pathway. HTC-8 monolayer data are adapted from Hochheimer et al. 2014 and were generated with RT-PCR. – means no data available and n.d. not detectable. The expression profile of HTC-8-G-GECO spheroids was analyzed using RNA transcriptome analysis (preliminary based on one 96-well plate of HTC-8-G-GECO spheroids).

Gene	Gene-ID	Name	monolayer expression	spheroid expression
SLC2A2	6514	Solute carrier family 2 member 2 (GLUT2)	n.d.	n.d.
SLC2A4	6517	Solute carrier family 2 member 4 (GLUT4)	n.d.	0.0355662
SLC2A5	6518	Solute carrier family 2 member 5 (GLUT5)	-	n.d.
SLC2A8	29988	Solute carrier family 2 member 8 (GLUT8)	n.d.	6.68082
SLC2A9	56606	Solute carrier family 2 member 9 (GLUT9)	n.d.	0.541399
SLC2A10	81031	Solute carrier family 2 member 10 (GLUT10)	-	49.8832
SLC2A13	114134	Solute carrier family 2 member 13 (GLUT13)	-	8.03344
SLC5A1	6523	Solute carrier family 5, member 1 (SGLT1)	n.d.	n.d.
SLC5A2	6524	Solute carrier family 5, member 2 (SGLT2)	n.d.	0.034832
SLC45A1	50651	Solute carrier family 45, member 1	-	1.62609
SLC45A2	511515	Solute carrier family 45, member 2	-	0.034832
SLC45A3	85414	Solute carrier family 45, member 3	-	0.955337
SLC45A4	57210	Solute carrier family 45, member 4	-	3.36511
KCNJ8	3764	Potassium inwardly rectifying channel subfamily J member 8 (Kir6.1)	-	1.03302
KCNJ10	3766	Potassium inwardly-rectifying channel, subfamily J, member 10 (Kir6.2)	n.d.	0.0102362
KCNJ11	3767	Potassium inwardly-rectifying channel, subfamily J, member 11 (Kir6.2)	n.d.	n.d.
KCNJ12	16515	Potassium inwardly-rectifying channel, subfamily J, member 12	n.d.	0.0169531
KCNJ14	3770	Potassium inwardly-rectifying channel, subfamily J, member 14	yes	0.158399
KCNJ15	3772	Potassium inwardly-rectifying channel, subfamily J, member 15	n.d.	0.182558
ABCC8	6833	ATP binding cassette subfamily C member 8 (SUR1)	-	n.d.
ABCC9	10060	ATP binding cassette subfamily C member 9 (SUR2)	-	1.02499
MGAM	8972	Maltase-glucoamylase	-	n.d.
LCT	3938	Lactase	-	n.d.
TREH	1181	Trehalase	-	n.d.
SIS	69983	Sucrase-isomaltase	-	n.d.
AMY1A	276	Amylase alpha 1A	-	n.d.

AMY1B	277	Amylase alpha 1B	-	n.d.
AMY1C	278	Amylase alpha 1C	-	n.d.
GANC	2595	Glucosidase alpha, neutral C	-	4.22942
GBA	2629	Glucosylceramidase beta	-	74.1861
GBA2	57704	Glucosylceramidase beta 2	-	8.11921
GBA3	57733	Glucosylceramidase beta 3	-	n.d.
GALC	2581	Galactosylceramidase	-	7.37882
GLB1	2720	Galactosidase beta 1	-	40.5395
DPP4	1803	Dipeptidyl-peptidase 4	-	4.74049
GCG	2641	Glucagon-like-peptide 1	-	n.d.
PCSK1	5122	Proprotein convertase subtilisin/kexin type (PC1, PC3)	-	0.327803
PCSK2	5126	Proprotein convertase subtilisin/kexin type 2 (PC2)	-	7.185
PCSK7	9159	Proprotein convertase subtilisin/kexin type 7 (PC7)	-	17.8021
PCSK5	5125	Proprotein convertase subtilisin/kexin type 5 (PC5,6)	-	3.66509
LRRC8A	56262	Leucine rich repeat containing 8 VRAC subunit A	-	35.9621
AQP1	358	Aquaporin 1	-	0.77696
AQP2	359	Aquaporin 2	-	n.d.
AQP3	360	Aquaporin 3	-	0.126306
AQP4	361	Aquaporin 4	-	n.d.
AQP5	362	Aquaporin 5	-	n.d.
AQP6	363	Aquaporin 6	-	n.d.
AQP7	364	Aquaporin 7	-	0.100763
AQP8	343	Aquaporin 8	-	0.0479663
AQP9	366	Aquaporin 9	-	0.0185967
AQP10	89872	Aquaporin 10	-	n.d.
AQP11	282679	Aquaporin 11	-	0.674047

Table 19: Total mRNA levels of KRT and type III cell marker. HTC-8 monolayer data are adapted from Hochheimer et al. 2014 and were generated with RT-PCR. – means no data available and n.d. not detectable. The expression profile of HTC-8-G-GECO spheroids was analyzed using RNA transcriptome analysis (preliminary based on one 96-well plate of HTC-8-G-GECO spheroids).

Gene	Gene-ID	Name	monolayer expression	spheroid expression
KRT8	3856	Cytokeratin 8	yes	n.d.
KRT14	3861	Cytokeratin 14	n.d.	n.d.
KRT20	54474	Cytokeratin 20	-	n.d.
SNAP25	6616	Synaptosomal-associated protein, 25kDa	yes	8.14941
GAD1	2571	Glutamat decarboxylase 1	-	n.d.
GAD2	2572	Glutamat decarboxylase 2	-	n.d.
PKD2L1	9033	Polycystic kidney disease 2-like 1 protein	n.d.	n.d.
PKD1L3	342372	Polycystic kidney disease 2-like 3 protein	n.d.	n.d.

7 Publications

Klicks, J.*; **von Molitor, E.***; Ertongur-Fauth, T.; Rudolf, R.; Hafner, M. (2017): In vitro skin three-dimensional models and their applications. In JCB 3 (1), pp. 21–39. DOI: 10.3233/JCB-179004.

von Molitor, **E.**; Nürnberg, E.; Ertongur-Fauth, T.; Scholz, P.; Riedel, K.; Hafner, M. et al. (2020a): Analysis of calcium signaling in live human Tongue cell 3D-Cultures upon tastant perfusion. In *Cell calcium* 87, p. 102164. DOI: 10.1016/j.ceca.2020.102164.

von Molitor, E.; Riedel, K.; Hafner, M.; Rudolf, R.; Cesetti, T. (2020b): Sensing Senses: Optical Biosensors to Study Gustation. In *Sensors (Basel, Switzerland)* 20 (7). DOI: 10.3390/s20071811.

von Molitor, E.; Riedel, K.; Krohn, M.; Rudolf, R.; Hafner, M.; Cesetti, T. (2020c): An alternative pathway for sweet sensation: possible mechanisms and physiological relevance. In *Pflugers Archiv : European journal of physiology*. DOI: 10.1007/s00424-020-02467-1.

Nürnberg, E.; Vitacolonna, M.; Klicks, J.; **von Molitor, E**.; Cesetti, T.; Keller, F.; Bruch, R.; Ertongur-Fauth, T.; Riedel, K.; Scholz, P.; Lau, T.; Schneider, R.; Meier, J.; Hafner, M.; Rudolf, R. (2020): Routine Optical Clearing of 3D-Cell Cultures: Simplicity Forward. In *Frontiers in molecular biosciences* 7, p. 20. DOI: 10.3389/fmolb.2020.00020.

submitted:

von Molitor, E.; Riedel K.; Krohn K.; Hafner M.; Rudolf R.; Cesetti T. (2021): Sweet taste is complex: signalling cascades and circuits involved in sweet sensation. Submitted to: *Frontiers in human neuroscience*

* contributed equally as first authors

8 Statement on copyright and self-plagiarism

The major content of this thesis has been published in peer reviewed articles (Chapter 7). Text passages were written in accordance to manuscripts but the wording and structure has been modified. Articles have been cited correspondingly. As indicated in legends, figures and tables have been adapted and/or modified from manuscripts.

The introduction of this thesis is based on the following two reviews: von Molitor et al. 2020b and von Molitor et al. 2020c. Further contents of the manuscript “Sweet taste is complex: signaling cascades and circuits involved in sweet sensation”, which has not been published yet, were implemented. I, E. von Molitor was involved in conceptualization, data collection and writing the original draft with the support of T. Cesetti. R. Rudolf was the main supervisor and involved in proof reading and editing. K. Riedel, M. Krohn and M. Hafner reviewed the manuscript.

The experimental data presented in this thesis have been partially published in von Molitor et al. 2020a. I, E. von Molitor planned the study, carried out experiments, analyzed/validated data and wrote the manuscript with the support of T. Cesetti. E. Nürnberg helped in LSFM data acquisition. R. Rudolf and M. Hafner are the principal supervisors and were involved in conceptualization, study design, and reviewing the manuscript. K. Riedel, P. Scholz and T. Ertongur-Fauth from BRAIN AG kindly provided HTC-8, HTC-8-G-GECO and HTP-76 cells. They all have been supportive in conceptualization and reviewing the publication. The results of clearing protocols tested on HTC-8 spheroids have been published in Nürnberg et al. 2020. I, Elena von Molitor conducted experiments and data analysis for HTC-8 (and HaCaT) spheroids with the support of T. Cesetti. E. Nürnberg and M. Vitacolonna provided clearing protocols and were responsible for confocal data acquisition of provided pre-stained and cleared spheroids. M. Vitacolonna conducted the segmentation analysis. The manuscript was written by E. Nürnberg, M. Vitacolonna. R. Rudolf and M. Hafner. The other authors reviewed the manuscript. The mRNA sequencing data analysis has not been published and was performed by P. Scholz from provided HTC-8-G-GECO spheroid mRNA. Further, BRAIN AG provided slides with human taste papillae for antibody testing.